**UNIVERSIDADE FEDERAL DO CEARÁ**
**CENTRO DE CIÊNCIAS**
**DEPARTAMENTO DE QUÍMICA ORGÂNICA E INORGÂNICA**
**PROGRAMA DE PÓS-GRADUAÇÃO EM QUÍMICA**

**MARIA DAIANE DE FREITAS**

# DETERMINAÇÃO DO PERFIL METABÓLICO DAS CASCAS DE *Citrus aurantium* USANDO CL-EMAR E AVALIAÇÃO DO POTENCIAL BIOLÓGICO

**FORTALEZA**
**2024**

MARIA DAIANE DE FREITAS

# DETERMINAÇÃO DO PERFIL METABÓLICO DAS CASCAS DE *Citrus aurantium* USANDO CL-EMAR E AVALIAÇÃO DO POTENCIAL BIOLÓGICO

Dissertação apresentada ao Programa de Pós-Graduação em Química da Universidade Federal do Ceará, como requisito final à obtenção do título Mestre em Química. Área de concentração: Química Orgânica.

Orientadora: Profa. Dra. Telma Leda Gomes de Lemos.

FORTALEZA

2024

Dados Internacionais de Catalogação na Publicação
Universidade Federal do Ceará
Sistema de Bibliotecas
Gerada automaticamente pelo módulo Catalog, mediante os dados fornecidos pelo(a) autor(a)

---

F937d Freitas, Maria Daiane de.
Determinação do perfil metabólico das cascas de Citrus aurantium usando CL-EMAR e avaliação do potencial biológico / Maria Daiane de Freitas. – 2024.
129 f. : il. color.

Dissertação (mestrado) – Universidade Federal do Ceará, Centro de Ciências, Programa de Pós-Graduação em Química, Fortaleza, 2024.
Orientação: Profa. Dra. Telma Leda Gomes de Lemos.

1. Espectrometria de massas. 2. Desreplicação. 3. Atividade antioxidante. 4. Fusarium jinanense. I. Título.
CDD 540

---

MARIA DAIANE DE FREITAS

# DETERMINAÇÃO DO PERFIL METABÓLICO DAS CASCAS DE *Citrus aurantium* USANDO CL-EMAR E AVALIAÇÃO DO POTENCIAL BIOLÓGICO

Dissertação apresentada ao Programa de Pós-Graduação em Química da Universidade Federal do Ceará, como requisito final à obtenção do título Mestre em Química. Área de concentração: Química Orgânica.

Aprovada em: 27 / 03 / 2024

BANCA EXAMINADORA

_____

Profa. Dra. Telma Leda Gomes de Lemos (Orientadora)
Universidade Federal do Ceará (UFC)

_____

Prof. Dr. Marcos Carlos de Mattos
Universidade Federal do Ceará (UFC)

_____

Profa. Dra. Fátima Miranda Nunes
Universidade Federal do Ceará (UFC)

## AGRADECIMENTOS

Primeiramente quero agradecer a Deus por me fortalecer nas minhas dificuldades e me permitir vivenciar essa fase tão importante para minha formação acadêmica e pessoal.

Aos meus pais, Antônio e Gorete pelos valores que me passaram e pelo incentivo em todas as minhas decisões.

Aos meus irmãos, Dalvan, Delvânia, Digiane e meus avós, Amélia, Josias e Francisca e ao meu tio Gerson, por serem sempre a minha base em todos os momentos.

À minha orientadora profa. Dra. Telma Leda Gomes de Lemos, pela oportunidade de trabalhar com ela durante seis anos da minha vida acadêmica, como ela fala, é uma mãe cientifica com quem tive a honra de aprender sobre a beleza dos produtos naturais. Agradeço por toda a motivação, confiança durante essa etapa do mestrado e pela ótima orientação profissional e pessoal.

Ao Departamento de Fitotecnia da Universidade Federal do Ceará por ceder o material vegetal para o estudo.

Ao Prof. Cristiano, Mayumi, Erivaldo e a Profa. Davila pela realização da atividade antifúngica do extrato e das frações.

Ao Rodolfo, doutorando da Unicamp, quero expressar meu profundo agradecimento pela parceria e disponibilidade que ele teve para me ajudar em todas as etapas do projeto.

Ao Rodolfo e profa. Taicia Pacheco pelas análises de massas de alta resolução do extrato, frações e padrões.

Aos amigos que fiz durante esse período acadêmico, Vitor, Marilia, Rebeca, Vanessa, Leomar, Jéssica, Erivaldo e Nicaely, pessoas com quem vivenciei momentos muito especiais e com certeza irei levar para fora dos muros da universidade.

Aos meus amigos adquiridos durante minha estadia no Laboratório de Biotecnologia e Produtos Naturais (LBPN), Iolanda, Renan, Patrícia e Ingrid que não mediram esforços para me ajudar, tanto profissionalmente como pessoalmente, é muito bom poder contar com vocês sempre.

A banca composta pelo Prof. Marcos e a Profa. Fátima Miranda por ter aceitado o convite para contribuir com o trabalho.

O presente trabalho foi realizado com apoio da Coordenação de Aperfeiçoamento de Pessoal de Nível Superior - Brasil (CAPES) - Código de Financiamento 001. Agradecer, aos órgãos de fomento CNPq e CAPES que foram cruciais para realização desse trabalho.

Nada te perturbe, nada te espante, tudo passa! Só Deus não passa. A paciência, por fim, tudo alcança. Quem a Deus tem, nada lhe falta, pois só Deus basta.

*Santa Tereza D' Ávila*

## RESUMO

A *Citrus aurantium* conhecida como laranja amarga é uma das muitas espécies do gênero *Citrus,* muito usada na medicina tradicional chinesa, como digestivo, anti-inflamatório, ansiolítico etc. Muitos estudos descreveram o uso do óleo essencial em diferentes aplicações, mas, pouco se sabe sobre a composição química e o potencial biológico obtido a partir das cascas do fruto. O presente trabalho tem como objetivo reportar a composição química e avaliar a capacidade antifúngica e antioxidante do decocto obtido das cascas de *C. aurantium*. Inicialmente, o extrato obtido do decocto por partição com acetato de etila (EAE-CA) foi submetido a extração em fase sólida (SPE) seguido de análise por cromatografia liquida de alta eficiência (CLAE). Então, o extrato EAE-CA e as frações obtidas foram submetidas a ensaios biológicos tais como: atividade antifúngica frente ao fitopatógeno *Fusarium jinanense* e atividade antioxidante usando o método de captura do radical 2,2-Difenil-1-Picril-Hidrazil (DPPH). O extrato EAE-CA e duas frações com potencial antifúngico FR3 e FR4 foram analisadas por Cromatografia Líquida acoplada a Espectrometria de Massas de Alta Resolução (CL-EMAR). Esses dados permitiram a anotação de 65 metabólitos secundários, sendo 57 substâncias no modo positivo e 8 no modo negativo, entre estes flavonoides, cumarinas, terpenos, limonóide, compostos aromáticos e nitrogenados. As frações FR3 e FR4 cujos compostos anotados foram predominantemente polimetoxiflavonas e cumarinas apresentou uma inibição de 60,97% do crescimento micelial do fungo *F. jinanense*, valor superior ao alcançado pelo atual antifúngico comercial Cercobin® (47,92%). A atividade antioxidante apresentou resultado moderado com concentração inibitória a 50% ($CI_{50}$) do extrato de 0,0602 mg/mL e o padrão positivo Trolox mostrou um $CI_{50}$ de 0,0061 mg/mL. Dessa forma, a busca de compostos ou frações enriquecidas por substâncias com potencial biológico em fontes de refugo industrial pouco exploradas como as cascas, atribui valor agregado, e pode ser uma alternativa no controle de diferentes fitopatologias.



**Palavras-chave**: espectrometria de massas; desreplicação; atividade antioxidante; *Fusarium jinanense*.

**ABSTRACT**

*Citrus aurantium*, known as bitter orange, is one of the many species of the genus *Citrus* and is widely used in traditional Chinese medicine as a digestive, anti-inflammatory, anxiolytic, etc. While many studies have described the use of its essential oil in various applications, little is known about the chemical composition and biological potential derived from the fruit peels. This study aims to report the chemical composition and evaluate the antifungal and antioxidant capacities of the decoction obtained from *C. aurantium* peels. Initially, the extract obtained from the decoction through partitioning with ethyl acetate (EAE-CA) underwent solid-phase extraction (SPE) followed by analysis using high-performance liquid chromatography (HPLC). Then, the EAE-CA extract and the fractions obtained were subjected to biological assays, such as antifungal activity against the phytopathogen *Fusarium jinanense* and antioxidant activity using the 2,2-Diphenyl-1-Picrylhydrazyl (DPPH) radical scavenging method. The EAE-CA extract and two fractions with antifungal potential, FR3 and FR4, were analyzed by Liquid Chromatography coupled with High-Resolution Mass Spectrometry (LC-HRMS). This data allowed the annotation of 65 secondary metabolites, with 57 substances in positive mode and 8 in negative mode, including flavonoids, coumarins, terpenes, limonoids, aromatic compounds, and nitrogenous compounds. Fractions FR3 and FR4, whose annotated compounds were predominantly polymethoxyflavones and coumarins, showed a 60.97% inhibition of fungal mycelial growth of *F. jinanense*, a value higher than that achieved by the current commercial antifungal Cercobin® (47.92%). The antioxidant activity showed moderate results with an Inhibitory Concentration at 50% ($IC_{50}$) of 0.0602 mg/mL for the extract, while the positive control Trolox presented an $IC_{50}$ of 0.0061 mg/mL. Thus, the search for compounds or fractions enriched with biologically active substances from underexplored industrial waste sources such as peels adds value and maybe an alternative for the control of different phytopathologies.

**Keywords**: mass spectrometry; dereplication; antioxidant activity; *Fusarium jinanense.*

## LISTA DE FIGURAS

## LISTA DE TABELAS

## LISTA DE ABREVIATURAS E SIGLAS

| | |
|---|---|
| CLAE C18 | Cromatografia Liquida de Alta Eficiência Octadecil |
| DAD | Detector de arranjo de diodos |
| DDA | Análise de dados dependente (do inglês, *data dependent analysis)* |
| DP | Desvio padrão |
| EAE-CA | Extrato em Acetato de Etila *Citrus aurantium* |
| *Full scan* | Espectro completo |
| LC-MS | Cromatografia Liquida acoplada a Espectrometria de Massas (do inglês, *Liquid Chromatography-Mass Spectrometry*) |
| MS | Espectrometria de massas (do inglês, *mass spectrometry*) |
| PA | Puro para análise |
| PTFE | Politetrafluoretileno |
| PDA | ágar batata dextrose (do inglês, *Potato Dextrose Agar*) |
| ppm | Partes por milhão |
| SPE | Extração em fase solida (do inglês, *Solid-phase extraction*) |
| UV- Vis | Ultravioleta visível |

## LISTA DE SÍMBOLOS

| | |
|---|---|
| λ | Comprimento de onda |
| ® | Marca Registrada Micro |
| μ | ($10^{-6}$) |
| *m/z* | Razão massa/carga |
| nm | Nanômetro |
| % | Porcentagem |

**SUMÁRIO**

# 1 INTRODUÇÃO

*Citrus aurantium* L., conhecida como laranja amarga ou laranja azeda, é uma espécie originária do Sudeste Asiático que pertence à ordem Geraniales e a família Rutaceae (DEGIRMENCI; ERKURT, 2020). Essa espécie, não ganha notoriedade na fabricação de suco, pois o fruto apresenta polpa amarga, no entanto, possui uma variedade de aplicações, como o uso em sobremesas, suplemento alimentar e obtenção de óleo essencial (OULEBSIR *et al.,* 2022).

A gama de aplicações de *C. aurantium* aumenta quando se trata da sua relevância na medicina tradicional chinesa, apresentando benefícios em diferentes quadros clínicos como indigestão, diarreia, doença de Alzheimer (ABOU *et al.,* 2020), doenças inflamatórias, anti-nociceptiva (HAMEDI *et al.,* 2019), agente anticatarata (KULKARNI *et al.,* 2017), ansiedade, doenças cardiovasculares (MORADI *et al.,* 2021) e anticâncer (NAZARI; AZARPIRA; HELI, 2018).

Os frutos do gênero *Citrus* apresentam em sua constituição química diversos compostos das classes dos flavonoides e das cumarinas, tais substâncias são relatadas como potenciais antifúngicos sobre cepas de fungos dos gêneros, *Candida*, *Aspergillus* e *Fusarium (*MONTAGNER *et al*., 2008; AL ABOODY; MICKYMARAY, 2020). No Brasil, patógenos do gênero *Fusarium* são responsáveis por grandes perdas na produção de melões, tendo sido descoberto atualmente novas espécies de fungos do complexo *Equiseti-Incarnatum*, como *Fusarium jinanense*, capazes de causar podridão do fruto a partir de um mecanismo quiescente de infecção que se inicia ainda no campo e pode comprometer hectares de produção (LIMA *et al.,* 2021).

Apesar da variedade de aplicações do óleo essencial *C. aurantium* contra fungos do gênero *Fusarium*, até a presente data não foram encontrados estudos na literatura dessa espécie com o objetivo de avaliar a composição química e o potencial antifúngico do decocto obtido das cascas do fruto sobre fitopatógenos desse gênero. Dessa forma, este trabalho tem como objetivo integrar uma estratégia de fracionamento bioguiado à técnica de alto desempenho como a Cromatografia Líquida acoplada a Espectrometria de Massas de Alta Resolução (CL-EMAR) a fim de agregar valor a este subproduto pouco explorado e principalmente apontar quais compostos estão envolvidos no potencial antifúngico frente a *F. jinanense.* agente causal da podridão em melão amarelo e avaliar a atividade antioxidante do extrato e de frações.

# 2 REVISÃO BIBLIOGRÁFICA

## 2.1 Considerações sobre espécie e constituição química de *Citrus aurantium* L.

*Citrus aurantium*, que é tipicamente conhecida como laranja amarga, laranja da terra ou laranja azeda, é uma árvore que pertence à ordem Geraniales e a família Rutaceae. A árvore apresenta porte de médio a grande, as folhas contêm características morfológicas laminares, com pontas, base arredondada, flores grandes, os frutos de aspecto sensorial ácido e amargo, de difícil consumo. Sua maior importância em citricultura decorre de seu uso como porta-enxerto (MOURA; AREAS, 2013).

A composição química de *C. aurantium* inclui uma série de compostos fixos e voláteis diversificada, como: vitaminas, minerais, cumarinas, flavonoides glicosilados, terpenóides e aminas biogênicas (SIMÕES *et al*., 2007). Dentre os compostos fixos, a classe das cumarinas e dos flavonoides ganham notoriedade devido a sua importância no papel fisiológico e farmacológico, com diversos benefícios para a saúde tais como: atividade antioxidante, antidiabética e vasodilatadora (SUNTAR *et al*.,2018).

As cumarinas apresentam uma biossíntese pela via do ácido chiquímico, através do metabolismo da fenilalanina, estruturalmente são lactonas derivadas do ácido *o*-hidróxi-cinâmico conforme expresso na **Figura 1**. Essa classe de compostos é amplamente distribuída nas plantas, encontradas principalmente nas famílias Apiaceae e Rutaceae (SIMÕES *et al*., 2007; DEWICK, 2002). As cumarinas são relatadas como componentes que apresentam diversas atividades biológicas tais como; antimicrobiana, anti-inflamatória, anticâncer, antidiabética entre outras (ANNUNZIATA *et al.,* 2020).

**Figura 1**: Estrutura base das cumarinas

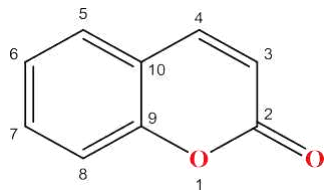


Fonte: Adaptação de ANNUNZIATA *et al.,* 2020.

Os flavonoides, biossintetizados a partir de fenilpropanóides podem ser encontrados em diversas formas estruturais. Entretanto, a maioria possui 15 átomos de carbono em seu núcleo fundamental **Figura 2 (**Pág.14), constituído por duas fenilas ligadas por uma

cadeia de carbonos entre elas. Geralmente os flavonoides de origem natural apresentam oxigênio em sua estrutura, podendo estar conjugados com açúcares (SIMÕES *et al.,* 2007).

**Figura 2**: Estrutura base dos flavonoides

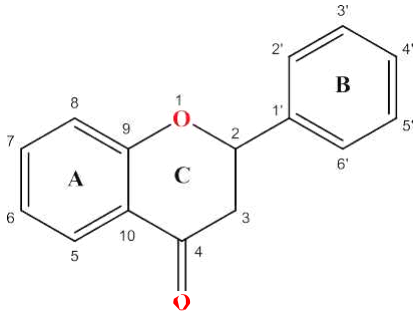


Fonte: Adaptação de Simões *et al.,* 2007.

## 2.2 Doenças pós-colheita causadas por fungos em frutos tropicais.

A segurança alimentar no consumo de frutas *in natura*, é uma preocupação de agencias nacionais e internacionais. Dessa forma, há legislações especificas para o uso de defensivos agrícolas. O Cercobin®, registrado pelo Ministério da Agricultura, Pecuária e Abastecimento (MAPA), com número 9318, cujo princípio ativo é o tiofanato metílico é um antifúngico do grupo químico Benzimidazol, esse é aplicado em partes aéreas de culturas como abacate, abacaxi, café, citros, mamão, maracujá, melão amarelo entre outros (OSTER *et al.,* 2018).

O melão amarelo (*Cucumis melo*), é um produto de grande importância econômica mundial. Segundo a FAO em 2021 esse fruto gerou um montante de 165 mil US$. No entanto, esse fruto é acometido por doenças infecciosas pós-colheita tais como: podridão-por-*Rhizopus*, antracnose, podridão negra e podridão-por-*Fusarium* etc. A podridão-por-*Fusarium* é uma das principais infecções fúngicas no melão, essas doenças apresentam um mecanismo quiescentes se expressando frequentemente no transporte ou armazenamento do fruto (KIST; CARVALHO; BELING, 2022; OSTER *et al.,* 2018; DIAS; TERAO, 2006).

Os fungos do gênero *Fusarium* causadores de patologias vegetais, sintetizam micotoxinas como os tricotecenos, zearalenona e fumonisina, que são substâncias nocivas para os humanos e a organização mundial de saúde (OMS) adverte que muitas dessas substâncias são carcinógenos humanos e o uso prolongado de fungicidas na agricultura pode ocasionar a seleção de fungos fitopatogênicos resistentes, que não são controlados pelo produto. Tal problema pode gerar graves consequências, tais como elevação de custos, resíduos em

alimentos e contaminações ambientais (APARECIDO; ROSA, 2019; OMOTAYO *et al*., 2017; GHINI; HIROSHI, 2002).

## 2.3 Estratégias de anotação e identificação de metabólitos secundários usando dados de Cromatografia Líquida acoplada a Espectrometria de Massas de Alta Resolução (CL-EMAR)

A espectrometria de massas é uma técnica analítica usada para identificar e confirmar diversas estruturas químicas. Em meados dos anos 90 essa técnica foi unida a técnicas de cromatografia. Essas técnicas hifenadas tais como: Cromatografia Líquida acoplada a Espectrometria de Massas (CL-EM) e a Cromatografia Gasosa acoplada a Espectrometria de Massas (CG-EM) possibilitou uma grande melhoria em termos analíticos, com análises amostrais fidedignas (NICOLESCU, 2017).

A cromatografia líquida é aplicada para a separação de compostos mais polares como: compostos fenólicos, alcaloides, nucleotídeos, peptídeos etc. Já a cromatografia gasosa é uma técnica aplicada para compostos com menor polaridade esse são: terpenos, fenilpropanóides, voláteis, esteroides e outros, esses também têm menor massa molecular e precisam apresentar duas características que são ser termicamente estáveis e lábeis (LI *et al*., 2016).

Nos equipamentos de CL-EM a amostra é injetada em instrumentos do tipo CLAE (Cromatografia Líquida de Alta Resolução), ou de maior resolução CLUE (Cromatografia Líquida de Ultra Eficiência) na qual ocorre a separação de substâncias presentes na amostra, essa separação se dá pela diferença entre as interações químicas dos analitos com a fase móvel e com a fase estacionária da coluna, em seguida essas substâncias seguem através de um tubo capilar para fonte de ionização no espectrômetro de massas (PAVIA et al., 2010).

Na fonte de ionização por *electrospray* ocorre a formação de íons através da diferença de potencial entre o cone (contra-eletrodo) e o capilar contendo a solução vinda da parte cromatográfica. Os íons gerados podem ser de três tipos: íons moleculares, moléculas protonadas/desprotonadas (íons quasi-moleculares) e moléculas cationizadas ou anionizadas (CROTTI *et al*., 2006). O spray que é expelido do capilar contém gotículas com solventes e íons, também é chamado de cone de Taylor devido o formato de cone durante o jato. A formação do spray ocorre porque há um gás inerte no sentido desse fluxo chamado de gás de bainha e

contra esse fluxo há um gás inerte, conhecido como gás de secagem cujo objetivo é diminuir a gota, com a diminuição do tamanho da gota as forças repulsivas serão maiores do que as forças atrativas então a gota se rompe, esse fenômeno é chamado de explosão coulômbica e as partículas carregadas são expelidas e fragmentadas gerando uma resposta que conhecemos como espectro (NICOLESCU, 2017; CROTTI *et al*., 2006).

O estudo de CL-EM com amostras complexas como extratos, geram um alto volume de espectros, a desreplicação ou comparação individual dos espectros pode se tornar um processo muito laborioso e demorado, por isso os avanços em técnicas estatísticas, quimiométricas e de bioinformática contribuiu para a organização e interpretação desses dados. A análise na forma de redes moleculares (do inglês, *Molecular Networking*), se baseia em comparar espectros experimentais com espectros de referência, a semelhança espectral é determinada por parâmetros estatísticos que podem ser alterados pelo usuário dessas ferramentas (PILON *et al*., 2021).

Os espectros de referência, são espectros de centenas de substâncias já identificadas que são armazenados em bancos de dados espectrais, essas bibliotecas sevem de subsídios para o confronto com dados adquiridos. Uma plataforma que permite o estudo de dados de espectrometria de massas usando redes moleculares é a *Global Natural Products Social Networking* (GNPS). Essa é uma ferramenta gratuita e online que foi criada para estudo de proteômica, mas que atualmente é muito usada por pesquisadores da área de produtos naturais (PILON *et al*., 2021).

Um dos modos de construção das redes moleculares no GNPS é através do *Feature Based Molecular Networking* (FBMN), um módulo de análise criado para resolver as limitações do MSCluster, o algoritmo do "classical'' *Molecular Networking* (MN). No FBMN os espectros adquiridos por técnicas acopladas como por exemplo CLAE-EM, $EM^n$ são associados ao tempo de retenção de cada respectivo valor de razão massa-carga, permitindo a anotação de isômeros e isóbaros. O modo FBMN requer uma etapa de pré-processamento dos dados, uma vez que é necessário a geração dos *features* que são dados de associação dos dados de cromatografia por exemplo: tempo de retenção com dados de massas, *m/z* do íon (NOTHIAS *et al*., 2020).

## 2.4 Atividade antioxidante

Um agente antioxidante é uma substância sintética ou natural que tem a função de prevenir ou retardar a deterioração causada pela ação do oxigênio presente no ar, podendo ser

substâncias orgânicas ou enzimas, capazes de agir contra danos de oxidação nos tecidos animais (PREVEDELLO; COMACHIO, 2021).

A atividade antioxidante *in vitro*, pode ser avaliada por diversos métodos, tais como: método baseado na captura de radical: 2,2-difenil-1-picrilhidrazil (DPPH) representado na **Figura 3** e ABTS (2,2'-azino-bis (ácido 3-etilbenzotiazolina-6-sulfônico)), ensaio da capacidade de absorção do radical oxigênio (ORAC) e verificação do poder antioxidante pela redução férrica (FRAP). O uso de tais testes se faz necessário para promover uma seleção inicial de substâncias que possam ser candidatos a fármacos (DING; ZHANG, X; ZHANG J, 2021; ALVES *et al.,* 2010).

**Figura 3**: Reação de captura do radical DPPH frente a um agente antioxidante

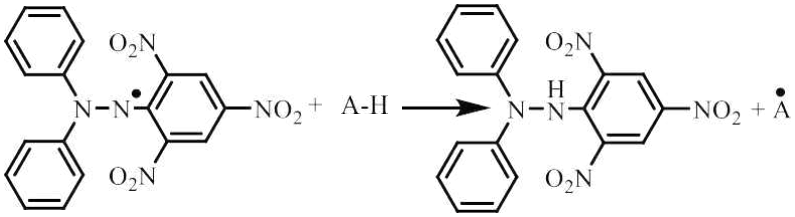


Cor: Violeta Cor: Amarelo

Fonte: adaptação de Oliveira, (2015).

# 3 OBJETIVOS

## 3.1 Objetivo Geral

Realizar estudo de desreplicação usando dados de espectrometria de massas de extrato e frações proveniente das cascas de *Citrus aurantium* L. e avaliar o potencial antifúngico frente a espécie *Fusarium jinanense* e antioxidante pelo método de captura de radical DPPHº.

## 3.2 Objetivos Específicos

• Obter o extrato em acetato de etila das cascas de *Citrus aurantium* L (EAE-CA), usando processo de decocção;

• Fracionar o extrato EAE-CA usando a técnica de Extração em Fase Sólida (SPE);

• Analisar o perfil cromatográfico do extrato EAE-CA e das frações obtidas por SPE, usando a Cromatografia Líquida de Alta Eficiência (CLAE);

• Avaliar o potencial antifúngico do extrato EAE-CA e das frações frente ao fitopatógeno do melão amarelo, *F. jinanense*. (UFCM-0611);

• Obter os dados de Cromatografia Líquida acoplada a Espectrometria de Massas de Alta Resolução (CL-EMAR) e realizar o processo de desreplicação através da comparação dos dados de fragmentação do extrato EAE-CA e frações bioativas com dados de fragmentação relatadas na literatura e em bibliotecas espectrais utilizando o fluxo de trabalho do *Feature Based Molecular Networking* (FBMN) uma ferramenta do *Global Natural Product Social Molecular Networking* (GNPS);

• Anotar e/ou identificar metabolitos secundários usando dados de fragmentação dos espectros de massas;

• Avaliar o potencial antioxidante do extrato EAE-CA e das frações usando o método de captura de radical DPPHº.

# 4 MATERIAIS E MÉTODOS

## 4.1 Coleta do material

Os dados de coleta da planta, obtenção do extrato e frações, tratamento cromatográfico, isolamento do fungo, atividade antifúngica sobre o fitopatógeno *Fusarium jinanense*, obtenção dos dados de CL-EMAR e a desreplicação dos compostos estão pressentes no manuscrito (Pág. 28-33).

## 4.2 Análise por CLAE das amostras EAE-CA, FR1-FR5 obtidas em SPE

As amostras EAE-CA, FR1-FR5 foram analisadas por Cromatografia Liquida de Alta Eficiência (CLAE), verificando assim a eficiência do fracionamento em SPE, nesse processo foi usado um Cromatógrafo da marca Shimadzu® com o sistema de bomba binário (L201147), equipado com detector de UV- Vis, com arranjo de Diodo (DAD). Utilizou-se coluna de fase reversa, Luna $C_{18}$ 5 μm com as dimensões de 250 x 4,6 mm, da marca Phenomenex®. Como fase móvel foi usado água deionizada (A) obtida através de um sistema de purificação Milli-Q e acetonitrila (MeCN) (B) grau CLAE da marca SK Chemicals®, ambos solventes foram filtrados separadamente através de uma membrana de náilon de 45 μm (Millipore). Cada amostra foi dissolvida separadamente em MeOH grau CLAE fornecida pela SK Chemicals® e filtradas em membrana de nylon 0,45 μm.

A metodologia usada nas injeções baseou-se em gradiente de eluição: 5% B (0-2 min), 5-98% B (2-10 min), 98% B (10-15 min), 98-5% B (15-16,2 min) e 5% B (16,2-20 min). O fluxo aplicado durante as corridas foi de 1 mL/min, temperatura de 40 ºC, e com a detecção por varredura de UV-Vis no comprimento de onda (λ) de 280 nm.

## 4.3 Espectroscopia de absorção na região infravermelho (IV)

Os espectros de absorção na região do infravermelho do extrato e das frações, foram adquiridos no Departamento de Química Orgânica e Inorgânica da Universidade Federal do Ceará, usando um Espectrômetro de Infravermelho com Transformada de Fourier (IV-TF), marca Perckin Elmer®, modelo FT-IR SPECTRUM 100. Utilizou-se pastilhas de brometo de potássio (KBr) na proporção de 1% de amostra. A análise foi adquirida na faixa de número de onda de 4000 a 400 $cm^{-1}$.

## 4.4 Atividade Antioxidante

A análise antioxidante foi baseada no método de Hegazi e El Hady (2002). O método consistiu primeiramente em preparar uma solução etanólica de DPPH 60 μM, seguida das respectivas concentrações das amostras (0,25; 0,0625; 0,0156; 0,0039; 0,0019 e 0,0009 mg/ mL). Depois da adição da solução de DPPH nas soluções contendo a amostra, estas foram armazenadas na ausência de luz por 30 minutos. Após esse período transferiu-se individualmente cada solução para uma cubeta de quartzo e as leituras foram realizadas em um espectrofotômetro da marca Shimadzu, modelo UV mini-1240. Antes das leituras o equipamento foi calibrado com metanol PA da marca Synth® e em seguida ajustou-se o comprimento de onda (λ) em 520 nm. A medida do branco foi realizada com 2 mL de metanol e 2 mL da solução de DPPH o procedimento foi realizado em triplicata utilizando ácido ascórbico (vitamina C) e o ácido 6-hidroxi-2,5,7,8-tetrametilcromano-2-carboxílico (Trolox) como padrões positivos.

Os dados obtidos foram analisados usando a Equação 1 descrita abaixo, onde AA% corresponde a porcentagem da atividade antioxidante.

$$AA\% = \left[1 - \left(\frac{Abs\ branco}{Abs\ DPPH}\right)\right] \text{ X } 100 \qquad (1)$$

A partir dos resultados foi construída uma curva de porcentagem da capacidade inibitória (eixo y) *vs* concentração em mg/mL (eixo x), permitindo assim o cálculo da Concentração Inibitória de 50% ($CI_{50}$) e 30% ($CI_{30}$), tanto das amostras como dos padrões positivos.

# 5 RESULTADOS E DISCUSSÃO

## 5.1 Informe sobre os resultados

Os resultados da atividade antifúngica sobre o *Fusarium jinanense*, desreplicação dos 65 compostos estão presentes no manuscrito (Pág. 33-49) e material suplementar (Pág. 56-125).

## 5.2 Análise do fracionamento por SPE do extrato EAE-CA

O extrato EAE-CA, apresentou rendimento de 0,36% m/m (1,4270 g). As frações FR1, FR2, FR3, FR4 e FR5 resultantes do fracionamento por SPE obtiveram as seguintes massas: 19,6 mg; 49,8 mg; 15,5 mg; 5,3 mg; 3, 2 mg, respectivamente. O perfil cromatográfico do extrato e das frações (FR1-FR5) evidenciaram que o fracionamento por SPE apresentou-se eficaz, as substâncias são eluidas em ordem decrescente de polaridade (mais polares, de polaridade intermediaria e menos polares), conforme expresso na **Figura 4**.

**Figura 4:** Cromatogramas do extrato EAE-CA e das frações FR1- FR5 obtidas por SPE, análise em 280 nm

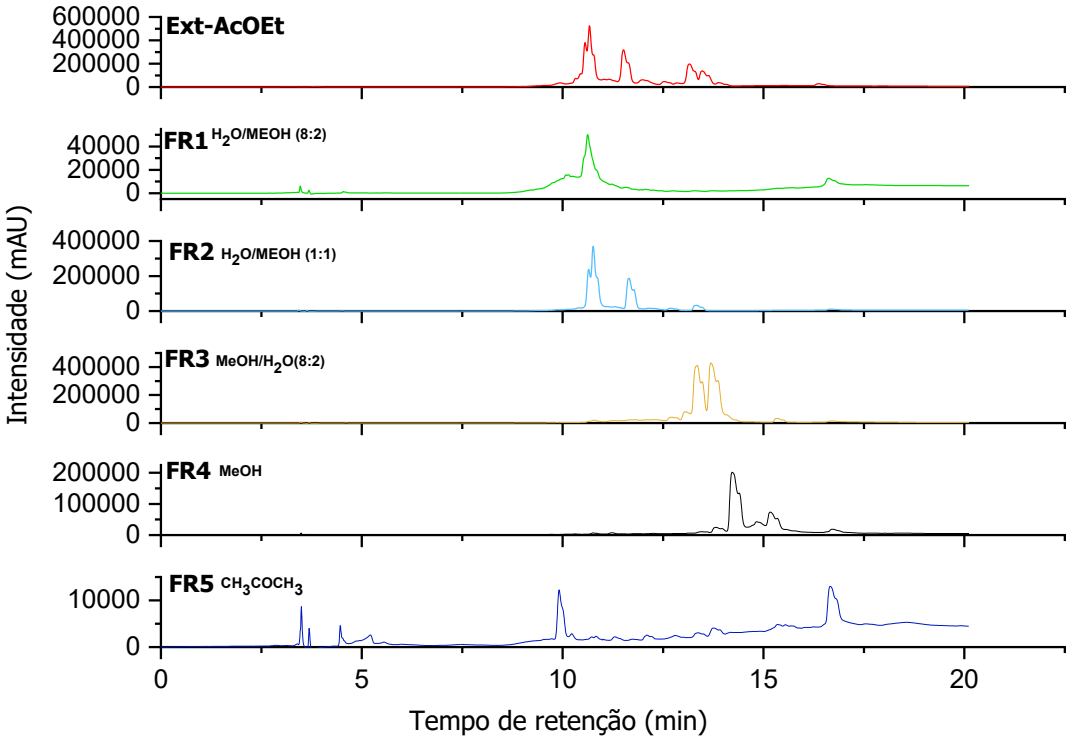


Fonte: Autoria própria.

## 5.3 Espectros de absorção na região do infravermelho do extrato EAE-CA, FR3 e FR4

Optou-se por obter os espectros na região do infravermelho apenas do extrato e das frações bioativas (FR3 e FR4), contra o fungo *Fusarium jinanense.* Assim, buscar as diferenças e semelhança espectral que corroborasse para justificar a atividade.

Os espectros de absorção na região do infravermelho (IV) do extrato EAE-CA**,** FR3 e FR4 (**Figura 5**), apresentam banda em 2926 $cm^{-1}$ que indica a vibração de estiramento relativo à presença de hidrogênio de carbono metilênico (-$CH_2$-). A banda em 1710 $cm^{-1}$ característica de carbonila cetônica. A banda de absorção em 1606 $cm^{-1}$ evidencia a deformação axial de ligação C-O e a região de 1500-750 $cm^{-1}$ (região de ligação C-O, C-N e C-C) há sobreposição de várias bandas dificulta a identificação. O extrato apresenta um declive próximo a 3250 $cm^{-1}$ que pode ser por conta da presença das hidroxilas de flavonoides glicosilados presentes no extrato. (SILVERSTEIN; WEBSTER; KIEMLE, 2007; PAVIA *et al.,* 2010).

**Figura 5:** Espectros de absorção na região do infravermelho das amostras EAE-CA, FR3 e FR4

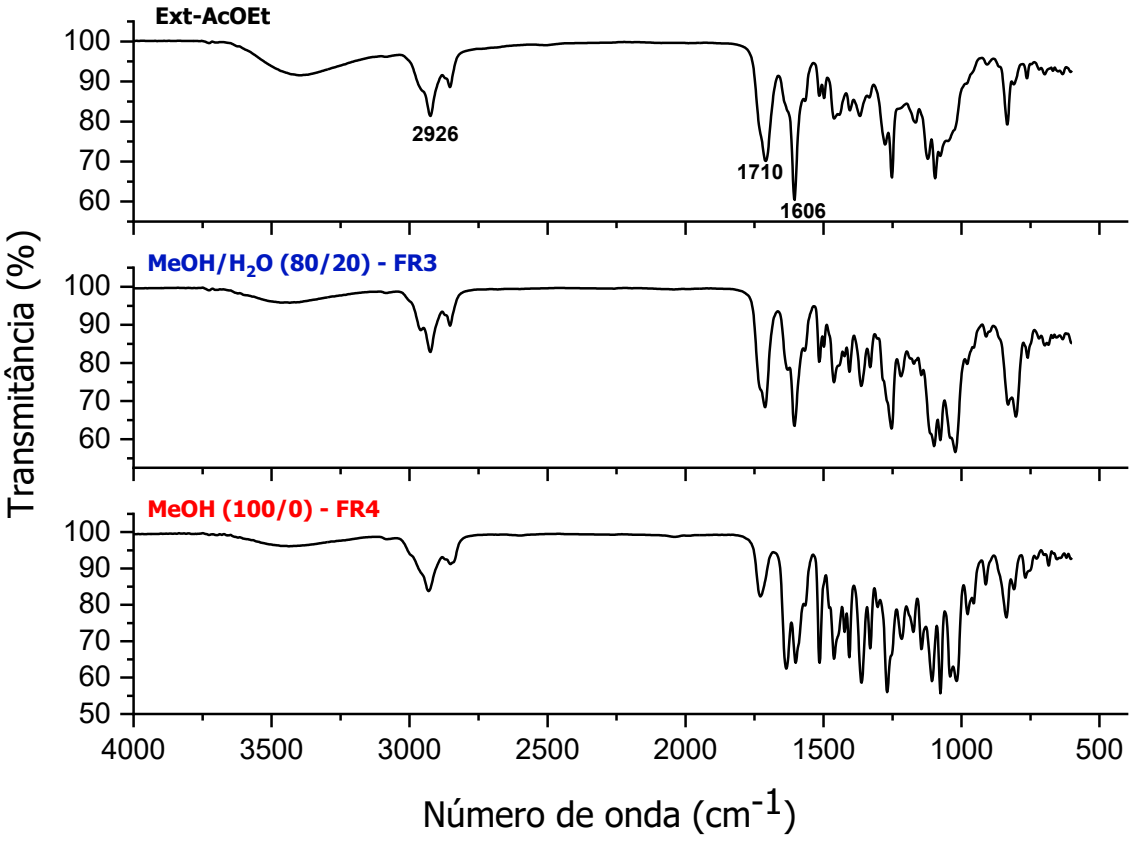


Fonte: Autoria própria.

## 5.4 Análise da atividade antioxidante pelo método de captura de radical DDPH nas amostras EAE-CA, FR1- FR5

Após o procedimento experimental descrito no item 4.4 (Pág. 21) os gráficos para cada amostra foram plotados no Excel, no eixo y os dados de porcentagem de inibição e concentração das amostras em mg/mL no eixo x, possibilitando a assim o cálculo da concentração inibitória a 50 % e 30% pela equação da reta, mostrados na **Tabela 1**.

Por definição o $CI_{50}$ é a concentração necessária para inibir 50% dos radicais livre formado em solução, enquanto o $CI_{30}$ é a concentração do composto antioxidante que diminui a concentração de radicais para 30%, então quanto menor for o $CI_{50}$ e $CI_{30}$, maior é o potencial de captura dessa amostra e por consequência maior a atividade antioxidante (PUTON *et al.,* 2018; JABEEN *et al.,* 2018).

**Tabela 1**: Dados de concentração inibitória a 50% e a 30 % de inibição do radical DPPH pelas amostras EAE-CA, FR1-FR5 e padrões positivos

| Amostras | $CI_{50}$ | DP (±) | $R^2$ (médio) | $CI_{30}$ | DP (±) |
|---|---|---|---|---|---|
| EAE-CA | 0,0602 | 0,0115 | 0,9713 | 0,0147 | 0,0097 |
| FR1 | 0,1952 | 0,0103 | 0,9867 | 0,086 | 0,0067 |
| FR2 | x | x | 0,9231 | 0,0914 | 0,0113 |
| FR3 | x | x | x | x | x |
| FR4 | x | x | x | x | x |
| FR5 | x | x | x | x | x |
| Ácido ascórbico* | 0,0032 | 0,0021 | 0,9796 | 0,0013 | 0,0003 |
| Trolox* | 0,0061 | 0,0001 | 0,9614 | 0,0016 | 0,0011 |

*Padrões positivos. [x] Frações que não apresentaram inibição significativa do radical DPPH.

Fonte: Autoria própria.

O extrato EAE-CA apresentou $CI_{50}$ cerca de dez vezes maior do que o padrão positivo Trolox (**Tabela 1)**, sendo um resultado moderado para esse ensaio, observou-se também que o fracionamento em extração em fase sólida (SPE) não favoreceu a atividade antioxidante, pois todas as frações tiveram uma porcentagem de inibição menor do que o extrato EAE-CA. Dessa forma, pode ser atribuir o potencial de inibição do extrato a interações sinérgicas entre as substâncias que foi modificada no fracionamento.

## 5.5 Manuscrito

O manuscrito foi escrito em inglês e submetido em revista Internacional de *Qualis* A1 conforme a classificação vigente da CAPES.

# Unraveling the antifungal composition of bitter orange decoction against melon pathogen *Fusarium jinanense*

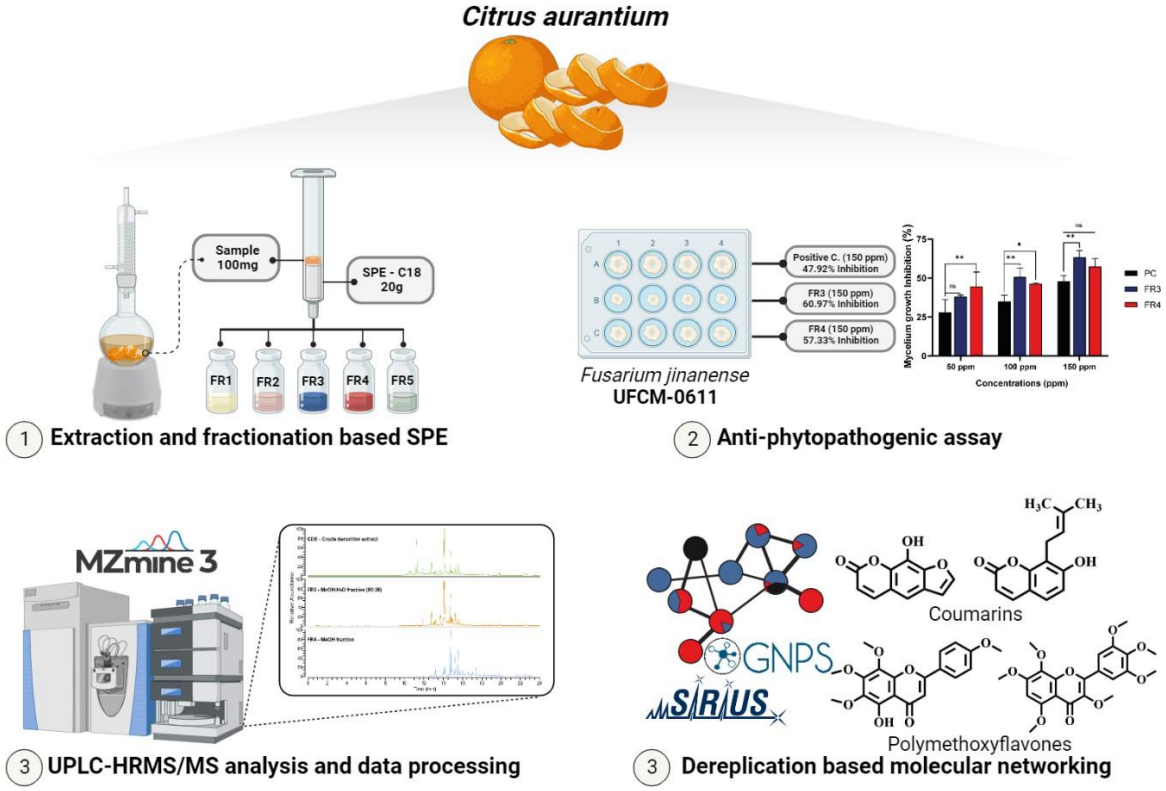

**Title: Unraveling the antifungal composition of bitter orange decoction against melon pathogen *Fusarium jinanense***

**Author(s):** Maria Daiane de Freitas [a,1], Rodolfo Dantas Lima Junior [b,1], Taicia Pacheco Fill [b], Francisco Erivaldo Freitas da Silva [a], Davila Zampieri[a], Cristiano Souza Lima [c], Eliane Mayumi Inokuti [c], Andréia Hansen Oster [d], Telma Leda Gomes de Lemos [a, *]

**Affiliation(s):**

[a] Departamento de Química Orgânica e Inorgânica, Universidade Federal do Ceará, Campus do Pici, 60021-940, Fortaleza, Ceará, Brasil.

[b] Instituto de Química, Universidade de Campinas, 13083-970, Campinas, SP, Brasil.

[c] Departamento de Fitotecnia, Universidade Federal do Ceará, Campus do Pici, 60440-554, Fortaleza, Ceará, Brasil.

[d] Empresa Brasileira de Pesquisa Agropecuária, Embrapa Uva e Vinho, 95701-008, Bento Gonçalves, Rio Grande do Sul, Brasil.

*Corresponding author: Telma Leda Gomes de Lemos, Departamento de Química Orgânica e Inorgânica, Universidade Federal do Ceará, Campus do Pici, 60021-940, Fortaleza, Ceará, Brasil.

E-mail: tlemos@dqoi.ufc.br

[1]The authors equally contribut

**Abstract**

Bitter orange (*Citrus aurantium*) is an important source of essential oils with high antimicrobial activities, however the composition and antifungal potential of the decoction peels is little explored. This study assessed the peel decoction's chemical profile at the secondary metabolism level and its antifungal activity against the melon phytopathogen *Fusarium jinanense*. The decoction's antifungal potential was investigated using a bioassay-guided fractionation approach based on Solid-Phase Extraction (SPE) and LC-HRMS/MS analysis. Coumarins and flavones were the most abundant classes of compounds in the high-value fractions responsible for up to 61% of the mycelial inhibition of *F. jinanense*. Overall, this study has presented for the first time the chemical composition, the antifungal potential of the decoction of *C. aurantium* peels and the compounds associated with these results. This strategy can guide the exploration of under-explored food sources and add value to compounds or fractions enriched with bioactive compounds.

**Keywords:** *Citrus aurantium*; phenolic compounds; molecular networking; SIRIUS; anti-phytopathogenic activity; fusarium rot melon.

# 1 Introduction

The citrus industry is essential to Brazil's fruit industry, with 137.5 million tonnes of citrus exported in 2019, including lemons, limes, oranges, pomelos, and tangerines (FAO, 2020). In 2021, Brazil exported 3.5 thousand tonnes of fresh oranges and 22.5 million t of orange juice, produced mainly by São Paulo, Minas Gerais, and Paraná states. These numbers figures position the country as the world's leading producer of fresh oranges and the world's largest exporter of orange juice, ahead of countries such as the United States and China (Kist et al., 2022).

Among the varieties of orange species, *Citrus aurantium* L., typically known as bitter orange or sour orange, is a Southeast Asia native species that belongs to the Geraniales order and the Rutaceae family (Degirmenci & Erkurt, 2020). Although the fruit has a bitter pulp and is not commonly used for juices, it has a variety of applications, including obtaining essential oils, and food supplements (Onakpoya et al., 2011; Deterre et al., 2014; Oulebsir et al., 2022).

Literature reports the antimicrobial action of *C. aurantium* essential oil against different microorganisms, including phytopathogenic fungi of important crops, such as *Aspergillus flavus*, *Aspergillus niger*, *Aspergillus terreus*, and *Fusarium culmorum* (Abo Elgat et al., 2020). In addition, Perczak et al. (2019) and Okwu et al., 2007 verified the antifungal potential of *C. aurantium* essential oil against strains of the *Fusarium* genus (*Fusarium graminearum*, *Fusarium culmorum,* and *Fusarium oxysporum*).

Fungi of the *Fusarium* genus are associated with plant diseases of various tropical fruit crops such as avocado, banana, mango, pineapple, and yellow melon (Zakaria, 2023). The yellow melon (*Cucumis melo*) is one of the most economically important crops worldwide. According to the FAO, in 2021, Brazil produced 607,000 t of melons and exported 257,000 t of fruit, which corresponded to 165,000 dollars. The primary melon production in Brazil is concentrated in the Vale do Rio São Francisco region, which accounts for around 95% of the Brazilian production, with the State of Rio Grande do Norte as the leading producer (Kist et al., 2022; IBGE, 2023; Medeiros Araújo et al., 2021). However, in Brazil, pathogens of the *Fusarium* genus are responsible for significant losses in melon production. New fungal species from the *Fusarium incarnatum-equiseti* species complex (FIESC) have now been discovered, such as *Fusarium jinanense* for Han, Wang & Cai, capable of causing fruit rot that can compromise production in the post-harvest stage (Lima et al., 2021; Han et al., 2023).

Despite the variety of applications of *C. aurantium* as a source of bioactive compounds against fungi of the Fusarium genus, to date, no studies have been focused on the chemical composition and the antifungal potential of the decoction obtained from the peel of the fruit against phytopathogens of this genus. Thus, here we integrated a bioguided fractionation strategy based on solid-phase extraction with high-performance platforms such as liquid chromatography coupled with mass spectrometry and analysis by Feature-Based Molecular Networking (FBMN) to add value to this little-exploited by-product and, above all, to identify, using a Global Natural Product Social Molecular Networking (GNPS) repository and SIRIUS software, which compounds are involved in the antifungal potential against *Fusarium jinanense*, the causal agent of yellow melon rot.

## 2 Materials and methods

### *2.1 Reagents and materials*

Ethyl acetate (EtAc) and methanol (MeOH) were purchased from Synth (Diadema, Brazil), while acetone (HPLC-grade) was obtained from Tedia Company (Fairfield, USA). HPLC-MS-grades solvents (methanol and acetonitrile (ACN)) and formic acid were used while ultrapure water (18 MΩ cm at 23 °C) was prepared using a Milli-Q purification system (Merck Millipore; Burlington, MA, USA). Potato dextrose agar (PDA) was purchased from KASVI$^{TM}$ (São José do Pinhais, Brazil). Antifungal Cercobin® 875 WG was purchased from Iharabras S.A. (Indústrias Químicas, Sorocaba, Brazil). PTFE (0.22 μm) membrane syringe filters (Millipore) were bought from Merck Millipore Co., Ltd. (Cork, Ireland). The chromatography column (C18) was obtained from Bruker Daltonics (Bruker, Bremen, Germany). The standards naringin, hesperidin, and hesperitin were purchased from Sigma Aldrich (St. Louis, MO, USA).

### *2.2 Citrus sample and preparation of the crude extract*

Specimens of *C. aurantium* fruits were collected at the Department of Plant Sciences of the Federal University of Ceará (UFC), with the following coordinates (3.7406° S, 38.5764° W), Campus do Pici in Fortaleza, Ceará, on the 26th September 2019 at 3:45 pm. The exsiccates are deposited in the Prisco Bezerra Herbarium under number 50434.

Twelve oranges were collected and properly rinsed with deionized water. The

orange peels were separated into flavedo and albedo fractions using a vegetable peeler. This resulted in 398 g of flavedo, which was decocted with 3 liters of distilled water and refluxed for 3 hours. Subsequently, the *C. aurantium* peels were subjected to decoction using 3 liters of distilled water and kept under reflux for 3 hours. Subsequently, a simple filtration was carried out, and the decoction obtained was partitioned with ethyl acetate, where for every 100 mL of the aqueous fraction, 100 mL of solvent was used three times. The partitions were concentrated under reduced pressure in a rotary evaporator with a bath temperature of 40 ºC.

### *2.3 Fractionation-based SPE*

The crude decoction extract (CDE) was fractionated through the solid phase extraction process using a cartridge (Strata$^{TM}$ C18, 20g/60 mL, 55µm, 70 Å) supplied by Phenomenex (Torrance, CA, U.S.A). The cartridge was previously activated using 10 mL of MeOH and adjusted with 10 mL of $H_2O$/MeOH (80:20, v/v) as already described in the literature (Nair & Clarke, 2016). Then, 100 mg of the extract was subjected to chromatography, using 150 mL of eluent per fraction $H_2O$/MeOH (80:20; 50:50; 20:80; 0:100) and $CH_3COCH_3$ (100), resulting in five fractions that they were named FR1, FR2, FR3, FR4, and FR5, respectively. The CDE and fractions samples were subjected to antifungal assay against the phytopathogen *F. jinanense* (UFCM-0611).

### *2.4 Fungal isolate*

The isolate UFCM-0611 of *F. jinanense* (isolate 41 or LPPC072 in Lima et al., 2021) was obtained in the 2015's growing season from yellow melon fruit showing typical symptoms of fusarium rot in Maracanaú city in Ceará State, Brazil. Specie identification and pathogenicity assay were carried out according to the methodology described by Lima et al. (2021) and Han et al. (2023). The isolate (UFCM-0611) is maintained at the Federal University of Ceará Mycological Collection (UFCM), Department of Plant Sciences, Fortaleza, Ceará, Brazil.

### *2.5 Antifungal assays of the extract and fractions*

The *in vitro* antifungal assay of the CDE and fractions FR1-FR5 against *F. jinanense* (UFCM-0611) was performed using a potato dextrose agar (PDA) culture medium. The PDA

was sterilized in an autoclave at 101 KPa (120 °C) for 15 min. Subsequently, the extract and fractions were solubilized separately in methanol (100 µL) and added to molten (45 °C) PDA medium at three concentrations: 50, 100, and 150 ppm. The commercial fungicide Cercobin (active ingredient: methyl thiophanate) was used as a positive control. For this, the fungicide was dissolved in sterilized distilled water. Then, serial dilutions were performed to obtain thiophanate methyl solutions at three concentrations (50, 100 and 150 ppm). Mycelial plugs (3 mm in diameter) were removed from the margins of a four-day-old culture of UFCM-0611 and transferred to the center of the wells in the plates amended with the different concentrations of the crude extract and fungicide used as positive control. Wells on the plates containing only PDA and mycelial plugs (3 mm in diameter) were used as a negative control.

All treatments were performed using technical replicates in triplicate. Tests were also conducted using only methanol as negative control. After a 25h incubation period at 25 °C and under a 12h photoperiod, the diameter of the colonies was measured, and the mean of two perpendicular mycelial-growth diameters for each replicate was calculated. The original diameter of the mycelial plug (3 mm) was subtracted from this measurement. The percentage of inhibition of radial mycelial growth (% IR) related to the negative control was calculated for all the tested concentrations. The rate of radial growth (IR) was determined according to Simionato et al., (2017) using the formula below.

$$\% IR = \frac{Dc - Dt}{Dc} x\ 100$$

Where Dc = average diameter of the fungal mycelial of the negative control (methanol), Dt = average diameter of the fungal mycelial treated with the extracts or the positive control. Only the fractions that showed promising results in the antifungal test and the CDE were analyzed by LC-MS/MS.

*2.6 UHPLC-MS/MS Analysis and Data Processing*

Samples of the CDE and fractions FR3 and FR4 were weighed (1.0 mg), solubilized in 1.0 mL of MeOH (HPLC grade), and filtered through a PTFE 0.22µm filter. UHPLC-MS/MS data were obtained using a Thermo Fisher RSLCnano U3000 UHPLC instrument coupled with a Q-Exactive Orbitrap-MS spectrometer (Thermo Fisher Scientific, Waltham, MA, USA) equipped with a heated electrospray ionization (HESI) source. The chromatographic elution was performed using Intensity Solo C18 (Bruker Daltonics, Bremen, Germany) with the

following specifications: 100 mm x 2.1 mm, 2.2 mm particle size. The mobile phase flow was maintained at 250 µL/min at 40 °C. A mixture of $H_2O$ (A) and MeCN (B), both acidified with 0.1% formic acid, was used as a mobile phase. The elution gradient for the positive and negative modes consisted of 5% B (0-5 min), 5-40% B (5-10 min), 40-45% B (10-12 min), 45-98% B (12-18 min), 98% B (18-20 min), 98-5% B (20-22 min) and 5% B (22-24 min).

The samples were analyzed in Full-scan mode and DDA (data-dependent acquisition) mode with a range of *m/z* 100-1500 Da. Ionization was carried out in positive and negative ionization modes, with the following parameters: auxiliary gas flow, 10 (arbitrary unit); spray voltage +3.5 kV (positive mode) and -3.2 kV (negative mode); capillary temperature of 300 °C, equipment resolution of 70,000 (200 *m/z*). MS/MS data were acquired by selecting five precursors per cycle and normalized collision energy (NCE) of 30 eV. The Q-Exactive Orbitrap-MS was operated using the Xcalibur 3.0 software (Thermo Fisher Scientific, Waltham, MA, USA).

Next to the positive mode ionization analysis, the raw data files (.raw) were converted to .mzXML format using MSConvert (ProteoWizard, Palo Alto, CA, USA) (Adusumilli & Mallick, 2017). After that, the files (.mzXML) were submitted for processing by MZmine (version 2.53) (Pluskal, et al., 2010) using feature detection, chromatogram builder, chromatogram deconvolution, isotope grouping, alignment, and filtering. The values for these parameters can be consulted in the supplementary material (**Supplementary Table 1**). After processing, files containing a quantification table of the detected features (.csv) were exported, as well as a file (.mgf) containing the MS/MS data information associated with the precursor ions (MS). The files were submitted for analysis on the Global Natural Products Social Molecular Networking (GNPS) platform (https://gnps.ucsd.edu) to annotate the features belonging to the samples and obtain molecular networks based on the similarity of the fragmentation profile of the features.

### *2.7 Feature-Based Molecular Networking Analysis and Metabolite Annotation*

To evaluate the chemical composition of the crude extract and fraction samples, the processed UHPLC-MS/MS data (.csv and .mgf) from MZmine 2.53, together with a metadata table containing the main characteristics of the samples (.tsv), were processed for molecular networking creation based on Feature-Based Molecular Networking (FBMN) workflow on the GNPS platform (Nothias et al., 2020). The parameters are present in (**Supplementary Table**

**2**). The FBMN job on GNPS can be found at https://gnps.ucsd.edu/ProteoSAFe/status.jsp?task=f336f310b7314351bdacdfc7a2288a11.

The molecular network obtained was visualized using the Cytoscape software (version 3.7.2, Cytoscape Consortium, San Diego, CA, United States) (Shannon et al., 2003), where each node corresponds to ion features of specific *m/z* ratio and retention time. The edges represent the similarity cosine scores calculated between the nodes based on the fragmentation spectra (MS/MS). The node size was scaled proportionally to the relative sum of the peak areas obtained in the samples where the feature was detected. The edge width was adjusted proportionally to the cosine of the similarity between the nodes, which ranged from 0.7 to 1.0. The nodes were represented in the network as a pie chart, where the colors were associated with sample groups: crude decoction extract (CDE), fraction 3 (FR3), and fraction (FR4).

The annotation of the compounds was performed according to the annotation levels reported by Metabolomics Standards Initiative (MSI) (Fiehn et al., 2007; Sumner et al., 2007), using the GNPS library and a manual curation from the comparison of the mass accuracy with a mass tolerance of 5 ppm for MS1 and characteristic fragments (MS/MS). Manual dereplication was performed using reference spectral data of substances produced in *C. aurantium* species and already reported in the ACS publication, Google Scholar, SciELO, ScienceDirect, Springer, Web of Science, Massbank and Pubchem. The data obtained were compared with precursor mass ions (MS1) and the mass fragments ions (MS/MS) contained in the CDE, FR3, and FR4 samples. The molecular formula of the ion fragments was predicted using the "elementary composition" provided by the Xcalibur 3.0 software (Thermo Fisher Scientific, Waltham, MA, USA), considering an error of ± 5 ppm for positive and negative modes.

The SIRIUS software (version 4.0.1) (Dührkop et al., 2019) was used to explore possible chemical structures of substances corresponding to the obtained features and the prediction of molecular formulas associated with these features. The structure propagation of the compounds occurred from comparing the isotopic distribution of the precursor ions and *in silico* prediction of the molecular formulas and fragments acquired in the LC-MS/MS analysis with a library of experimental and *in silico* data. The molecular formula prediction by ZODIAC, molecular structure prediction based on CSI:FingerID, and, finally, chemical class evaluation by CANOPUS were used for this data set. The parameters used to predict the formula took into account the possible adducts associated with the feature ($[M+H]^+$, $[M+H-H_2O]^+$, $[M+Na]^+$, and $[M+K]^+$), the analyzer used (Orbitrap), the maximum error in ppm (5 ppm), and the association

of features with molecular formulas present in databases (Bio database).

## 3 Results and discussion

### *3.1 SPE fractionation of Citrus aurantium peels decoction revealed a potent inhibition of Fusarium jinanense*

After obtaining 1.4270 g of crude decoction extract (CDE) (yield 0.36%, w/w), 100 mg of the CDE was subjected to the SPE fractionation method where five fractions were obtained: FR1 (19.6 mg), FR2 (49.8 mg), FR3 (15.5 mg), FR4 (5.3 mg) and FR5 (3.2 mg). In order to select the fractions with the highest antifungal activity against *F. jinanense* (UFCM-0611), the mycelial inhibition potential of each fraction was compared with the positive control containing the active ingredient methyl thiophanate. Methyl thiophanate is currently used as a synthetic fungicide (Cercobin®) to control fungal diseases in yellow melon.

The antifungal microdilution plate assay showed potent inhibition of the mycelial growth of the pathogenic fungus for fractions 3 and 4 compared to the positive control in a concentration range of 100 - 150 ppm. Compared to the inhibition values obtained for the crude extract in the same concentration range tested, it was possible to observe an increased antifungal effect after fractionation. Tests performed at 100 ppm showed inhibition of 51% (FR3) and 46% (FR4) compared to 42% for crude extract under the same conditions. At a concentration of 150 ppm, the activity of fraction 3 (MeOH:$H_2O$ fraction (80:20)) and fraction 4 (MeOH fraction) was higher than that of crude extract, reaching 61% (FR3) and 57% (FR4), respectively, in comparison with 50% for crude extract. Compared to the inhibition values obtained for the positive control at 100 ppm (35%) and 150 ppm (48%), fractions 3 and 4 showed higher results of 51% and 46%, respectively. **Figure 1** illustrates the results presented and outlines the clear statistically significant difference in antifungal activity between the extract and the active fractions at different concentrations compared to the positive control under the same conditions. Graphs showing the inhibition percentage of all fractions tested are provided in the supplementary material **(Supplementary Figure 1)**. Based on these results, samples of the crude extract and fractions 3 and 4 were then selected for analysis by UHPLC-MS/MS to verify the variation in chemical composition after fractionation and thus be able to associate the bioactivity observed with the active compounds present in each fraction.

**Figure 1:** Crude decoction extract (CDE) and fractions of *Citrus aurantium* peels showed potent dose-dependent inhibition of mycelial growth of *Fusarium jinanense*. **A.** Antifungal microdilution plate assay at concentrations of 50, 100, and 150 ppm for the CDE, fraction 3 (FR3), fraction 4 (FR4), and the positive control (PC) methyl thiophanate. The dashed black line emphasizes the level of mycelial growth inhibition for positive control. **B.** Inhibition potential of mycelial growth of *F. jinanense* using the most active fractions (FR3 and FR4) compared to the positive control at different concentrations (50, 100, and 150 ppm). Statistical analysis: ANOVA was performed with post-hoc Tukey's multiple comparisons tests. *, ** and ns = statistically significant differences with $p < 0.05$, $p < 0.005$, and no significant, respectively. **C** and **D.** Photos of the microdilution plate assay after 72h

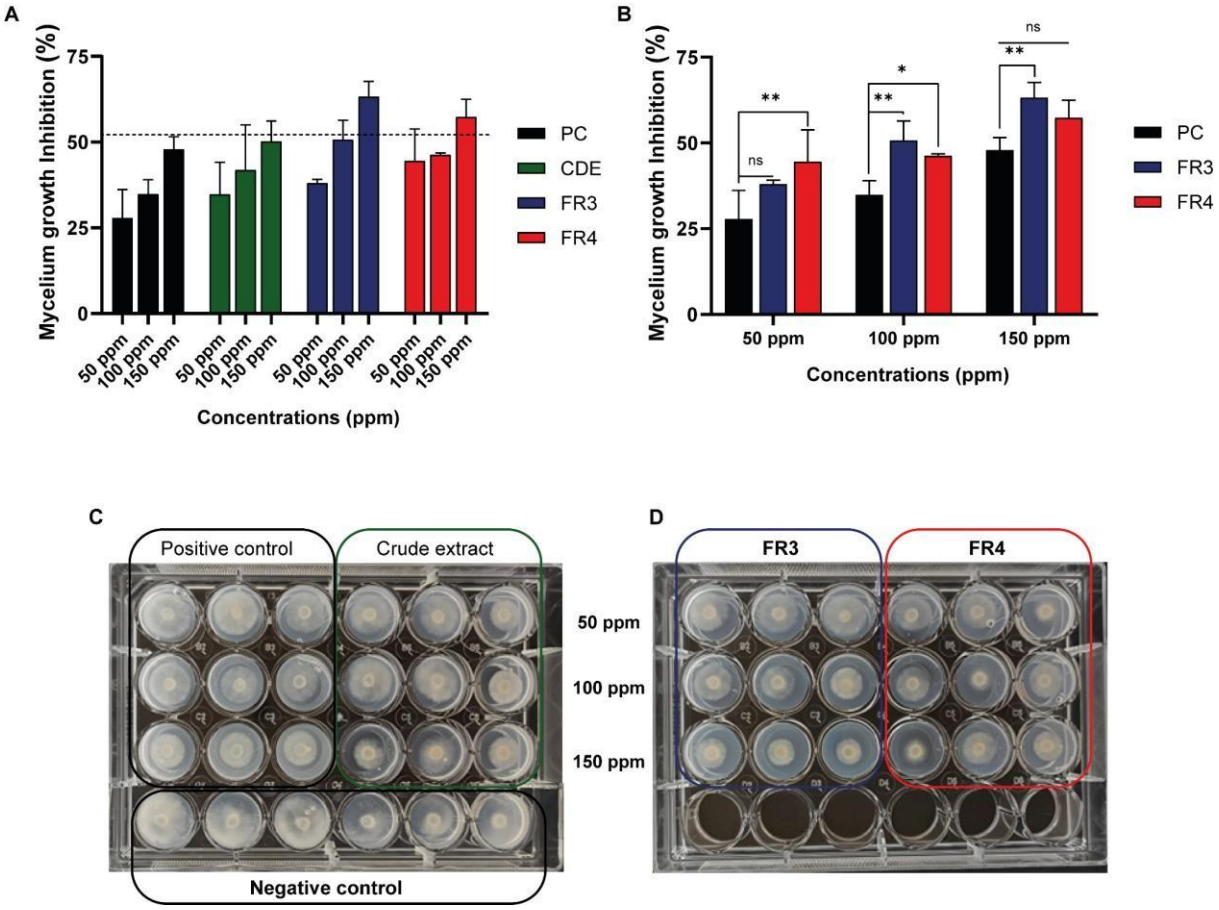


Source: Author's own.

## *3.2 Active fractions and crude extract chemical profiles*

From the UHPLC-MS/MS analyses of the active fractions and the CDE, it was possible to observe the separation capacity, pre-concentration, differentiation of the chemical profile, and composition of the samples after fractionation by SPE from 100 mg of the crude extract. The chromatograms in positive ionization mode presented in **Figure 2** show the success

of the fractionation based on the evident differentiation of the relative abundances associated with the secondary metabolites present at different retention times.

**Figure 2:** Chemical profile through base peak chromatograms (BPCs) obtained from crude decoction extract (CDE) and active fractions (FR3 and FR4) from *Citrus aurantium* L. in positive ionization mode. BPCs from the ethyl acetate CDE are shown on the top (green), and those of the active fractions 3 and 4 obtained from proportions MeOH:H2O (80:20) and MeOH (100%) are shown in orange and blue, respectively

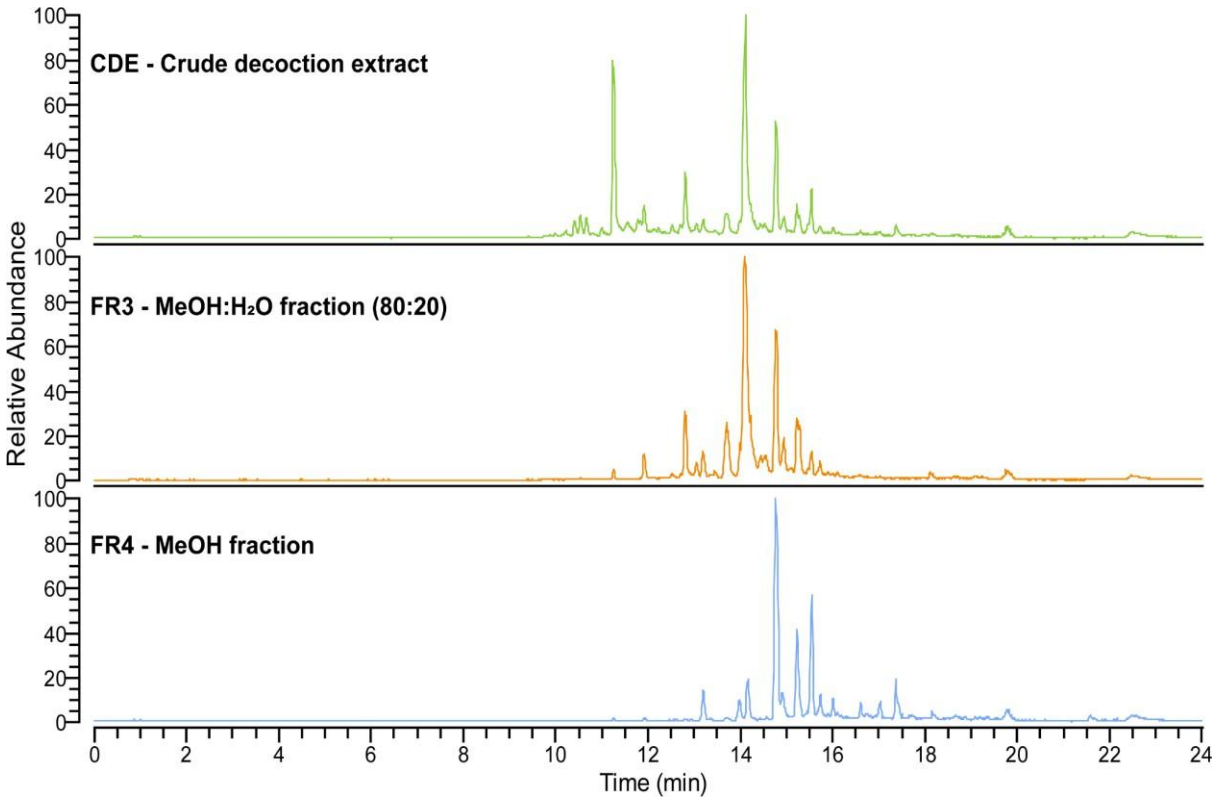


Source: Author's own.

This pattern is highlighted in the base peak chromatograms (BPC) of FR3, where it was possible to see a decrease in the abundance of the metabolites present in the 10-12 min range compared to the crude extract. For fraction 4, eluted with 100% methanol, there was a decrease in the relative abundance of the secondary metabolites previously present between 13-14.5 min in FR3. The variation in relative abundances throughout the fractionation shows important physicochemical characteristics about the nature of the compounds involved in the antifungal activity observed for these fractions, such as intermediate polarity, which is directly related to the molecular structure of the secondary metabolites analyzed, and affinity with the long carbon chains contained in the stationary phase of the SPE cartridge (C18).

To summarize, the increase in antifungal activity against *F. jinanense* observed in

fractions 3 and 4 is directly related to the contribution of the SPE fractionation, which reduces the complexity of the chemical composition of the starting samples and the consequent preconcentration of compounds with intermediate polarity, compared to the distribution of these compounds in the crude extract.

The molecular networks obtained from the FBMN workflow for the positive ionization mode were analyzed to better understand the composition of the crude extract and the active fractions and to point out which compounds may be involved in the antifungal activity based on the distribution of these metabolites after fractionation. The molecular network was generated with 605 precursor ions and their respective fragmentation spectra, responsible for forming 48 spectral families (clusters) and 348 self-loops nodes (**Supplementary Figure 2**). Comparison of the MS/MS spectra of these nodes with the GNPS spectral library generated 50 spectral matches for the positive mode, corresponding to 8.26% of the total nodes that comprise the entire molecular network. All fragmentation spectra associated with a spectral match to the GNPS library were evaluated for annotation at confidence level 2 (Schymanski et al., 2014), and manual curation of the spectra was performed according to previous literature for this citrus cultivar. The GNPS library's annotations of features with secondary metabolite matches that still need to be reported for the species were considered level 3 annotations (Schymanski et al., 2014). The annotated metabolites are listed in **Table 1**, and their spectral matches are in the **Supplemental Material**.

*3.3 Putative annotation and identification of compounds by UHPLC-MS/MS from Citrus aurantium peels with potential antifungal activity*

LC-MS/MS analysis of the ethyl acetate extract of the decoction and active fractions allowed the annotation of 57 compounds in the positive ionization mode and eight in the negative mode with confidence levels 1, 2 and 3 (**Supplementary Table 3**). The annotation matches of the compounds from the GNPS library indicated the presence of different classes of substances including flavonoids, limonoids, coumarins, terpenes, aromatic compounds, and nitrogen compounds. Among the annotated compounds, 36 are flavonoids belonging to the flavone, flavanone, and flavonol subclasses; 17 were classified as coumarins, and the remaining 12 compounds are distributed among the other classes, as shown in **Table 1** and **Supplementary Table 3**. In addition to the annotation based on the similarity of fragmentation patterns obtained by tandem mass spectrometry (MS/MS) analysis using the GNPS library, the

chemical structures of 23 compounds from the flavonoid (12) and coumarin (11) classes were proposed from the annotation propagation based on GNPS annotations, the construction of the molecular network and the construction of fragmentation trees using the CSI:Finger ID module of the SIRIUS software (**Supplementary Table 4 and 5**). This tool uses a pipeline based on constructing fragmentation trees from MS/MS spectra of a training dataset to construct fingerprints (molecular properties), as well as constructing fragmentation trees and fingerprints from the experimental dataset. Finally, the similarity of the fingerprints of the compounds to be identified (experimental) is searched against fingerprints from databases such as PubChem, with the aim of predicting different structures with a high similarity index through the confidence score (Dührkop et al., 2019). All the structural proposals provided by the SIRIUS software were based only on nodes present in molecular networks containing level 2 annotations obtained from the GNPS spectral library. This strategy allowed to gain insights concerning the chemical composition of the active fractions based on the fragmentation trees proposed for each compound.

### *3.3.1 Flavones, flavanones, and flavonols*

Several molecular families and self-loops related to the flavonoid class were obtained, including flavonoids *O*-glycosylated of the flavanones, flavones, and flavonols subclasses, which can be observed by the several green coloring nodes in the molecular network **(Figure 3**).

From the analysis of the molecular network and manual curation, it was possible to observe the presence of a greater abundance of *O*-glycosylated flavonoids (compounds 3, 6, 8, 10, 11, 12, 13, 16, 17, 19, 21 and 22 (**Table 1**)), and compounds 3N, 4N, 5N and 6N (**Supplementary Table 3**) in nodes corresponding to the CDE sample, indicating that after fractionation by SPE these compounds remained in the initial fractions containing more aqueous character (FR1 and FR2) than when compared to the final fractions with more organic character (FR3 and FR4).

**Figure 3:** Molecular families of flavonoids from the Feature-Based Molecular Networking workflow and annotation based on spectral matches in the public spectral libraries on the GNPS (black arrow) and SIRIUS (blue arrow). The pie chart legend shows that the different nodes' colors represent the sample groups (CDE, FR3, and FR4). Each node represents a mass spectrometry spectrum (MS/MS), and width edges represent MS/MS fragmentation similarity as a cosine score range between 0.7 (less thick) and 1.0 (thicker). The black diamond shape of some nodes represents the hits obtained by the GNPS spectral library, and the node size is proportional to a sum precursor intensity of features area in MS1 scans. The acronym CI (cluster index), followed by the values of the nodes found in the molecular network, refers to putative structural proposals based on the SIRIUS software

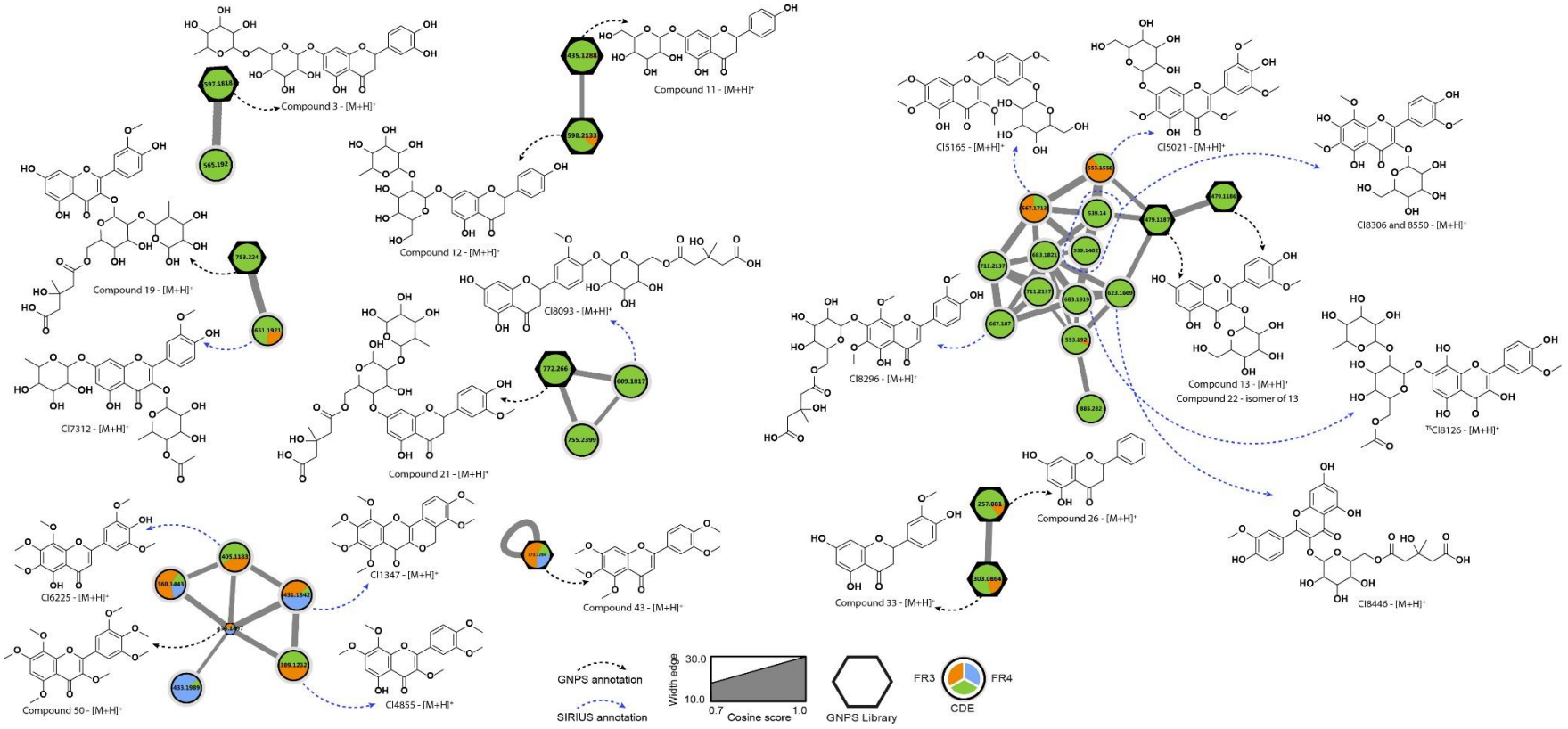


Source: Author's own.

Glycosylated flavonoids are highly polar compounds containing mono- or disaccharides modified or not by other substituents, which do not favor interaction with the C-18 stationary phase used in SPE, thus facilitating rapid elution with a predominantly aqueous mobile phase gradient.

The typical fragmentation of these protonated molecules involves the sugar moiety loss, as shown in the tandem mass spectra (MS/MS) (**Supplementary Figure 6, 9, 13, 17, 19, 21, 22, 25, 28, 29, 31, 33, 34, 75, 76, 77, 78, 79 and 80**).

In *O*-glycosylated flavonoids, there is the presence of a C-O bond connected to different sugars, which appears in the MS/MS spectra on electrospray ionization as characteristic neutral losses, such as 146 Da for a rhamnoside, *m/z* 162 for a glucoside and *m/z* 308 for a neohesperidoside losses (see **Supplementary Material**). The aglycone structure of flavonoids showed characteristic fragments (**Figure 4**), such as $^{1,3}A^+$ (153 Da) and $^{1,3}B^+$, whose mechanism is *retro*-Diels-Alder type. It can be observed in flavones, flavanones, and flavonols. Other fragments present in the spectra were $^{0,2}A^+$, $^{0,2}B^+$, $^{0,3}B^+$, and $^{1,4}B^+$ formed from cleavages in the aglycone skeleton (Ma et al., 1997).

**Figure 4:** Structure of flavonoid subclasses and the main fragmentations observed in MS/MS spectra.

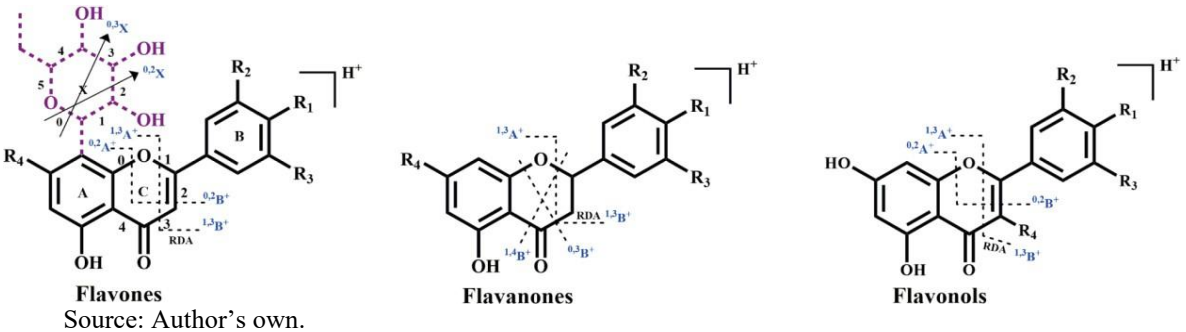


Source: Author's own.

The *C*-glycosylated flavonoids joined by a C-C bond, such as compounds 18, 1N, and 2N (**Table 1** and **Supplementary Table 3**), showed the base peak referring to the $^{0,2}X^+$ fragment at *m/z* 120. The presence of 90 Da fragments corresponding to the $^{0,3}X^+$ ion is also notable; these are fragments of part of the glycone, whose mechanism is cross-cleavage (Cuyckens & Claeys, 2004), as shown in **Figure 4**.

All the flavonoids annotated by the GNPS library showed excellent spectral match, and two of them were annotated as gold annotation by the GNPS library (flavonoids 12 and 21). This classification brings greater robustness to the annotation since a gold annotation is understood to present a higher level of spectral quality within the database, as it matches

experimental spectra with spectra of pure substances of synthetic or isolated origins with complete structural characterization. In addition to the annotations classified as gold, some compounds present in the fractions were identified as level 1 by comparison with analytical standards, such as naringin (6), hesperidin (16) and hesperitin (34), founds in greater abundance in FR3 compared to FR4 (spectra are available in **Supplementary Figure 10**, **Supplementary Figure 26** and **Supplementary Figure 48**).

The **Figure 3** also shows the presence of flavonoids containing a methoxyl and a sugar unit in the same structure, such as compounds 13 and 22, within the more prominent molecular family of flavonoids. Since these compounds have not yet been reported for the species, even though they are annotated by the GNPS spectral library, they were considered as level 3 annotations. From the annotation of these two compounds, it was possible to perform a structural propagation through the CSI:Finger ID module contained in SIRIUS. As a result, the putative structure of polymethoxylated flavonoids CI5165 and CI5020 was observed in nodes directly linked to compounds 13 and 22, which are present in greater abundance in fraction 3 when compared to CDE. This result reinforces that the compounds' presence in the fractions is due to their interaction with the mobile phase and stationary phase during SPE fractionation.

The partial absence of *O*-glycosylated flavonoids in fractions 3 and 4 (**Supplementary Figure 106**) makes it possible to infer that they do not actively participate in the antifungal activity observed for these fractions and that other compounds, such as polymethoxyflavones, may be associated with the bioactivity, as will be discussed below. From this perspective, the presence of flavones belonging to the polymethoxyflavone subclass was also noted, and these were more abundant in the active fractions. As illustrated in **Figure 3**, it is possible to observe a molecular family containing a node referring to compound 50 and three other polymethoxyflavones (CI4855, CI1347 and CI6225) employing structural propagation using the SIRIUS software. The spectral match obtained for compound 50 and the fragmentation trees for the structures obtained by structural propagation is in the supplementary material in **Supplementary Figure 67** and **Supplementary Figure 94**, **Supplementary Figure 93** and **Supplementary Figure 92**.

The annotated polymethoxyflavones (32, 38, 41, 42, 43, 44, 48, 49, 50, and 57) showed a similar spectral pattern, with the most intense peaks corresponding to the protonated molecule $[M+H]^+$ and the loss of the $2CH_3$ fragments associated with the adult $[M+H-(2CH_3)]^+$, at *m/z* 30. Between the two most abundant signals, this subclass showed a low-intensity peak equivalent to the loss of $CH_3$ (15 Da) expressed in the fragmentation spectra (Wang et al., 2021). (see **Supplementary Figure 45**, **55**, **58**, **59**, **60**, **61**, **65**, **66**, **67** and **74**).

The literature reports the antifungal activity of flavonoids of the flavanone subclass, such as eriodictiol (2), naringenin (9), and hesperitin (34), against fungi of the genus *Aspergillus*, *Candida*, and *Fusarium* (Al Aboody & Mickymaray, 2020). In consensus, Förster et al. (2022) investigated the activity of naringenin (9) and its *O*-methylated tautomers against two fungal species, *Fusarium graminearum*, and *Fusarium verticillioides*, and ultimately confirmed the antifungal potential of these phenolic compounds.

Among the 36 flavonoids that were annotated in this work, 10 of them are polymethoxyflavones (PMFs), which include tangeritin (57), nobiletin (48), 5-demethylnobiletin (32) and sinensetin (43). These compounds were previously found to be present in the peel of *Citrus reticulata Blanco* and showed inhibition against *Aspergillus niger*. The authors reported a minimum inhibitory concentration (MIC) of 1.5 mg/mL for tangeritin, a value close to that found for the alcoholic extract of *C. reticulata Blanco* bark. The explanation for the antifungal effects of polymethoxyflavones includes altering the permeability of the cytomembrane, causing fragility in the cell walls, and inhibiting chitin synthase, so they are considered natural antifungals that can be widely applied in the food industry (Wu et al., 2014).

*Citrus* species are known to have high levels of different classes of flavonoids in the composition of their peels, and several studies have reported that the fruit uses these compounds as a defense strategy against phytopathogenic fungi (Ortuño et al., 2011). Studies have shown that the fruit uses defense strategies through the accumulation of flavones (hesperidin, 16) and polymethoxyflavones (nobiletin, 48; heptametoxyflavone, 50, and tangeritin, 57) during infection by pathogenic fungi, such as *Penicillium digitatum* (Ortuño et al., 2006). This evidence reiterates that using these compounds, or products enriched with these compounds, can promote a fungicidal action against pathogens of different genera and species.

### *3.3.2 Coumarins*

The two largest networks generated (**Figure 5A and B**) showed library matches predominantly with coumarins. These compounds were also widely distributed in fractions 3 and 4 (orange and blue nodes) after fractionation, thus being associated with high values of mycelial inhibition presented for FR3 and FR4, as discussed above about fractionation efficiency applied.

**Figure 5:** (**A**) and (**B**) Molecular families with coumarins as major compounds obtained from the Feature-Based Molecular Networking workflow and annotated based on spectral matches in the GNPS (black arrow) and SIRIUS (blue arrow) public spectral libraries. The pie chart legend shows that the different nodes' colors represent the sample groups (CDE, FR3, and FR4). Each node represents a mass spectrometry spectrum (MS/MS), and width edges represent MS/MS fragmentation similarity as a cosine score range between 0.7 (less thick) and 1.0 (thicker). The black diamond shape of some nodes represents the hits obtained by the GNPS spectral library, and the node size is proportional to a sum precursor intensity of features area in MS1 scans. The acronym CI (cluster index), followed by the values of the nodes found in the molecular network, refers to structural proposals based on the SIRIUS software

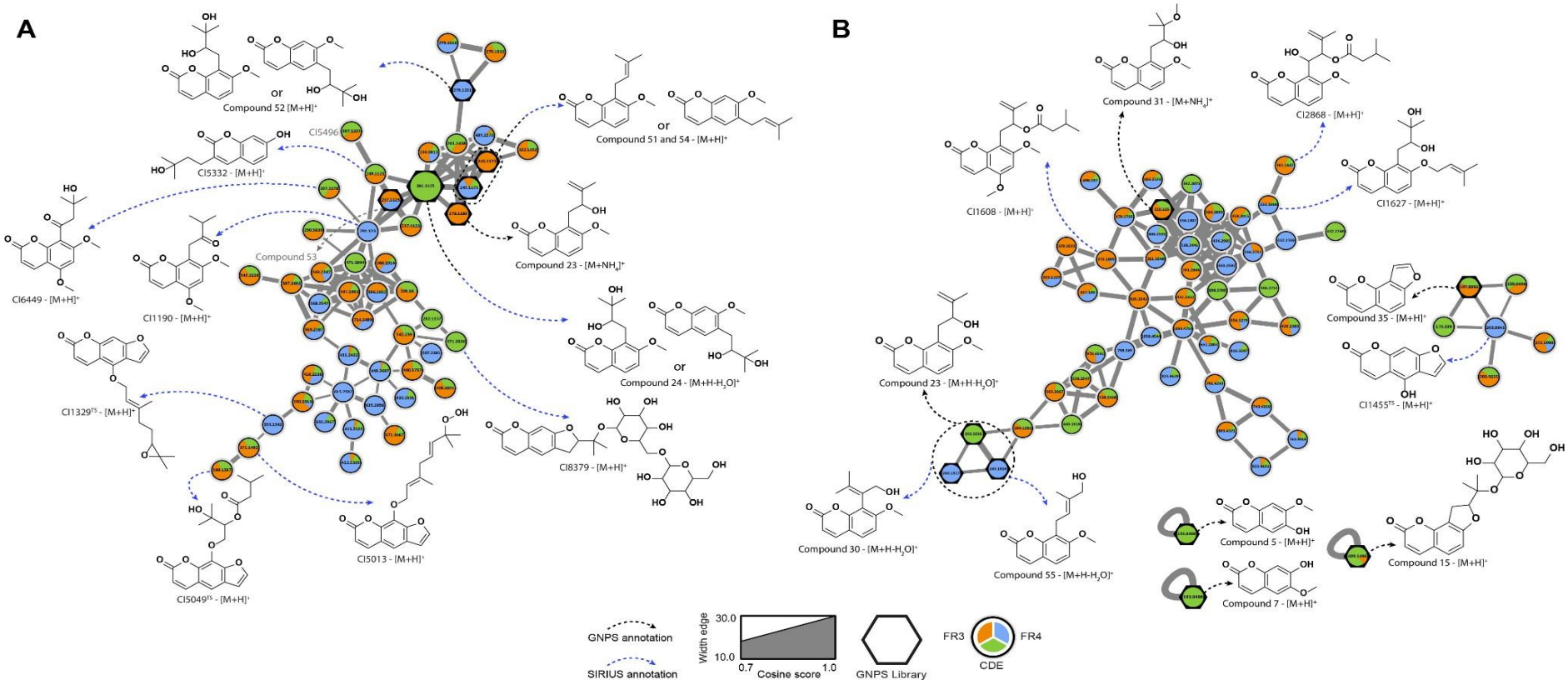


Source: Author's own.

The samples' coumarins belong to the lactonic compound class, derived from *O*-hydroxycinnamic acid and belonging to two subclasses: simple coumarins and furanocoumarins (Simões et al., 2007). Simple coumarins have a 1,2 benzopyrone nucleus containing hydroxyl, methoxyl, alkyl, and glycoside substituents. Among the 17 coumarins reported at level 2 in the present work, 13 are simple coumarins, with substances 5, 7, 23, 24, 25, 30, 31, 40, 46, 51, 52, 54, 55 presented in **Table 1**. Compounds 15, 31 and 35, which had yet to be reported for the *Citrus aurantium* species, were considered a level 3 annotation, with only the chemical class suggested in the annotation table.

On the other hand, furanocoumarins are characterized by containing a furan ring attached to the benzene ring (Simões et al., 2007; Bruni et al., 2019) and have been annotated as compounds 15, 27, 35, and 39 (**Table 1** and **Supplementary Material**). In addition, a glycosylated furanocoumarin (compound 15) was found in the extract and bioactive fractions, whose base peak is formed by the loss of 162 Da, corresponding to one sugar unit.

In the MS/MS spectra of the simple coumarins and furanocoumarins present in the extract and the FR3 and FR4 fractions, it was possible to observe the loss of low molecular weight fragments, such as loss of $H_2O$, $CH_3$ and CO (Yu et al., 2020). In the MS/MS spectra of compounds 46, 51, and 54, the highest intensity signal was formed by the $[C_4H_8]^+$ fragment, whose *m/z* 56 corresponds to the loss of the alkyl group (prenyl) (Yu et al., 2020). Low abundance peaks were also observed in substances 27, 39, 40, and 46, corresponding to the formation of the tropylium cation $[C_7H_7]^+$ with an *m/z* 91, and the ion with an *m/z* 65, corresponding to the cyclopentadienylium cation $[C_5H_5]^+$ (Yu et al., 2020). The MS/MS spectra of all the substances listed can be found in the **Supplementary Material**.

Among the annotations present in the molecular network A (**Figure 5**), matches were obtained corresponding to compounds (24, 51, 52, and 54) that are structurally distinct only in the position of the substituent, but belong to the same chemical class, have the same exact mass and the same molecular formula. This limitation in annotation comes up against the similarity of these isomers in terms of MS/MS fragmentation, given that the GNPS spectral library is limited and dependent on the deposit of spectra by other users. This fact explains why most of the nodes that make up the networks were not annotated; however, even starting from a few spectral matches, it was possible to propagate the annotation and provide a greater knowledge of the structures putatively present in the active fractions.

As observed for the flavonoids, it was also possible to obtain annotations classified as gold for the furanocoumarins in the molecular network, such as compounds 5, 15, and 35. Specifically for compound 35, which clustered with other nodes in a smaller network, it was

possible to perform structural propagation using the SIRIUS software. An adjacent node with predominant abundance in FR4 was proposed (1455$^{TS}$, see **Supplementary Table 5**) as bergaptol, a compound containing one less hydroxyl group and a change in the position of the furan ring in its structure when compared to compound 35, an analog of psoralen. All the fragmentation trees obtained for the structural propagation by the SIRIUS software are available in the supplementary material.

The achievement of structures proposed specified as "Training set" (TS), as obtained for compound 1455 and other compounds of the furanocoumarin class (1329 and 5049, see **Supplementary Table 5**), points above all to the excellent quality of the structure propagation based on the predictive model trained using a database of experimental and theoretical data used to build the internal library of the SIRIUS software. Consequently, it was also possible to infer that the experimental data obtained for the fractions from the LC-MS/MS analyses are of high quality, allowing for greater reliability of the compound annotation process presented here.

An example of a structural propagation based on the SIRIUS TS software is for compound 1329, identified as an *O*-prenylated furanocoumarin called epoxybergamottin, derived from bergamottin since its only difference is the presence of an epoxide in the final double bond of the prenyl group. Furanocoumarins like this and others proposed here by SIRIUS as being present in the active fractions have already been shown to be components of various *Citrus* species, specifically in the fruit peels (Dugrand et al., 2013).

Coumarins are present in many *Citrus* species and are one of the most described classes of compounds with antimicrobial activity. Montagner et al. (2008) evaluated the antifungal activity of disubstituted structures such as scopoletin (7) and trisubstituted structures such as osthenol (46) and bergapten (39) against fungi of the genus *Fusarium*, *Candida* and *Aspergillus*. Trisubstituted coumarins have shown excellent antifungal results, especially in terms of prenylated coumarins such as osthenol (46). This activity is associated with an increase in the molecule's lipophilicity, which facilitates its permeation through the lipid layer.

As has been reported for flavonoids, several studies point to compounds from the coumarin class in the response to infection by phytopathogenic fungi. An example of this is the study carried out by Massana-Codina et al. (2020), in which it was possible to observe the pronounced accumulation of different coumarins during the infection of potatoes (*Solanum tuberosum*) by the pathogen *Colletotrichum coccodes*. Among the coumarins involved, scopoletin (7) showed antifungal activity against the potato pathogen, suggesting that the accumulation of coumarins is induced during infection by *C. coccodes* to limit the proliferation

of the phytopathogen. This natural strategy used by different hosts allows us to use the mechanisms existing in nature to control pests that affect significant commodities, such as yellow melon rot caused by *Fusarium jinanense*.

**Table 1:** Annotation of secondary metabolites in the *Citrus aurantium* L. peel decoction extract and its fractions by manual dereplication and based on spectral matches within the GNPS platform

| *Feature* | $R_t$ (min) | $[M+H]^+$; $^2[M+H-H_2O]^+$; $^3[M+NH_4]^+$; $^4[M+Na]^+$ | | | | Molecular formula[a] | Annotation | FR3 | FR4 | Node | Ref. |
|---|---|---|---|---|---|---|---|---|---|---|---|
| | | Theoretical mass (*m/z*) | Measured mass (m/z) | MS/MS | Error (ppm) | | | | | | |
| **1** | 9,96 | 211.1446 | 211.1442 | 183, 138, 114, 98, 86 | 0.358 | $C_{11}H_{18}O_2N_2$ | ❖Dipeptide[c] | - | - | 8230 | CCMSLIB00005739084 |
| **2** | 9.97 | 289.0707 | 289.0708 | 289, 153, 145 | 0.468 | $C_{15}H_{12}O_6$ | Eriodictyol[b] | - | - | - | Yu *et al*., 2020 |
| **3** | 10.0 | 597.1819 | 597.1818 | 289, 195, 153, 399 | 0.508 | $C_{27}H_{32}O_{15}$ | Eriocitrin[c] | - | - | 8029 | CCMSLIB00010124324 |
| **4** | 10.09 | 183.0657 | 183.0655 | 155, 140, 123, 95 | 1.500 | $C_9H_{10}O_4$ | Syringaldehyde[c] | - | - | 8269 | CCMSLIB00003136460 |
| **5** | 10.21 | 193.0500 | 193.0498 | 178, 165, 149, 137, 133 | 1.027 | $C_{10}H_8O_4$ | Isoscopoletin [c] | - | - | 8072 | CCMSLIB00006417685 |
| **6** | 10.27 | 581.1865 | 581.1869 | 435, 383, 273, 153, 121 | 0.719 | $C_{27}H_{32}O_{14}$ | Naringin[b] | x | x | - | Wang *et al*., 2021 |
| **7** | 10.35 | 193.0500 | 193.0498 | 178, 165, 161, 149, 133 | 1.027 | $C_{10}H_8O_4$ | Scopoletin[c] | - | - | 8153 | CCMSLIB00005778023 |
| **8** | 10.35 | 579.1708 | 579.1713 | 433, 271, 153 | 0.808 | $C_{27}H_{30}O_{14}$ | Rhoifolin[b] | - | - | - | Kim *et al*., 2023 |
| **9** | 10.39 | 273.0757 | 273.0759 | 273, 147, 153, 119 | 0.549 | $C_{15}H_{12}O_5$ | Naringenin[b] | x | x | - | Kim *et al*., 2023 |
| **10** | 10.41 | 595.1657 | 595.1654 | 431, 287, 263, 161, 153 | -0.582 | $C_{27}H_{30}O_{15}$ | Luteolin 7-*O*-neohesperidoside[b] | - | - | - | Mencherini *et al*., 2013 |
| **11** | 10.41 | 435.1286 | 435.1288 | 273, 153, 145 | 0.421 | $C_{21}H_{22}O_{10}$ | Naringenin-*O*-glucoside[d] | x | - | 6534 | CCMSLIB00010113073 |
| **12** | 10.42 | 598.2135[3] | 598.2133[3] | 273, 171, 153, 147, 85 | 0,510 | $C_{27}H_{32}O_{14}$ | ❖Flavanone[c] | x | - | 6905 | CCMSLIB00000845824 |
| **13** | 10.46 | 479.1189 | 479.1187 | 317, 302, 285, 145, 127 | 1.465 | $C_{22}H_{22}O_{12}$ | ❖Flavonol[cs] | - | - | 8479 | CCMSLIB00004718647 |
| **14** | 10.55 | 175.0371[4] | 175.0390[4] | 147, 119, 91 | 5.666 | $C_8H_8O_3$ | Vanillin[c] | - | - | 8516 | CCMSLIB00006357163 |
| **15** | 10.55 | 409.1498 | 409.1496 | 247, 229, 187, 175 | 1.492 | $C_{20}H_{24}O_9$ | ❖Furocoumarin[c] | x | x | 3959 | CCMSLIB00000846145 |
| **16** | 10.62 | 611.1970 | 611.1971 | 303, 195, 153, 85 | 0.087 | $C_{28}H_{34}O_{15}$ | Hesperidin | x | x | - | Yu *et al*., 2020 |
| **17** | 10.64 | 449.1442 | 449.1443 | 303, 153,129 | 0.171 | $C_{22}H_{24}O_{10}$ | Hesperetin-*O*-rhamnoside[b] | x | - | - | Yu *et al*., 2020 |
| **18** | 10.71 | 463.1235 | 463.1238 | 445, 427, 397, 367, 343 | 0.674 | $C_{22}H_{22}O_{11}$ | Diosmetin-8-C-glucoside[b] | x | - | 5444 | Wen *et al*., 2021 |
| **19** | 10.86 | 753.2242 | 753.2240 | 301, 145, 127, 103, 85 | 0.00 | $C_{34}H_{40}O_{19}$ | ❖Flavonol[c] | - | - | 8368 | CCMSLIB00004718799 |
| **20** | 10.95 | 531.1502 | 531.1502 | 177, 163, 149, 145, 135 | 2.298 | $C_{26}H_{26}O_{12}$ | ❖Cinnamic acids derivatives[cs] | - | - | 8796 | CCMSLIB00000848797 |
| **21** | 10.99 | 772.2664[3] | 772.2660[3] | 345, 303, 171, 127, 85 | 0.00 | $C_{34}H_{42}O_{19}$ | ❖Flavanone[c] | - | - | 8621 | CCMSLIB00000848270 |
| **22** | 11.18 | 479.1189 | 479.1186 | 317, 302, 153 | 0.828 | $C_{22}H_{22}O_{12}$ | ❖Flavonol[cs] | - | - | 8355 | CCMSLIB00000221170 |

(*continued on next page*)

**Table 1** (*continued*)

| *Feature* | $R_t$ (min) | $[M+H]^+$; $^2[M+H-H_2O]^+$; $^3[M+NH_4]^+$; $^4[M+Na]^+$ | | | | Molecular formula[a] | Annotation | FR3 | FR4 | Node | Ref. |
|---|---|---|---|---|---|---|---|---|---|---|---|
| | | Theoretical mass (*m/z*) | Measured mass (m/z) | MS/MS | Error (ppm) | | | | | | |
| **23** | 11.24 | 243.1021[2] | 243.1016[2] | 201, 189, 173, 159, 131 | 1.255 | $C_{15}H_{16}O_4$ | Auraptenol[c] or CHEMBL3590439[sp], or Micromarin F[s] | - | - | 8010 | CCMSLIB00005722959 |
| **24** | 11.24 | 261.1126[2] | 261.1125[2] | 243, 217, 201, 189, 131 | 1.519 | $C_{15}H_{18}O_5$ | Meranzin Hydrate or Ulopterol[ds] | - | - | 8007 | CCMSLIB00005722913 |
| **25** | 11.29 | 261.1126 | 261.1124 | 243, 189, 131, 103 | 1.013 | $C_{15}H_{16}O_4$ | Meranzin[b] | x | x | - | Wang *et al*., 2021 |
| **26** | 11.54 | 257.0813 | 257.0810 | 171, 153, 131, 103, 67 | 0.00 | $C_{15}H_{12}O_4$ | Pinocembrine[c] | x | - | 6603 | CCMSLIB00010116989 |
| **27** | 11.78 | 203.0339 | 203.0341 | 175, 147, 119 | 0.861 | $C_{11}H_6O_4$ | Xanthotoxol[b] | x | x | - | Yu *et al*., 2020 |
| **28** | 12.35 | 271.0601 | 271.0605 | 271, 153, 119, 91 | 1.476 | $C_{15}H_{10}O_5$ | Apigenin[b] | - | - | - | Horai *et at*., 2010 |
| **29** | 12.40 | 177.0551[2] | 177.0548[2] | 163, 145, 135, 117, 89 | 1.120 | $C_{10}H_{10}O_4$ | Ferulic acid[c] | x | - | 5157 | CCMSLIB00010111580 |
| **30** | 12.55 | 243.1021[2] | 243.1017[2] | 201, 189, 173, 159, 131 | 0.816 | $C_{15}H_{16}O_4$ | Auraptenol[c] or CHEMBL3590439[sp], or Micromarin F[s] | - | x | 1259 | CCMSLIB00005722959 |
| **31** | 12.64 | 310.1654[3] | 310.1650[3] | 261, 243, 201, 189, 131 | 0.00 | $C_{16}H_{20}O_5$ | ❖ Coumarin[c] | x | - | 5130 | CCMSLIB00004700679 |
| **32** | 12.65 | 389.1231 | 389.1233 | 374, 359, 356, 341, 328 | 0,529 | $C_{20}H_{20}O_8$ | 5-Demethylnobiletin[b] | x | x | - | Kim *et al*., 2023 |
| **33** | 12.69 | 303.0868 | 303.0864 | 285, 177, 171, 163, 153 | 1.309 | $C_{16}H_{14}O_6$ | Homoeriodictyol[c] | x | - | 4951 | CCMSLIB00003139732 |
| **34** | 12.71 | 303.0863 | 303.0865 | 285, 179, 177, 153 | 0.612 | $C_{16}H_{14}O_6$ | Hesperitin[b] | x | - | - | Kim *et al*., 2023 |
| **35** | 12.81 | 187.0395 | 187.0392 | 159, 143, 131, 115 | 4.242 | $C_{11}H_6O_3$ | ❖ Furocoumarin[c] | x | - | 4933 | CCMSLIB00006423586 |
| **36** | 12.88 | 133.1017[2] | 133.1014[2] | 115, 105, 91 | 2.980 | $C_{10}H_{14}O$ | Cumic Alcohol[c] | x | - | 5086 | CCMSLIB00005435949 |
| **37** | 13.02 | 201.1643[2] | 201.1640[2] | 173, 159, 145, 131, 119 | 0.00 | $C_{15}H_{22}O$ | Nootkatone[c] | x | x | 4184 | CCMSLIB00010118710 |
| **38** | 10.66 | 345.0969 | 345.0969 | 345, 330, 315, 84 | 0.640 | $C_{18}H_{16}O_7$ | 5,3′-Dihydroxy-3,7,4′-trimethoxyflavone[b] | - | - | - | Xu *et al*., 2018 |
| **39** | 13.66 | 217.0495 | 217.0497 | 202, 174, 161, 131, 115 | 0.759 | $C_{12}H_8O_4$ | Bergapten[b] | x | x | - | Yu *et al*., 2020 |
| **40** | 13.75 | 207.0652 | 207.0650 | 207, 192, 179, 151 | 0.554 | $C_{11}H_{10}O_4$ | Scoparone[b] | x | - | - | Kim *et al*., 2023 |
| **41** | 13.82 | 419.1337 | 419.1339 | 419, 404, 389, 371 | 0.576 | $C_{21}H_{22}O_9$ | 7-Hydroxy-3,5,6,8,3′,4′-hexamethoxyflavone[b] | x | x | - | Xu *et al*., 2018 |
| **42** | 13.93 | 359.1125 | 359.1126 | 359, 329, 311, 197 | 0.197 | $C_{19}H_{18}O_7$ | 5-Hydroxy-6,7,8,4′-tetramethoxyflavone[b] | x | - | - | Xu *et al*., 2018 |
| **43** | 13.99 | 373.1287 | 373.1284 | 358, 343, 328, 312 | 1.063 | $C_{20}H_{20}O_7$ | Sinensetin[c] | x | x | 1165 | CCMSLIB00010104830 |
| **44** | 14.14 | 343.1176 | 343.1177 | 328, 313, 285 | 0.248 | $C_{19}H_{18}O_6$ | 4’,5,6,7-Tetramethoxyflavone[b] | - | - | - | Yu *et al*., 2020 |
| **45** | 14.29 | 135.1173[2] | 135.1170[2] | 107, 105, 93, 91, 79 | 0.00 | $C_{10}H_{16}O$ | Carveol[c] | x | x | 1947 | CCMSLIB00010125872 |
| **46** | 14.46 | 231.1016 | 231.1018 | 175, 147, 119, 91 | 0.992 | $C_{14}H_{14}O_3$ | Osthenol[b] | x | x | - | Xu *et al*., 2018 |
| **47** | 14.61 | 473.2170 | 473.2174 | 427, 279, 161 | 0.857 | $C_{26}H_{32}O_8$ | Deacetylnomilin[b] | - | - | - | Pessoa *et al*., 2021 |
| **48** | 14.71 | 403.1387 | 403.1391 | 388, 373, 355, 327, 301 | 0.883 | $C_{21}H_{22}O_8$ | Nobiletin[b] | x | x | - | Xu *et al*., 2018 |
| **49** | 15.22 | 433.1497 | 433.1493 | 403, 388, 385, 360, 165 | 0.903 | $C_{22}H_{24}O_9$ | 3',4',5',3,5,6,7-Heptamethoxyflavone[b] | x | x | | Wang *et al*., 2021 |
| **50** | 15.23 | 433.1498 | 433.1497 | 418, 403, 385, 373, 211 | 1.620 | $C_{22}H_{24}O_9$ | 3',4',5',3,5,7,8-Heptamethoxyflavone[c] | x | x | 1160 | CCMSLIB00000847330 |

(*continued on next page*)

| *Feature* | $R_t$ (min) | $[M+H]^+$; $^2[M+H-H_2O]^+$; $^3[M+NH_4]^+$; $^4[M+Na]^+$ | | | Error (ppm) | Molecular formula[a] | Annotation | FR3 | FR4 | Node | Ref. |
|---|---|---|---|---|---|---|---|---|---|---|---|
| | | Theoretical mass (*m/z*) | Measured mass (m/z) | MS/MS | | | | | | | |
| **52** | 15.67 | 279.1232 | 279.1231 | 243, 189, 175, 149, 131 | 0.437 | $C_{15}H_8O_5$ | Meranzin Hydrate[d] or Ulopterol[s] | - | x | 1312 | CCMSLIB00004696513 |
| **53** | 16.24 | 237.1126 | 237.1123 | 219, 191, 165, 149, 135 | 1.287 | $C_{13}H_{16}O_4$ | ❖Coumaran | x | x | 1872 | CCMSLIB00000851098 |
| **54** | 16.60 | 245.1177 | 245.1173 | 203, 189, 161, 131, 103 | 1.183 | $C_{15}H_{16}O_3$ | Osthole[c] or Suberosin[s] | x | x | 1168 | CCMSLIB00010107493 |
| **55** | 17.04 | 243.1021[2] | 243.1016[2] | 201, 189, 173, 159, 131 | 1.255 | $C_{15}H_{16}O_4$ | Auraptenol[c] or CHEMBL3590439[sp], or Micromarin F[s] | - | x | 1175 | CCMSLIB00005722959 |
| **56** | 17.10 | 315.1960 | 315.1956 | 269, 199, 187, 171, 131 | 1.839 | $C_{20}H_{26}O_3$ | ❖Diterpenoid[c] | x | x | 1729 | CCMSLIB00004699027 |
| **57** | 18.47 | 373.1282 | 373.1284 | 358, 343, 325, 312 | 0.591 | $C_{20}H_{20}O_7$ | Tangeritin[b] | x | x | - | Xu *et al*., 2018 |

[a] The molecular formulas described here refer to neutral monoisotopic masses. [b] Compound annotated only by manual dereplication. [c] Compound annotated only by the GNPS library. [d] Compound annotated by manual dereplication and the GNPS library. [s] Compound annotated by SIRIUS. [p] Pubchem code. ❖Compound annotated level 3.
Source: Author's own.

## 4 Conclusion

The application of current methodologies to explore and characterize different matrices to add value within the food industry allows us to discover and redirect the use of different unexploited residues. Among the various possibilities involving the production of waste from the citrus industry, this work enabled the chemical characterization of an essential oil residue from *Citrus aurantium* as well as proving its efficiency in inhibiting the fungus *Fusarium jinanense*, which causes yellow melon rot.

Using a robust and efficient workflow based on SPE fractionation, UHPLC-MS/MS analysis and the use of molecular networking associated with different databases and softwares (GNPS and SIRIUS), it was possible to annotate 65 metabolites from different chemical classes distributed within the crude extract and active fractions from the *C. aurantium* decoction. Compounds from the class of polymethoxyflavones, coumarins and furanocoumarins were mostly present in the fractions that were responsible for inhibiting 61% of the mycelial growth of the fungus *F. jinanense*, a value higher than that achieved by the current antifungal Cercobin® (48%) used in the field.

Our results show the potential of the essential oil composition residue and demonstrate the importance of understanding this residue at a molecular level so that it is possible to plan new studies aimed at developing new eco-friendly products and understanding the mechanisms of action of the compounds presented here against this harmful causal agent responsible for significant losses in melon production.

### CRediT authorship contribution statement

**Maria Daiane de Freitas:** Conceptualization; Data curation; Investigation; Methodology; Project administration; Resources; Validation; Visualization; Roles/Writing - original draft; and Writing - review & editing. **Rodolfo Dantas Lima Junior:** Conceptualization; Data curation; Formal analysis; Investigation; Methodology; Project administration; Resources; Software; Validation; Visualization; Roles/Writing - original draft; and Writing - review & editing. **Taicia Pacheco Fill:** Funding acquisition; Project administration; Supervision; Roles/Writing - original draft; and Writing - review & editing. **Francisco Erivaldo Freitas da Silva:** Conceptualization; Data curation; Investigation and Methodology. **Davila Zampieri:** Supervision and Writing - review & editing. **Cristiano Souza Lima:** Funding acquisition; Supervision; Methodology; Roles/Writing - original draft; and Writing - review & editing. **Eliane Mayumi Inokuti:** Conceptualization; Data curation;

Investigation; Methodology; Roles/Writing - original draft; and Writing - review & editing. **Andréia Hansen Oster:** Roles/Writing - original draft; and Writing - review & editing. **Telma Leda Gomes de Lemos:** Funding acquisition; Project administration; Supervision; Roles/Writing - original draft; and Writing - review & editing.

## Declaration of Competing Interest

The authors declare that they have no known competing financial interests or personal relationships that could have appeared to influence the work reported in this paper.

## Data availability

Data will be made available on request.

## Acknowledgments and Funding Information

This study was financed by the Coordenação de Aperfeiçoamento de Pessoal de Nível Superior - Brazil (CAPES) - Funding Code 001 and 88887.474570/2020-00. The authors gratefully acknowledge the financial support of Conselho Nacional de Desenvolvimento Científico e Tecnológico (CNPq), Project nº 303273.2019-4 and Fundação de Amparo à Pesquisa do Estado de São Paulo (FAPESP), Project nº 2022/02992-0.

## REFERENCES

Abo Elgat, W. A. A., Kordy, A. M., Böhm, M., Černý, R., Abdel-Megeed, A., & Salem, M. Z. M. (2020). Eucalyptus camaldulensis, citrus aurantium, and citrus sinensis essential oils as antifungal activity against aspergillus flavus, aspergillus niger, aspergillus terreus, and fusarium culmorum. *Processes*, *8*(8). https://doi.org/10.3390/pr8081003

Aboody, M. S. Al, & Mickymaray, S. (2020). Anti-fungal efficacy and mechanisms of flavonoids. *Antibiotics*, *9*(2). https://doi.org/10.3390/antibiotics9020045

Adusumilli, R., & Mallick, P. (2017). Data Conversion with ProteoWizard msConvert. In: Comai, L., Katz, J., Mallick, P. (eds) *Proteomics. Methods in Molecular Biology*, *1550*. Humana Press, New York, NY. https://doi.org/10.1007/978-1-4939-6747-6_23

Bruni, R., Barreca, D., Protti, M., Brighenti, V., Righetti, L., Anceschi, L., Mercolini, L., Benvenuti, S., Gattuso, G., & Pellati, F. (2019). Botanical Sources, Chemistry, Analysis, and Biological Activity of Furanocoumarins of Pharmaceutical Interest. *Molecules*. *24*(11). doi: 10.3390/molecules24112163

Cuyckens, F., & Claeys, M. (2004). Mass spectrometry in the structural analysis of flavonoids. In *Journal of Mass Spectrometry*, *39*(1). https://doi.org/10.1002/jms.585

Degirmenci, H., & Erkurt, H. (2020). Chemical profile and antioxidant potency of Citrus aurantium L. flower extracts with antibacterial effect against foodborne pathogens in rice pudding. *Lebensmittel-Wissenschaft & Technologie*, *126*. https://doi.org/10.1016/j.lwt.2020.109273

Deterre, S. C., Rega, B., Delarue, J., Teillet, E., & Giampaoli, P. (2014). Classification of commercial bitter orange essential oils (Citrus aurantium L.), based on a combination of chemical and sensory analyses of specific odor markers. *Journal of Essential Oil Research*, *26*(4). https://doi.org/10.1080/10412905.2014.917337

Dugrand, A., Olry, A., Duval, T., Hehn, A., Froelicher, Y., & Bourgaud, F. (2013). Coumarin and furanocoumarin quantitation in citrus peel via ultraperformance liquid chromatography coupled with mass spectrometry (UPLC-MS). *Journal of Agricultural and Food Chemistry*, *61*(45). https://doi.org/10.1021/jf402763t

Dührkop, K., Fleischauer, M., Ludwig, M., Aksenov, A. A., Melnik, A. V., Meusel, M., Dorrestein, P. C., Rousu, J., Böcker, S. (2019). SIRIUS 4: a rapid tool for turning tandem mass spectra into metabolite structure information. *Nature Methods*.*16*(4). https://doi.org/10.1038/s41592-019-0344-8

FAO-Food and Agriculture Organization. (2020). *Citrus fruit fresh and processed-Statistical bulletin 2020*. Available at: https://www.fao.org/3/cb6492en/cb6492en.pdf . Accessed on: 08 April 2023.

Fiehn, O., Robertson, D., Griffin, J., vab der Werf, M., Nikolau, B., Morrison, N., Sumner, L. W., Goodacre, R., Hardy, N. W., Taylor, C., Fostel, J., Kristal, B., Kaddurah-Daouk, R., Mendes, P., van Ommen, B., Lindon, J. C., & Sansone, S. A. (2007). The metabolomics

standards initiative (MSI). *Metabolomics*, *3*(3). https://doi.org/10.1007/s11306-007-0070-6

Förster, C., Handrick, V., Ding, Y., Nakamura, Y., Paetz, C., Schneider, B., Castro-Falcón, G., Hughes, C. C., Luck, K., Poosapati, S., Kunert, G., Huffaker, A., Gershenzon, J., Schmelz, E. A., Köllner, T. G. (2022). Biosynthesis and antifungal activity of fungus-induced O-methylated flavonoids in maize. *Plant Physiology*, *188*(1). doi: 10.1093/plphys/kiab496

Han, S. L., Wang, M. M., Ma, Z. Y., Raza, M., Zhao, P., Liang, J. M., Gao, M., Li, Y. J., Wang, J. W., Hu, D. M., Cai, L. (2023). *Fusarium* diversity associated with diseased cereals in China, with an updated phylogenomic assessment of the genus. *Studies in Mycology,* 104. https://doi.org/10.3114/sim.2022.104.02

Horai, H., Arita, M., Kanaya, S., Nihei, Y., Ikeda, T., Suwa, K., Ojima, Y., Tanaka, K., Tanaka, S., Aoshima, K., Oda, Y., Kakazu, Y., Kusano, M., Tohge, T., Matsuda, F., Sawada, Y., Hirai, M. Y., Nakanishi, H., Ikeda, K., … Nishioka, T. (2010). MassBank: a public repository for sharing mass spectral data for life sciences. *Journal of Mass Spectrometry*, *45*(7). https://doi.org/10.1002/jms.1777

IBGE-Brazilian Institute of Geography and Statistics. (2023). *Municipal Agricultural Production*. Available at: https://sidra.ibge.gov.br/tabela/1612. Accessed on April 22, 2023.

Kim, S., Chen, J., Cheng, T., Gindulyte, A., He, J., He, S., Li, Q., Shoemaker, B. A., Thiessen, P. A., Yu, B., Zaslavsky, L., Zhang, J., & Bolton, E. E. (2023). PubChem 2023 update. *Nucleic Acids Research*, *51*(D1). https://doi.org/10.1093/nar/gkac956

Kist, B. B., Carvalho, D. C., & Beling, R. R. (2022). Anuário Brasileiro de Horti&Fruti 2022 – Santa Cruz do Sul : Editora Gazeta Santa Cruz, pp. 62–65. Available at: https://www.editoragazeta.com.br/sitewp/wp-content/uploads/2022/04/HORTIFRUTI_2022.pdf. Accessed on April 14, 2023.

Lima, E. N., Oster, A. H., Bordallo, P. N., Araújo, A. A. C., Silva, D. E. M., Lima, C. S. (2021). A novel lineage in the Fusarium incarnatum-equiseti species complex is one of the causal agents of fusarium rot on melon fruits in Northeast Brazil. *Plant Pathology*, *70*(1). https://doi.org/10.1111/ppa.13271

Ma, Y. L., Li, Q. M., Van den Heuvel, H., & Claeys, M. (1997). Characterization of flavone and flavonol aglycones by collision-induced dissociation tandem mass spectrometry. *Rapid Communications in Mass Spectrometry*, *11*(12). https://doi.org/10.1002/(SICI)1097-0231(199708)11:12<1357::AID-RCM983>3.0.CO;2-9

Massana-Codina, J., Schnee, S., Allard, P. M., Rutz, A., Boccard, J., Michellod, E., Cléroux, M., Schürch, S., Gindro, K., & Wolfender, J. L. (2020). Insights on the structural and metabolic resistance of potato (Solanum tuberosum) cultivars to tuber black dot (Colletotrichum coccodes). *Frontiers in Plant Science*, *11*. https://doi.org/10.3389/fpls.2020.01287

Medeiros Araújo, M. B., Moreira, G. M., Nascimento, L. V., Nogueira, G. de A., Nascimento, S. R. de C., Pfenning, L. H., & Ambrósio, M. M. de Q. (2021). Fusarium rot of melon is caused by several Fusarium species. *Plant Pathology*, *70*(3). https://doi.org/10.1111/ppa.13328

Mencherini, T., Campone, L., Piccinelli, A. L., García Mesa, M., Sánchez, D. M., Aquino, R. P., Rastrelli, L. (2013). HPLC-PDA-MS and NMR characterization of a hydroalcoholic extract of Citrus aurantium L. var. amara peel with antiedematogenic activity. *Journal of Agricultural and Food Chemistry*, *61*(8). https://doi.org/10.1021/jf302815t

Montagner, C., De Souza, S. M., Groposo, C., Delle Monache, F., Smânia, E. F. A., & Smânia, A. (2008). Antifungal activity of coumarins. *Zeitschrift für Naturforschung - Section C Journal of Biosciences, 63*(1-2). https://doi.org/10.1515/znc-2008-1-205

Nair, H., & Clarke, W. (2016). Mass Spectrometry for the Clinical Laboratory. In Mass Spectrometry for the Clinical Laboratory. https://doi.org/10.1016/c2013-0-19099-x

Nothias, L. F., Petras, D., Schmid, R., Dührkop, K., Rainer, J., Sarvepalli, A., Protsyuk, I., Ernst, M., Tsugawa, H., Fleischauer, M., Aicheler, F., Aksenov, A. A., Alka, O., Allard, P. M., Barsch, A., Cachet, X., Caraballo-Rodriguez, A. M., Da Silva, R. R., Dang, T., Garg, N., Gauglitz, J. M., Gurevich, A., Isaac, G., Jarmusch, A. K., Kameník, Z., Kang, K. B., Kessler, N., Koester, I., Korf, A., Le Gouellec, A., Ludwig, M., Martin, H. C., McCall, L. I., McSayles, J., Meyer, S. W., Mohimani, H., Morsy, M., Moyne, O., Neumann, S., Neuweger, H., Nguyen, N. H., Nothias-Esposito, M., Paolini, J., Phelan, V. V., Pluskal, T., Quinn, R. A., Rogers, S., Shrestha, B., Tripathi, A., van der Hooft, J. J. J., Vargas, F., Weldon, K. C., Witting, M., Yang, H., Zhang, Z., Zubeil, F., Kohlbacher, O., Böcker, S., Alexandrov, T., Bandeira, N., Wang, M., Dorrestein, P. C. (2020) Feature-based molecular networking in the GNPS analysis environment. *Nature Methods*, *17*(9). https://doi.org/10.1038/s41592-020-0933-6

Okwu, D. E., Awurum, A. N., & Okoronkwo, J. I. (2007). Phytochemical composition and in vitro antifungal activity screening of extracts from citrus plants against Fusarium oxysporum of okra plant (Hibiscus esculentus). *Summa Phytopathol*, *30*, 145-148. https://api.semanticscholar.org/CorpusID:55533842

Onakpoya, I., Davies, L., & Ernst, E. (2011). Efficacy of herbal supplements containing Citrus aurantium and synephrine alkaloids for the management of overweight and obesity: a systematic review. *Focus on Alternative and Complementary Therapies*, *16*(4). https://doi.org/10.1111/j.2042-7166.2011.01115.x

Ortuño, A., Báidez, A., Gómez, P., Arcas, M. C., Porras, I., García-Lidón, A., & Del Río, J. A. (2006). Citrus paradisi and Citrus sinensis flavonoids: Their influence in the defence mechanism against Penicillium digitatum. *Food Chemistry*, *98*(2). https://doi.org/10.1016/j.foodchem.2005.06.017

Ortuño, A., Díaz, L., Alvarez, N., Porras, I., García-Lidón, A., & Del Río, J. A. (2011). Comparative study of flavonoid and scoparone accumulation in different Citrus species and their susceptibility to Penicillium digitatum. *Food Chemistry*, *125*(1). https://doi.org/10.1016/j.foodchem.2010.09.012

Oulebsir, C., Mefti-Korteby, H., Djazouli, Z. E., Zebib, B., & Merah, O. (2022). Essential Oil of Citrus aurantium L. Leaves: Composition, antioxidant activity, elastase and collagenase inhibition. *Agronomy*, *12*(6). https://doi.org/10.3390/agronomy12061466

Perczak, A., Gwiazdowska, D., Marchwińska, K., Juś, K., Gwiazdowski, R., & Waśkiewicz, A. (2019). Antifungal activity of selected essential oils against Fusarium culmorum and F. graminearum and their secondary metabolites in wheat seeds. *Archives of Microbiology*, *201*(8). https://doi.org/10.1007/s00203-019-01673-5

Pessoa, L. G. A., Pessoa, L. A., Santos, É. da S., Pilau, E. J., Gonçalves, J. E., Gonçalves, R. A. C., & de Oliveira, A. J. B. (2021). Limonoid detection and profile in callus culture of sweet orange. *Acta Scientiarum-Biological Science*, *43*. https://doi.org/10.4025/actascibiolsci.v43i1.53075

Pluskal, T., Castillo, S., Villar-Briones, A., & Oresic, M. (2010). MZmine 2: modular framework for processing, visualizing, and analyzing mass spectrometry-based molecular profile data. *BMC Bioinformatics*, *11*. https://doi.org/10.1186/1471-2105-11-395

Schymanski, E. L., Jeon, J., Gulde, R., Fenner, K., Ruff, M., Singer, H.P., & Hollender, J. (2014). Identifying small molecules via high resolution mass spectrometry: Communicating confidence. In Environmental *Science & Technology*, *48*. https://doi.org/10.1021/es5002105

Shannon, P., Markiel, A., Ozier, O., Baliga, N. S., Wang, J. T., Ramage, D., Amin, N., Schwikowski, B., Ideker, T. (2003). Cytoscape: A Software Environment for Integrated Models of Biomolecular Interaction Networks. *Genome Research*, *13*, 2498–2504. https://doi.org/10.1101/GR.1239303

Simionato, A. S., Navarro, M. O. P., de Jesus, M. L. A., Barazetti, A. R., da Silva, C. S., Simões, G. C., Balbi-Peña, M. I., de Mello, J. C. P., Panagio, L. A., de Almeida, R. S. C., Andrade, G., de Oliveira, A. G. (2017). The effect of phenazine-1-carboxylic acid on mycelial growth of *Botrytis cinerea* produced by *Pseudomonas aeruginosa* LV strain. *Frontiers in Microbiology*, *8*, 1102. https://doi.org/10.3389/fmicb.2017.01102

Simões, C. M. O. (2007). *Farmacognosia: da planta ao medicamento*. *6*. ed. Porto Alegre: Editora da UFRGS; Florianópolis: Editora da UFSC, 537-55.

Sumner, L.W., Amberg, A., Barrett, D., Beale, M. H., Beger, R., Daykin, C. A., Fan, T. W. M., Fiehn, O., Goodacre, R., Griffin, J. L. and Hankemeier, T., Hardy, N., Harnly, J., Higashi, R., Kopka, J., Lane, A. N., Lindon, J. C., Marriott, P., Nicholls, A. W., … Viant, M. R. (2007). Proposed minimum reporting standards for chemical analysis. *Metabolomics*, *3*(3), 211–221. https://doi.org/10.1007/s11306-007-0082-2

Wang, Q., Zou, Z., Zhang, Y., Lin, P., Lan, T., Qin, Z., Xu, D., Wu, H. & Yao, Z. (2021). Characterization of chemical profile and quantification of major representative components of Wendan decoction, a classical traditional Chinese medicine formula. *Journal of Separation Science*, *44*(5). https://doi.org/10.1002/jssc.202000952

Wen, L., He, M., Yin, C., Jiang, Y., Luo, D., & Yang, B. (2021). Phenolics in Citrus aurantium fruit identified by UHPLC-MS/MS and their bioactivities. *Lebensmittel-Wissenschaft & Technologie*, *147*. https://doi.org/10.1016/j.lwt.2021.111671

Wu, T., Cheng, D., He, M., Pan, S., Yao, X., & Xu, X. (2014). Antifungal action and inhibitory mechanism of polymethoxylated flavones from Citrus reticulata Blanco peel against Aspergillus niger. *Food Control*, *35*(1). https://doi.org/10.1016/j.foodcont.2013.07.027

Xu, Y., Cai, H., Cao, G., Duan, Y., Pei, K., Tu, S., Zhou, J., Xie, L., Sun, D., Zhao, J., Liu, J., Wang, X., & Shen, L. (2018). Profiling and analysis of multiple constituents in Baizhu Shaoyao San before and after processing by stir-frying using UHPLC/Q-TOF-MS/MS coupled with multivariate statistical analysis. *Journal of Chromatography B: Analytical Technologies in the Biomedical and Life Sciences*, *1083*. https://doi.org/10.1016/j.jchromb.2018.03.003

Yu, L., Chen, M., Liu, J., Huang, X., He, W., Qing, Z., & Zeng, J. (2020). Systematic detection and identification of bioactive ingredients from Citrus aurantium L. var. amara using HPLC-Q-TOF-MS combined with a screening method. *Molecules*, *25*(2). https://doi.org/10.3390/molecules25020357

Zakaria, Latiffah. (2023). Fusarium Species Associated with Diseases of Major Tropical Fruit Crops. *Horticulturae*, *9*(3). https://doi.org/10.3390/horticulturae9030322

*Supplementary material*

**Title: Unraveling the antifungal composition of bitter orange decoction against the melon pathogen *Fusarium jinanense***

Maria Daiane de Freitas[a,1], Rodolfo Dantas Lima Junior[b,1], Francisco Erivaldo Freitas da Silva[a], Eliane Mayumi Inokuti[c], Andréia Hansen Oster[d], Davila Zampieri[a], Cristiano Souza Lima[d], Taicia Pacheco Fill[b], Telma Leda Gomes de Lemos[a,*], tlemos@dqoi.ufc.br

[a]Departamento de Química Orgânica e Inorgânica, Universidade Federal do Ceará, Campus do Pici, 60021-940, Fortaleza, Ceará, Brazil.

[b]Instituto de Química, Universidade de Campinas, CP 6154, 13083-970, Campinas, SP, Brazil.

[c]Departamento de Fitotecnia, Universidade Federal do Ceará, Campus do Pici, 60440-554, Fortaleza, Ceará, Brazil.

[d]Empresa Brasileira de Pesquisa Agropecuária, Embrapa Uva e Vinho, 95701-008, Bento Gonçalves, Rio Grande do Sul, Brazil.

[*]Corresponding author.

[1]The authors equally contributed.

## Summary

# TABLES

**Supplementary Table 1:** Parameters settled in the MZmine software (Version 2.53) for raw data processing

| **Feature detection** | |
|---|---|
| Mass detection (MS1) | 1.00E+05 |
| Mass detection (MS2) | 1.00E+03 |
| **ADAP Chromatogram builder** | |
| Scans | MS Level:1 |
| Min group size in # of scans | 4 |
| Group intensity threshold | 3.00E+05 |
| Min highest intensity | 3.00E+05 |
| *m/z* tolerance | 5 ppm |
| **Chromatogram deconvolution** | |
| Algorithm | Local minimum search |
| Chromatographic threshold | 10% |
| Search minimum in RT range (min) | 0.02 |
| Minimum relative height | 10% |
| Minimum absolute height | 3.00E+05 |
| Min ratio of peak top/edge | 2 |
| Peak duration range (min) | 0.02 - 1.50 |
| *m/z* center calculation | MEDIAN |
| *m/z* range for MS2 scan pairing (Da) | 0.01 |
| RT range for MS2 scan pairing (min) | 0.02 |
| **Isotope grouping (Isotopic peaks grouper)** | |
| *m/z* tolerance | 5 ppm |
| Retention time tolerance | 0.02 (absolute (min)) |
| Maximum charge | 2 |
| Representative isotope | Most intense |
| **Alignment (Join aligner)** | |
| *m/z* tolerance | 5 ppm |
| Weight for m/z | 75 |
| Retention time tolerance | 0.02 (absolute (min)) |
| Weight for RT | 25 |
| **MS row filter and Isotope filter (Feature list rows filter)** | |
| Minimum peaks in a row | 1 |
| Minimum peaks in na isotope pattern | 2 |
| keep peaks with MS2 for GNPS | TRUE |

Source: Author's own.

**Supplementary Table 2:** Parameters settled in Feature-Based Molecular Networking workflow

| **Description** | **Parameter settings** |
|---|---|
| Removing all MS/MS fragment ions within +/- 17 Da of window precursor | off |
| Only the top 6 fragment ions in the +/- 50 Da | off |
| The precursor ion mass tolerance | 0.02 Da |
| The MS/MS fragment ion tolerance | 0.02 Da. |
| Minimum cosine score to form an edge in a molecular network with more than 5 matched peaks. | 0.7 |
| Maximum number of nodes a single node can have. | 10 |
| Maximum size of a molecular family | 100 |
| The necessary matches between the network spectra and the library spectra | Score above 0.7 and at least 4 matched peaks. |

Source: Author's own.

**Supplementary Table 3:** Annotation of secondary metabolites in the *Citrus aurantium* L. peel decoction extract and its fractions in negative ionization mode

| *Feature* | $t_R$ (min) | Theoretical mass (*m/z*) | Measured mass (*m/z*) | $MS^2$ | Error (ppm) | Molecular formula | Annotation | FR3 | FR4 | Reference |
|---|---|---|---|---|---|---|---|---|---|---|
| **1N**[b] | 9.61 | 447.0933 | 447.0935 | 447, 327, 357, 299 | 2.935 | $C_{21}H_{20}O_{11}$ | Orientin | - | - | Zhang *et al*., 2022 |
| **2N**[b] | 9.92 | 431.0984 | 431.0983 | 431, 311, 283, 341 | 2.382 | $C_{21}H_{20}O_{10}$ | Vitexin | - | - | Zhang *et al*., 2022 |
| **3N**[b] | 10.05 | 449.1089 | 449.1091 | 449, 287, 151, 135 | 2.810 | $C_{21}H_{22}O_{11}$ | Eriodictyol-7-O-glucoside | - | - | Kim *et al.,* 2023 |
| **4N**[b] | 10.31 | 447.0933 | 447.0934 | 447, 285, 151 | 2.711 | $C_{21}H_{20}O_{11}$ | Luteolin-O- glucoside | - | - | Zhang *et al*., 2022 |
| **8**[a] | 10.34 | 577.1563 | 577.1563 | 578, 577, 270, 269, 268 | 1.937 | $C_{27}H_{30}O_{14}$ | Rhoifolin | x | - | Kim *et al.,* 2023 |
| **10**[a] | 10.40 | 593.1512 | 593.1509 | 593, 285, 284 | 1.355 | $C_{27}H_{30}O_{15}$ | Luteolin 7-O-neohesperidoside | x | - | Mencherini *et al.,* 2013 |
| **5N**[b] | 10.70 | 463.1246 | 463.1249 | 463, 301, 151, 286, 242 | 3.049 | $C_{22}H_{24}O_{11}$ | peretin 7-O-β-D- glucuronide | - | - | Zhang *et al*., 2022 |
| **6N**[b] | 10.80 | 579.1719 | 579.1721 | 579, 301, 286, 242,151 | 2.224 | $C_{27}H_{32}O_{14}$ | Narirutin | x | x | Zhang *et al*., 2022 |
| **18**[a] | 11.06 | 461.1089 | 461.1084 | 461, 341, 298 | 3.388 | $C_{22}H_{22}O_{11}$ | Diosmetin-8-C-glucoside | - | - | Wang *et al.,*2021 |
| **2**[a] | 11.55 | 287.0561 | 287.0562 | 287, 135, 151, 107 | 4.269 | $C_{15}H_{12}O_6$ | Eriodictyol | - | - | Zhang *et al*., 2022 |
| **7N**[b] | 11.60 | 285.0405 | 285.0406 | 285, 257, 199, 151 | 4.335 | $C_{15}H_{10}O_6$ | Kaempferol | x | - | McNab *et al.,* 2009 |
| **8N**[b] | 11.62 | 263.1289 | 263.1290 | 263, 219, 204, 201 | 4.615 | $C_{15}H_{20}O_4$ | Abscisic acid | - | - | Zhang *et al*., 2022 |
| **28**[a] | 12.34 | 269.0455 | 269.0458 | 269, 225, 151, 117 | 5.018 | $C_{15}H_{10}O_5$ | Apigenin | x | - | McNab *et al.,* 2009 |
| **9**[a] | 12.37 | 271.0612 | 271.0613 | 271, 177, 151, 119 | 4.427 | $C_{15}H_{12}O_5$ | Naringenin | - | - | Zhang *et al*., 2022 |
| **34**[a] | 12.71 | 301.0718 | 301.0717 | 301, 286, 257, 164,151 | 3.439 | $C_{16}H_{14}O_6$ | Hesperitin | x | - | s and Lopes, 2012 |

[a]These compounds were also identified in the positive mode as shown in Table 1. [b] Compounds identified only in negative mode.
Source: Author's own.

## REFERENCES

Gates, P.-J., and Lopes N.-P. (2012). Characterisation of flavonoid aglycones by negative ion chip-based nanospray tandem mass spectrometry. *International Journal of Analytical Chemistry,* 2012, 7.https://doi.org/10.1155/2012/259217

Kim, S., Chen, J., Cheng, T., Gindulyte, A., He, J., He, S., Li, Q., Shoemaker, B. A., Thiessen, P. A., Yu, B., Zaslavsky, L., Zhang, J., Bolton, E. E. (2023). PubChem 2023 update. *Nucleic Acids Research*, 51(D1), D1373-D1380. https://doi.org/10.1093/nar/gkac956

McNab, H., Ferreira, E.-S.-B., Hulme, A.-N., Quye, A. (2009) Negative ion ESI-MS analysis of natural yellow dye flavonoids-An isotopic labelling study, *International Journal of Mass Spectrometry*, 284, 57-65. https://doi.org/10.1016/j.ijms.2008.05.039

Mencherini, T., Campone, L., Piccinelli, A. L., García Mesa, M., Sánchez, D. M., Aquino, R. P., & Rastrelli, L. (2013). HPLC-PDA-MS and NMR characterization of a hydroalcoholic extract of Citrus aurantium L. var. amara peel with antiedematogenic activity. *Journal of Agricultural and Food Chemistry*, 61(8), 1686-1693.https://doi.org/10.1021/jf302815t

Wang, Q., Zou, Z., Zhang, Y., Lin, P., Lan, T., Qin, Z., Xu, D., Wu, H. and Yao, Z. (2021). Characterization of chemical profile and quantification of major representative components of Wendan decoction, a classical traditional Chinese medicine formula. *Journal of Separation Science*, 44(5), 1036-1061.https://doi.org/10.1002/jssc.202000952

Zhang, L., Qin, S., Tang, S., E, S., Li, K., Li, J., Cai, W., Sun, L., Li, H. (2022). Qualitative Analysis of Multiple Phytochemical Compounds in Tojapride Based on UHPLC Q-Exactive Orbitrap Mass Spectrometry. *Molecules*, 27(19), 6639. https://doi.org/10.3390/molecules271966

**Supplementary Table 4:** Annotation propagation of flavonoids present in fractions and crude decoction extract using SIRIUS software (CSI:FingerID and ZODIAC)

| Cluster Index (CI) | [1]*m/z* | Molecular formula | Zodiac (%) | Confidence score | Similarity (%) |
|---|---|---|---|---|---|
| 7312 | 651.1921 | $C30H_{34}O_{16}$ | 99.85 | 0.724 | 82.63 |
| 8093 | 609.1817 | $C_{28}H_{32}O_{15}$ | 100 | 0.937 | 87.42 |
| 5021 | 553.1558 | $C_{25}H_{28}O_{14}$ | 100 | 0.541 | 94.93 |
| 5165 | 567.1713 | $C_{26}H_{30}O_{14}$ | 100 | 0.431 | 93.30 |
| 8296 | 667.1870 | $C_{30}H_{34}O_{17}$ | 100 | 0.309 | 88.38 |
| 8306 | 539.1400 | $C_{24}H_{26}O_{14}$ | 100 | 0.274 | 93.58 |
| 8550 | 539.1402 | $C_{24}H_{26}O_{14}$ | 100 | 0.276 | 93.06 |
| [TS]8126 | 683.1819 | $C_{30}H_{34}O_{18}$ | 100 | 0.362 | 74.73 |
| 8446 | 623.1609 | $C_{28}H_{30}O_{16}$ | 100 | 0.331 | 95.05 |
| 6225 | 405.1183 | $C_{20}H_{20}O_9$ | 100 | 0.096 | 96.34 |
| 1347 | 431.1342 | $C_{22}H_{22}O_9$ | 99.47 | 0.320 | 80.14 |
| 4855 | 389.1232 | $C_{20}H_{20}O_8$ | 100 | 0.199 | 94.55 |

*1 – $[M+H]^+$
**TS – Training Set
Source: Author's own.

**Supplementary Table 5:** Annotation propagation of coumarins present in fractions and crude decoction extract using SIRIUS software (CSI:FingerID and ZODIAC)

| Cluster Index (CI) | [1]*m/z* | Molecular formula | Zodiac (%) | Confidence score | Similarity (%) |
|---|---|---|---|---|---|
| 1627 | 333.1698 | $C_{19}H_{24}O_5$ | 100 | 0.450 | 89.75 |
| 2868 | 361.1647 | $C_{20}H_{24}O_6$ | 100 | 0.597 | 82.49 |
| 1608 | 375.1805 | $C_{21}H_{26}O_6$ | 100 | 0.817 | 70.43 |
| 5332 | 249.1121 | $C_{14}H_{16}O_4$ | 100 | 0.183 | 74.60 |
| 6449 | 307.1178 | $C_{16}H_{18}O_6$ | 100 | 0.326 | 77.23 |
| 1190 | 291.1230 | $C_{16}H_{18}O_5$ | 100 | 0.224 | 83.87 |
| 8379 | 571.2026 | $C_{26}H_{34}O_{14}$ | 100 | 0.458 | 91.03 |
| [TS]1329 | 355.1542 | $C_{21}H_{22}O_5$ | 100 | 0.198 | 87.46 |
| 5013 | 371.1492 | $C_{21}H_{22}O_6$ | 100 | 0.361 | 78.80 |
| [TS]5049 | 389.5970 | $C_{21}H_{24}O_7$ | 100 | 0.546 | 80.47 |
| [TS]1455 | 203.0341 | $C_{11}H_6O_4$ | 100 | 0.300 | 98.98 |

*1 – $[M+H]^+$
**TS – Training Set
Source: Author's own.

## Figures

**Supplementary Figure 1:** Figure (**A**) and (**B**). Antifungal assay of extract (CDE) and fractions (FR1-FR5) of *C. aurantium* decoction against *Fusarium jinanense* (UFCM-0611) at concentrations of 50, 100, and 150 ppm

**A**

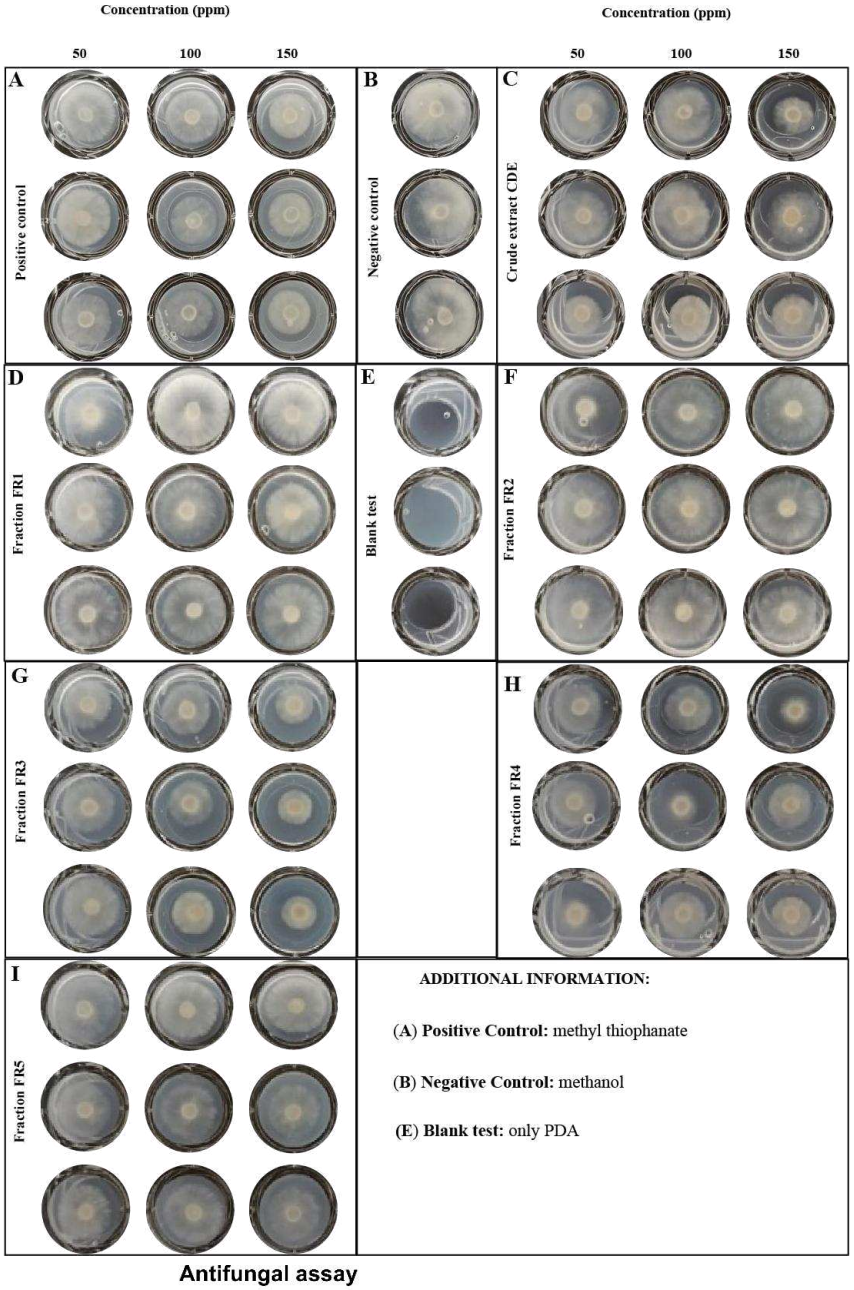


**B**

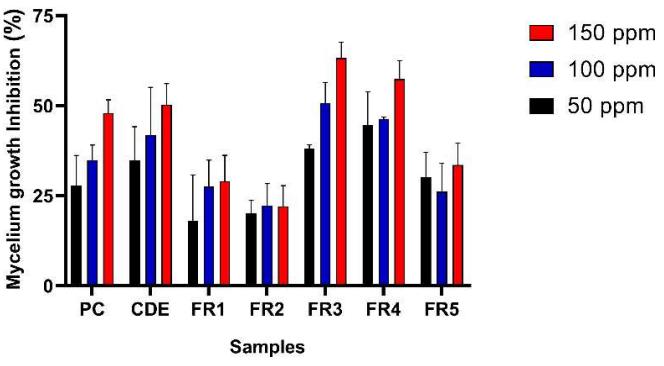


Source: Author's own.

**Supplementary Figure 2:** Molecular families and self-loop nodes obtained from the Feature- Based Molecular Networking workflow. The pie chart legend shows that the colors of the different nodes represent the sample groups

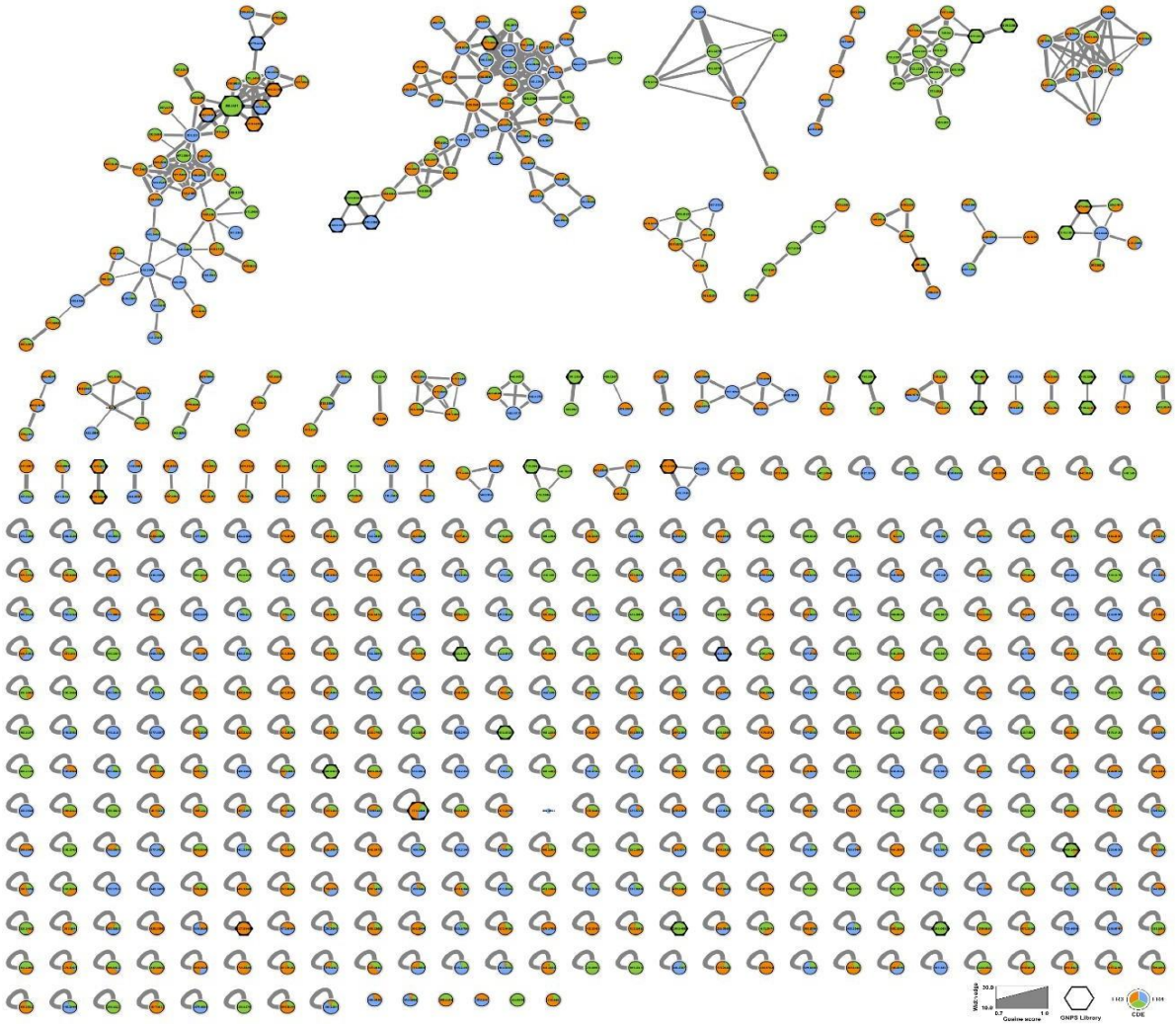

Source: Author's own.

**Supplementary Figure 3:** Spectral match obtained by comparison with GNPS library for compound (**1**)

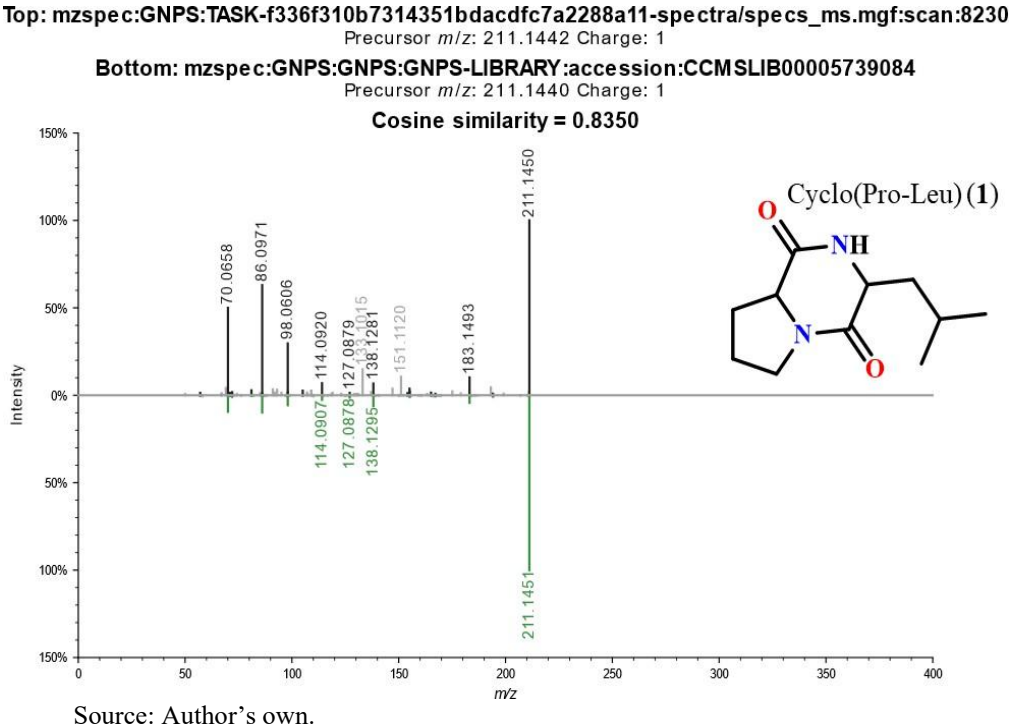


Source: Author's own.

**Supplementary Figure 4:** (+)- ESI MS/MS spectrum of the compound (**2**)

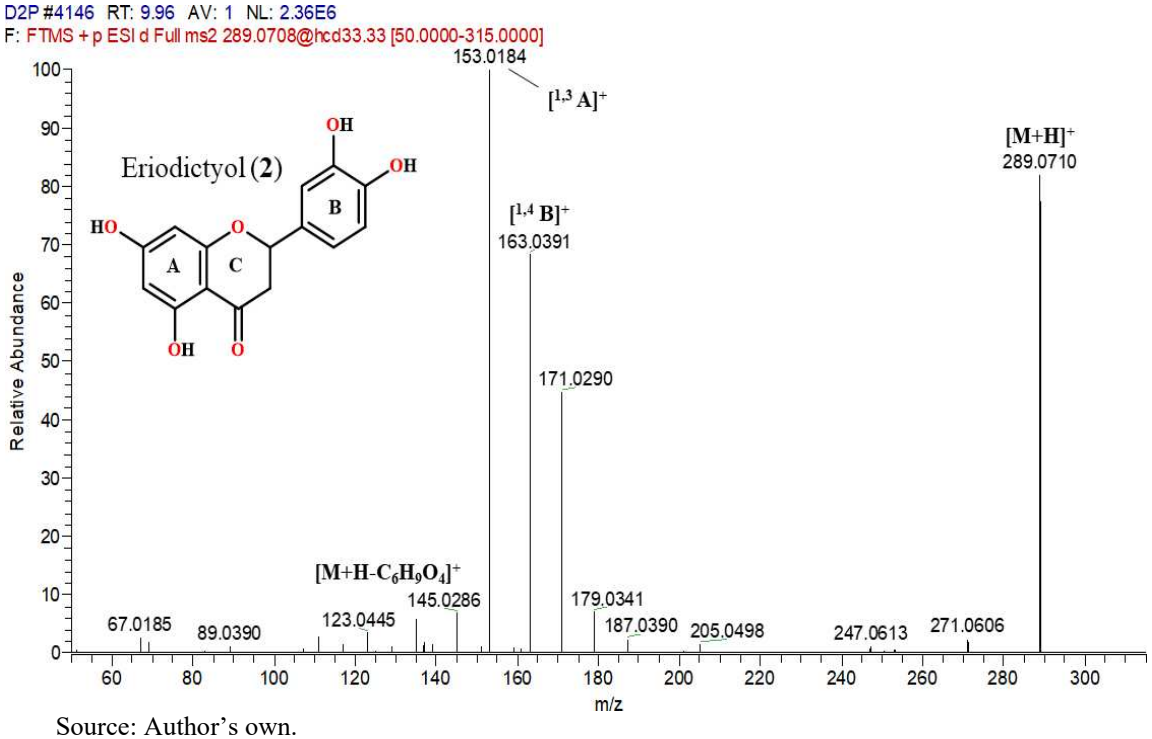


Source: Author's own.

**Supplementary Figure 5:** (-)- ESI MS/MS spectrum of the compound (**2**)

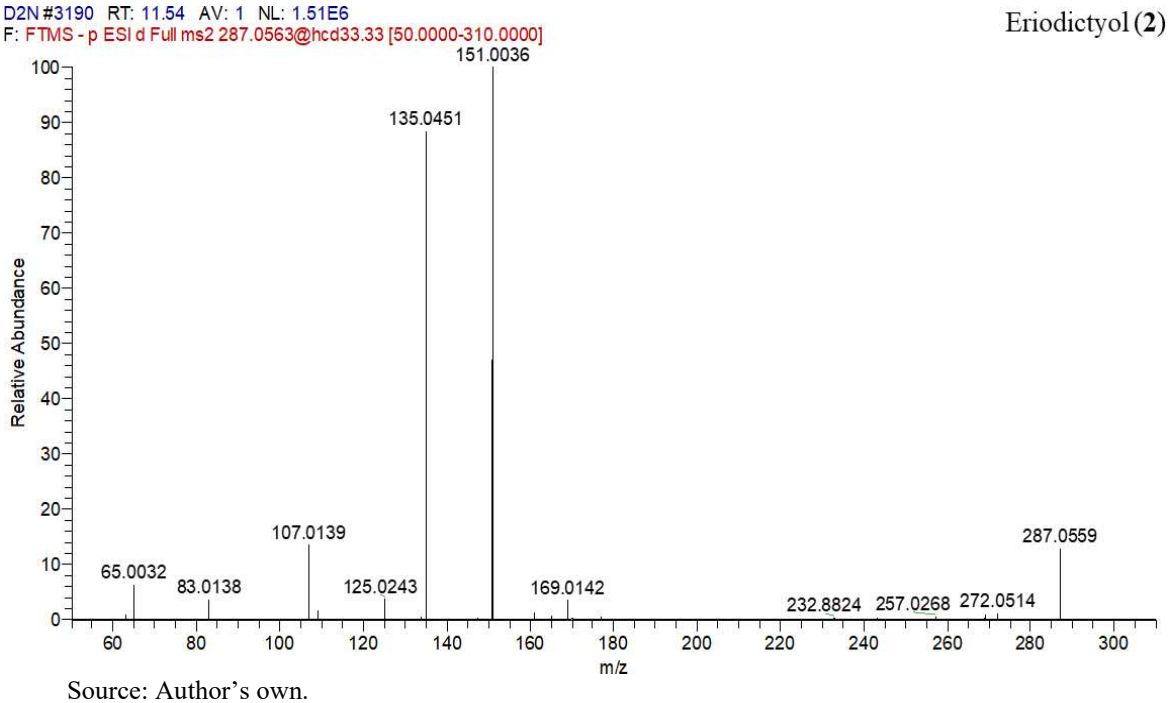


Source: Author's own.

**Supplementary Figure 6:** Spectral match obtained by comparison with GNPS library for compound (**3**)

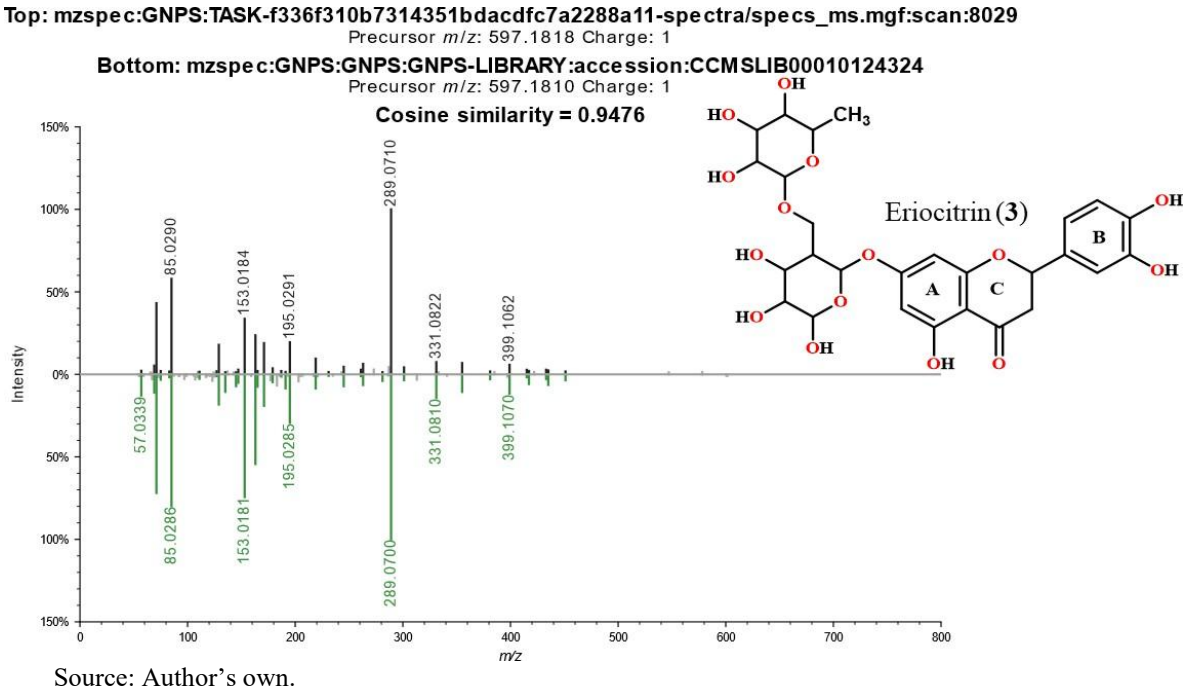


Source: Author's own.

**Supplementary Figure 7:** Spectral match obtained by comparison with GNPS library for compound (4)

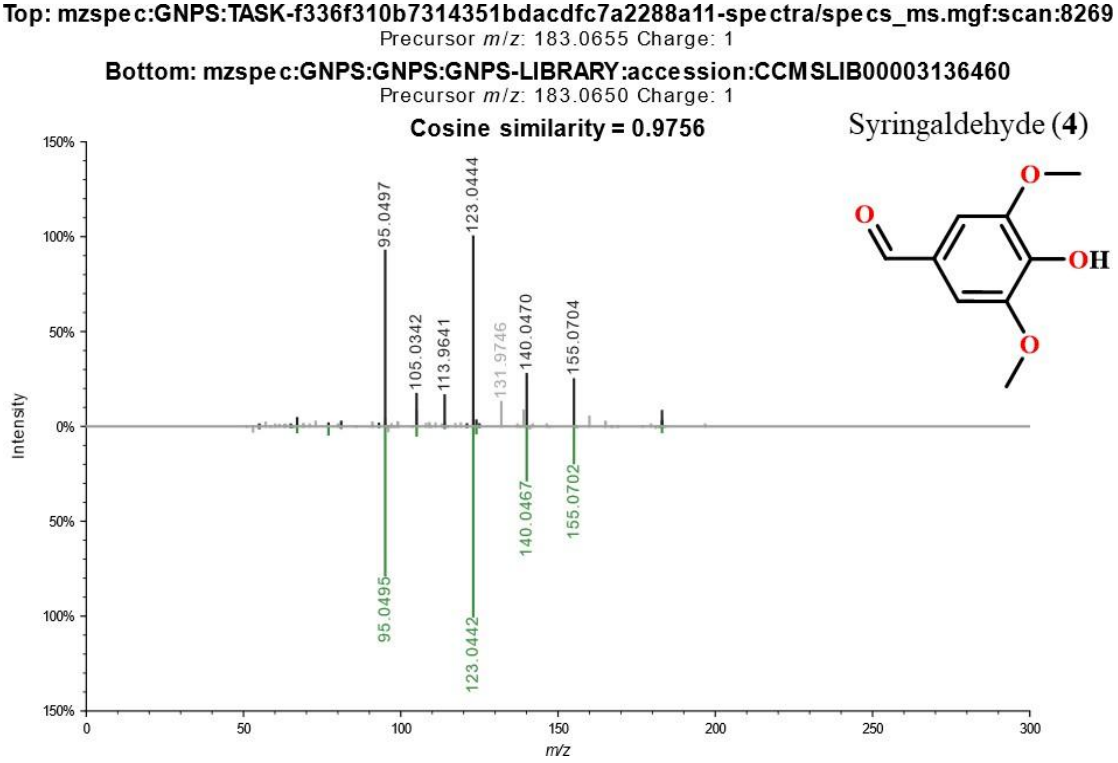


Source: Author's own.

**Supplementary Figure 8:** Spectral match obtained by comparison with GNPS library for compound (**5**)

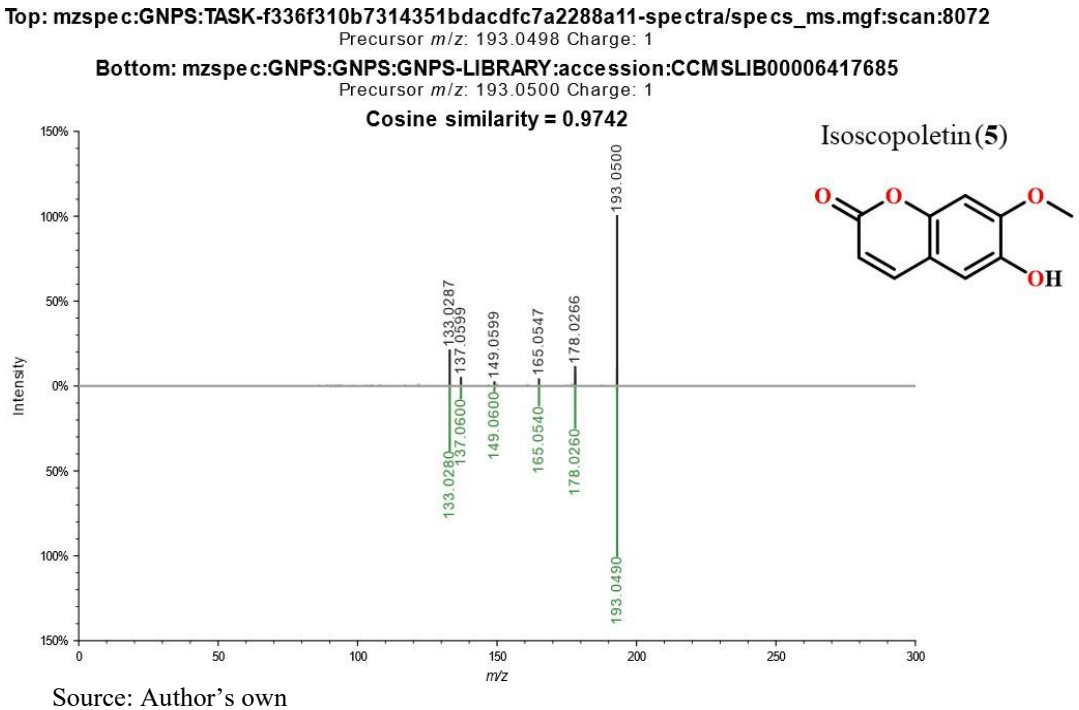


Source: Author's own

**Supplementary Figure 9:** Base peak chromatograms (BPCs) present in the fractions of *Citrus aurantium* compared to the standard naringin (**6**)

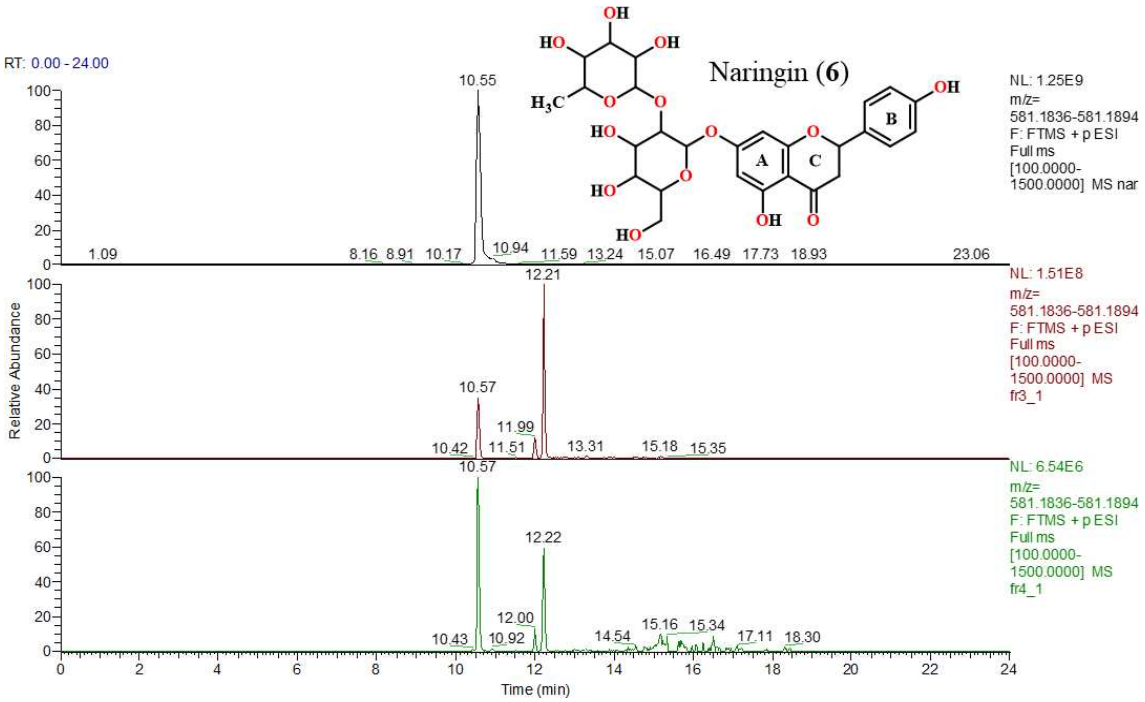


Source: Author's own.

**Supplementary Figure 10:** (+)- ESI MS/MS spectra for naringin (**6**) present in the crude extract and fractions of *Citrus aurantium* decoction compared to a standard

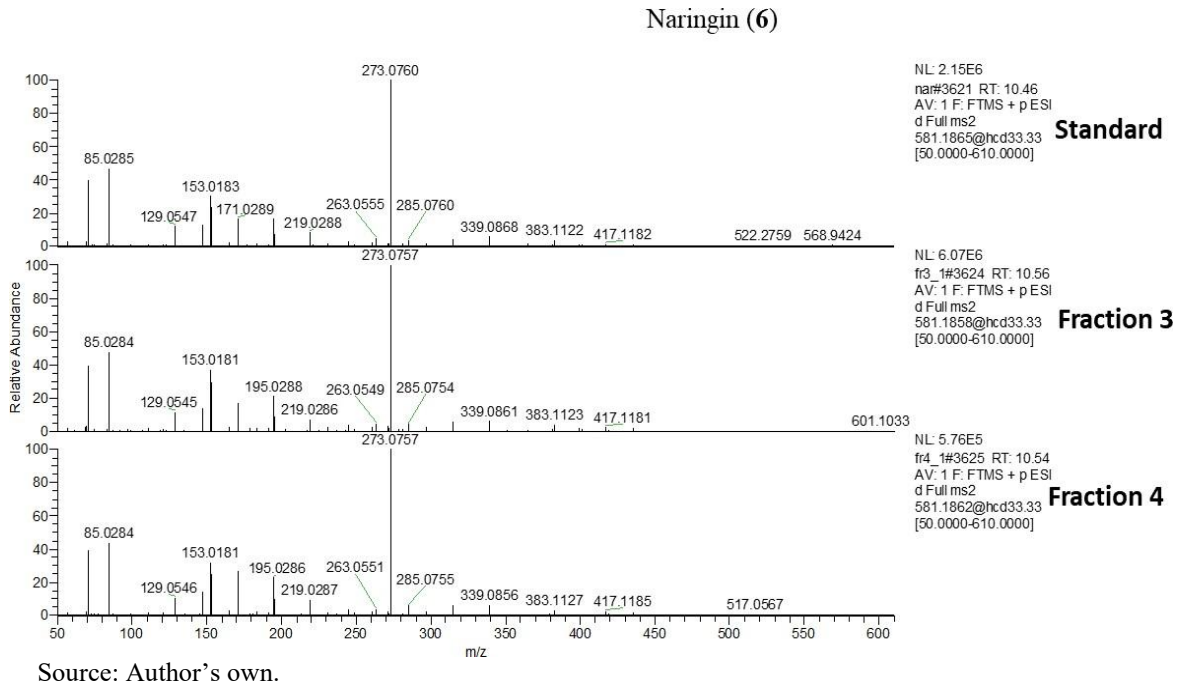


Source: Author's own.

**Supplementary Figure 11:** (+)- ESI MS/MS spectrum of the compound (**6**)

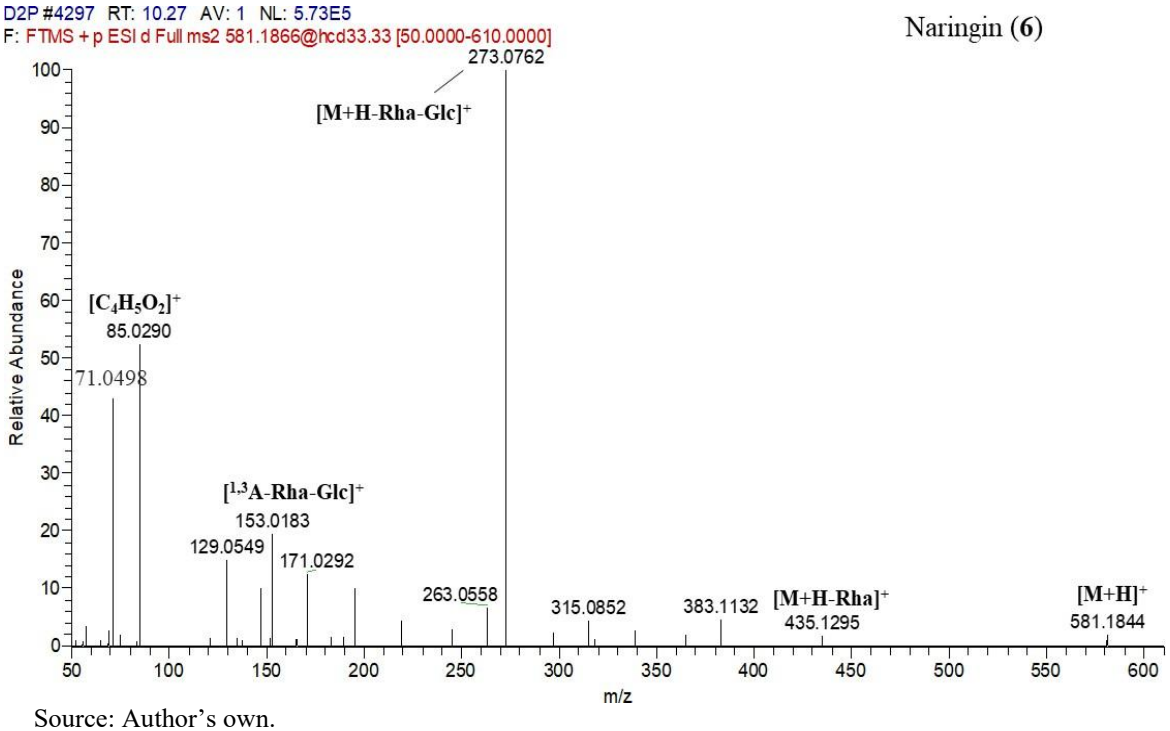


Source: Author's own.

**Supplementary Figure 12:** Spectral match obtained by comparison with GNPS library for compound (**7**)

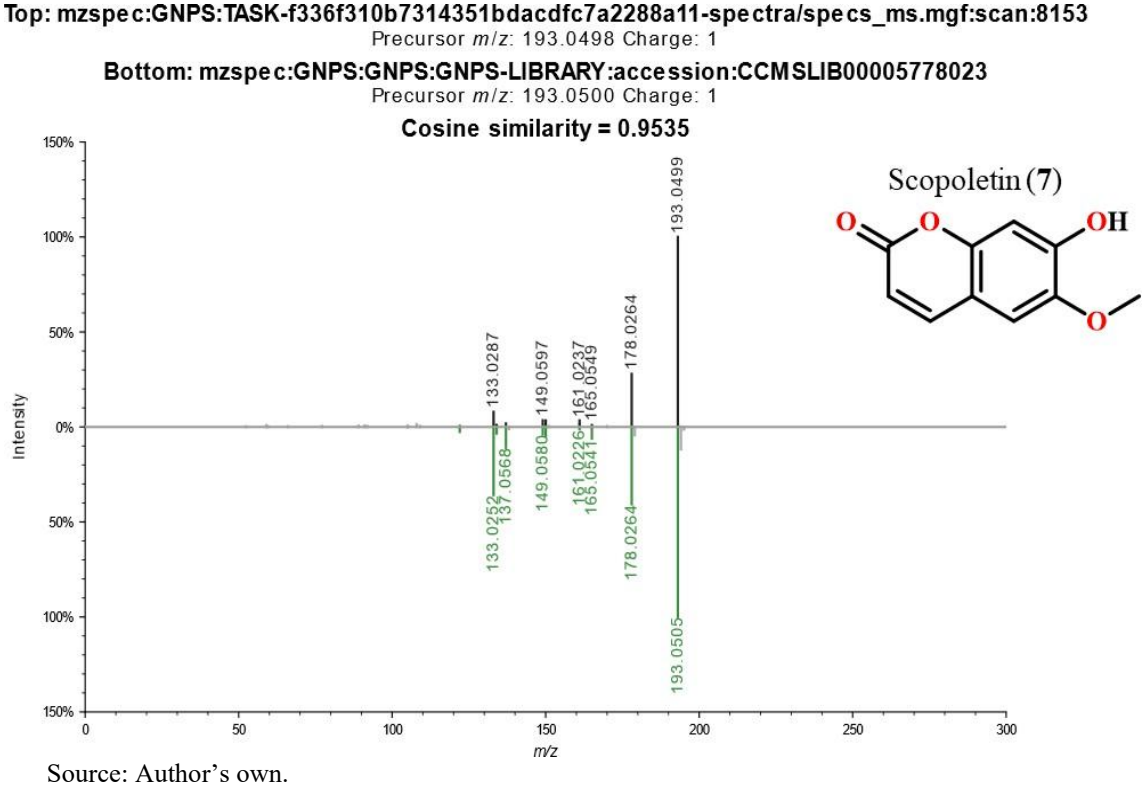


Source: Author's own.

**Supplementary Figure 13:** (+)- ESI MS/MS spectrum of the compound (**8**)

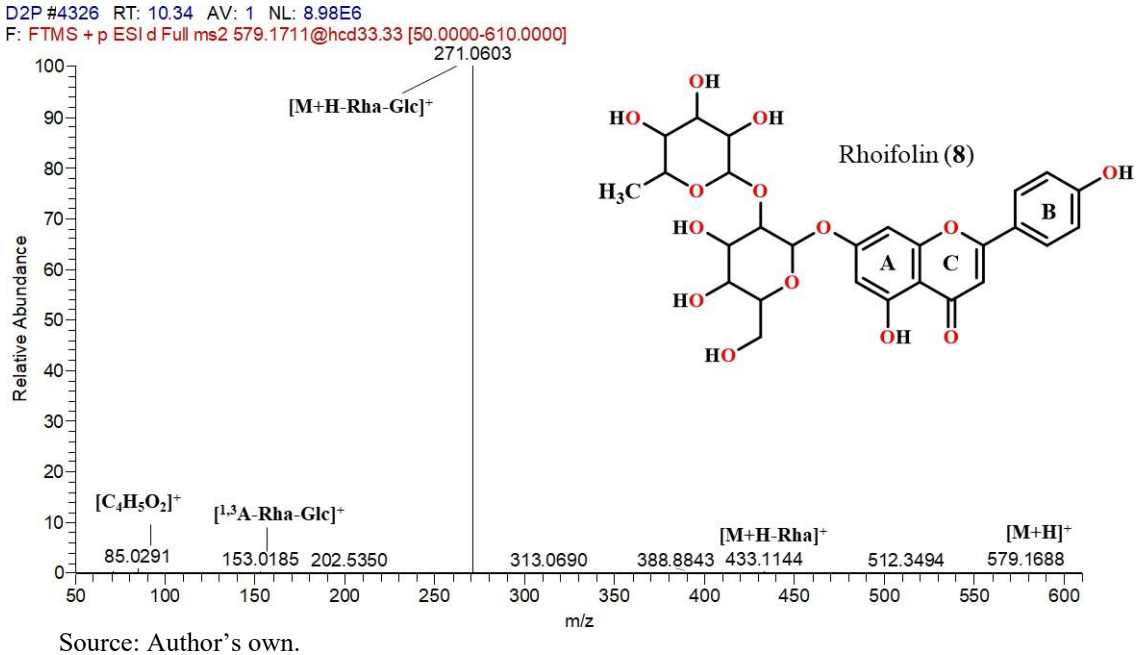


Source: Author's own.

**Supplementary Figure 14.** (-)- ESI MS/MS spectrum of the compound (**8**)

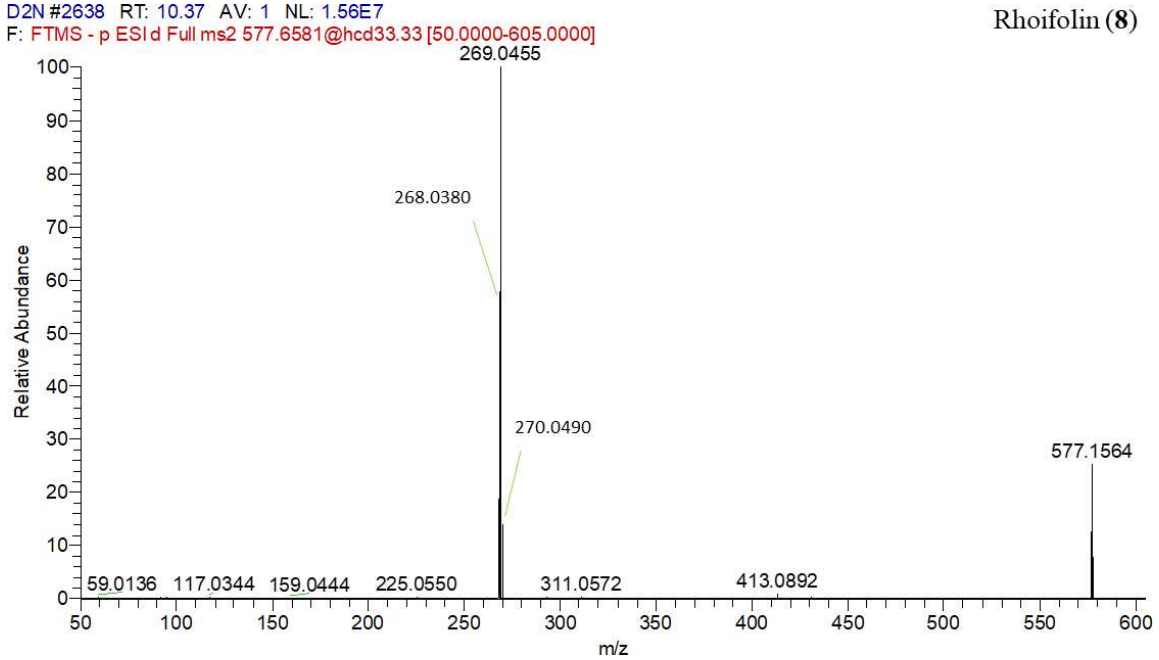


Source: Author's own.

**Supplementary Figure 15:** (+)- ESI MS/MS spectrum of the compound (**9**)

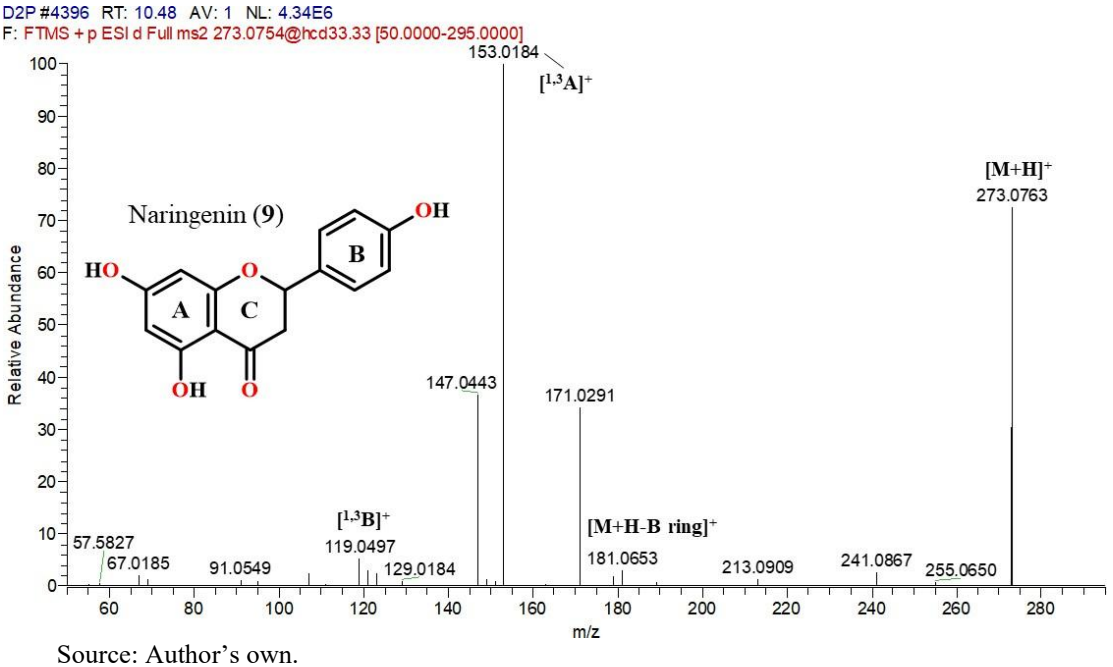


Source: Author's own.

**Supplementary Figure 16:** (-)- ESI MS/MS spectrum of the compound (**9**)

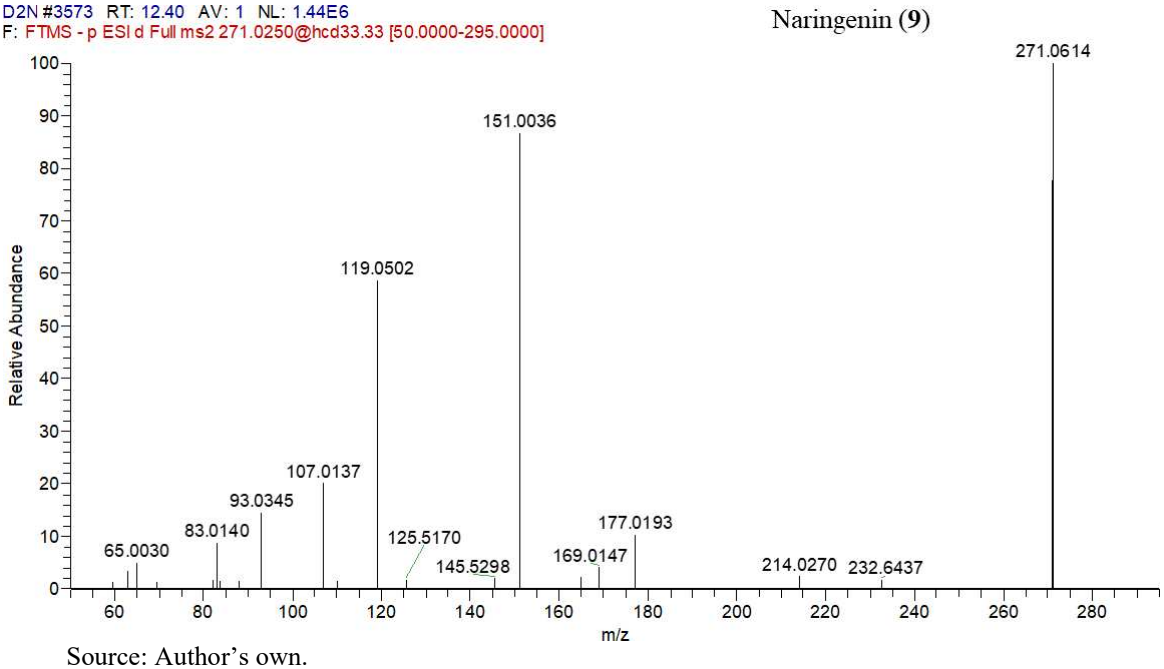


Source: Author's own.

**Supplementary Figure 17:** (+)- ESI MS/MS spectrum of the compound (**10**)

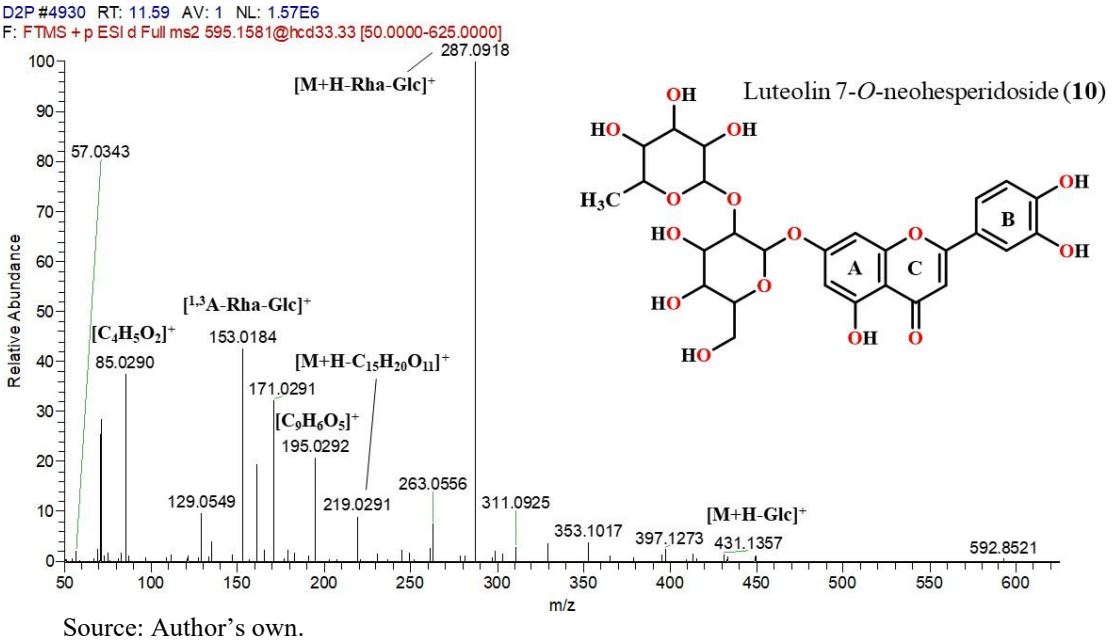


Source: Author's own.

**Supplementary Figure 18:** (-)- ESI MS/MS spectrum of the compound (**10**)

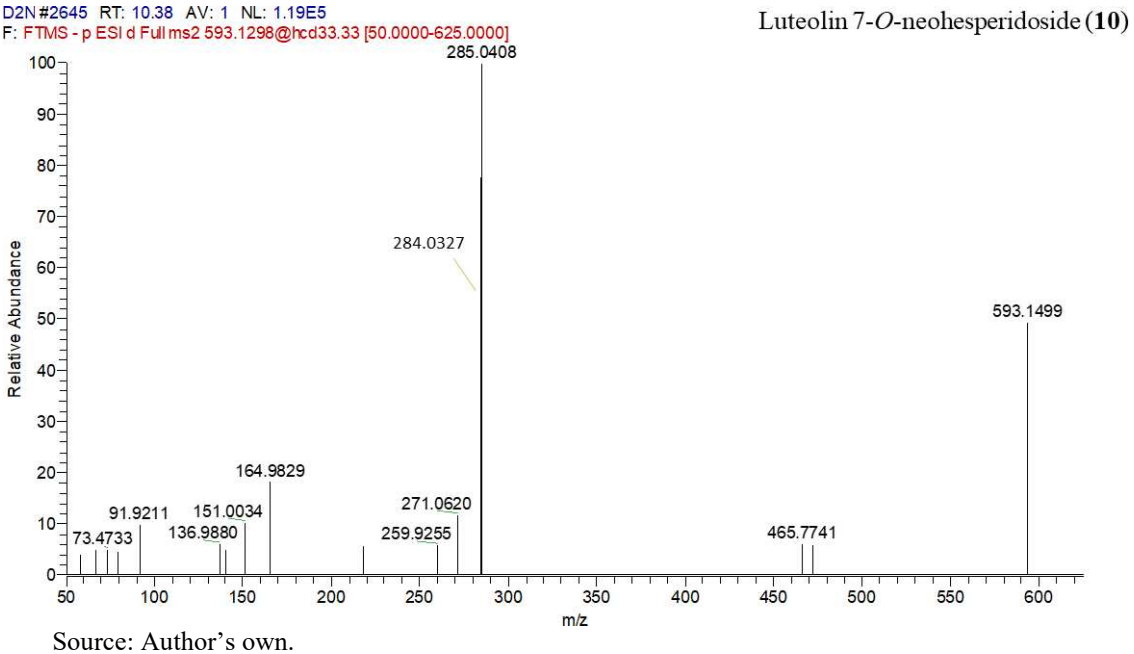


Source: Author's own.

**Supplementary Figure 19:** Spectral match obtained by comparison with GNPS library for compound (**11**)

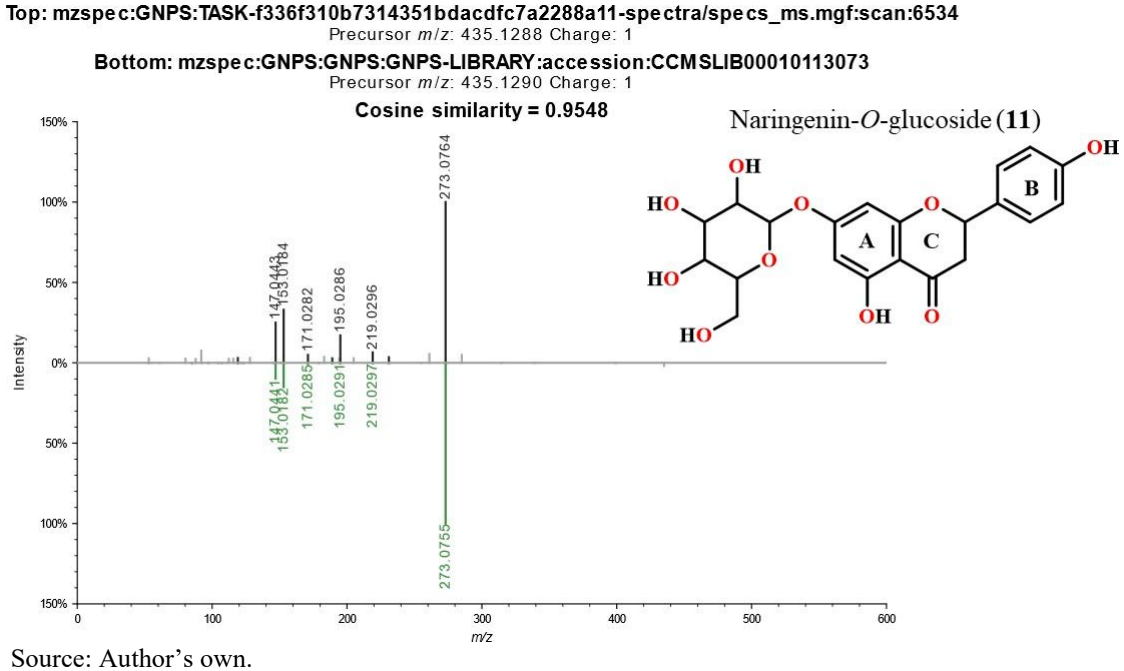


Source: Author's own.

**Supplementary Figure 20:** (+)- ESI MS/MS spectrum of the compound (**11**)

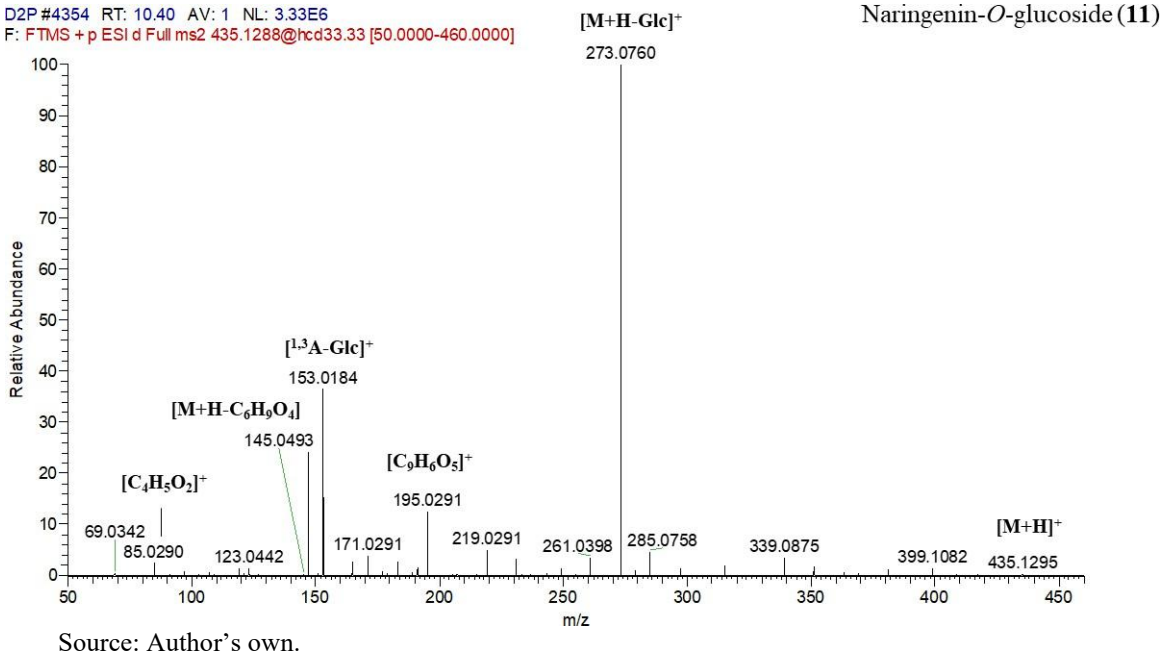


Source: Author's own.

**Supplementary Figure 21:** Spectral match obtained by comparison with GNPS library for compound (**12**)

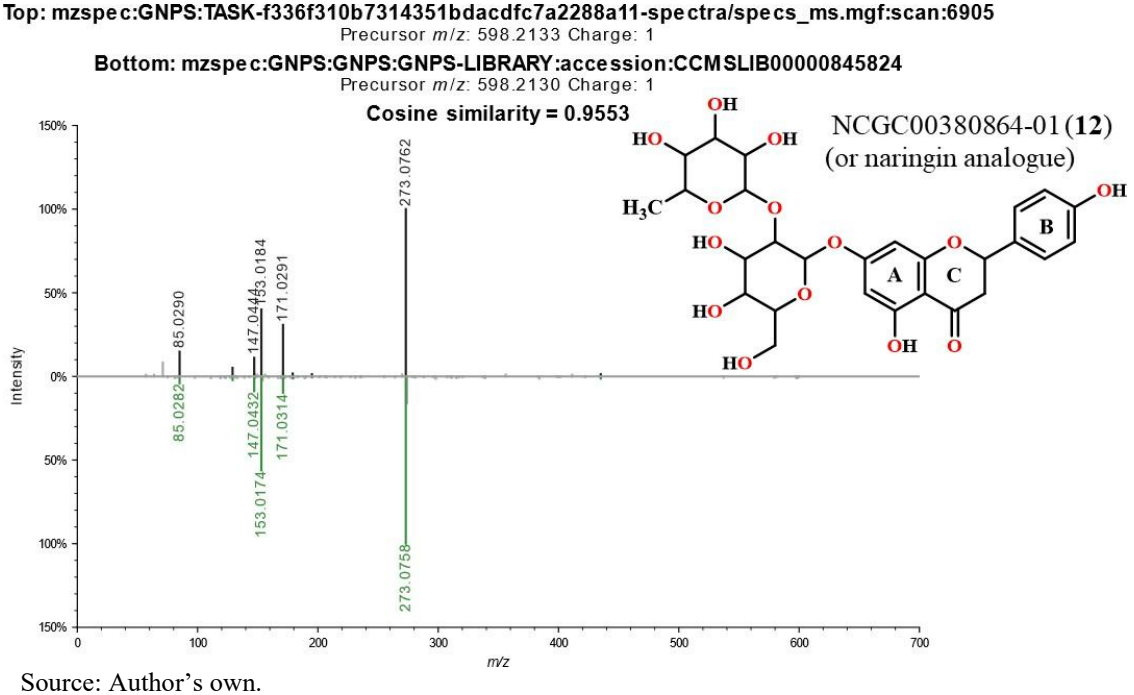


Source: Author's own.

**Supplementary Figure 22:** Spectral match obtained by comparison with GNPS library for compound (**13**)

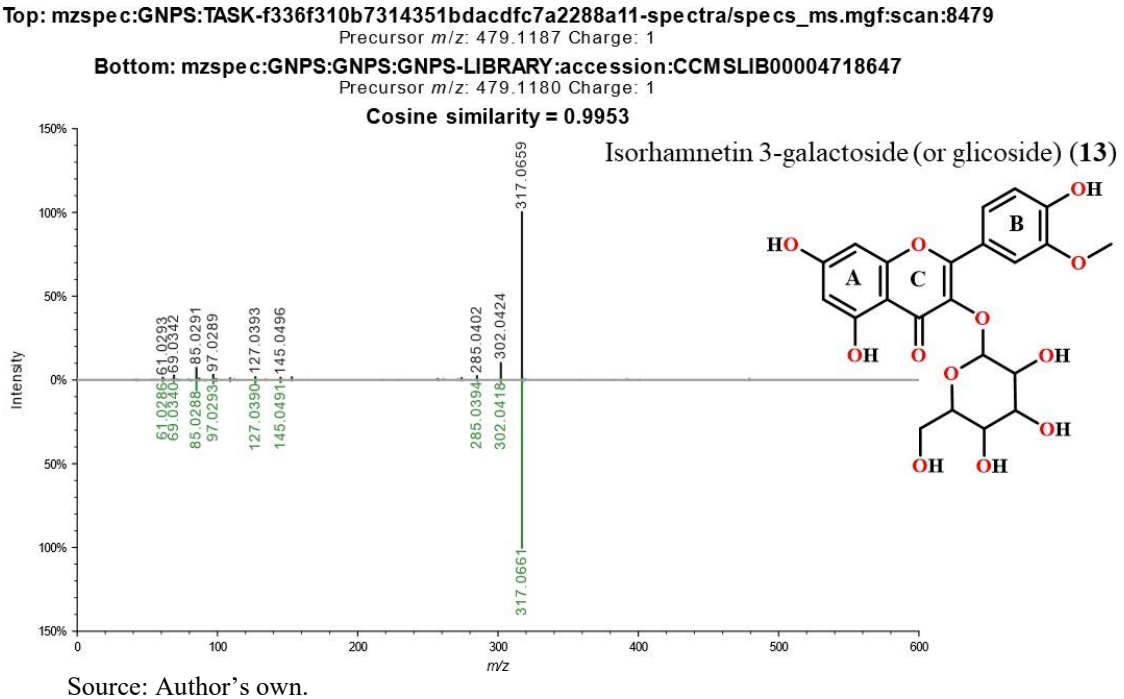


Source: Author's own.

**Supplementary Figure 23:** Spectral match obtained by comparison with GNPS library for compound (**14**)

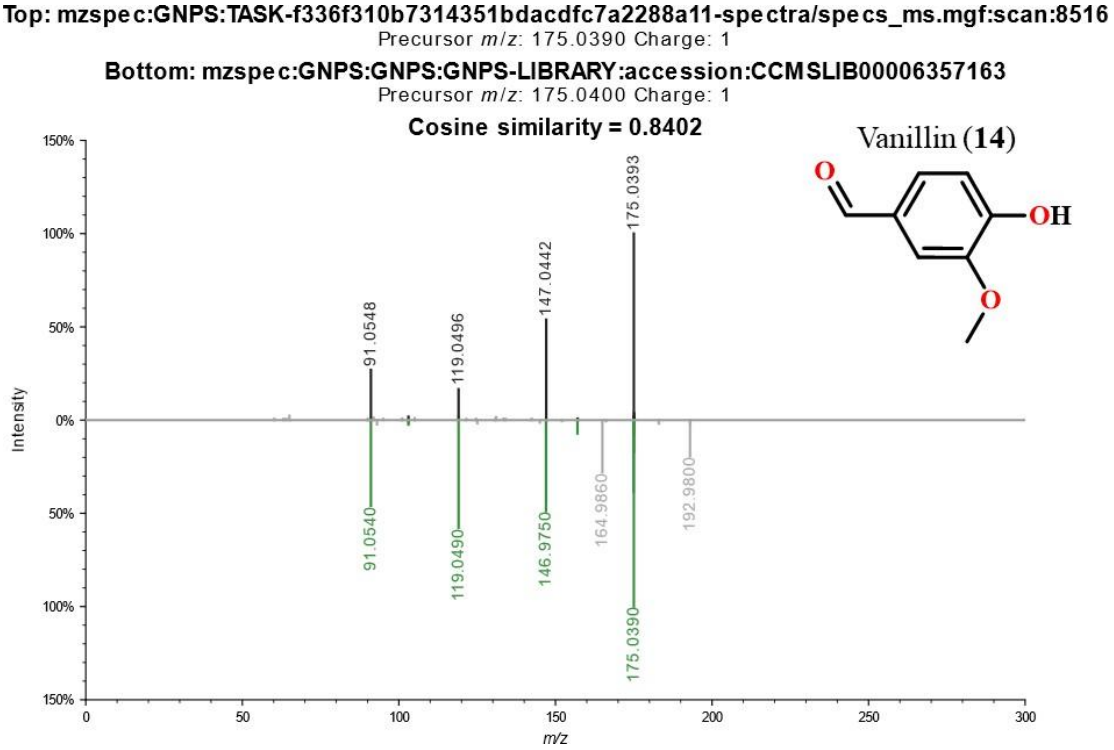


Source: Author's own.

**Supplementary Figure 24:** Spectral match obtained by comparison with GNPS library for compound (**15**)

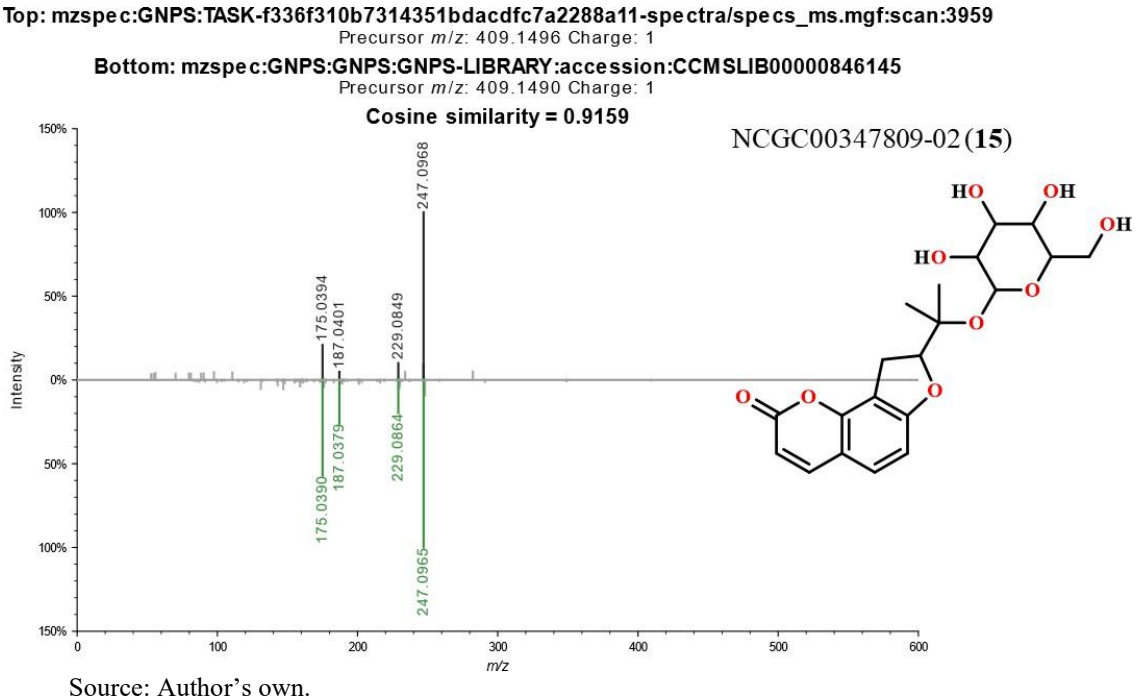


Source: Author's own.

**Supplementary Figure 25:** Base peak chromatograms (BPCs) present in the fractions of *Citrus aurantium* compared to the standard hesperidin (**16**)

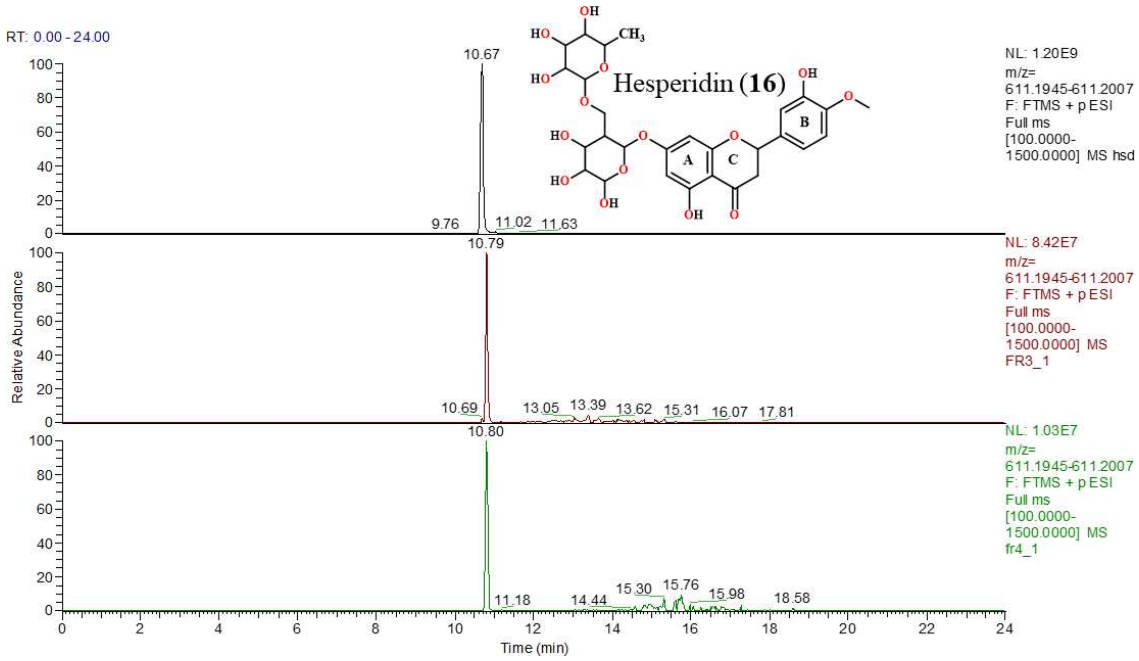


Source: Author's own.

**Supplementary Figure 26:** (+)- ESI MS/MS spectra for hesperidin (**16**) present in the crude extract and fractions of *Citrus aurantium* decoction compared to a standard

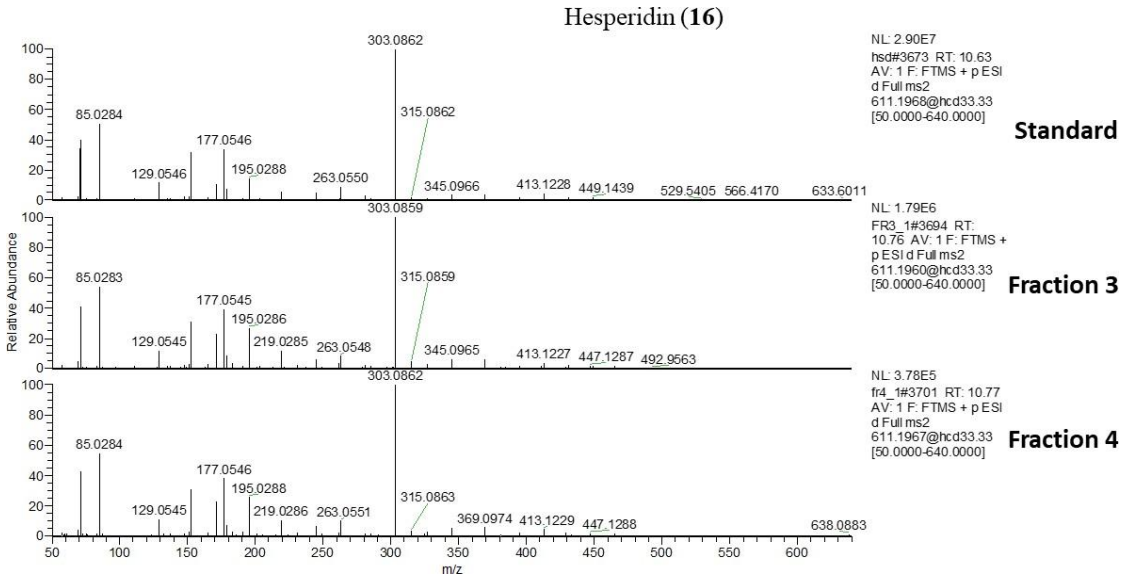


Source: Author's own.

**Supplementary Figure 27:** (+)- ESI MS/MS spectrum of the compound (**16**)

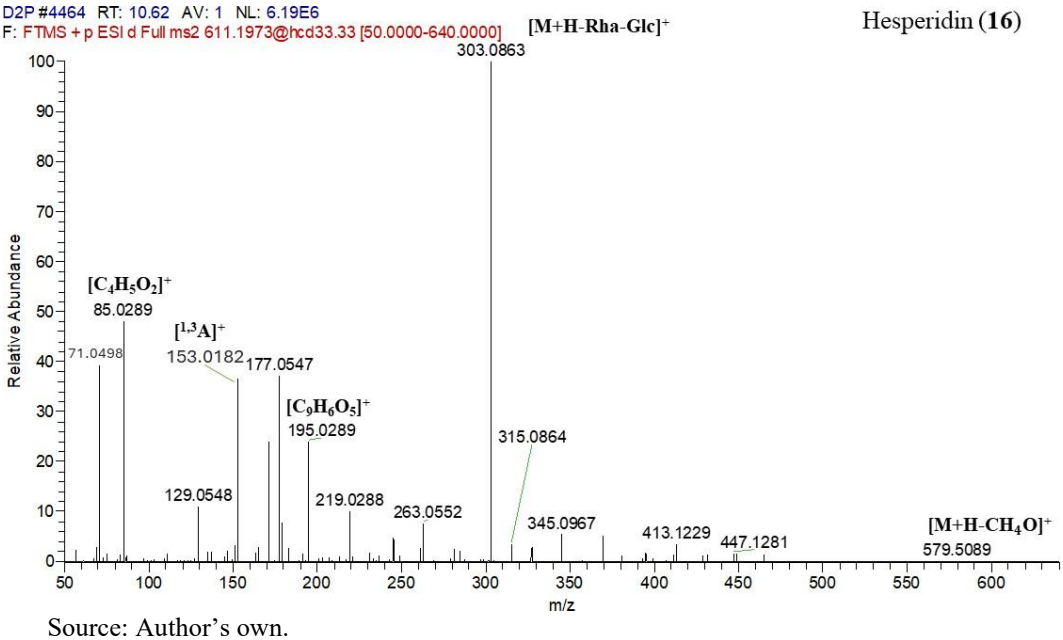


Source: Author's own.

**Supplementary Figure 28:** (+)- ESI MS/MS spectrum of the compound (**17**)

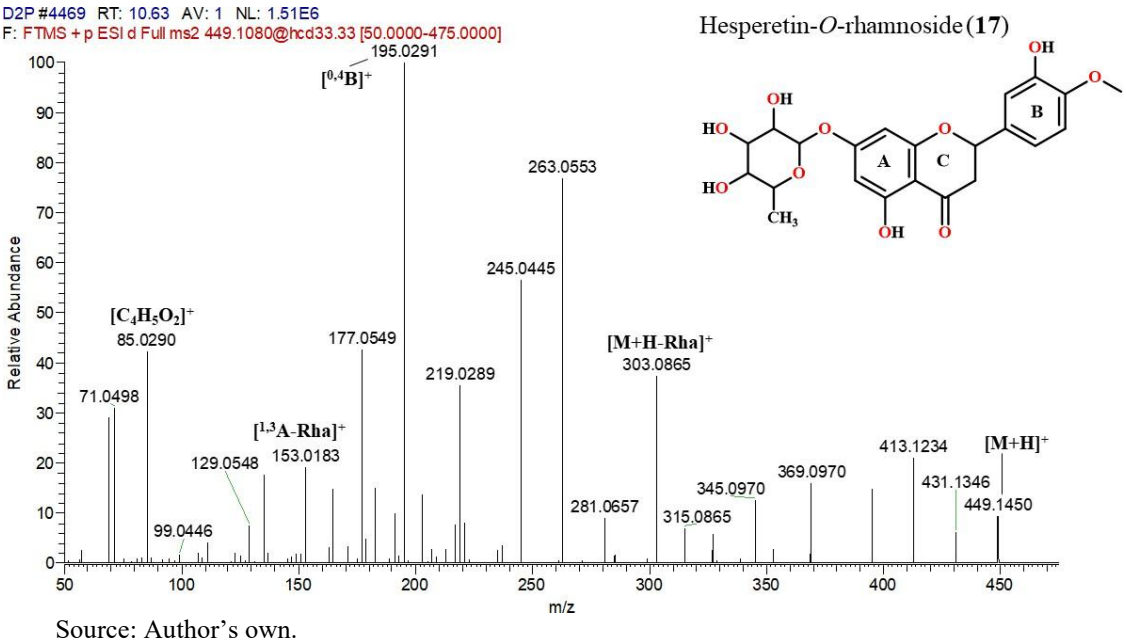


Source: Author's own.

**Supplementary Figure 29:** (+)- ESI MS/MS spectrum of the compound (**18**)

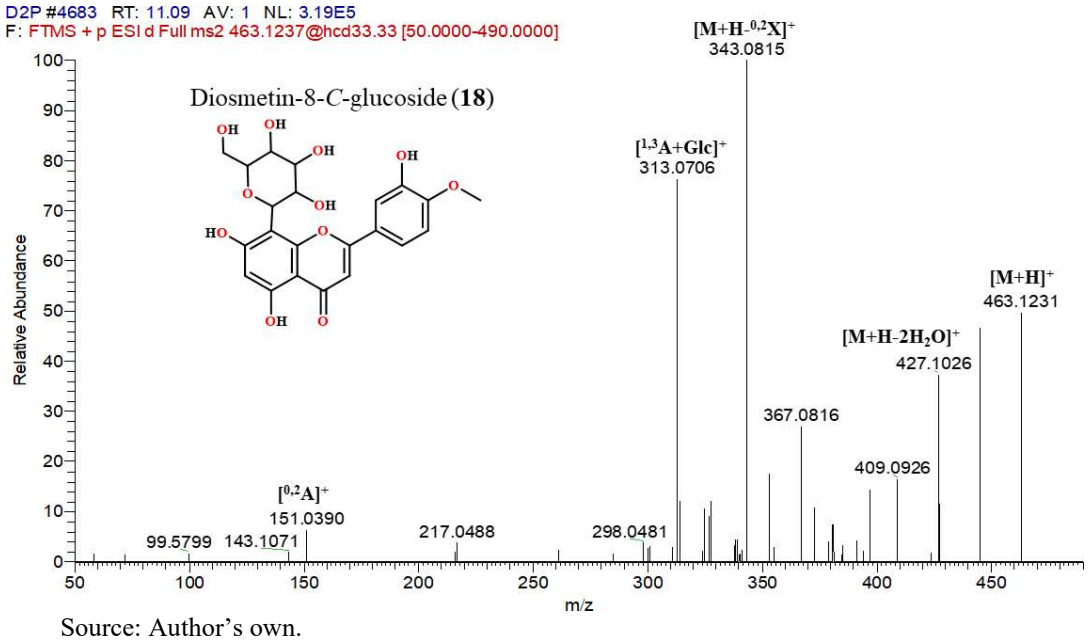


Source: Author's own.

**Supplementary Figure 30:** (-)- ESI MS/MS spectrum of the compound (**18**)

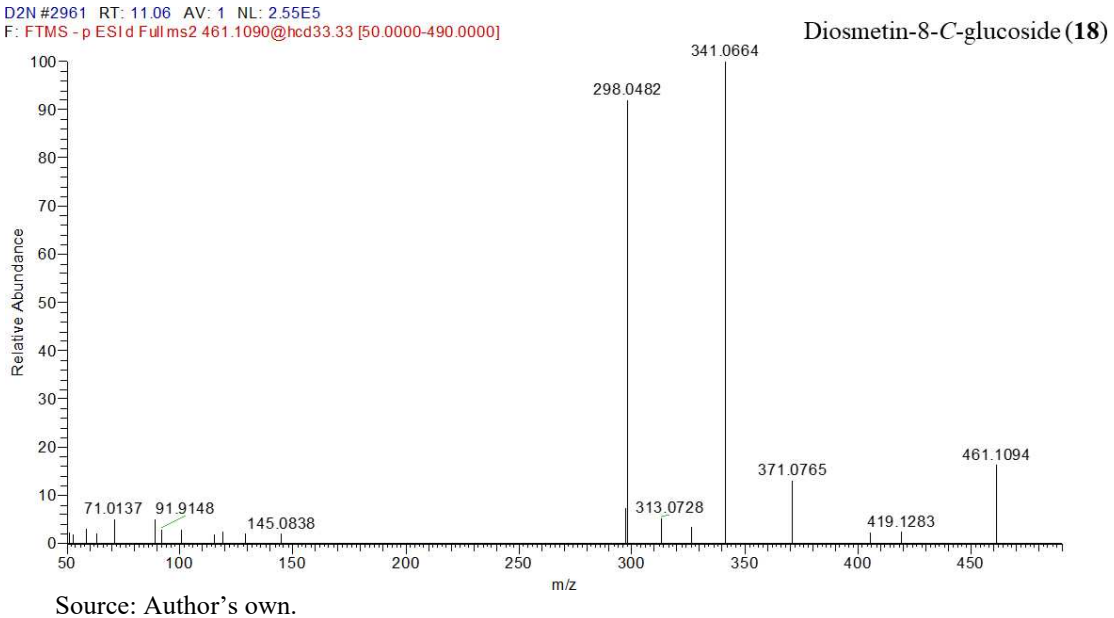


Source: Author's own.

**Supplementary Figure 31:** Spectral match obtained by comparison with GNPS library for compound (**19**)

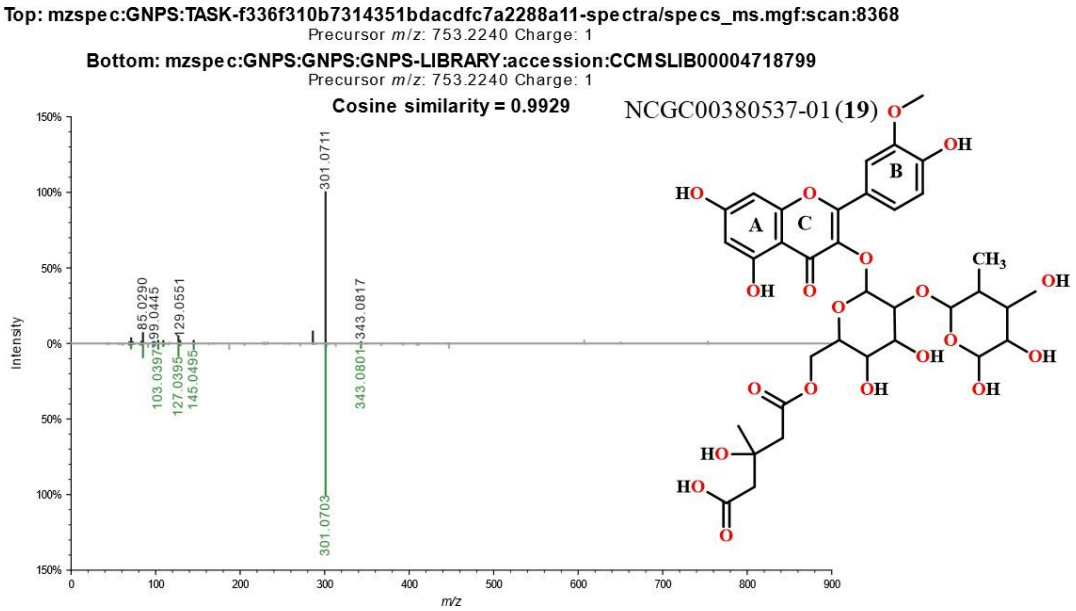


Source: Author's own.

**Supplementary Figure 32:** Spectral match obtained by comparison with GNPS library for compound (**20**)

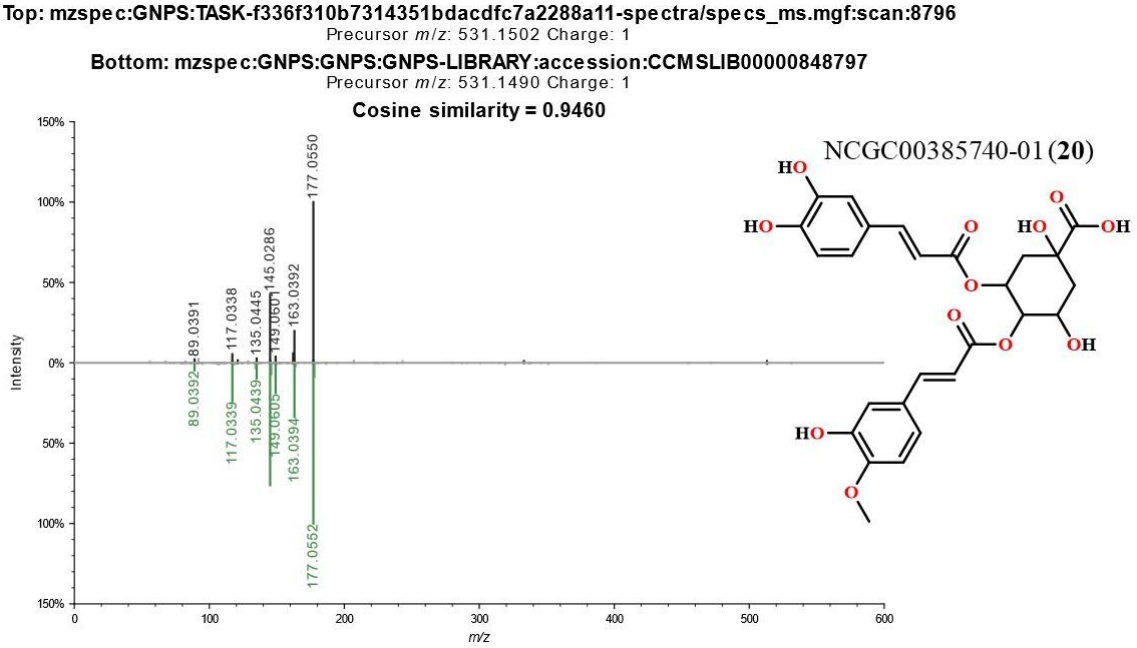


Source: Author's own.

**Supplementary Figure 33:** Spectral match obtained by comparison with GNPS library for compound (**21**)

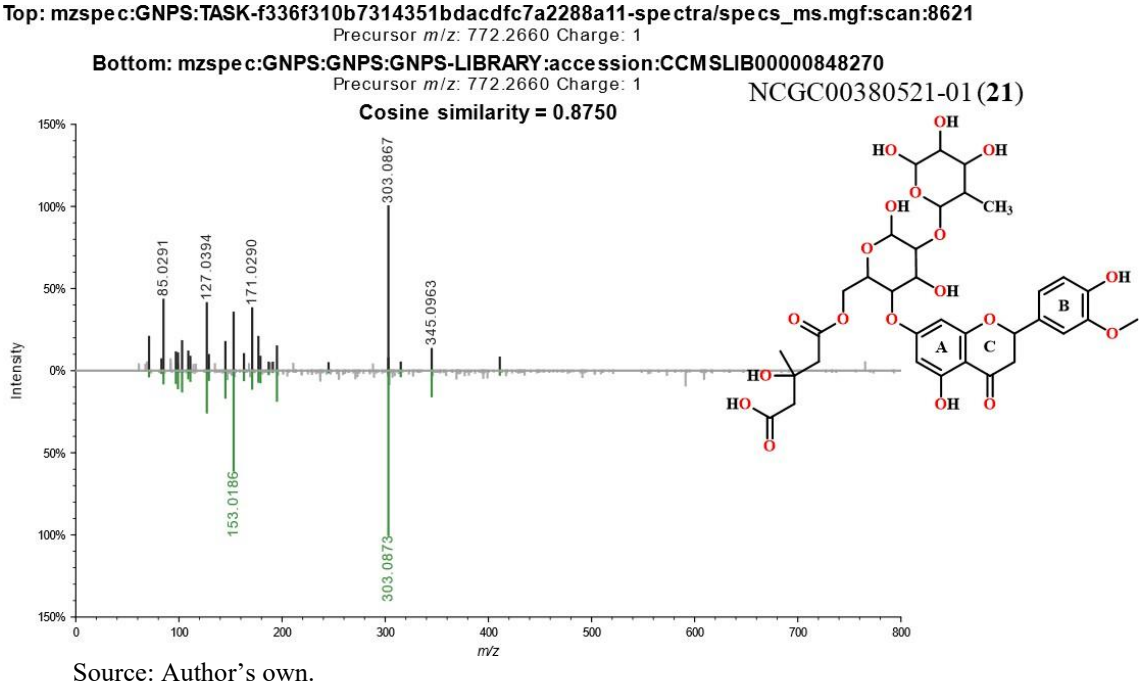


Source: Author's own.

**Supplementary Figure 34:** Spectral match obtained by comparison with GNPS library for compound **22**)

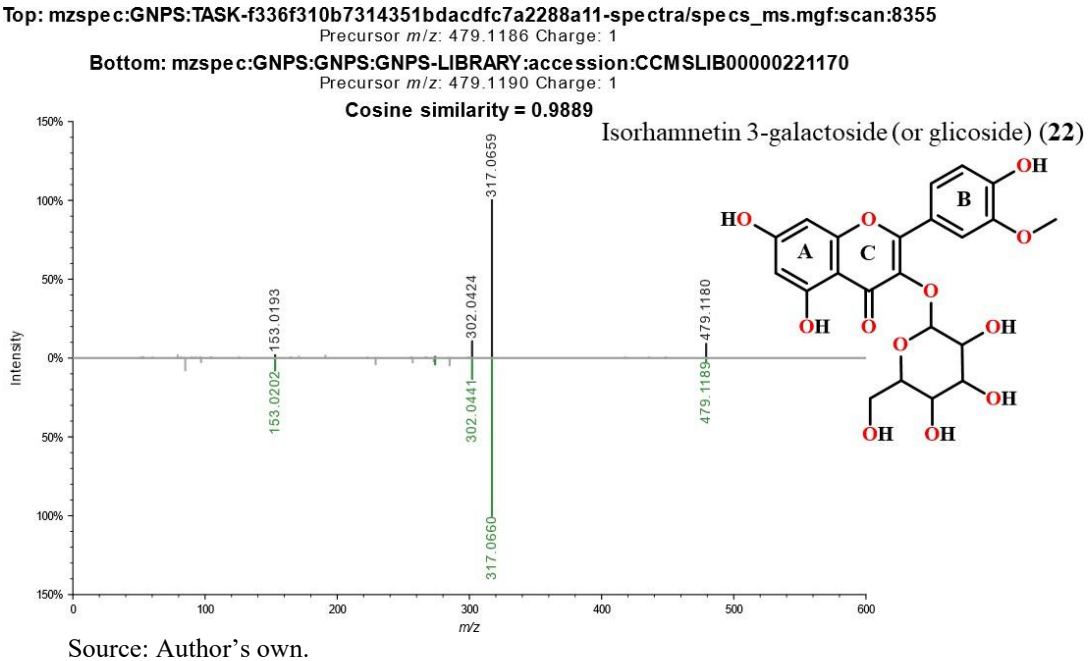


Source: Author's own.

**Supplementary Figure 35:** Spectral match obtained by comparison with GNPS library for compound (**23**)

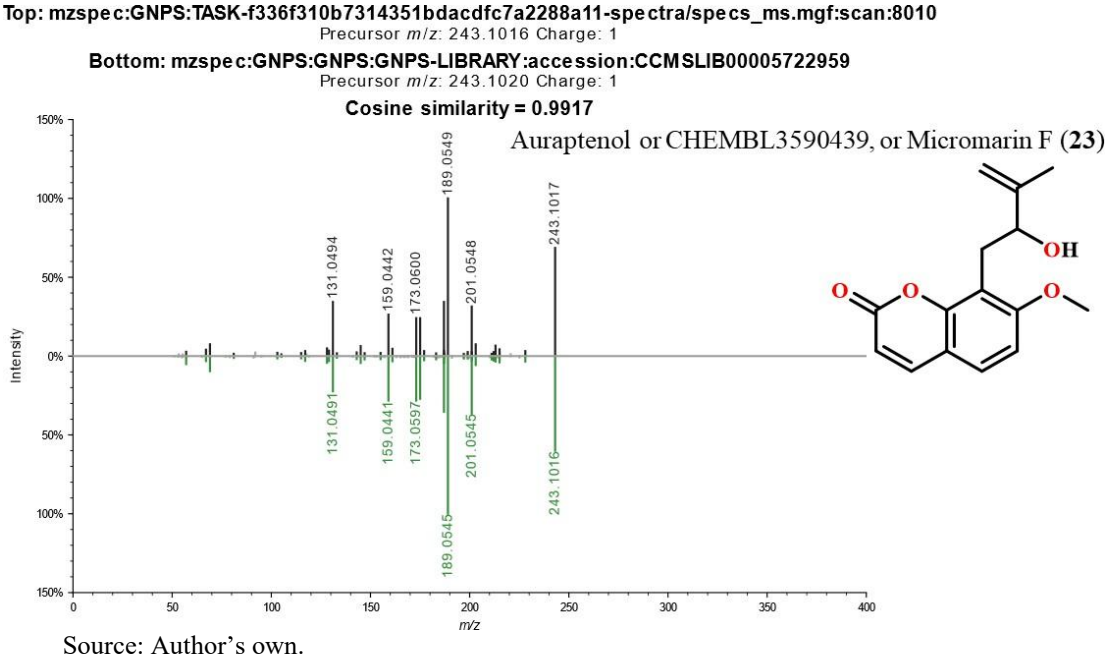


Source: Author's own.

**Supplementary Figure 36:** Spectral match obtained by comparison with GNPS library for compound (**24**)

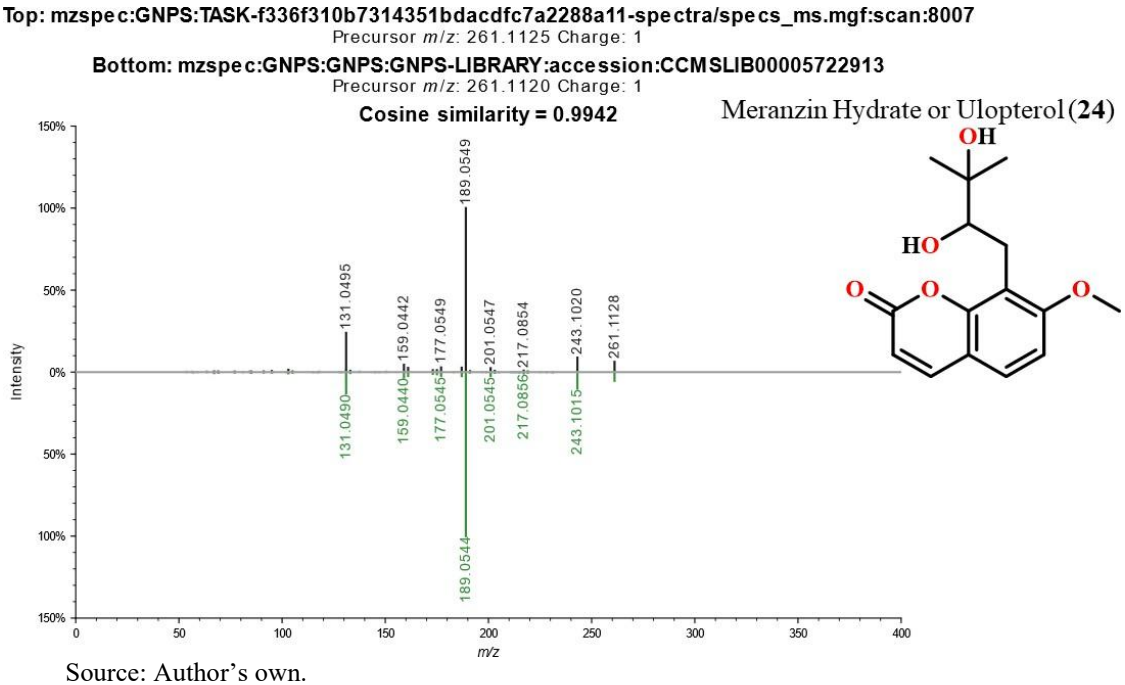


Source: Author's own.

**Supplementary Figure 37:** (+)- ESI MS/MS spectrum of the compound (**25**)

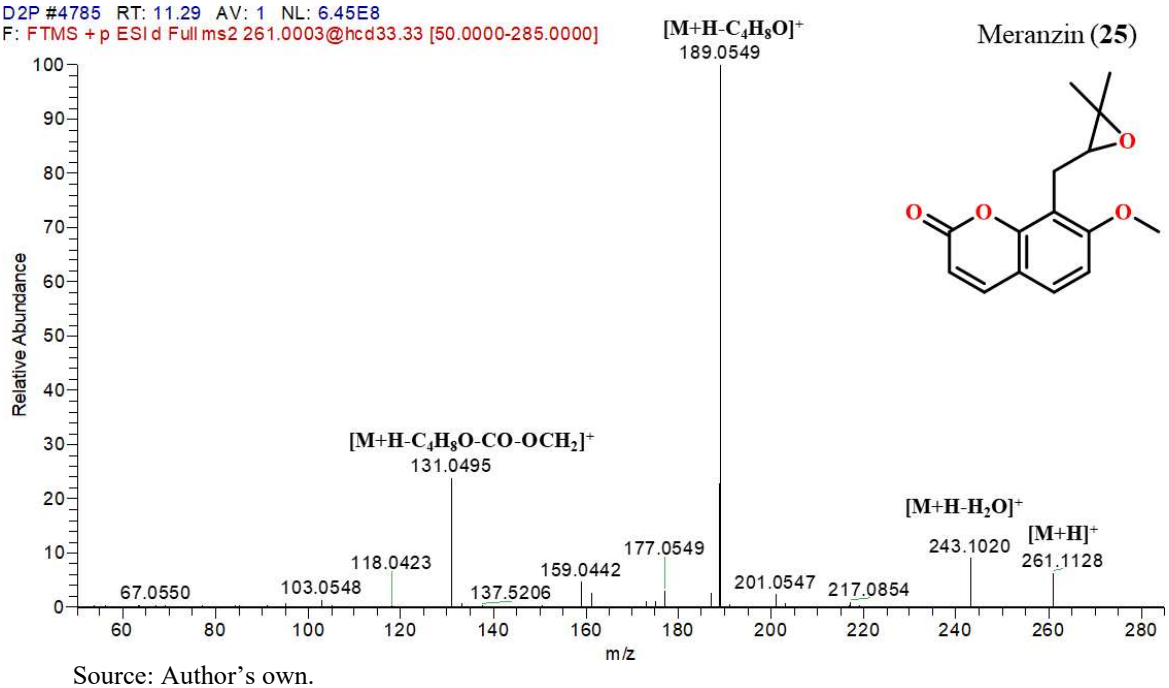


Source: Author's own.

**Supplementary Figure 38:** Spectral match obtained by comparison with GNPS library for compound (**26**)

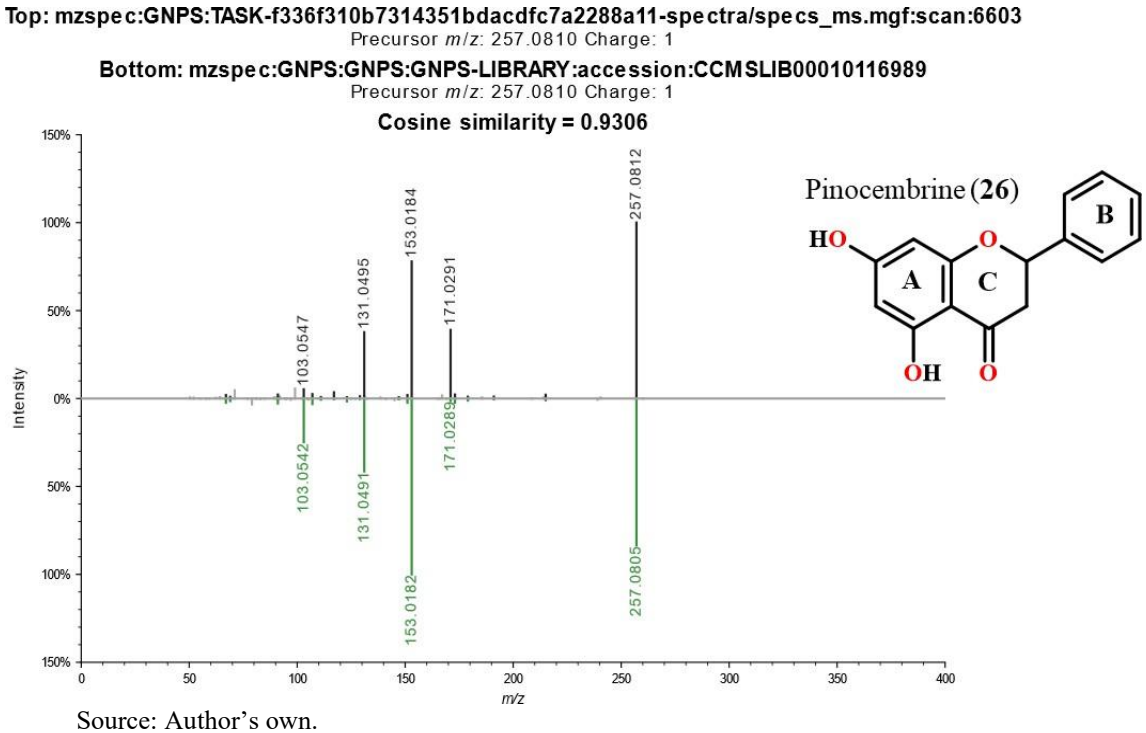


Source: Author's own.

**Supplementary Figure 39:** (+)- ESI MS/MS spectrum of the compound (**27**)

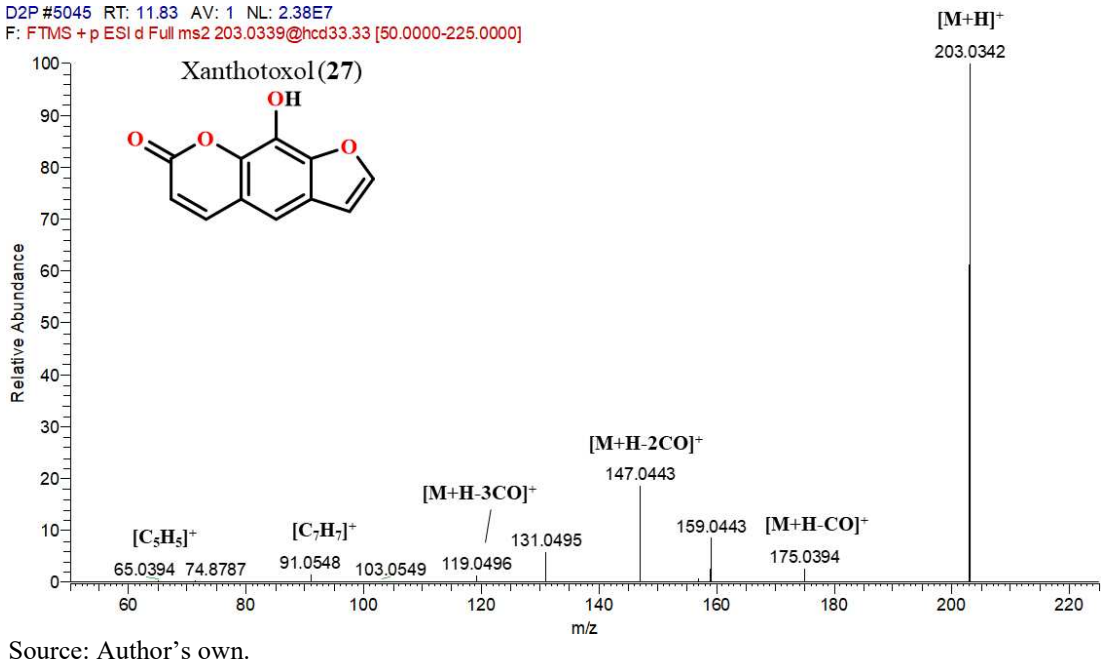


Source: Author's own.

**Supplementary Figure 40:** (+)- ESI MS/MS spectrum of the compound (**28**)

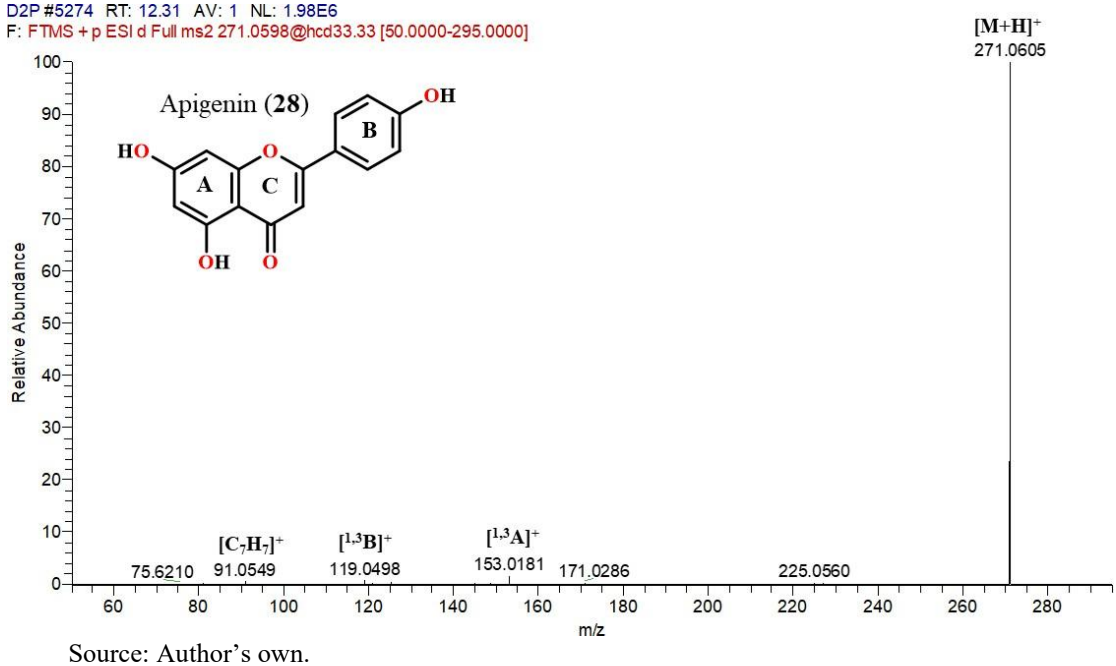


Source: Author's own.

**Supplementary Figure 41:** (-)- ESI MS/MS spectrum of the compound (**28**)

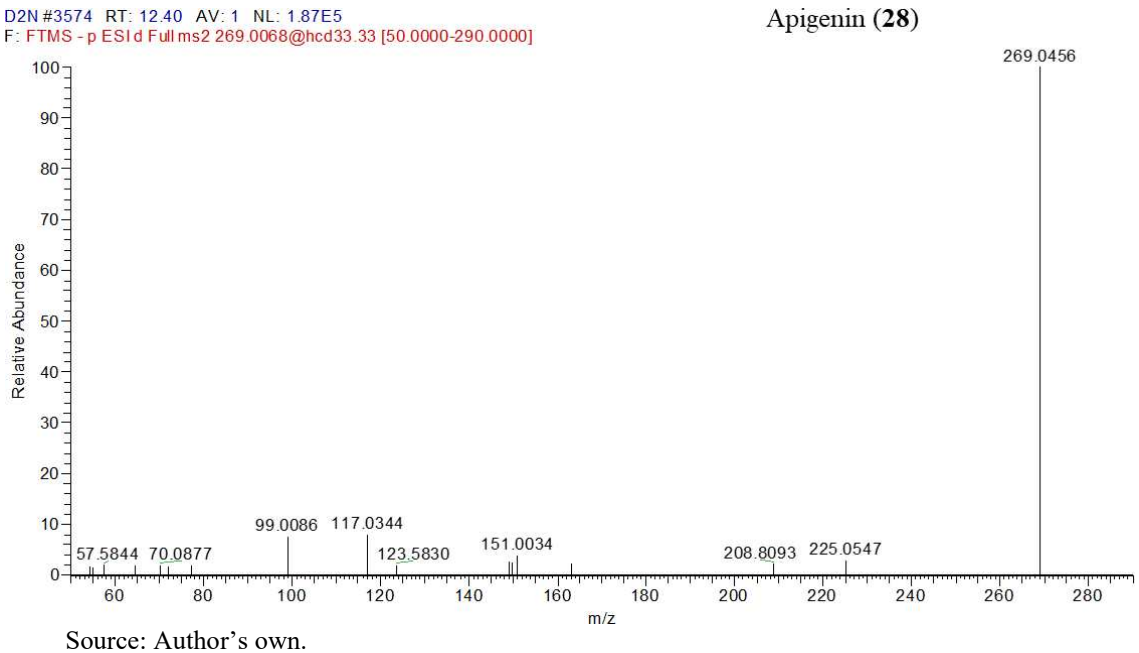


Source: Author's own.

**Supplementary Figure 42:** Spectral match obtained by comparison with GNPS library for compound (**29**)

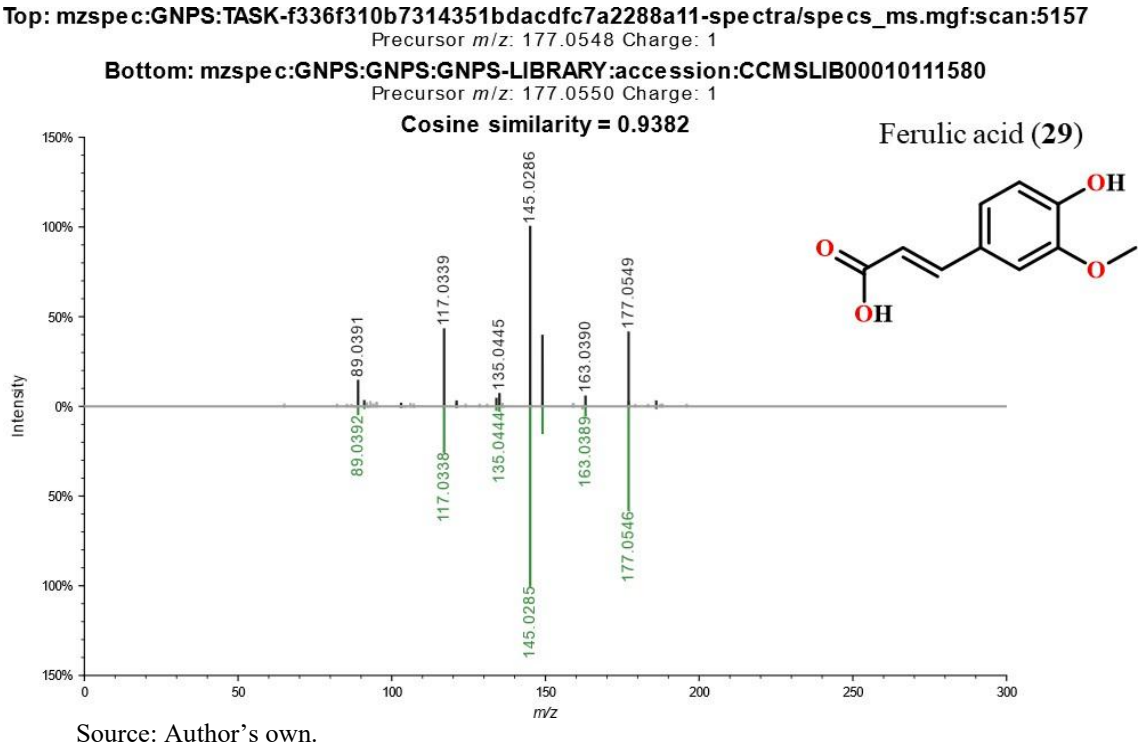


Source: Author's own.

**Supplementary Figure 43:** Spectral match obtained by comparison with GNPS library for compound (**30**)

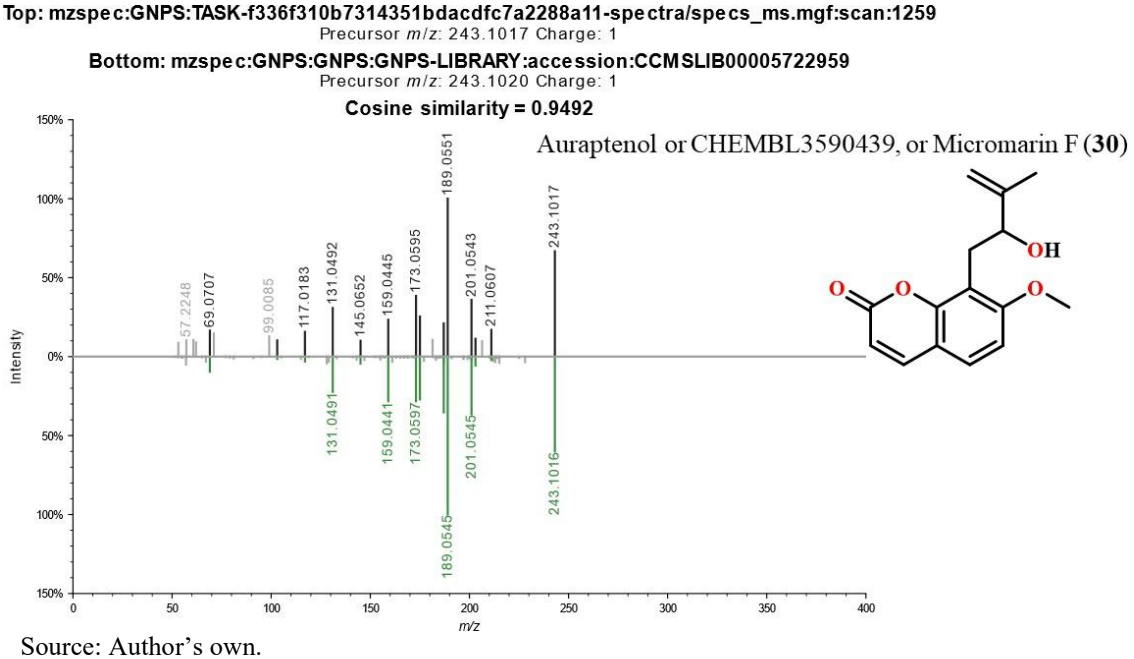


Source: Author's own.

**Supplementary Figure 44:** Spectral match obtained by comparison with GNPS library for compound (**31**)

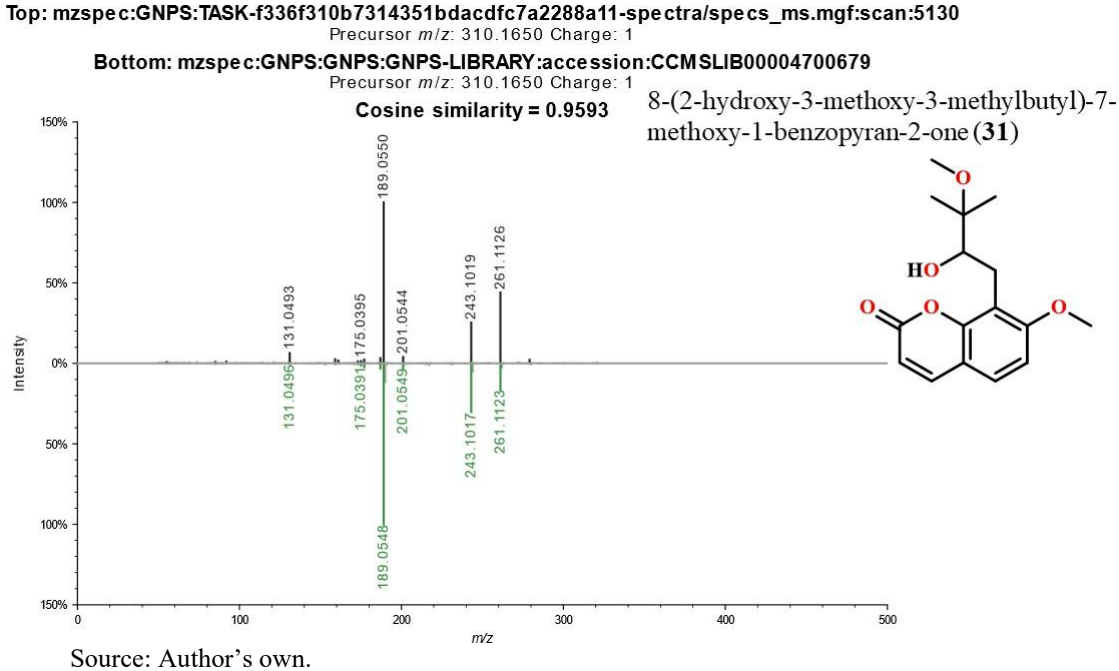


Source: Author's own.

**Supplementary Figure 45:** (+)- ESI MS/MS spectrum of the compound (**32**)

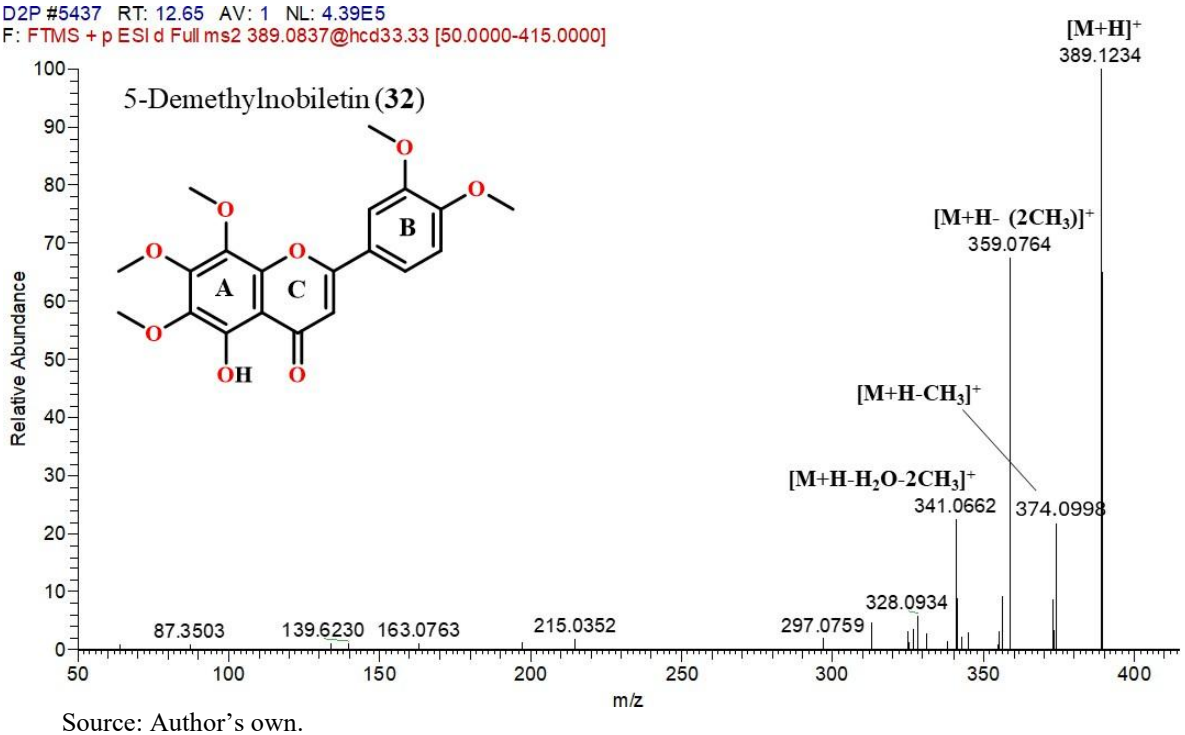


Source: Author's own.

**Supplementary Figure 46:** Spectral match obtained by comparison with GNPS library for compound (**33**)

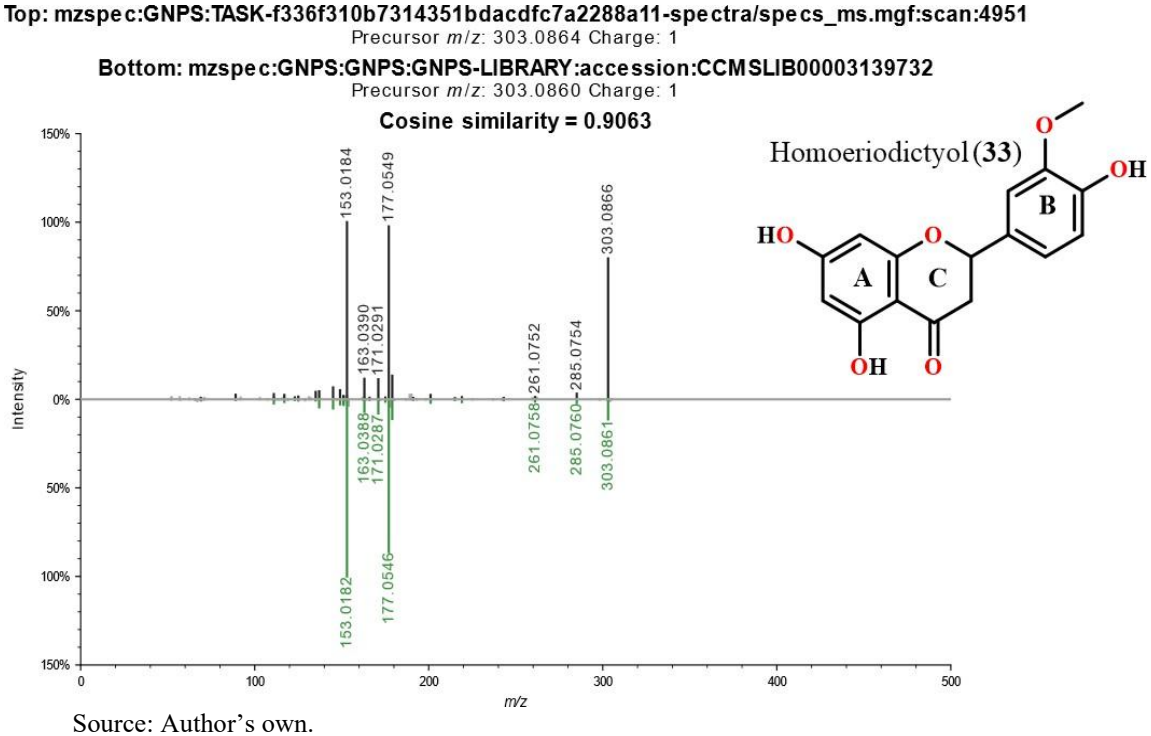


Source: Author's own.

**Supplementary Figure 47:** Base peak chromatograms (BPCs) present in the fractions of *Citrus aurantium* compared to the standard hesperitin (**34**)

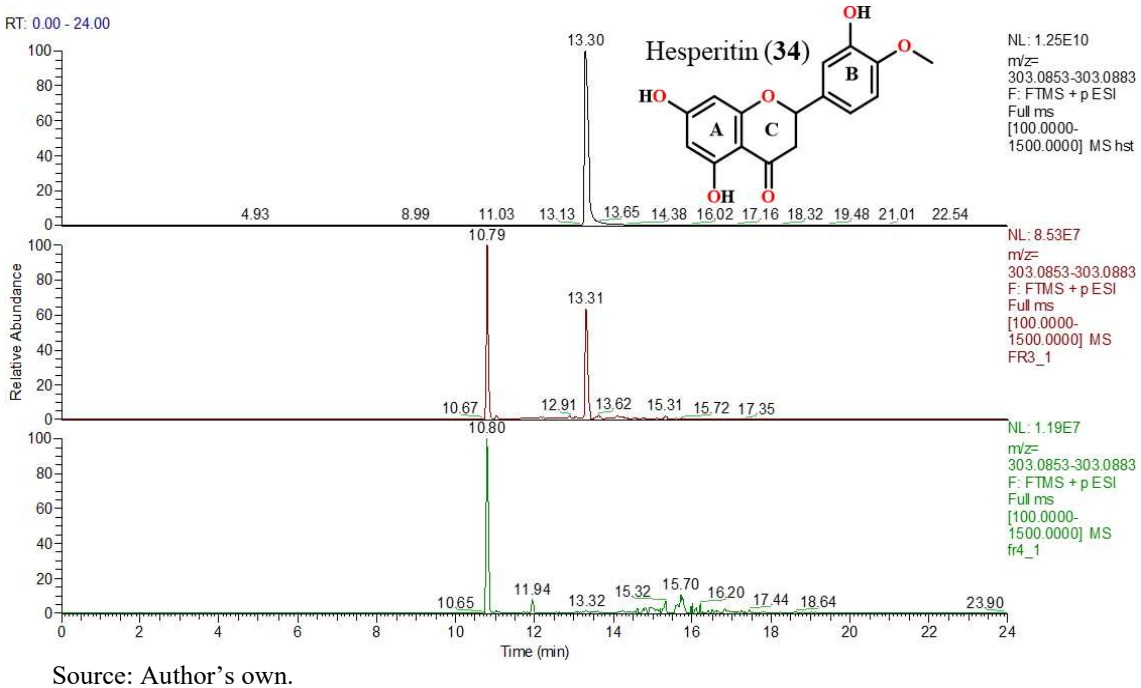


Source: Author's own.

**Supplementary Figure 48:** (+)- ESI MS/MS spectra for hesperitin (**34**) present in the crude extract and fractions of *Citrus aurantium* decoction compared to a standard

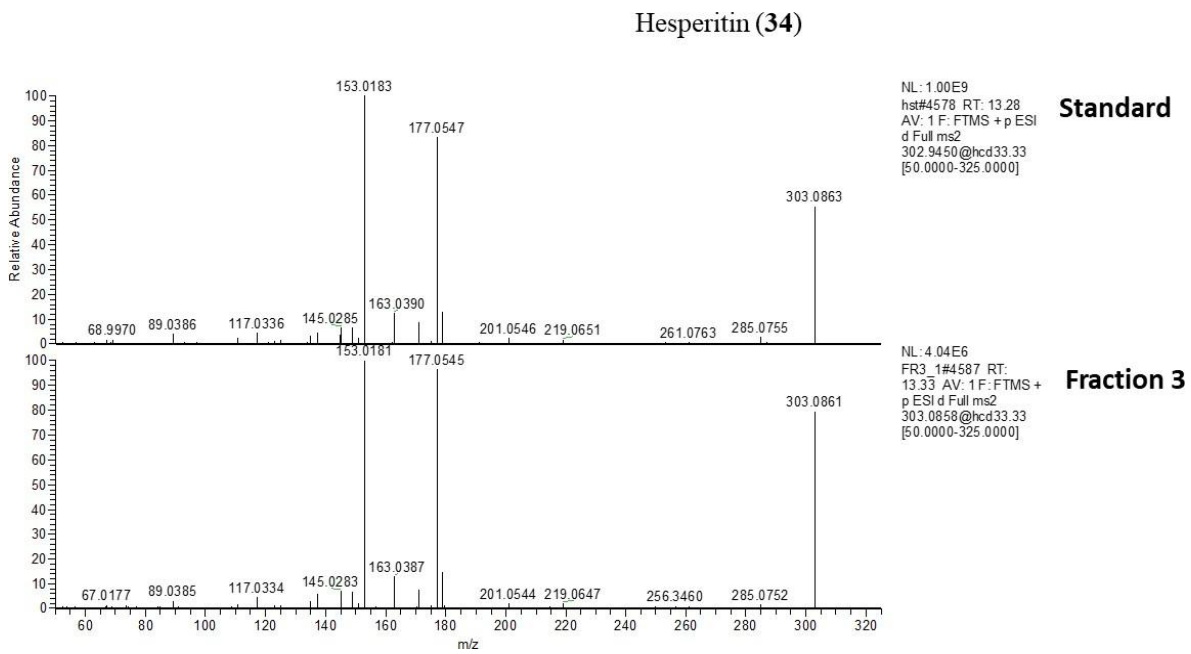


Source: Author's own.

**Supplementary Figure 49:** (+)- ESI MS/MS spectrum of the compound (**34**)

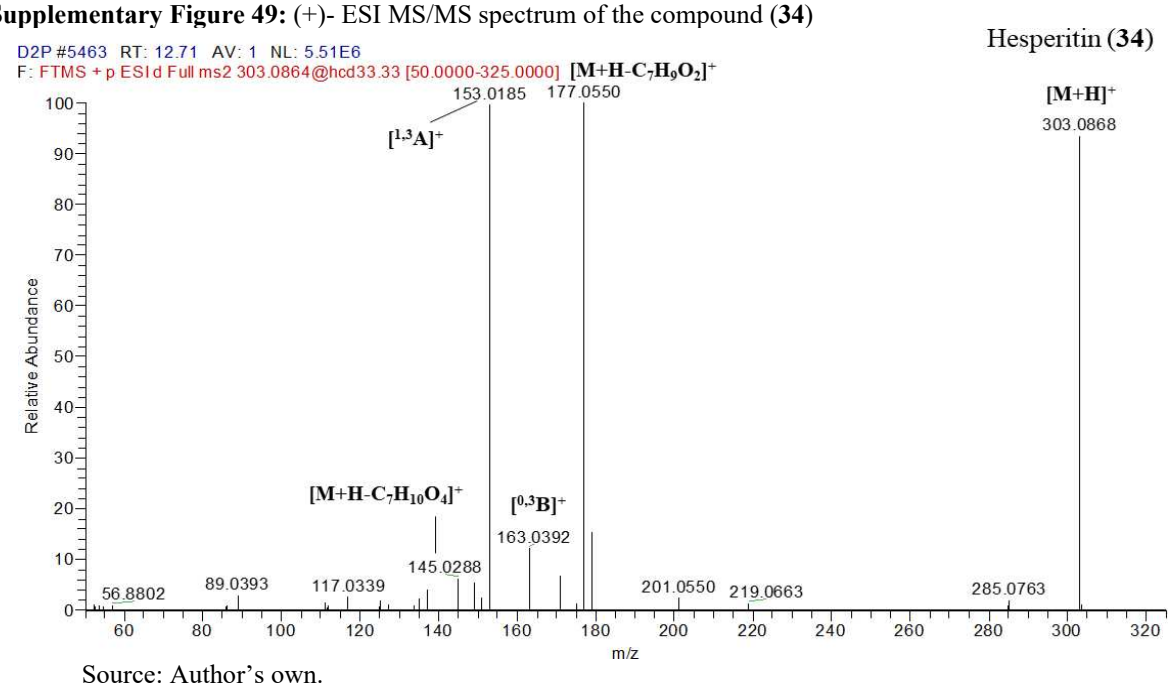


Source: Author's own.

**Supplementary Figure 50:** (-)- ESI MS/MS spectra for hesperitin (**34**) present in the crude extract and fractions of *Citrus aurantium* decoction compared to a standard

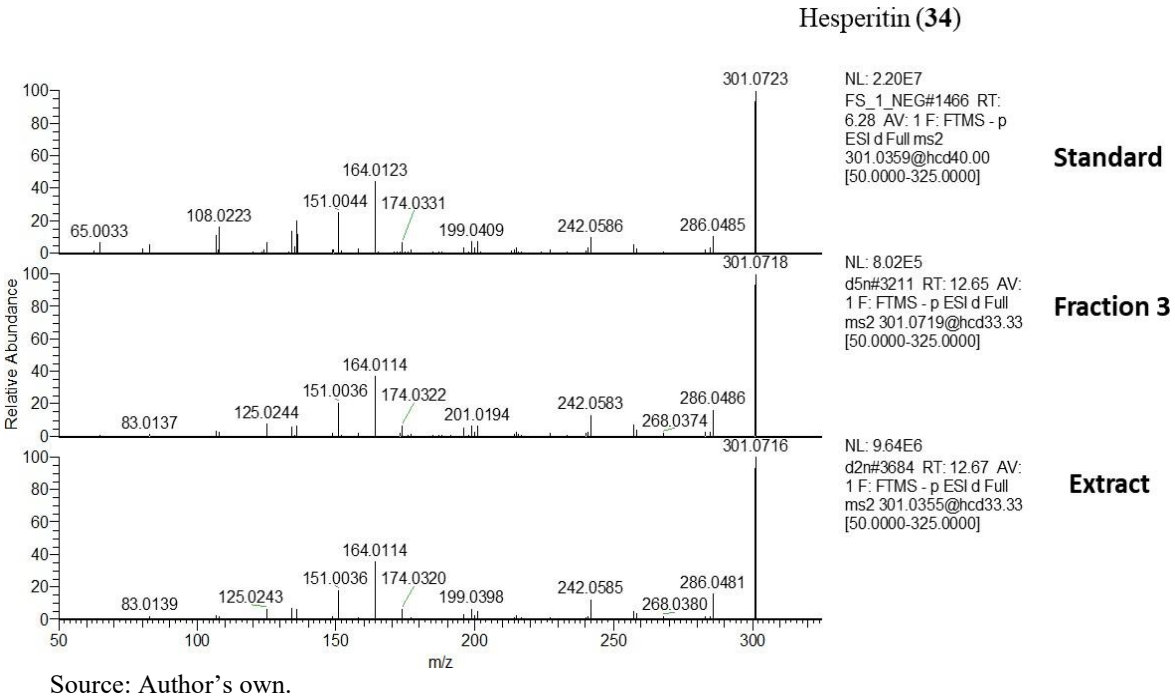


Source: Author's own.

**Supplementary Figure 51:** (-)- ESI MS/MS spectrum of the compound (**34**)

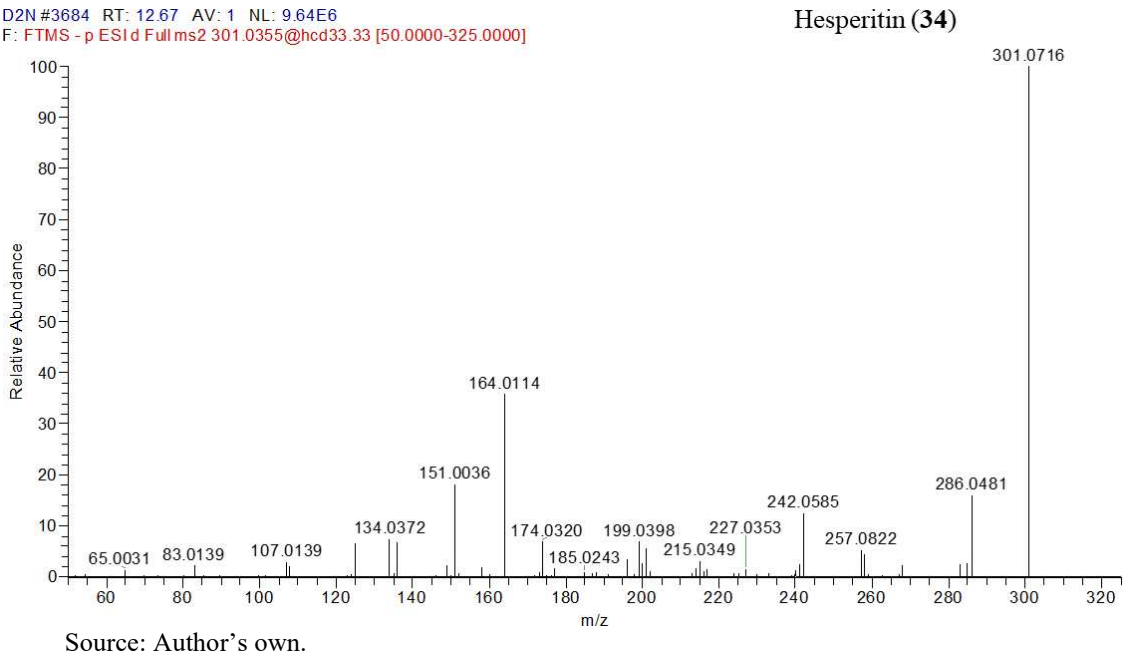


Source: Author's own.

**Supplementary Figure 52:** Spectral match obtained by comparison with GNPS library for compound (**35**)

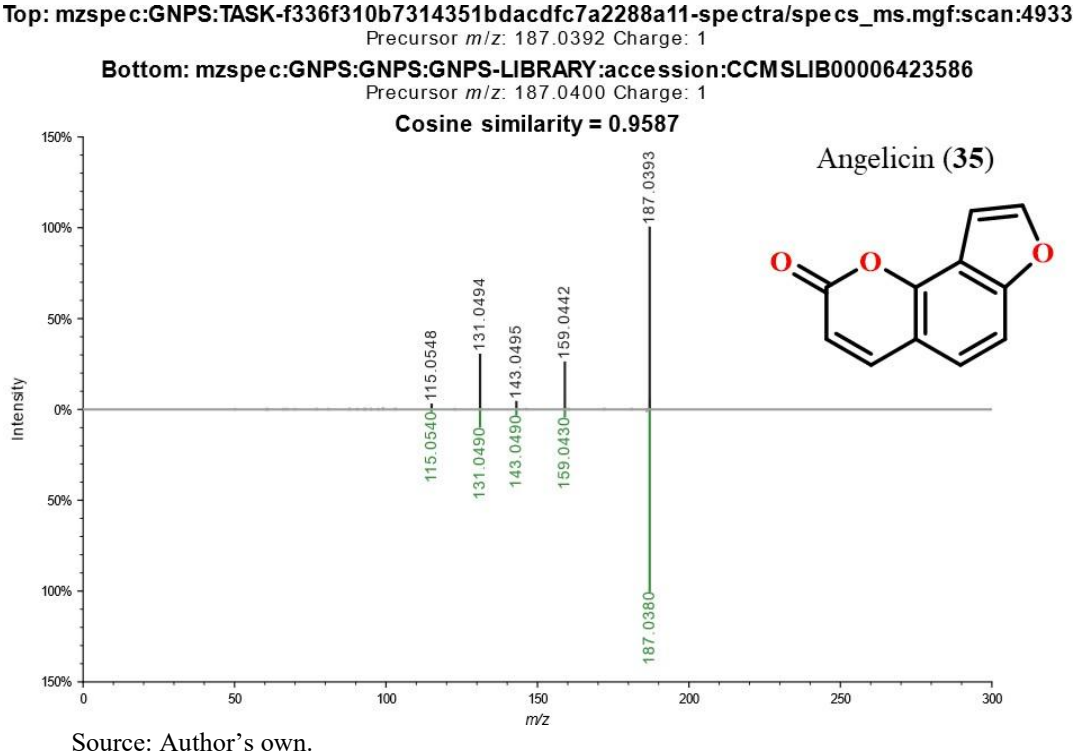


Source: Author's own.

**Supplementary Figure 53:** Spectral match obtained by comparison with GNPS library for compound (**36**)

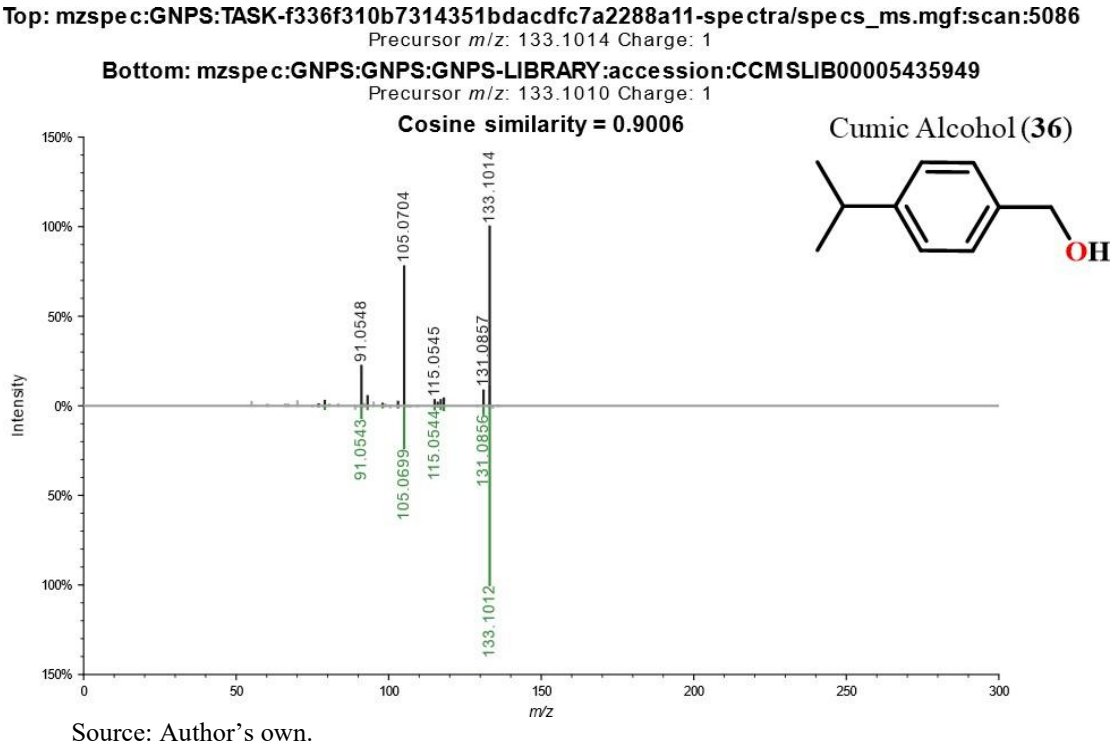


Source: Author's own.

**Supplementary Figure 54:** Spectral match obtained by comparison with GNPS library for compound (**36**)

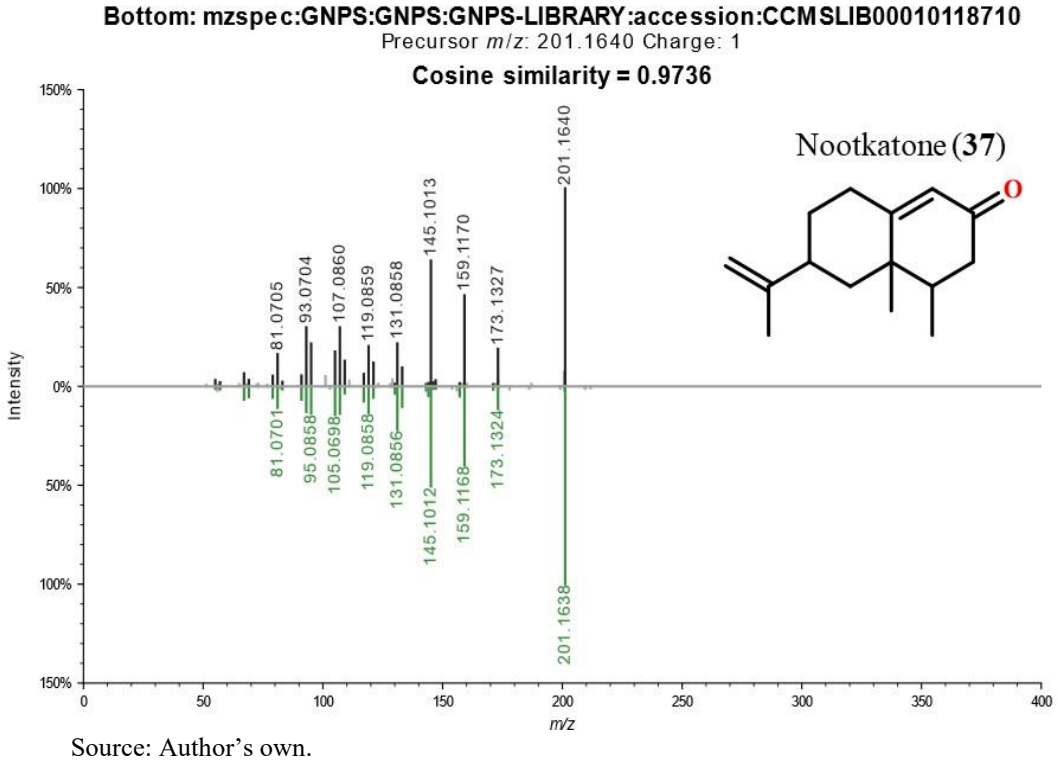


Source: Author's own.

**Supplementary Figure 55:** (+)- ESI MS/MS spectrum of the compound (**38**)

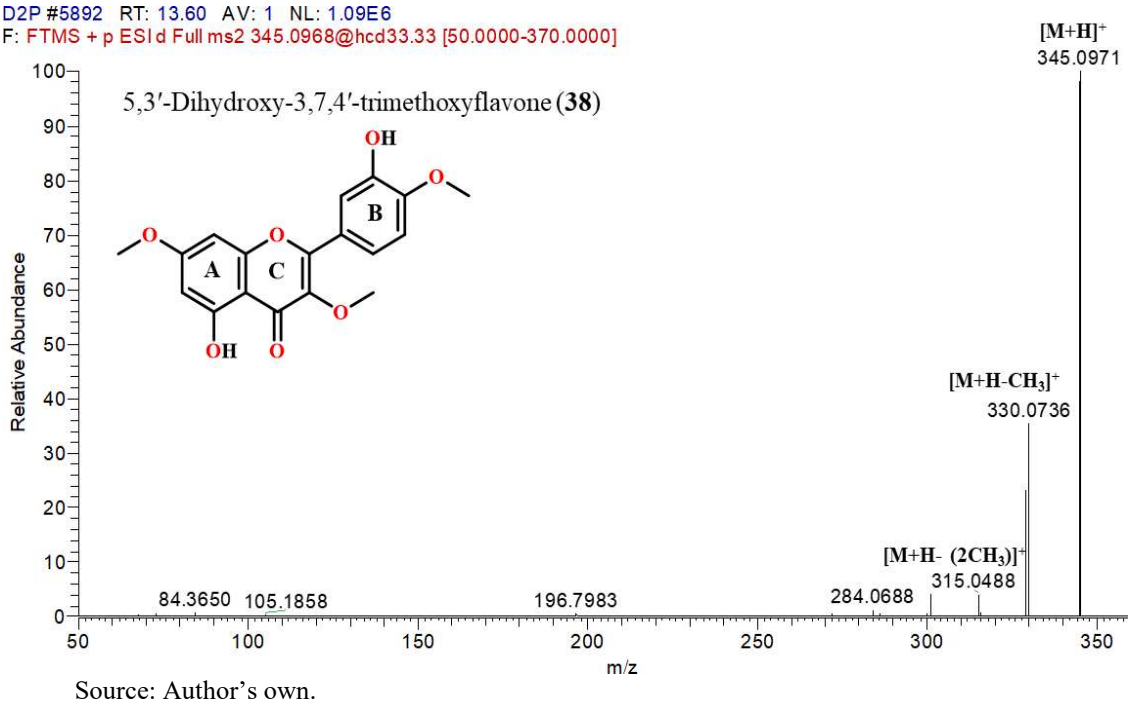


Source: Author's own.

**Supplementary Figure 56:** (+)- ESI MS/MS spectrum of the compound (**39**)

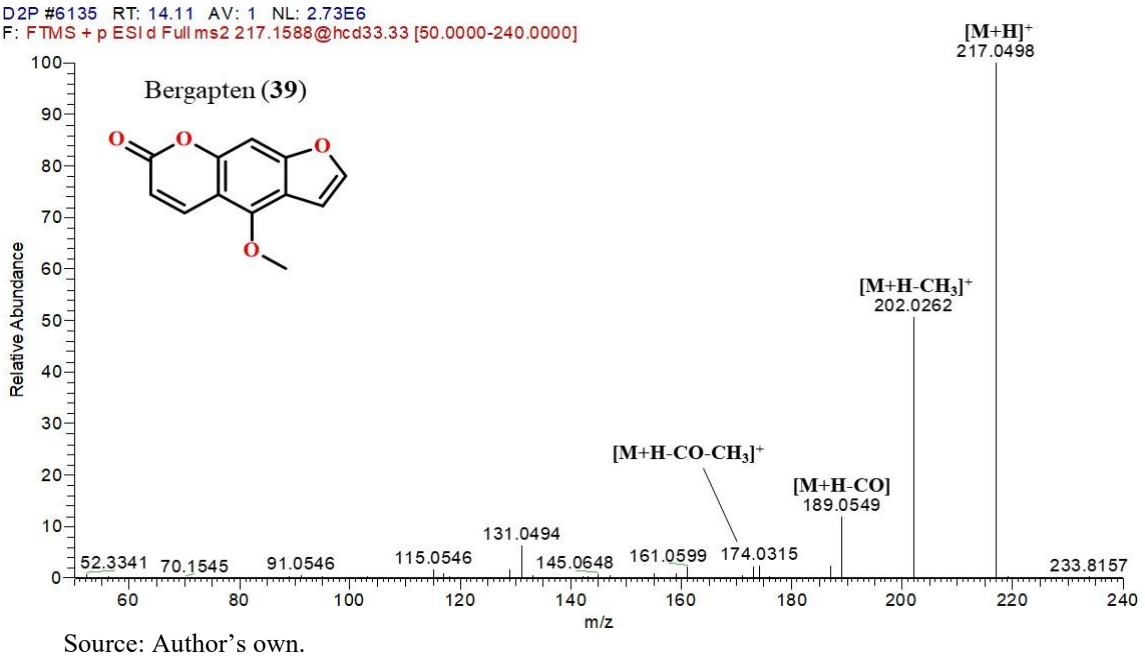


Source: Author's own.

**Supplementary Figure 57:** (+)- ESI MS/MS spectrum of the compound (**40**)

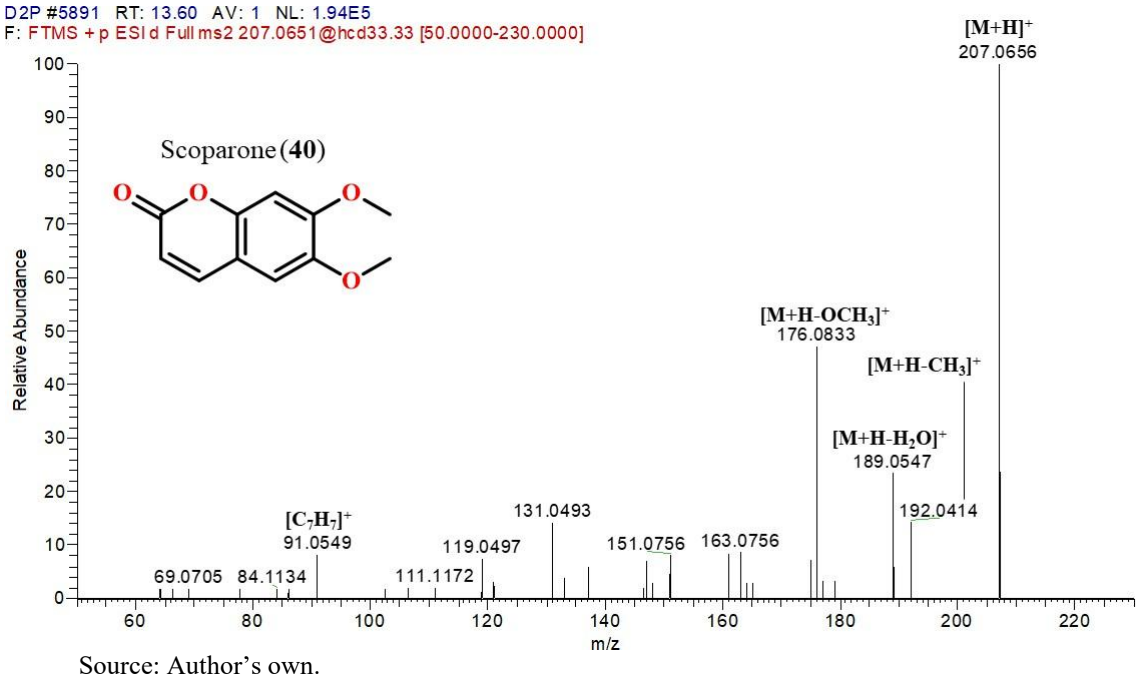


Source: Author's own.

**Supplementary Figure 58:** (+)- ESI MS/MS spectrum of the compound (**41**)

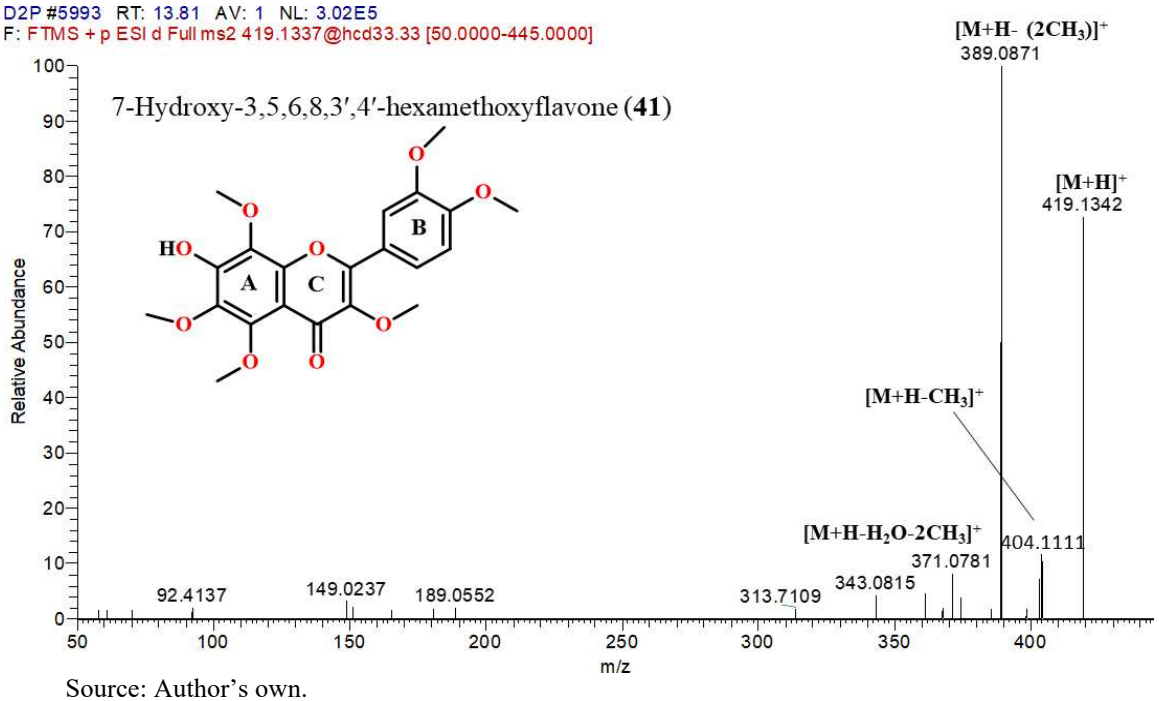


Source: Author's own.

**Supplementary Figure 59:** (+)- ESI MS/MS spectrum of the compound (**42**)

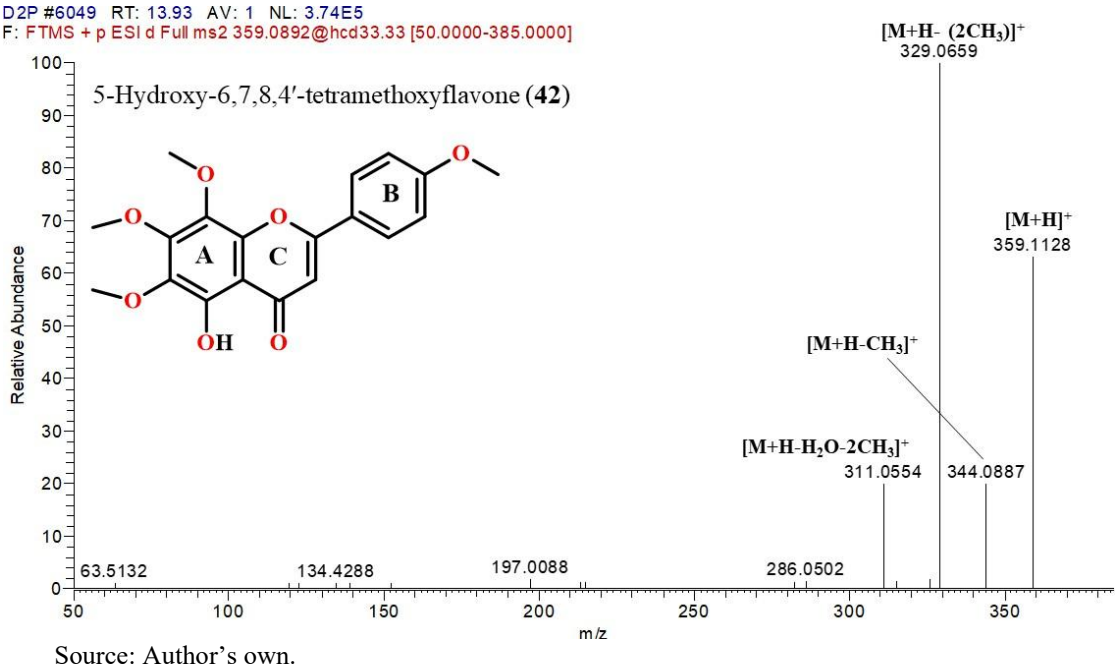


Source: Author's own.

**Supplementary Figure 60:** Spectral match obtained by comparison with GNPS library for compound (**43**)

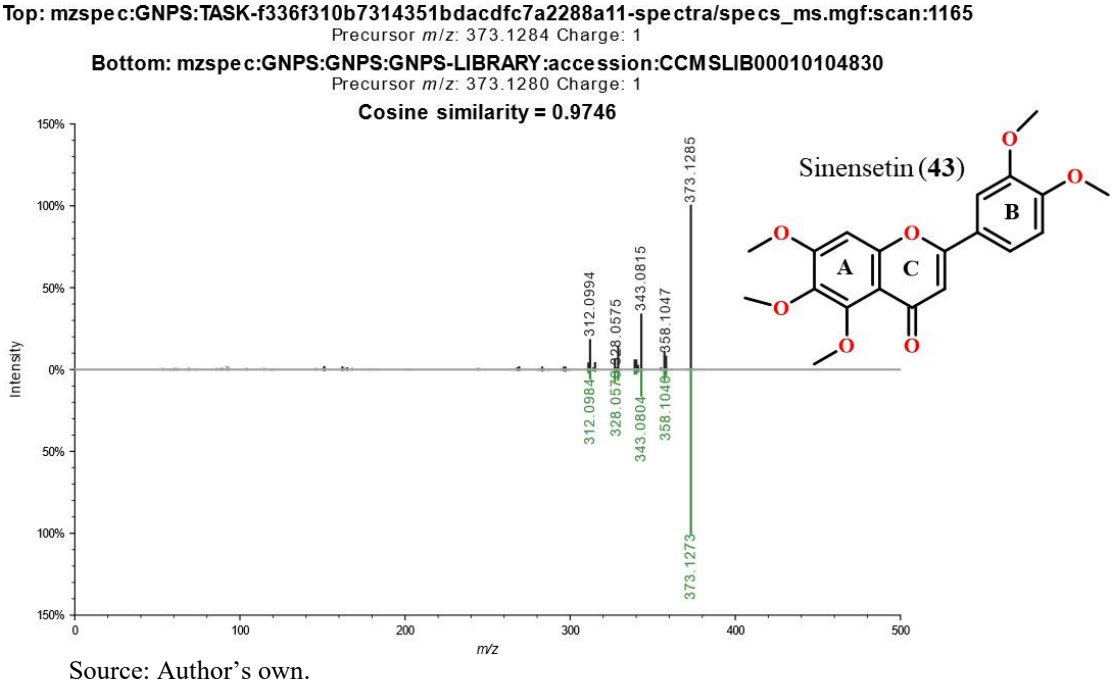


Source: Author's own.

**Supplementary Figure 61:** (+)- ESI MS/MS spectrum of the compound (**44**)

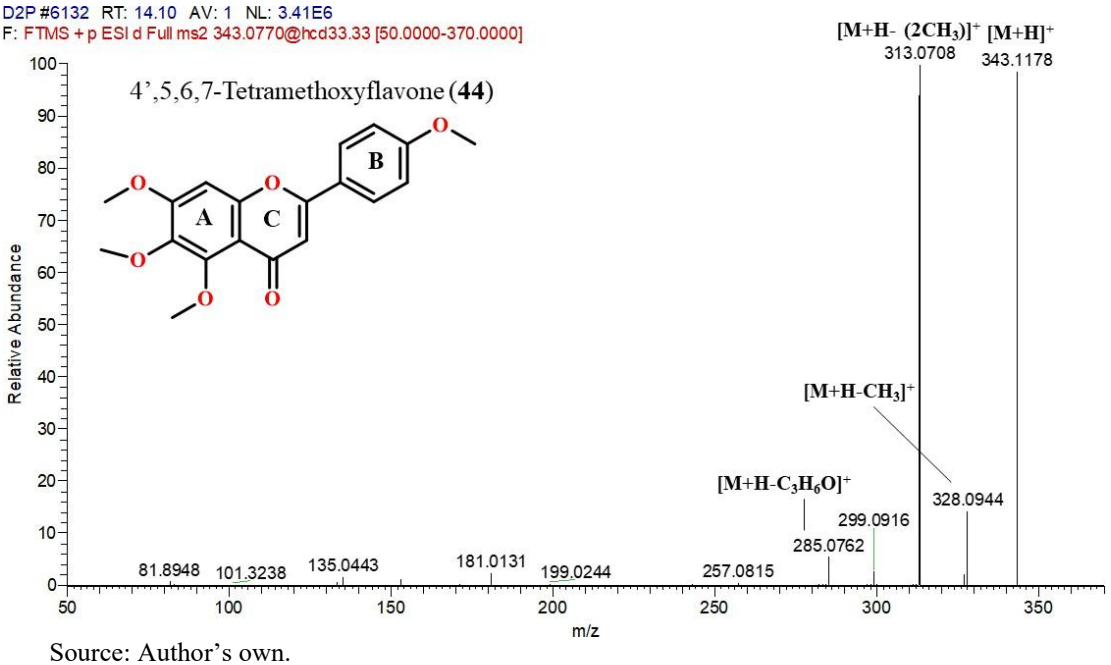


Source: Author's own.

**Supplementary Figure 62:** Spectral match obtained by comparison with GNPS library for compound (**45**)

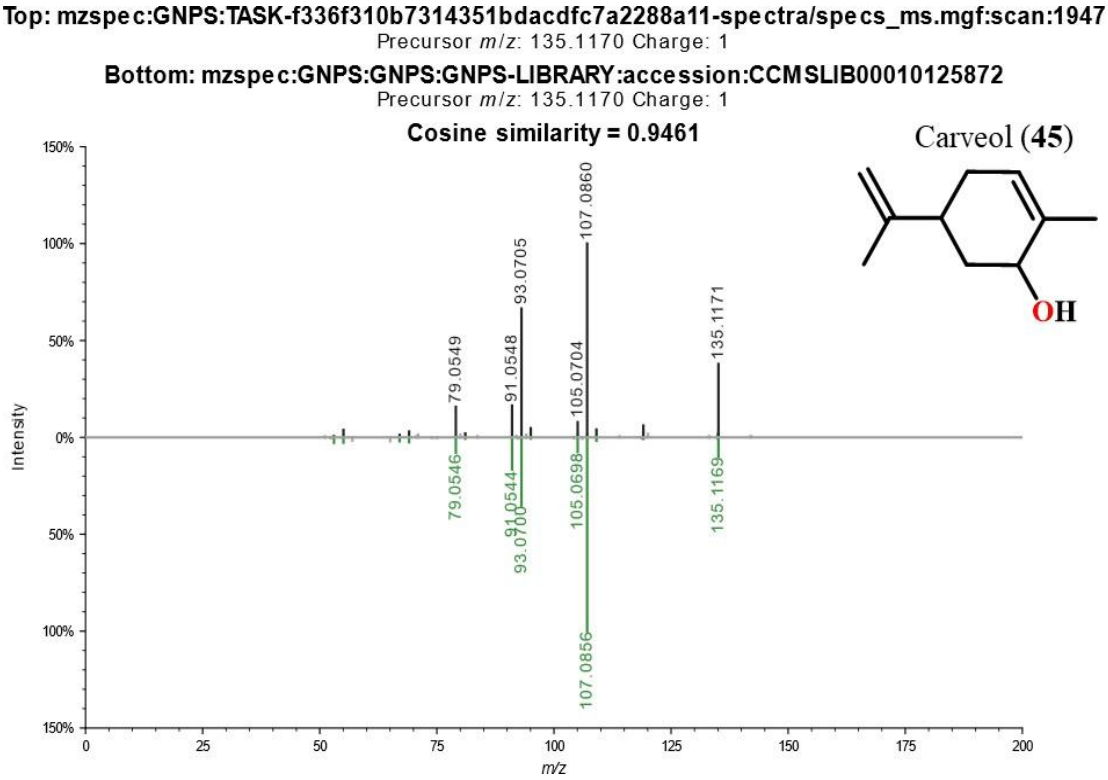


Source: Author's own.

**Supplementary Figure 63:** (+)- ESI MS/MS spectrum of the compound (**46**)

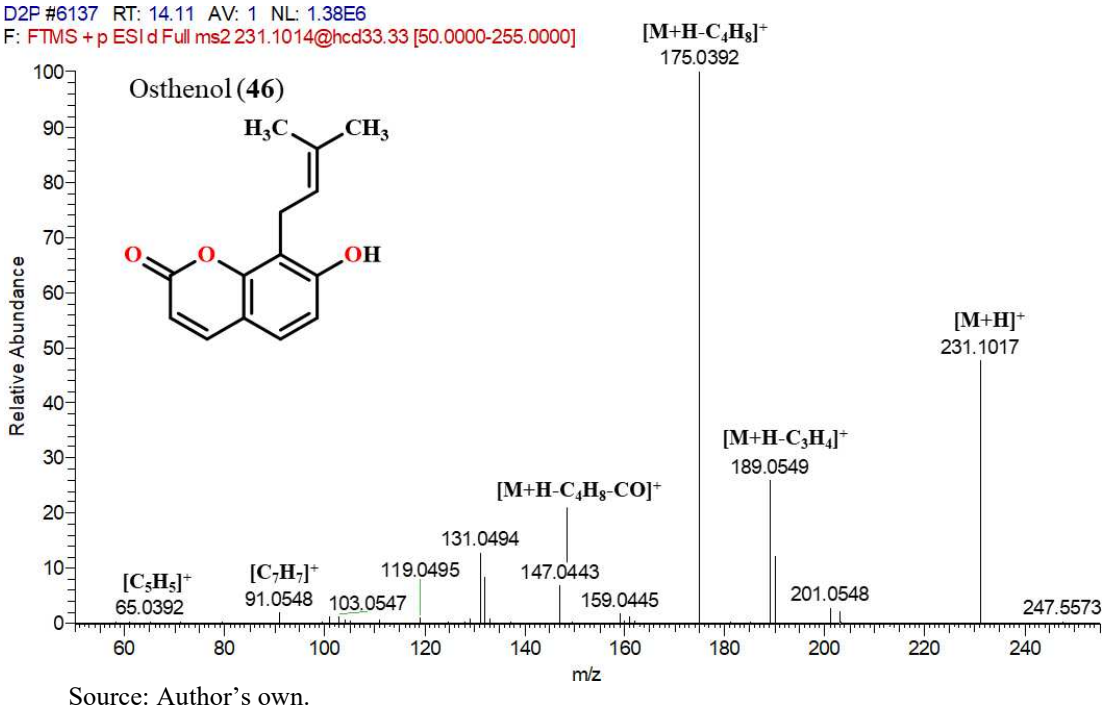


Source: Author's own.

**Supplementary Figure 64:** (+)- ESI MS/MS spectrum of the compound (**47**)

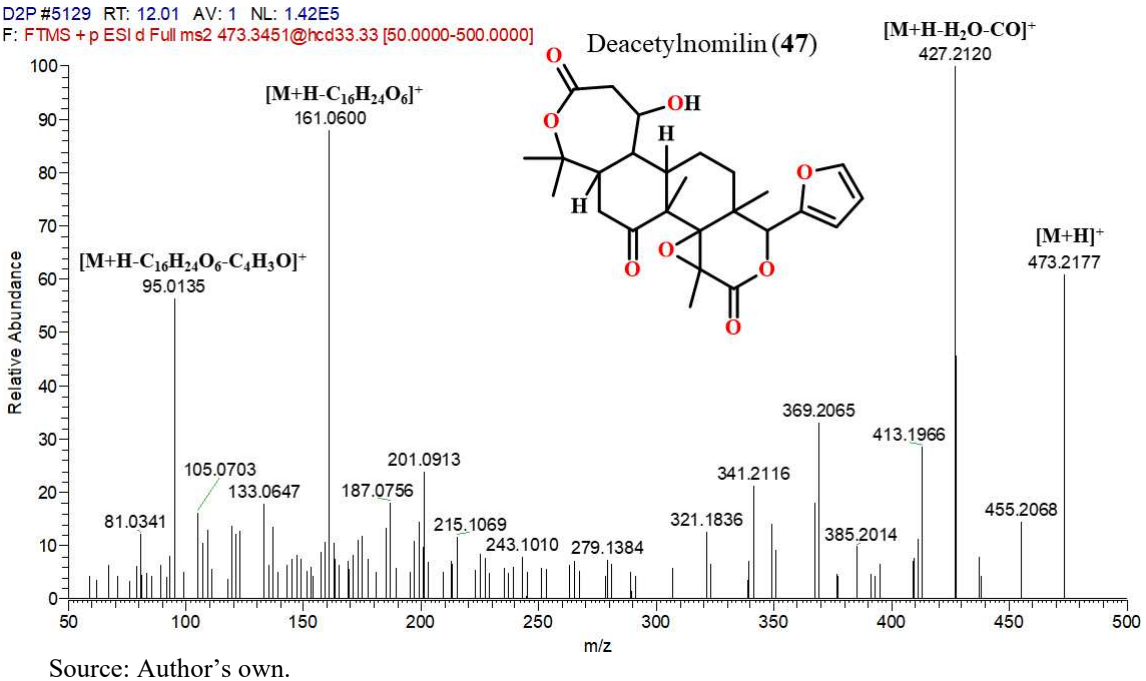


Source: Author's own.

**Supplementary Figure 65:** (+)- ESI MS/MS spectrum of the compound (**48**)

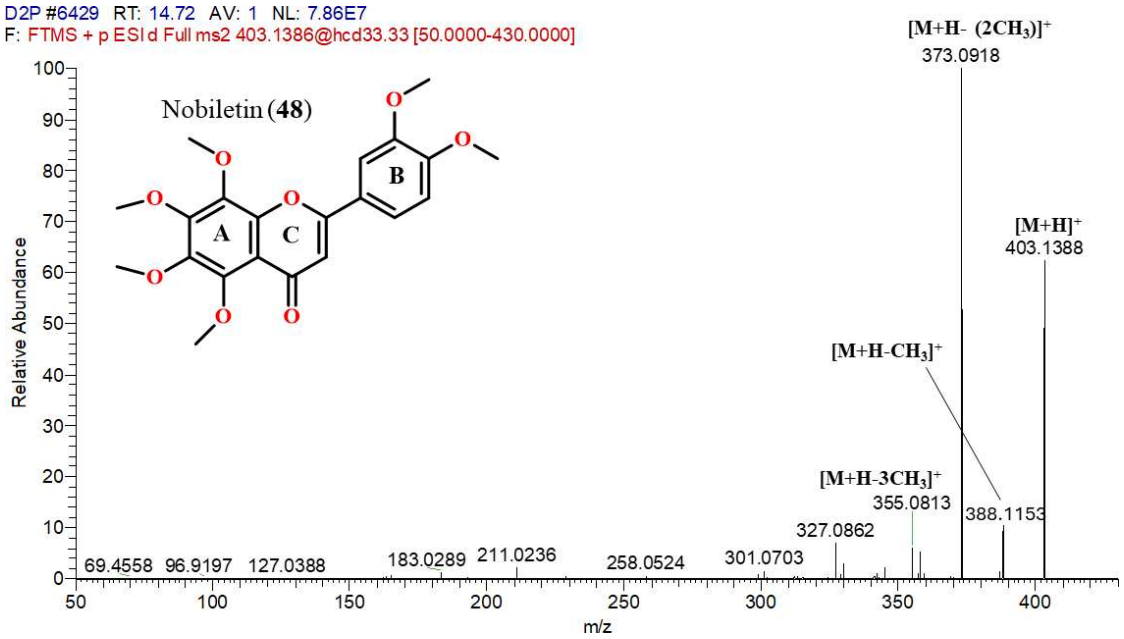


Source: Author's own.

**Supplementary Figure 66:** (+)- ESI MS/MS spectrum of the compound (**49**)

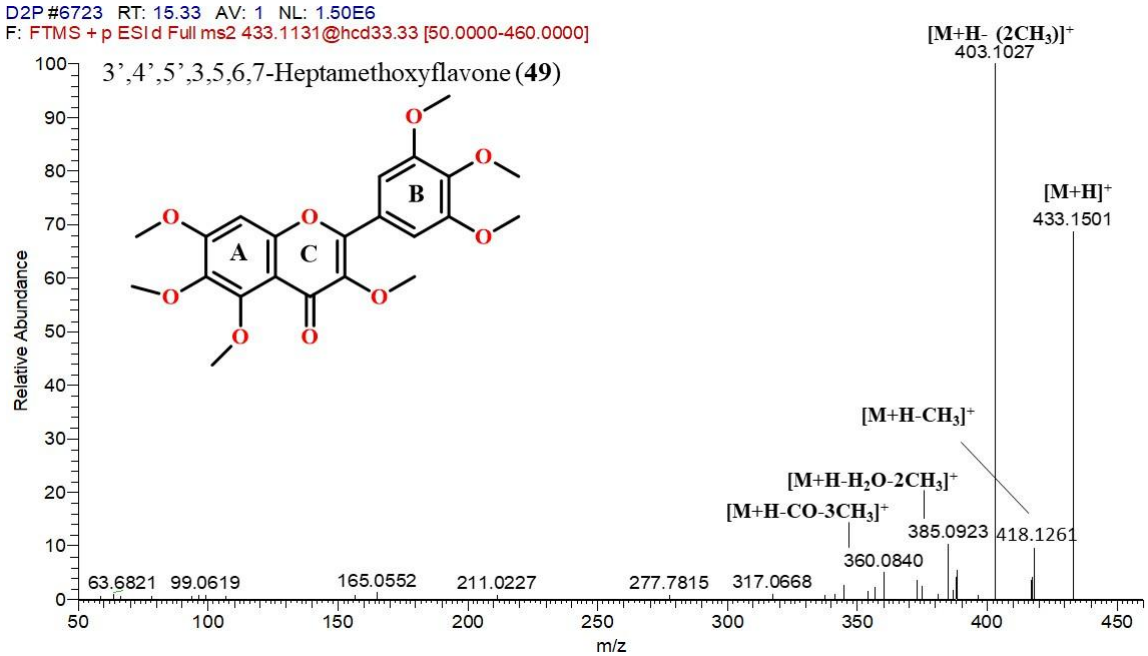


Source: Author's own.

**Supplementary Figure 67:** Spectral match obtained by comparison with GNPS library for compound (**50**)

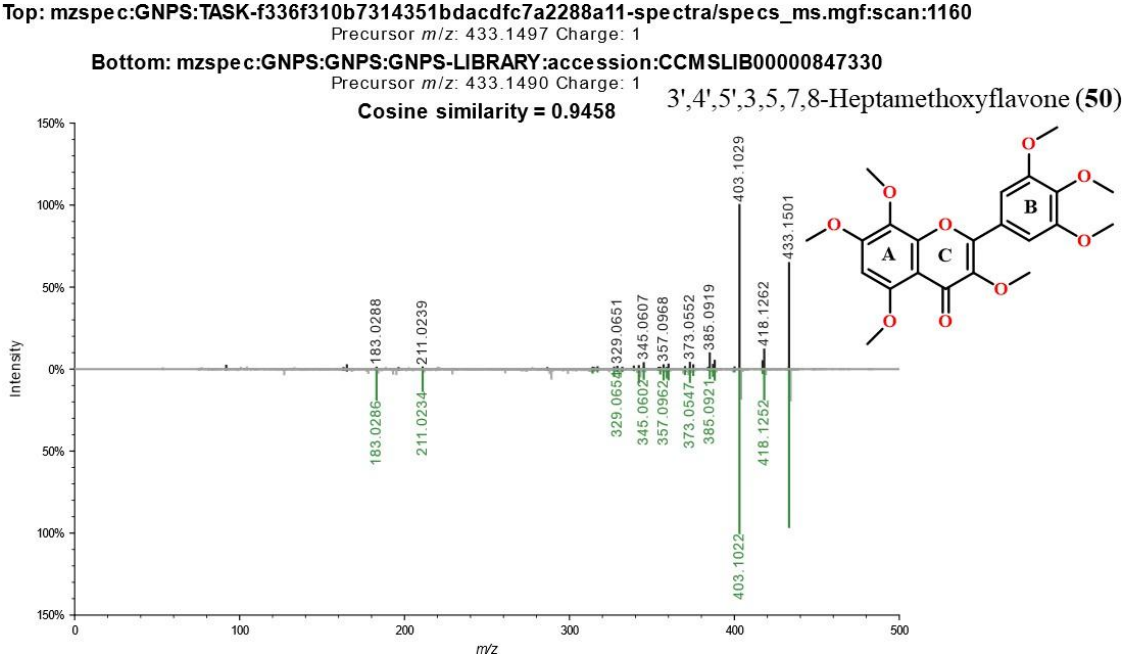


Source: Author's own.

**Supplementary Figure 68:** Spectral match obtained by comparison with GNPS library for compound (**51**)

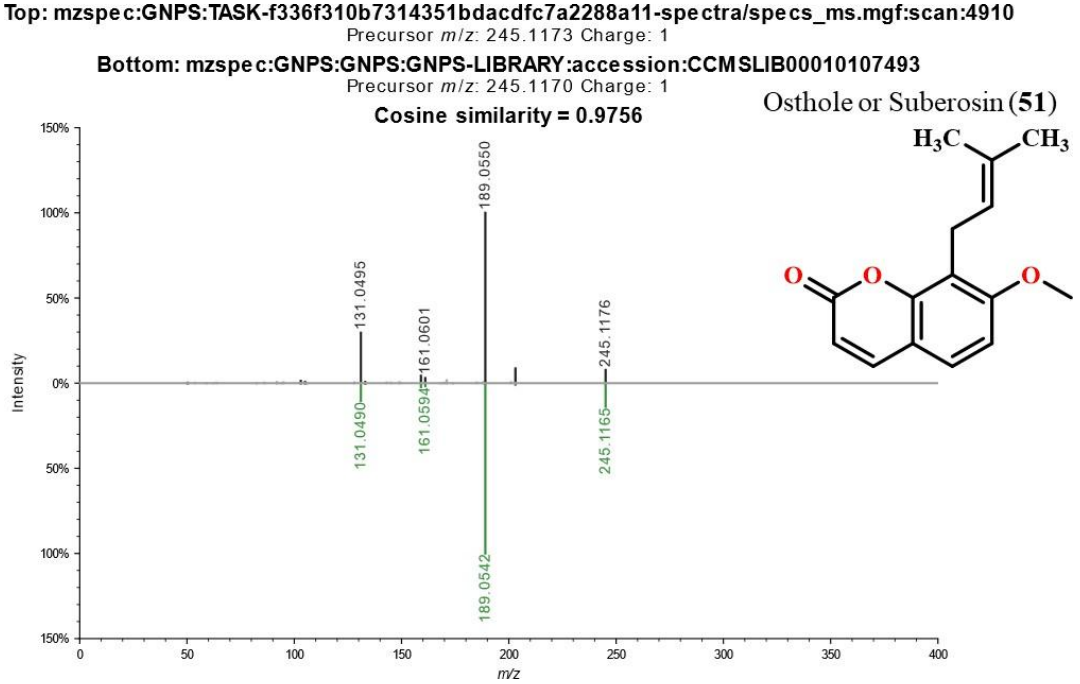


Source: Author's own.

**Supplementary Figure 69:** Spectral match obtained by comparison with GNPS library for compound (**52**)

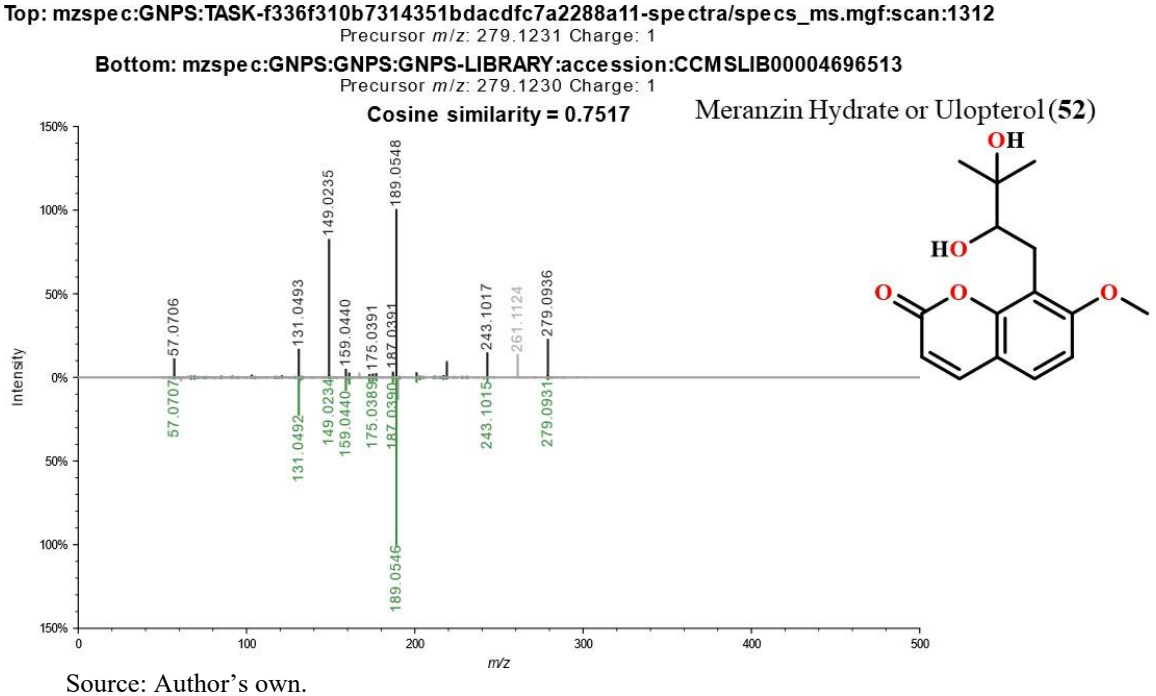


Source: Author's own.

**Supplementary Figure 70:** Spectral match obtained by comparison with GNPS library for compound (**53**)

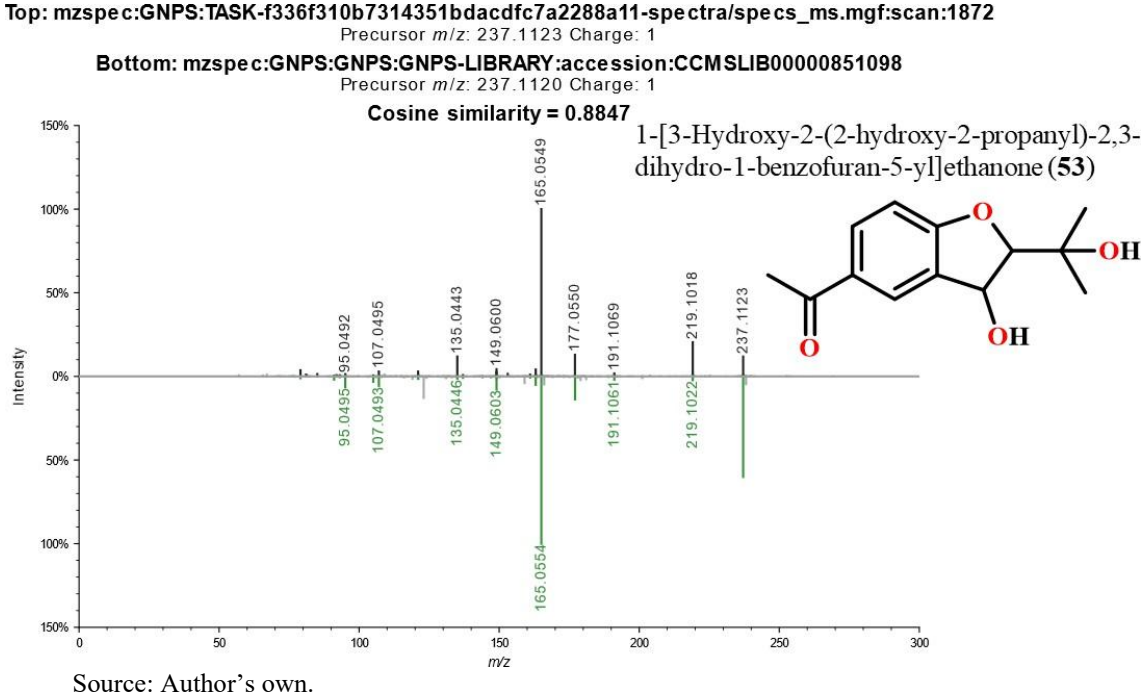


Source: Author's own.

**Supplementary Figure 71:** Spectral match obtained by comparison with GNPS library for compound (**54**)

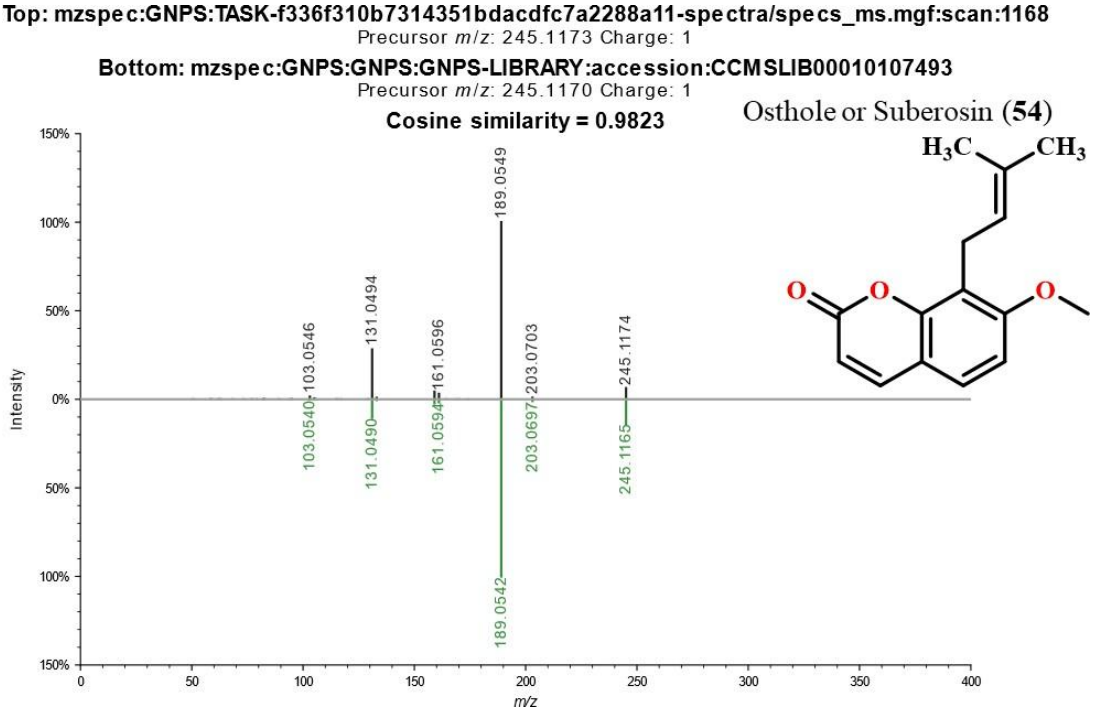


Source: Author's own.

**Supplementary Figure 72:** Spectral match obtained by comparison with GNPS library for compound (**55**)

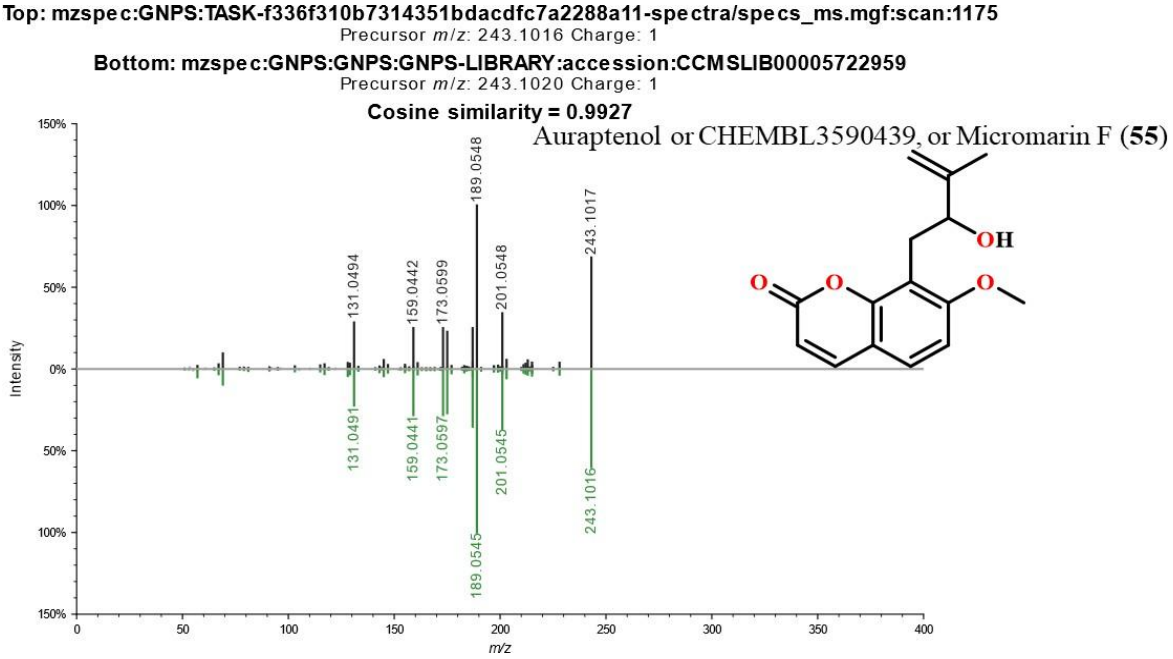


Source: Author's own.

**Supplementary Figure 73:** Spectral match obtained by comparison with GNPS library for compound (**56**)

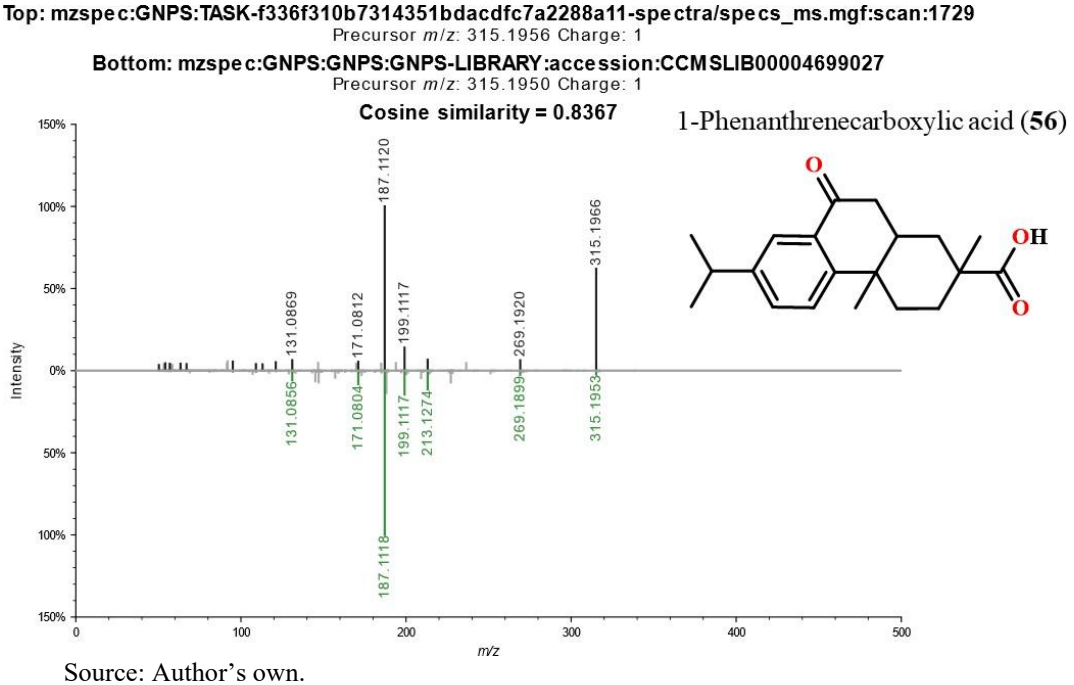


Source: Author's own.

**Supplementary Figure 74:** (+)- ESI MS/MS spectrum of the compound (**57**)

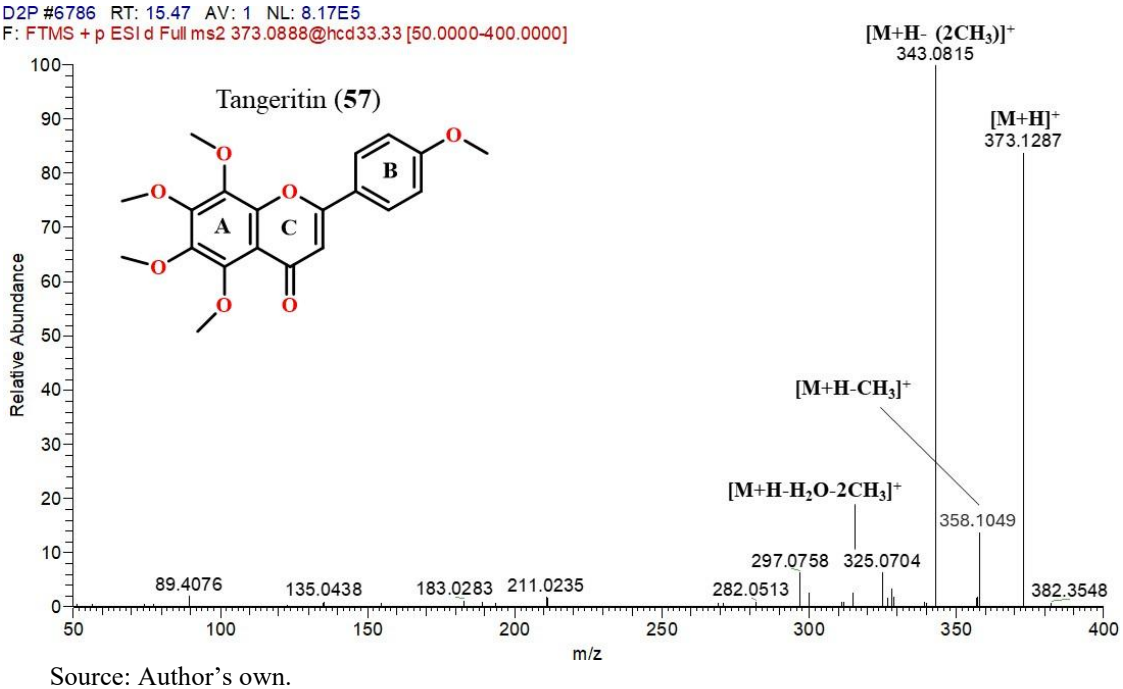


Source: Author's own.

**Supplementary Figure 75:** (-)- ESI MS/MS spectrum of the compound (**1N**)

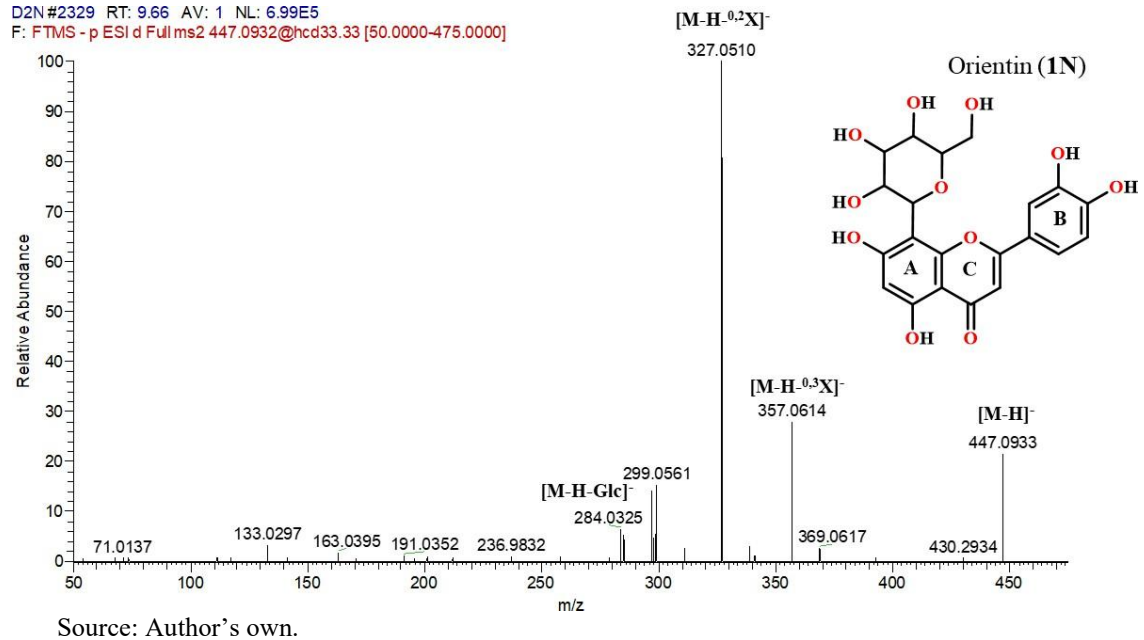


Source: Author's own.

**Supplementary Figure 76:** (-)- ESI MS/MS spectrum of the compound (**2N**)

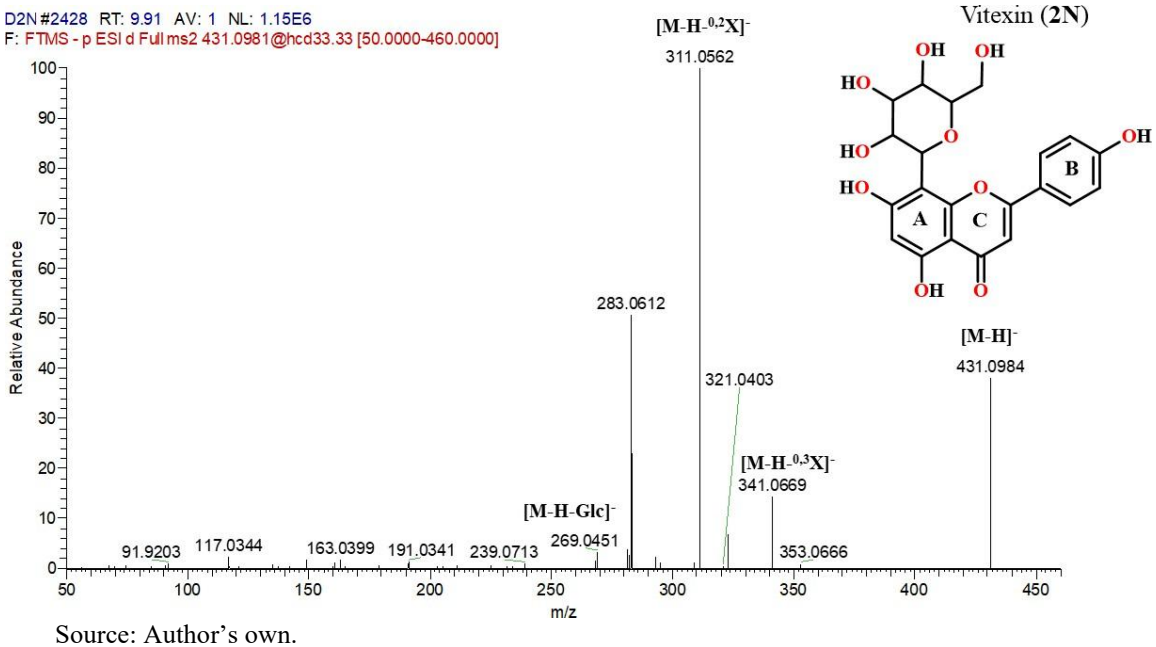


Source: Author's own.

**Supplementary Figure 77:** (-)- ESI MS/MS spectrum of the compound (**3N**)

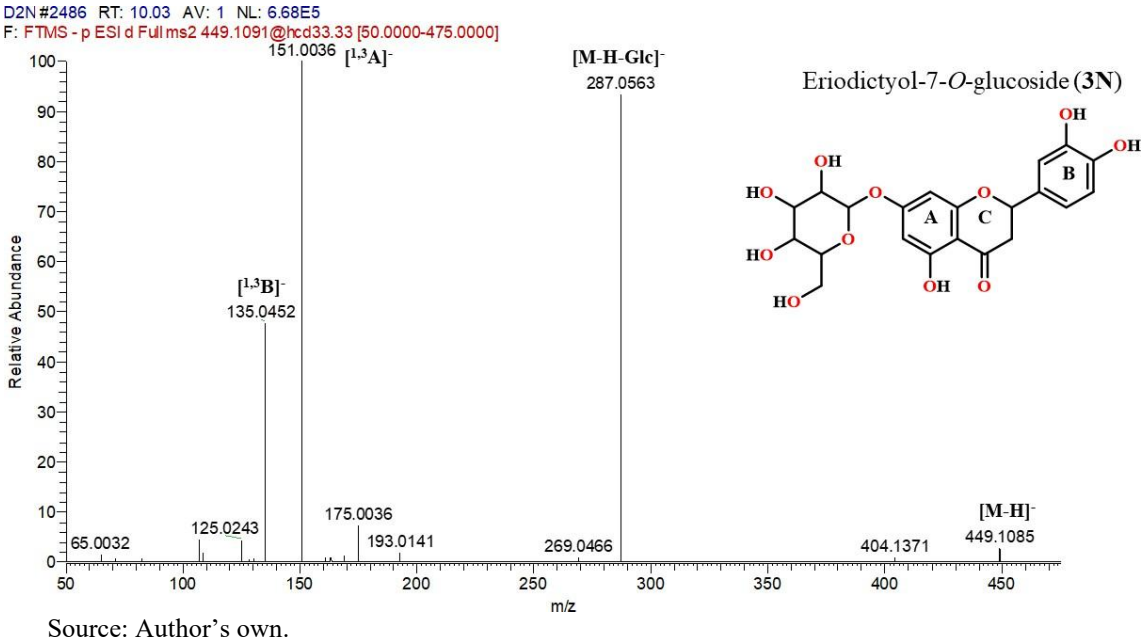


Source: Author's own.

**Supplementary Figure 78:** (-)- ESI MS/MS spectrum of the compound (**4N**)

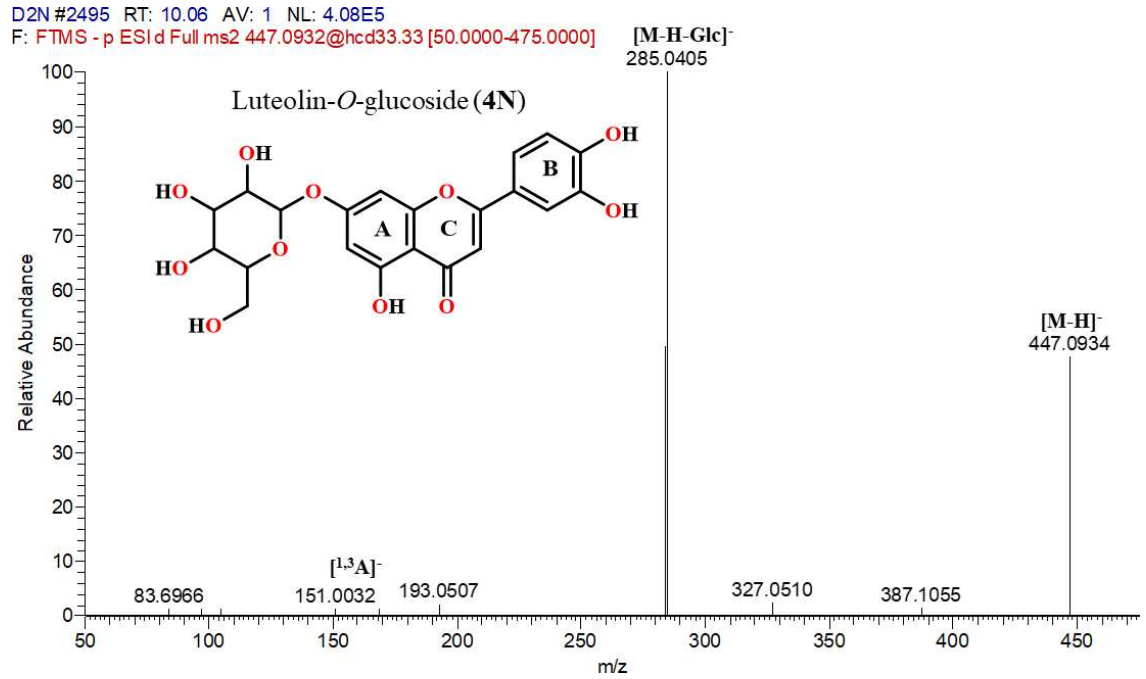


Source: Author's own.

**Supplementary Figure 79:** (-)- ESI MS/MS spectrum of the compound (**5N**)

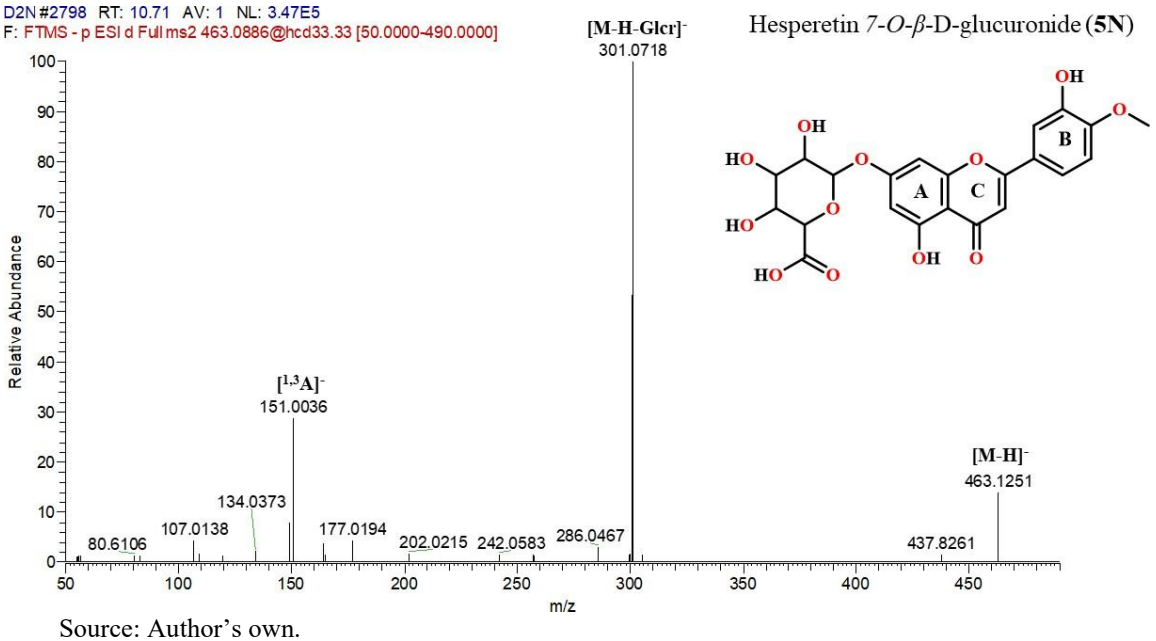


Source: Author's own.

**Supplementary Figure 80:** (-)- ESI MS/MS spectrum of the compound (**6N**)

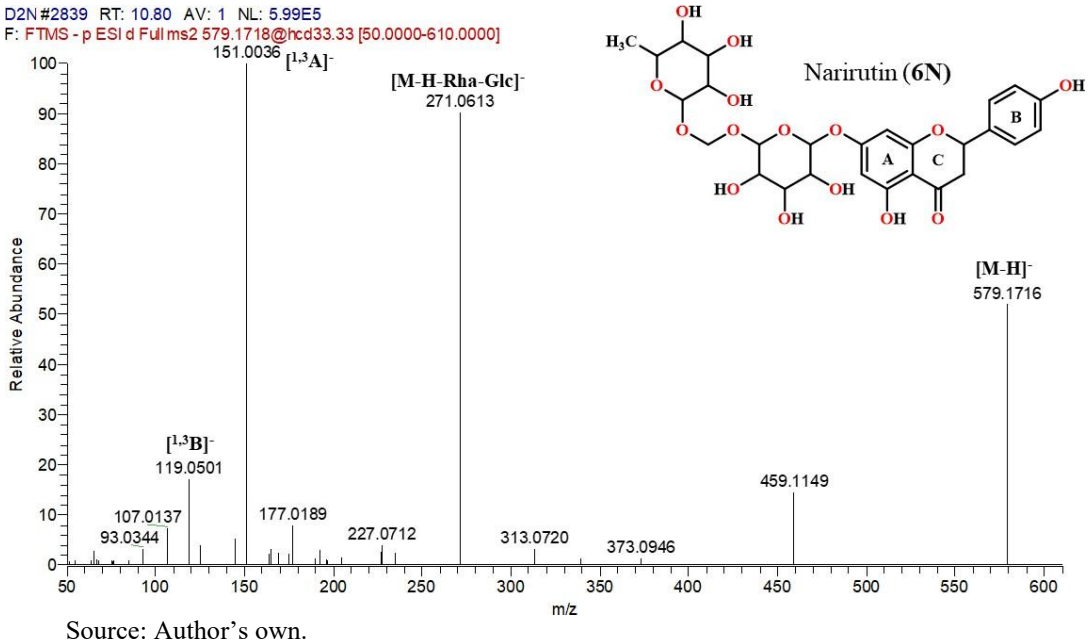


Source: Author's own.

**Supplementary Figure 81:** (-)- ESI MS/MS spectrum of the compound (**7N**)

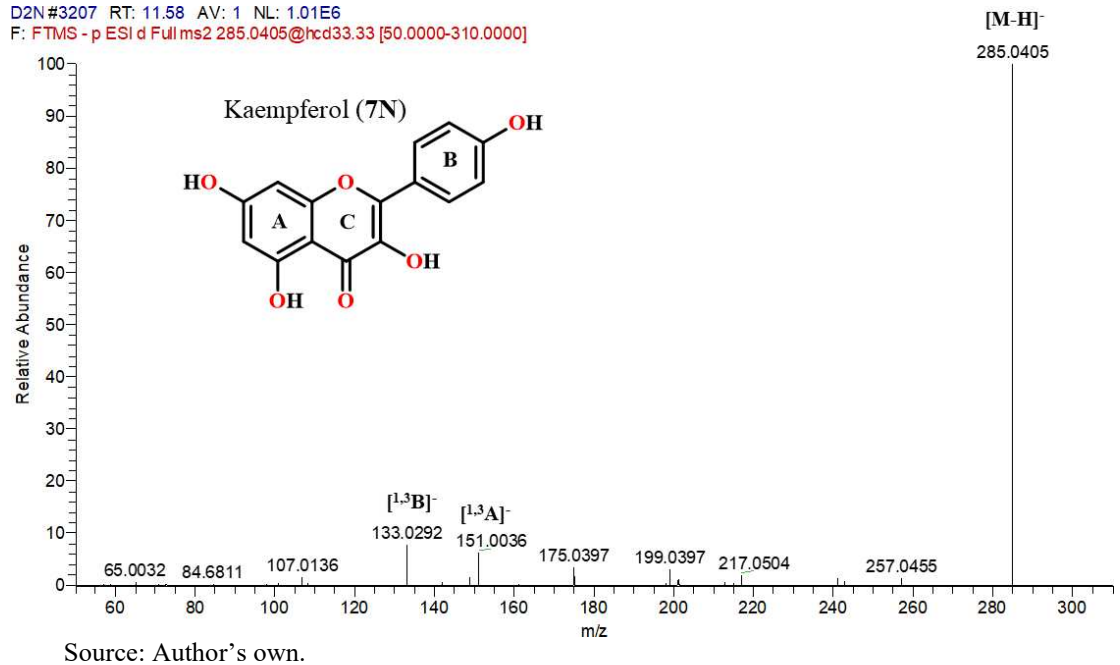


Source: Author's own.

**Supplementary Figure 82:** (-)- ESI MS/MS spectrum of the compound (**8N**)

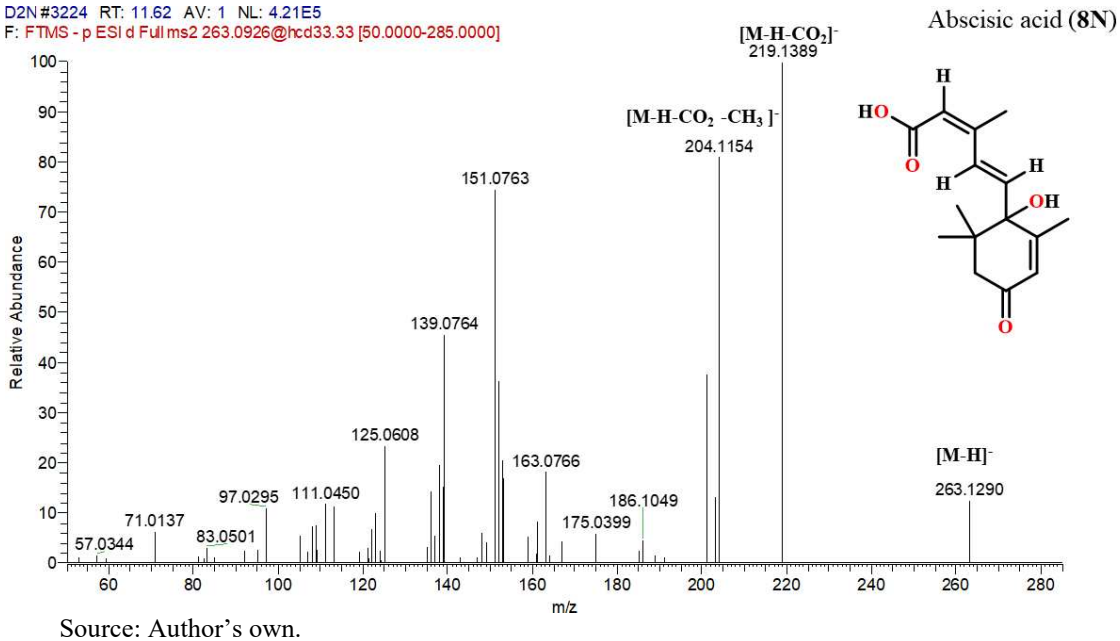


Source: Author's own.

**Supplementary Figure 83:** (+)- ESI MS/MS spectrum of compound CI 7312, fragmentation and structures proposed by CSI:Finger ID. Purple peaks represent the fragments present in the experimental data that were explained by in silico fragmentation based on the databases used by SIRIUS

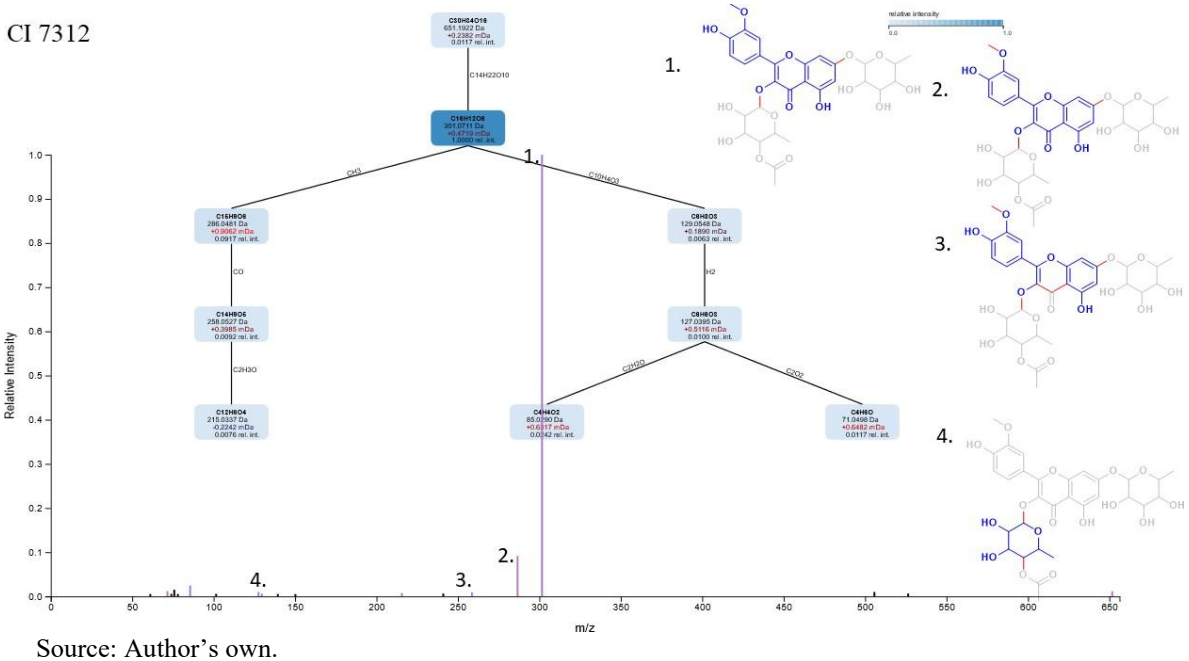


Source: Author's own.

**Supplementary Figure 84:** (+)- ESI MS/MS spectrum of compound CI 8093, fragmentation and structures proposed by CSI:Finger ID. Purple peaks represent the fragments present in the experimental data that were explained by in silico fragmentation based on the databases used by SIRIUS

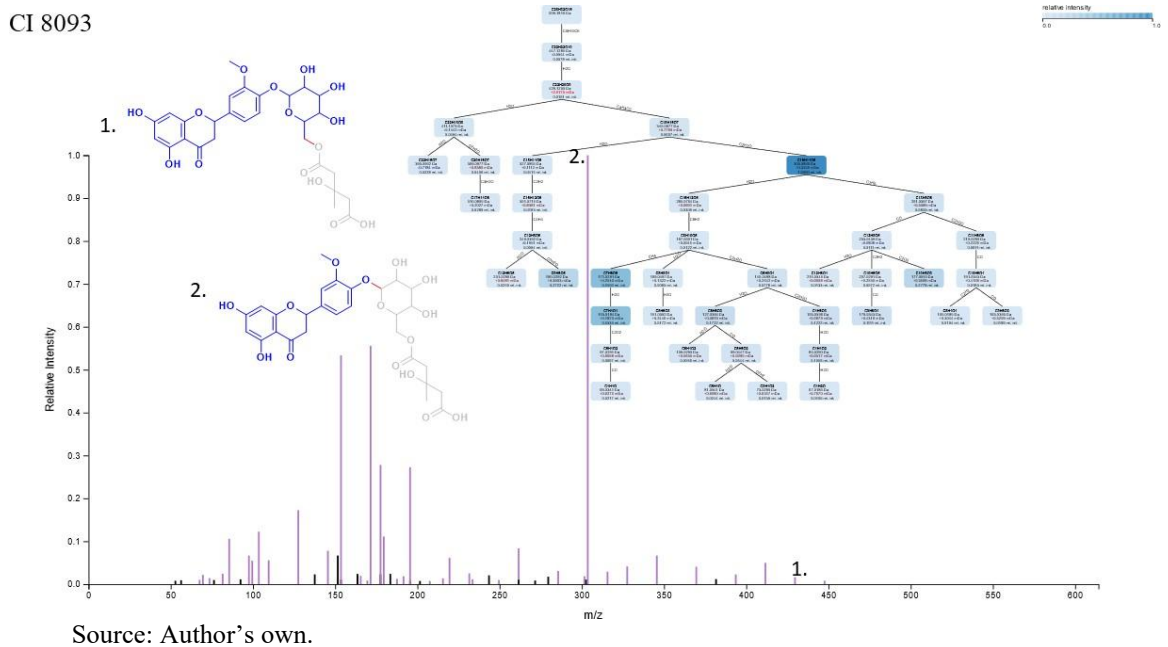


Source: Author's own.

**Supplementary Figure 85:** (+)- ESI MS/MS spectrum of compound CI 5021, fragmentation and structures proposed by CSI:Finger ID. Purple peaks represent the fragments present in the experimental data that were explained by in silico fragmentation based on the databases used by SIRIUS

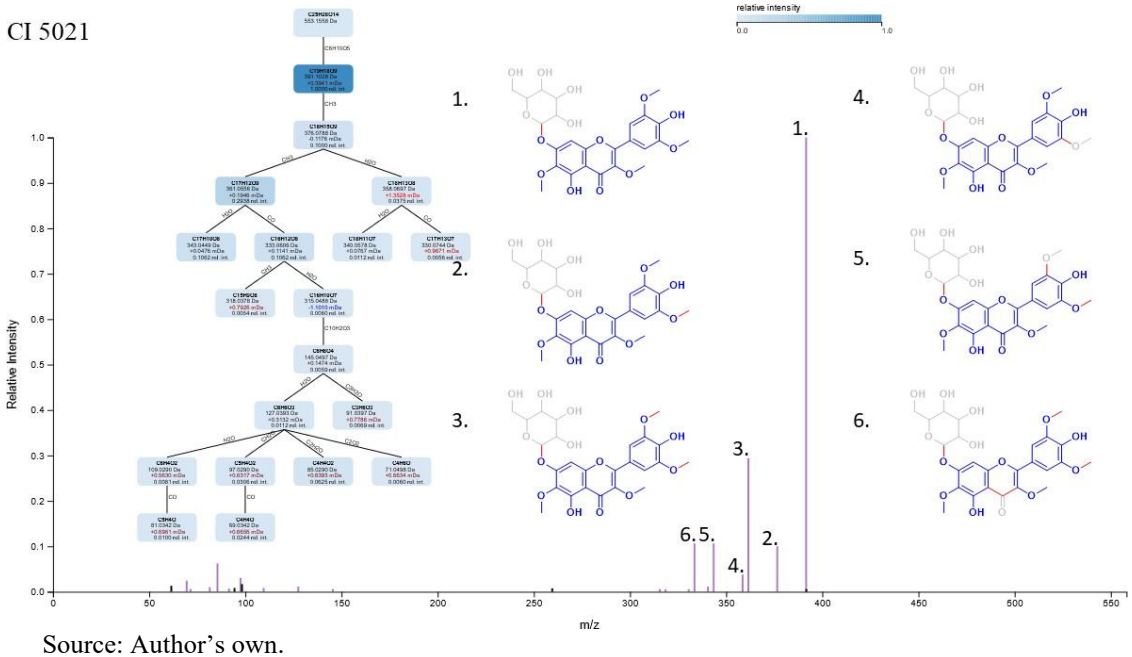


Source: Author's own.

**Supplementary Figure 86:** (+)- ESI MS/MS spectrum of compound CI 5165, fragmentation and structures proposed by CSI:Finger ID. Purple peaks represent the fragments present in the experimental data that were explained by in silico fragmentation based on the databases used by SIRIUS

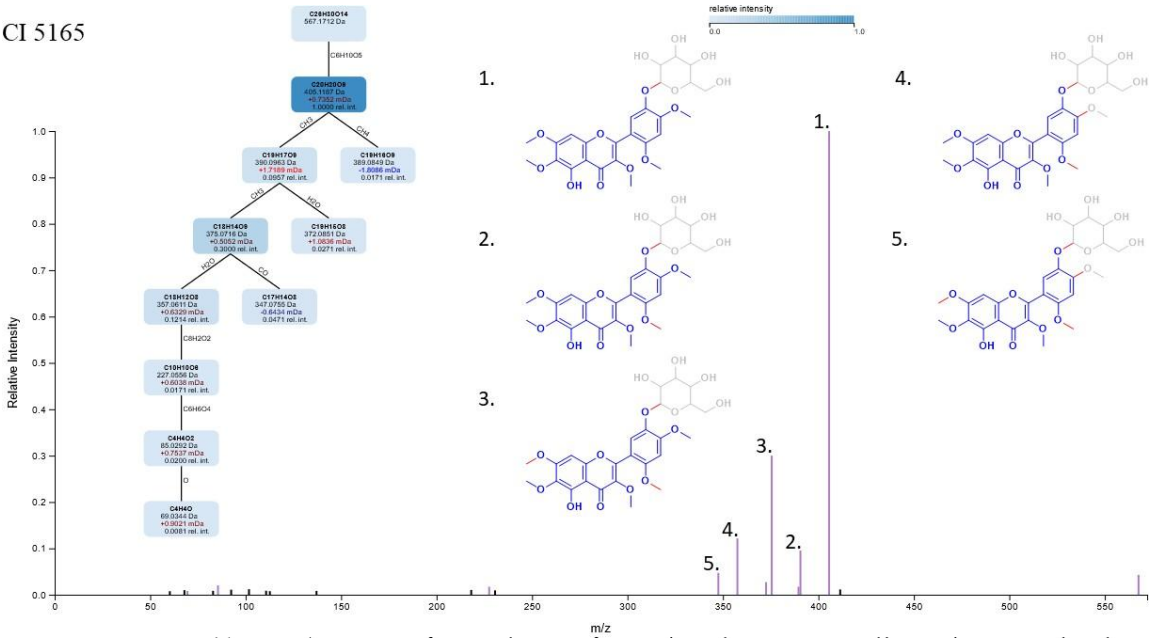


Source: Author's own.

**Supplementary Figure 87:** (+)- ESI MS/MS spectrum of compound CI 8296, fragmentation and structures proposed by CSI:Finger ID. Purple peaks represent the fragments present in the experimental data that were explained by in silico fragmentation based on the databases used by SIRIUS

CI 8296

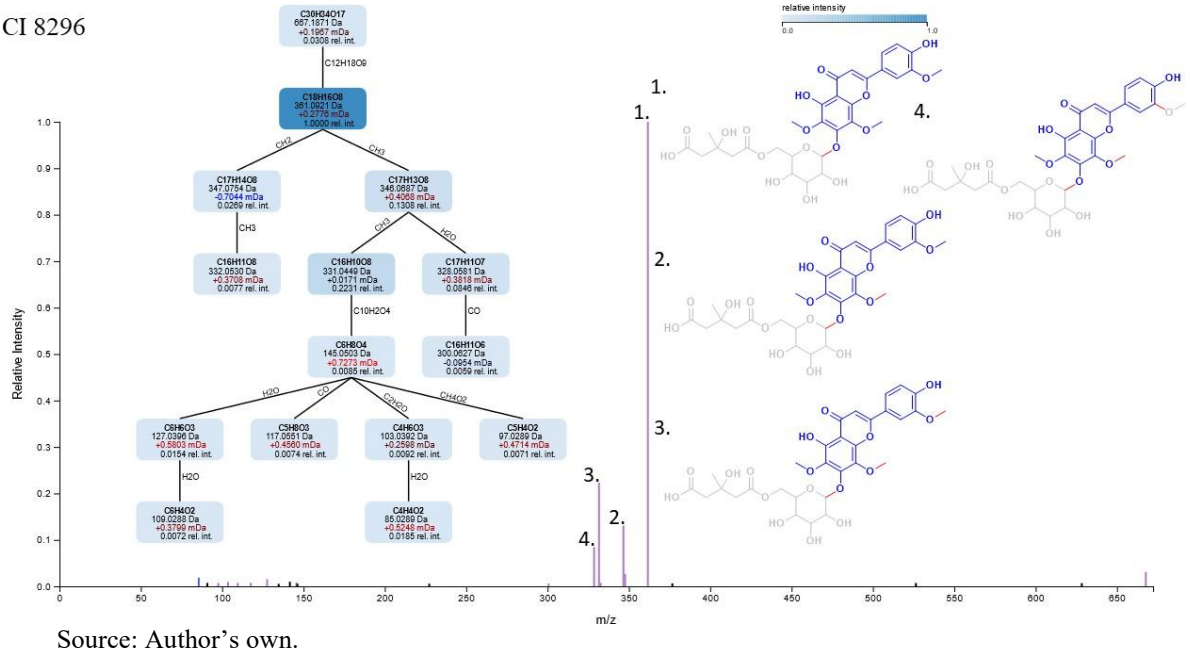


Source: Author's own.

**Supplementary Figure 88:** (+)- ESI MS/MS spectrum of compound CI 8306, fragmentation and structures proposed by CSI:Finger ID. Purple peaks represent the fragments present in the experimental data that were explained by in silico fragmentation based on the databases used by SIRIUS

CI 8306

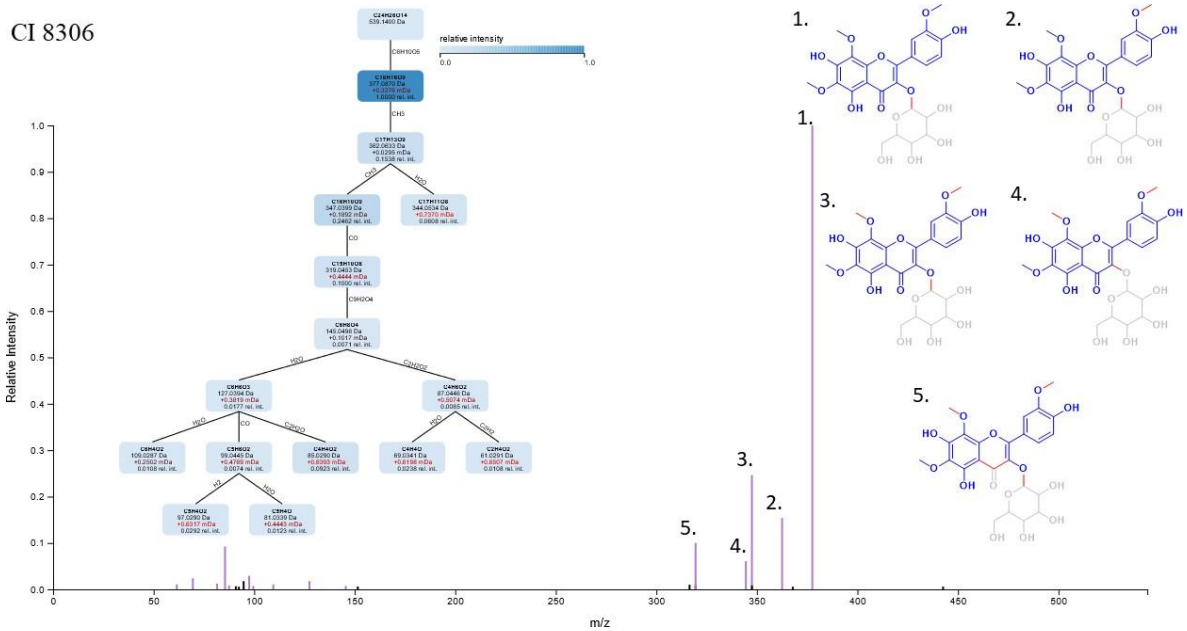


Source: Author's own.

**Supplementary Figure 89:** (+)- ESI MS/MS spectrum of compound CI 8550, fragmentation and structures proposed by CSI:Finger ID. Purple peaks represent the fragments present in the experimental data that were explained by in silico fragmentation based on the databases used by SIRIUS

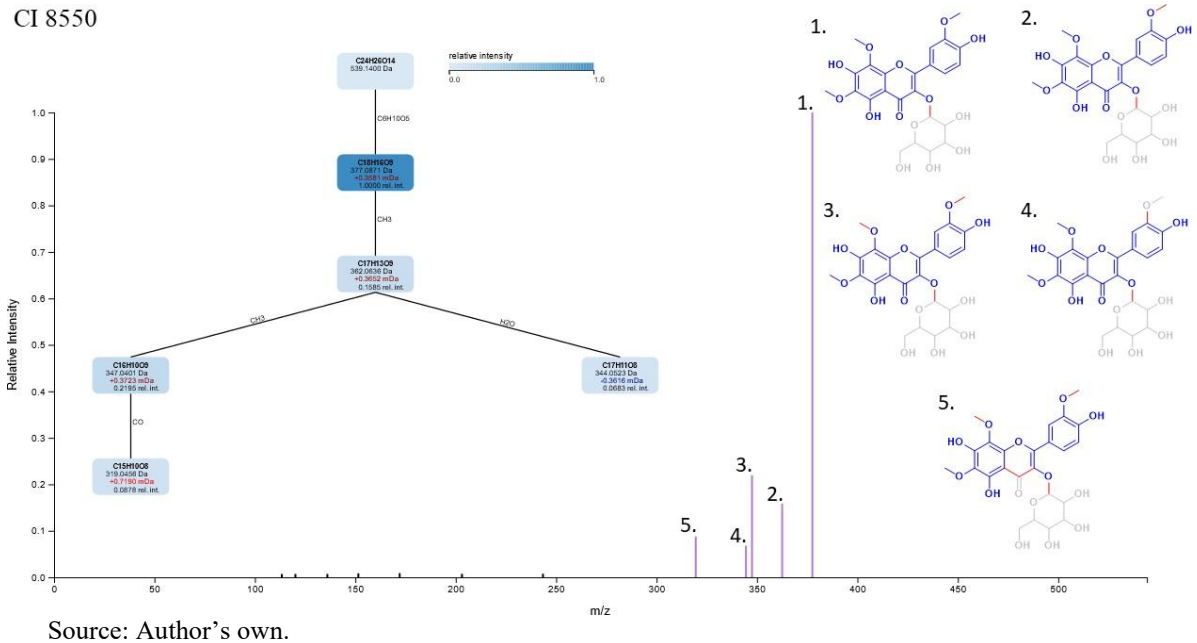


Source: Author's own.

**Supplementary Figure 90:** (+)- ESI MS/MS spectrum of compound CI $^{TS}$8126, fragmentation and structures proposed by CSI:Finger ID. Purple peaks represent the fragments present in the experimental data that were explained by in silico fragmentation based on the databases used by SIRIUS

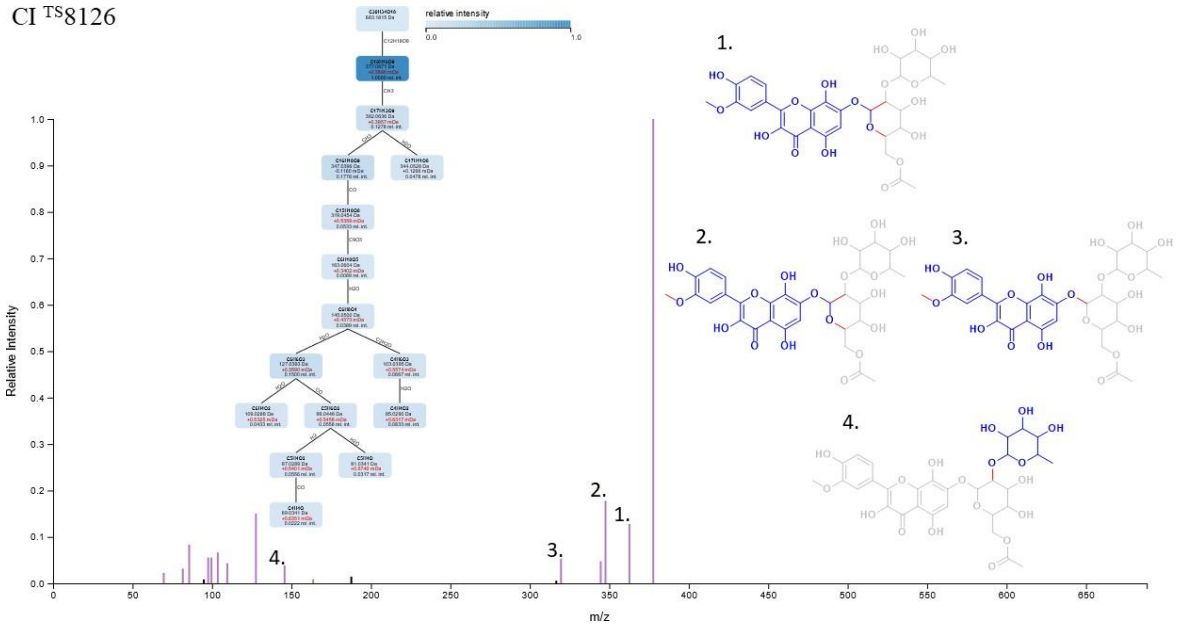


Source: Author's own.

**Supplementary Figure 91:** (+)- ESI MS/MS spectrum of compound CI 8446, fragmentation and structures proposed by CSI:Finger ID. Purple peaks represent the fragments present in the experimental data that were explained by in silico fragmentation based on the databases used by SIRIUS

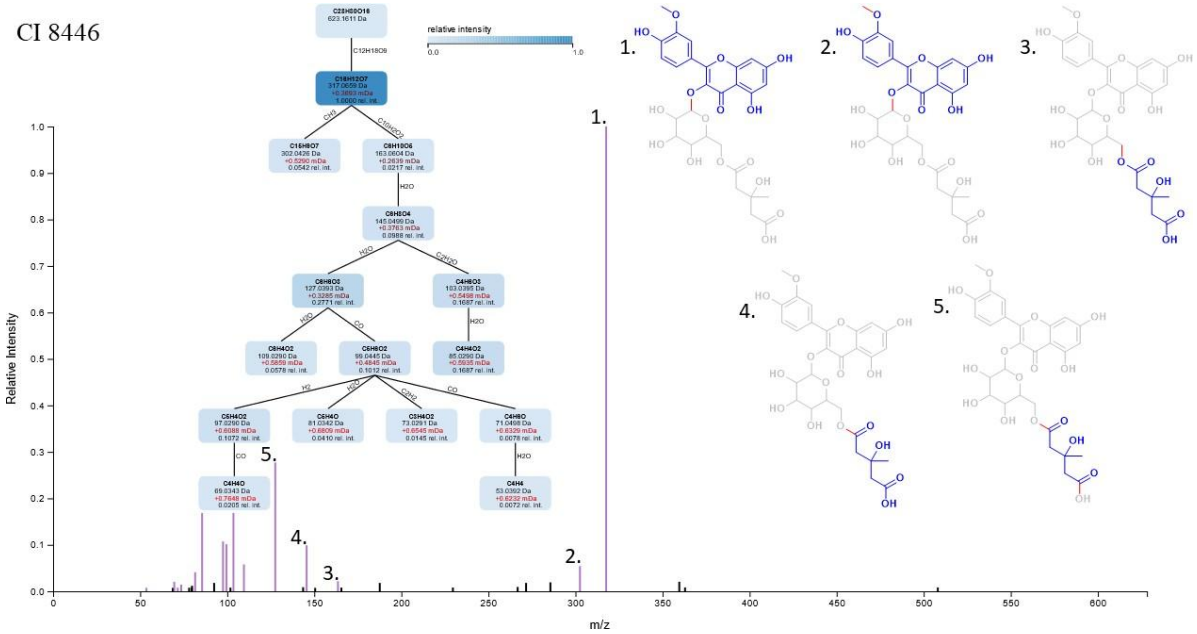


Source: Author's own.

**Supplementary Figure 92:** (+)- ESI MS/MS spectrum of compound CI 6225, fragmentation and structures proposed by CSI:Finger ID. Purple peaks represent the fragments present in the experimental data that were explained by in silico fragmentation based on the databases used by SIRIUS

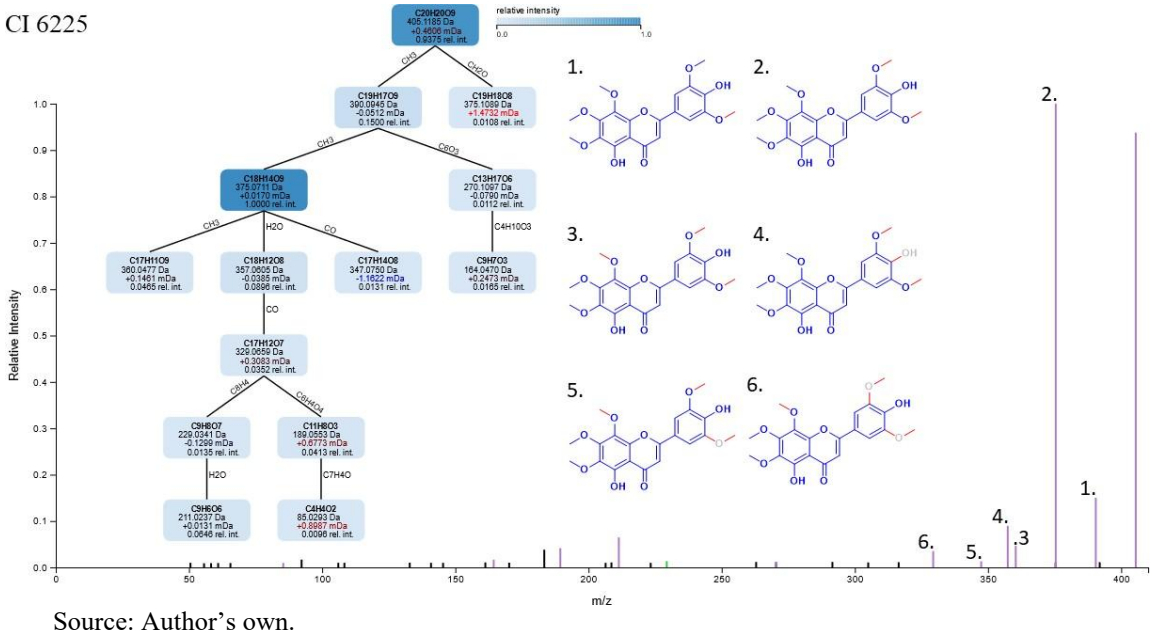


Source: Author's own.

**Supplementary Figure 93:** (+)- ESI MS/MS spectrum of compound CI 1347, fragmentation and structures proposed by CSI:Finger ID. Purple peaks represent the fragments present in the experimental data that were explained by in silico fragmentation based on the databases used by SIRIUS

CI 1347

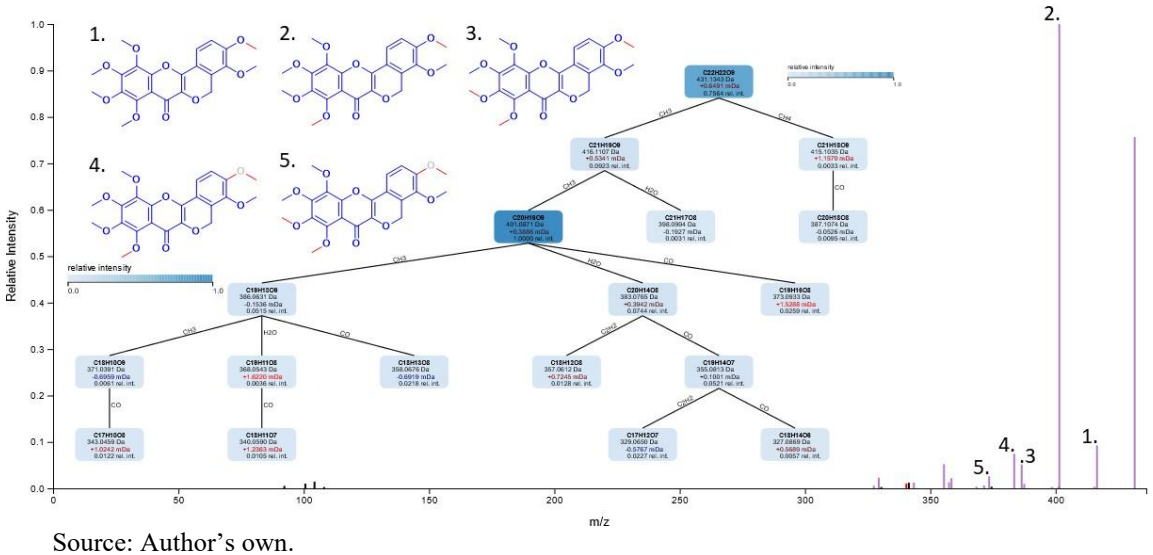


Source: Author's own.

**Supplementary Figure 94:** (+)- ESI MS/MS spectrum of compound CI 4855, fragmentation and structures proposed by CSI:Finger ID. Purple peaks represent the fragments present in the experimental data that were explained by in silico fragmentation based on the databases used by SIRIUS

CI 4855

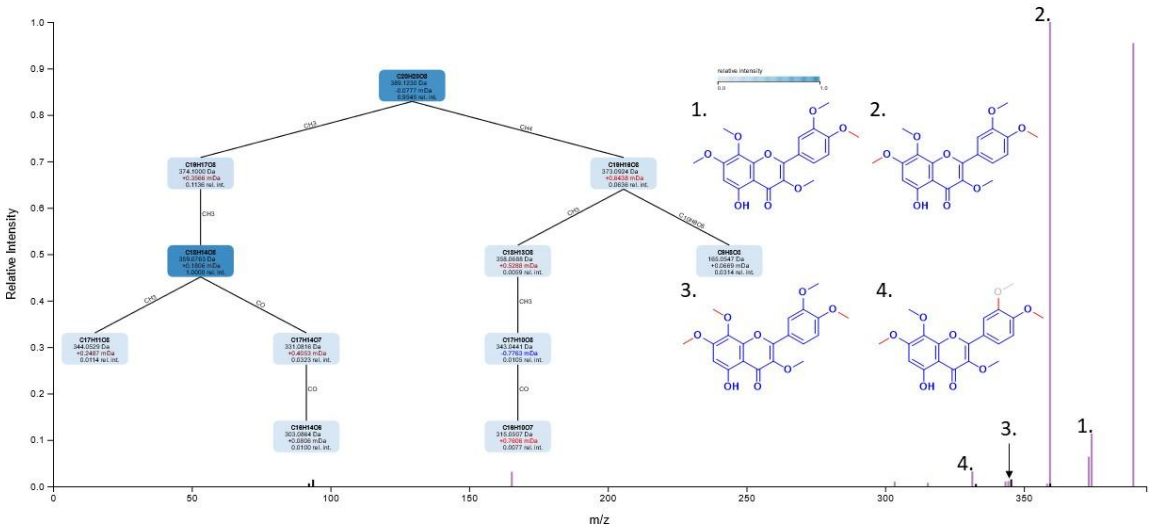


Source: Author's own.

**Supplementary Figure 95:** (+)- ESI MS/MS spectrum of compound CI 1627, fragmentation and structures proposed by CSI:Finger ID. Purple peaks represent the fragments present in the experimental data that were explained by in silico fragmentation based on the databases used by SIRIUS

CI 1627

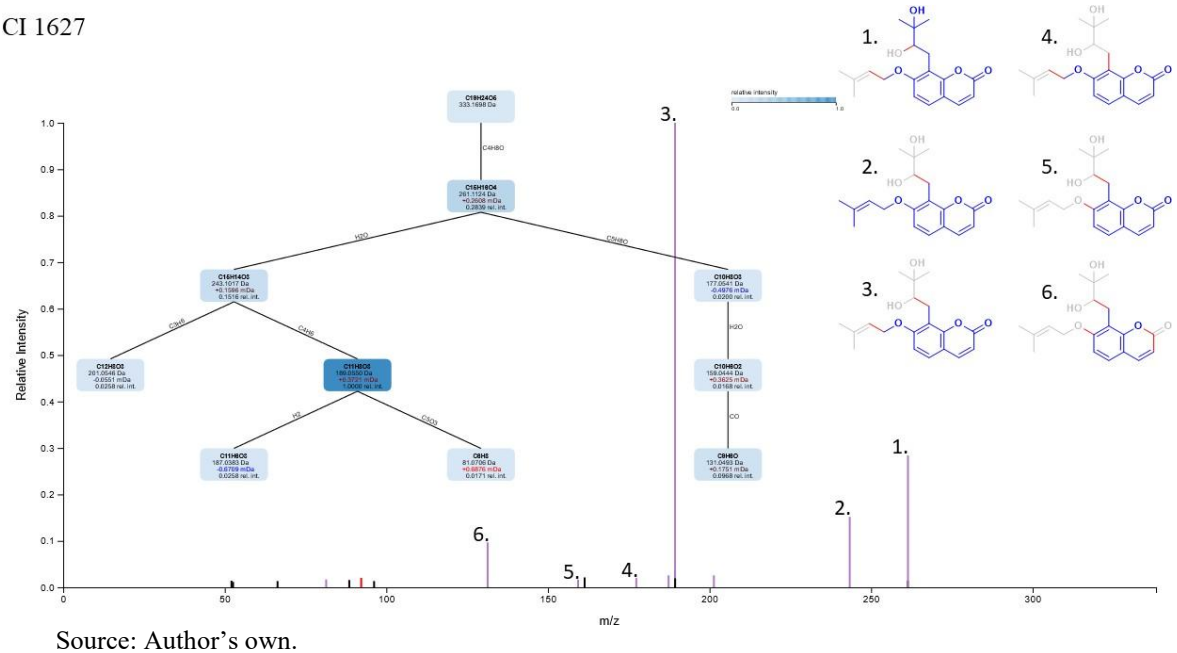


Source: Author's own.

**Supplementary Figure 96:** (+)- ESI MS/MS spectrum of compound CI 2868, fragmentation and structures proposed by CSI:Finger ID. Purple peaks represent the fragments present in the experimental data that were explained by in silico fragmentation based on the databases used by SIRIUS

CI 2868

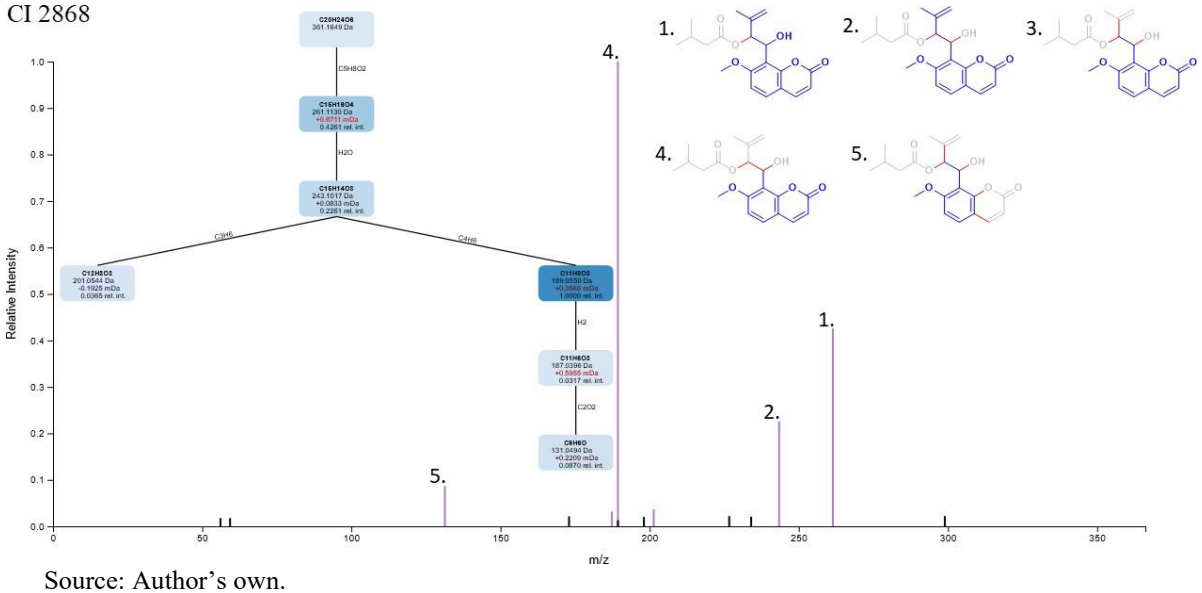


Source: Author's own.

**Supplementary Figure 97:** (+)- ESI MS/MS spectrum of compound CI 1608, fragmentation and structures proposed by CSI:Finger ID. Purple peaks represent the fragments present in the experimental data that were explained by in silico fragmentation based on the databases used by SIRIUS

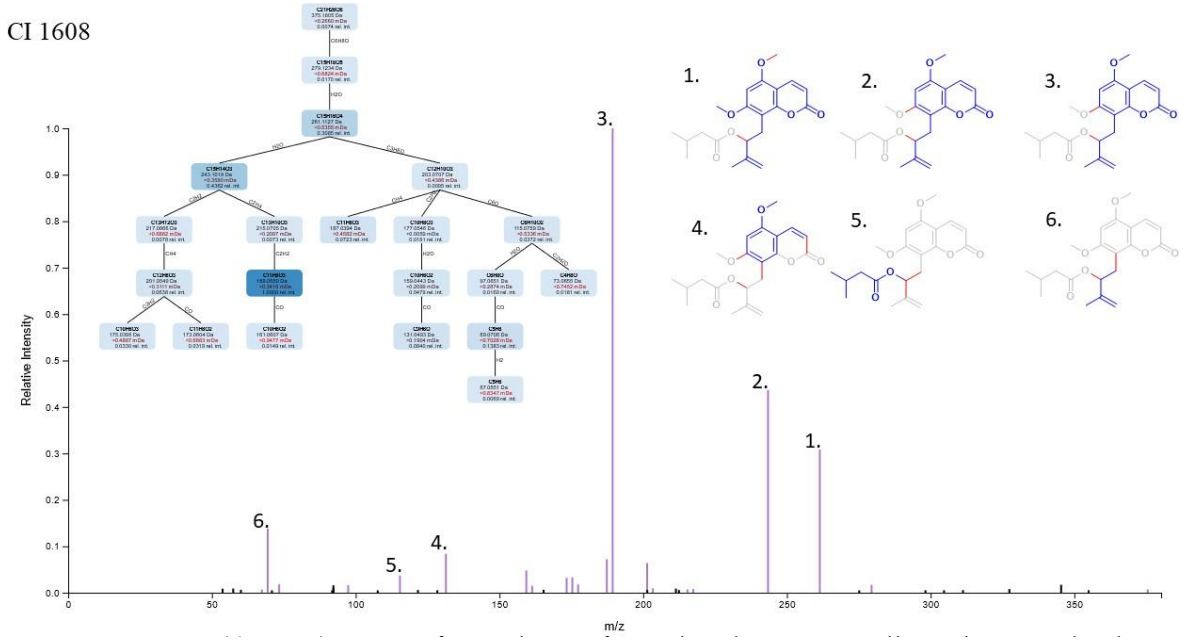


Source: Author's own.

**Supplementary Figure 98:** (+)- ESI MS/MS spectrum of compound CI 5332, fragmentation and structures proposed by CSI:Finger ID. Purple peaks represent the fragments present in the experimental data that were explained by in silico fragmentation based on the databases used by SIRIUS

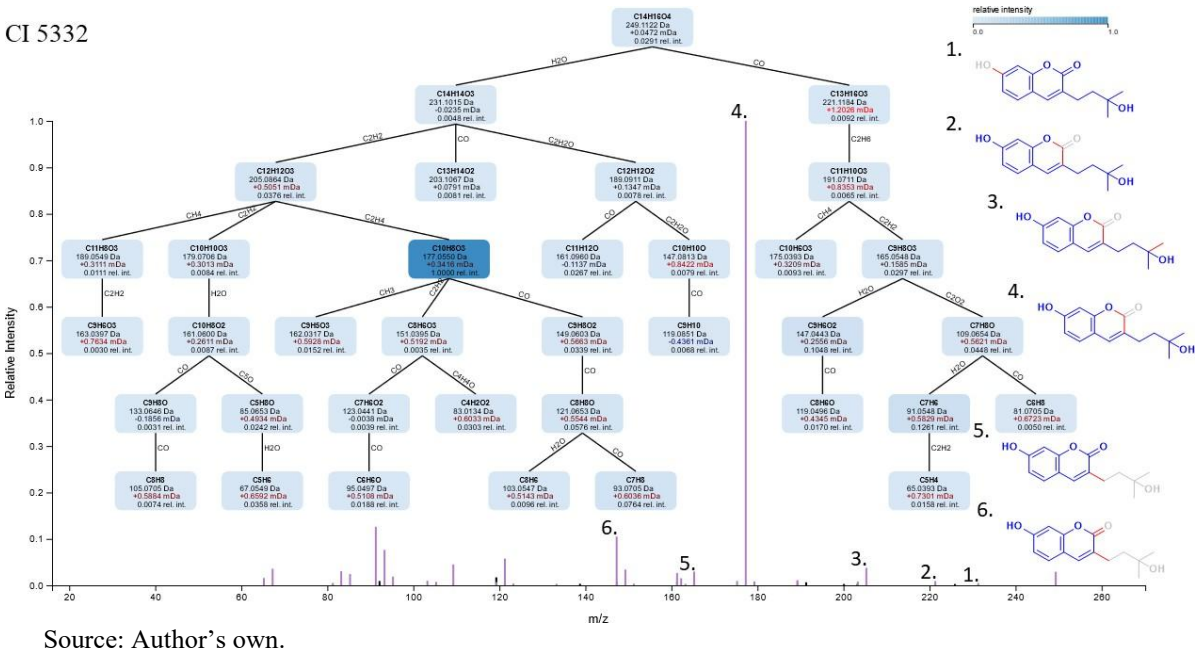


Source: Author's own.

**Supplementary Figure 99:** (+)- ESI MS/MS spectrum of compound CI 6449, fragmentation and structures proposed by CSI:Finger ID. Purple peaks represent the fragments present in the experimental data that were explained by in silico fragmentation based on the databases used by SIRIUS

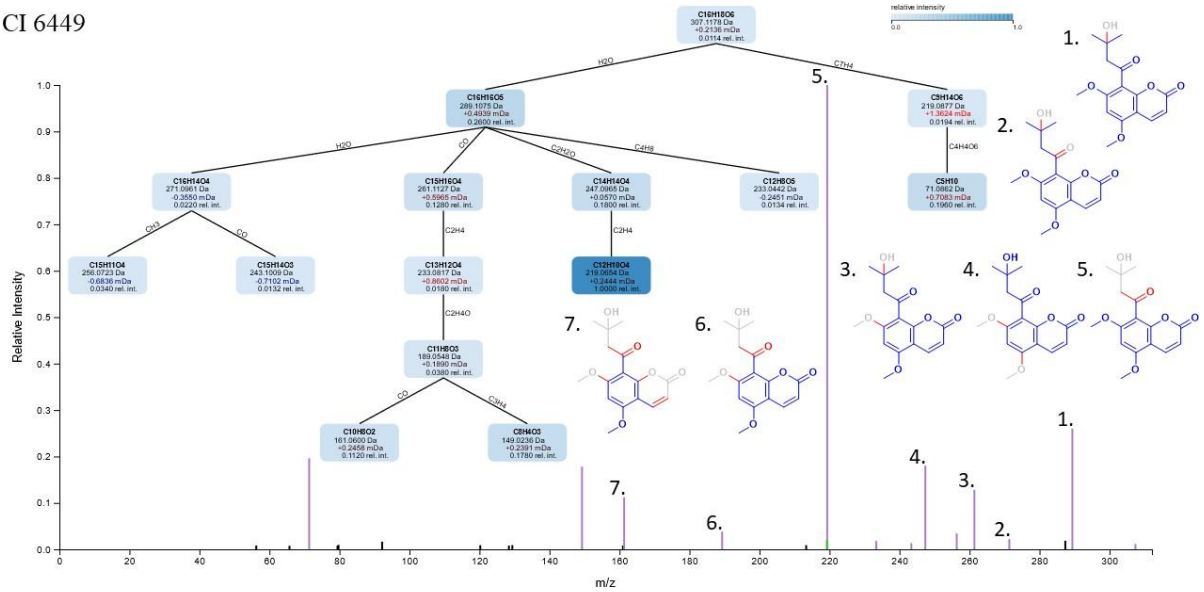


Source: Author's own.

**Supplementary Figure 100:** (+)- ESI MS/MS spectrum of compound CI 1190, fragmentation and structures proposed by CSI:Finger ID. Purple peaks represent the fragments present in the experimental data that were explained by in silico fragmentation based on the databases used by SIRIUS

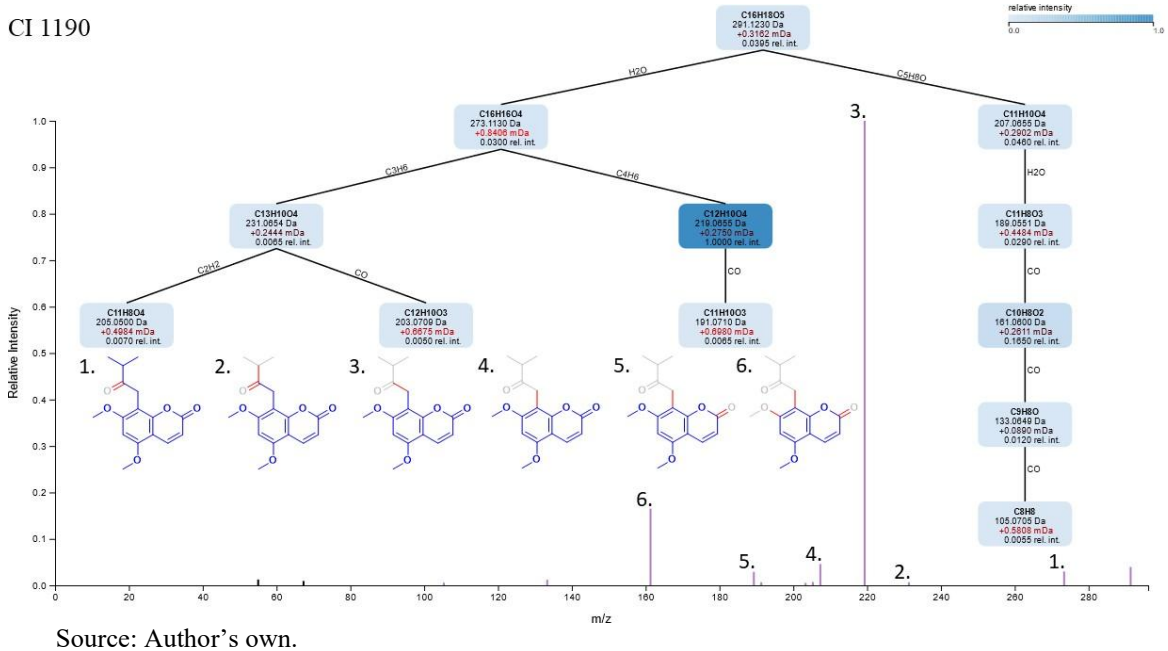


Source: Author's own.

**Supplementary Figure 101:** (+)- ESI MS/MS spectrum of compound CI 8379, fragmentation and structures proposed by CSI:Finger ID. Purple peaks represent the fragments present in the experimental data that were explained by in silico fragmentation based on the databases used by SIRIUS

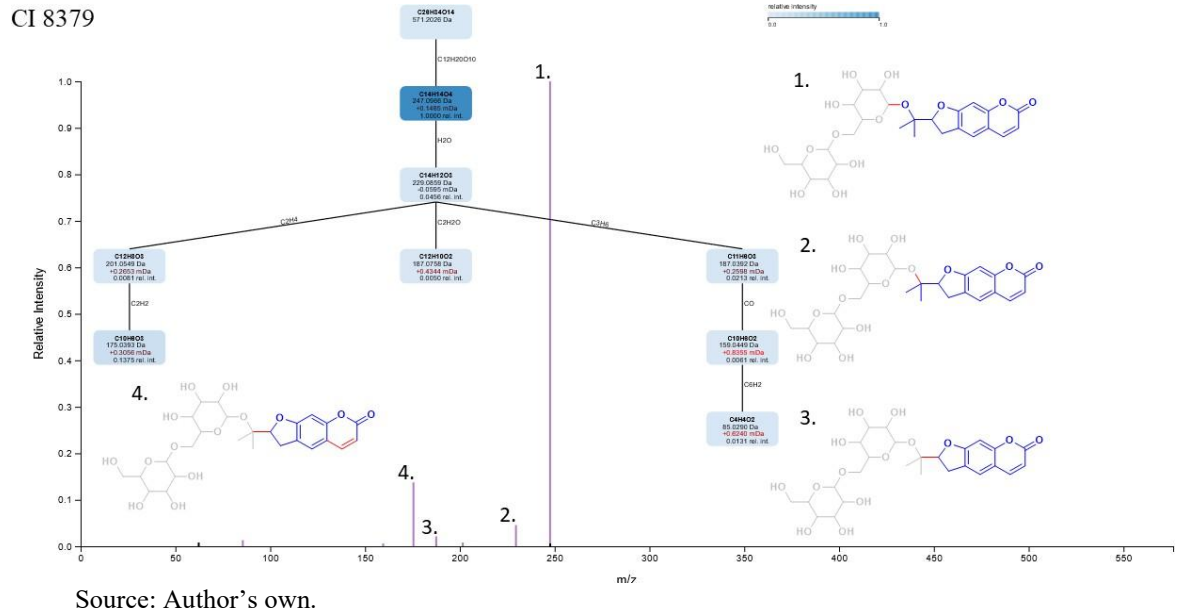


Source: Author's own.

**Supplementary Figure 102:** (+)- ESI MS/MS spectrum of compound CI $^{TS}$1329, fragmentation and structures proposed by CSI:Finger ID. Purple peaks represent the fragments present in the experimental data that were explained by in silico fragmentation based on the databases used by SIRIUS

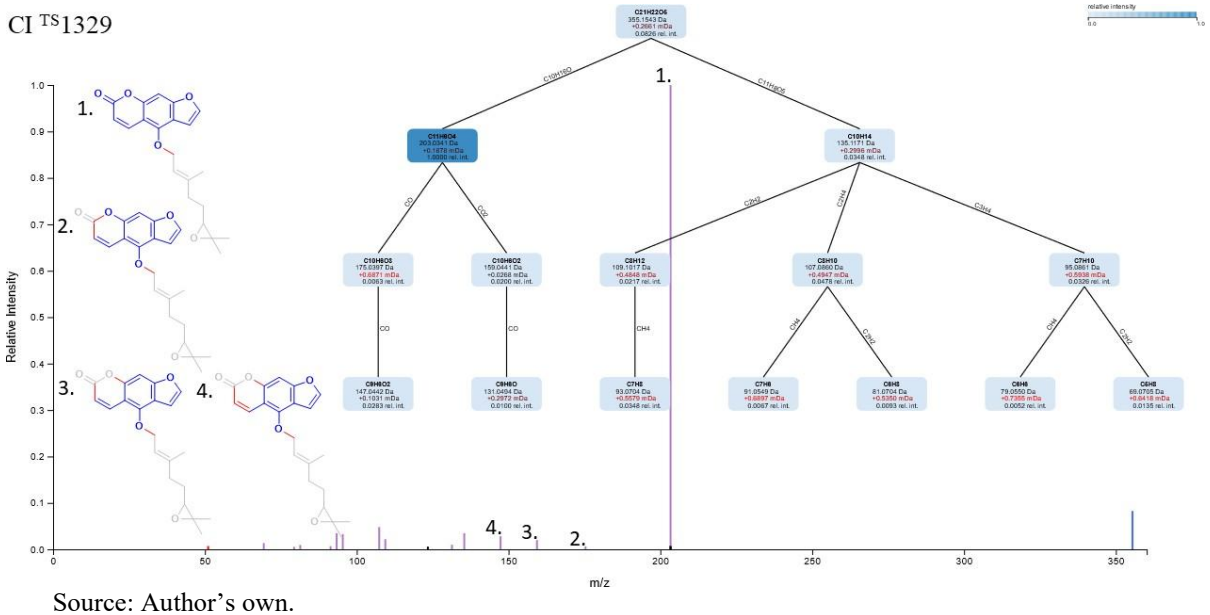


Source: Author's own.

**Supplementary Figure 103:** (+)- ESI MS/MS spectrum of compound CI 5013, fragmentation and structures proposed by CSI:Finger ID. Purple peaks represent the fragments present in the experimental data that were explained by in silico fragmentation based on the databases used by SIRIUS

CI 5013

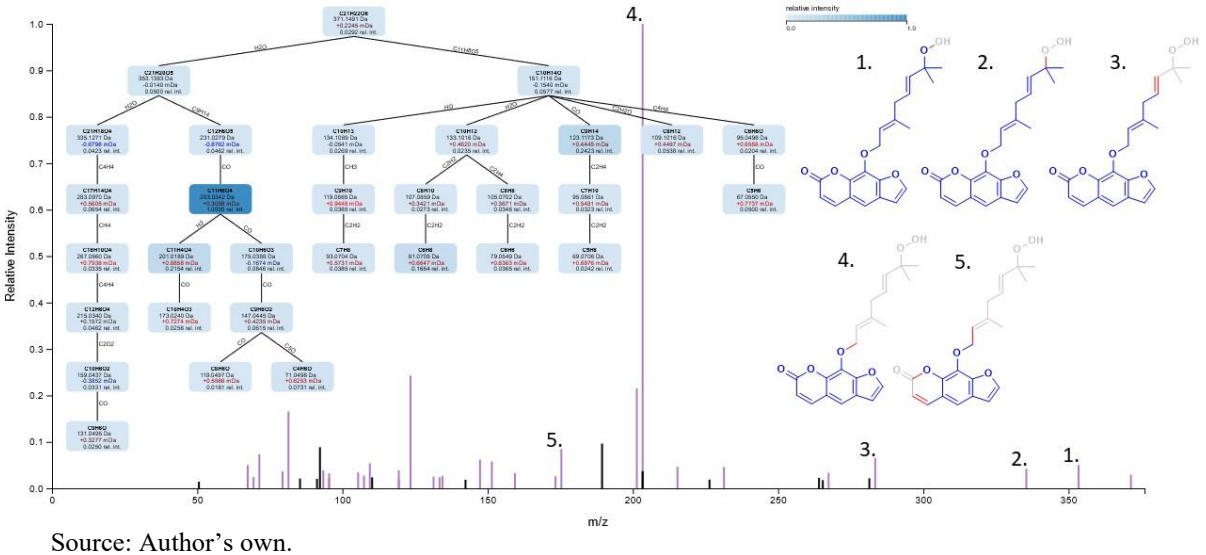


Source: Author's own.

**Supplementary Figure 104:** (+)- ESI MS/MS spectrum of compound CI $^{TS}$5049, fragmentation and structures proposed by CSI:Finger ID. Purple peaks represent the fragments present in the experimental data that were explained by in silico fragmentation based on the databases used by SIRIUS

CI $^{TS}$5049

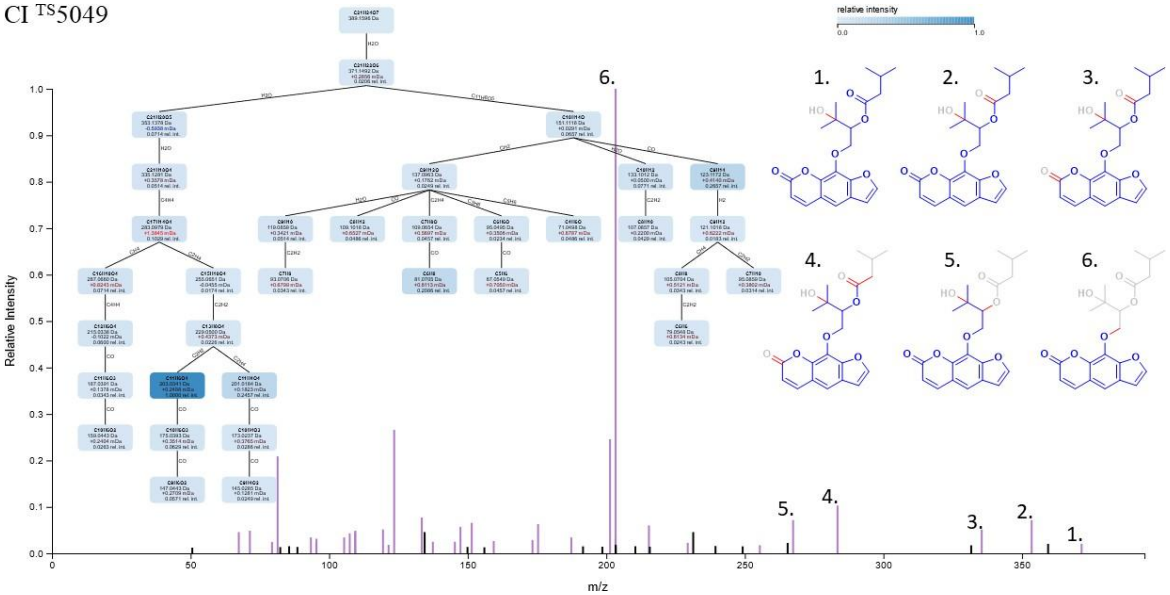


Source: Author's own.

**Supplementary Figure 105:** (+)- ESI MS/MS spectrum of compound CI 1455, fragmentation and structures proposed by CSI:Finger ID. Purple peaks represent the fragments present in the experimental data that were explained by in silico fragmentation based on the databases used by SIRIUS

CI $^{TS}$1455

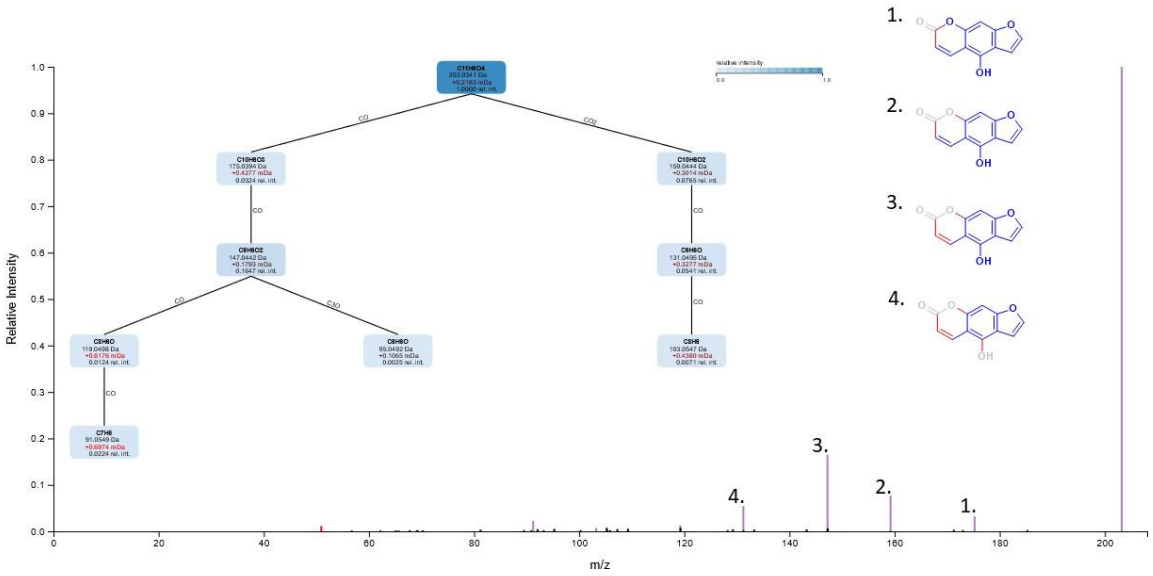


Source: Author's own.

**Supplementary Figure 106:** Graphs (2D) showing the relative abundance of glycosylated flavonoids in all the fractions obtained by SPE. In the Heatmap, each row represents a compound (numbered 1-13), and each column represents a fraction (FR1-FR5). The values of the heatmap cells represent the averages of the relative abundances of each triplicate. The scale on the side represented by a color gradient shows the most abundant (dark blue) and least abundant (light blue-white) compounds

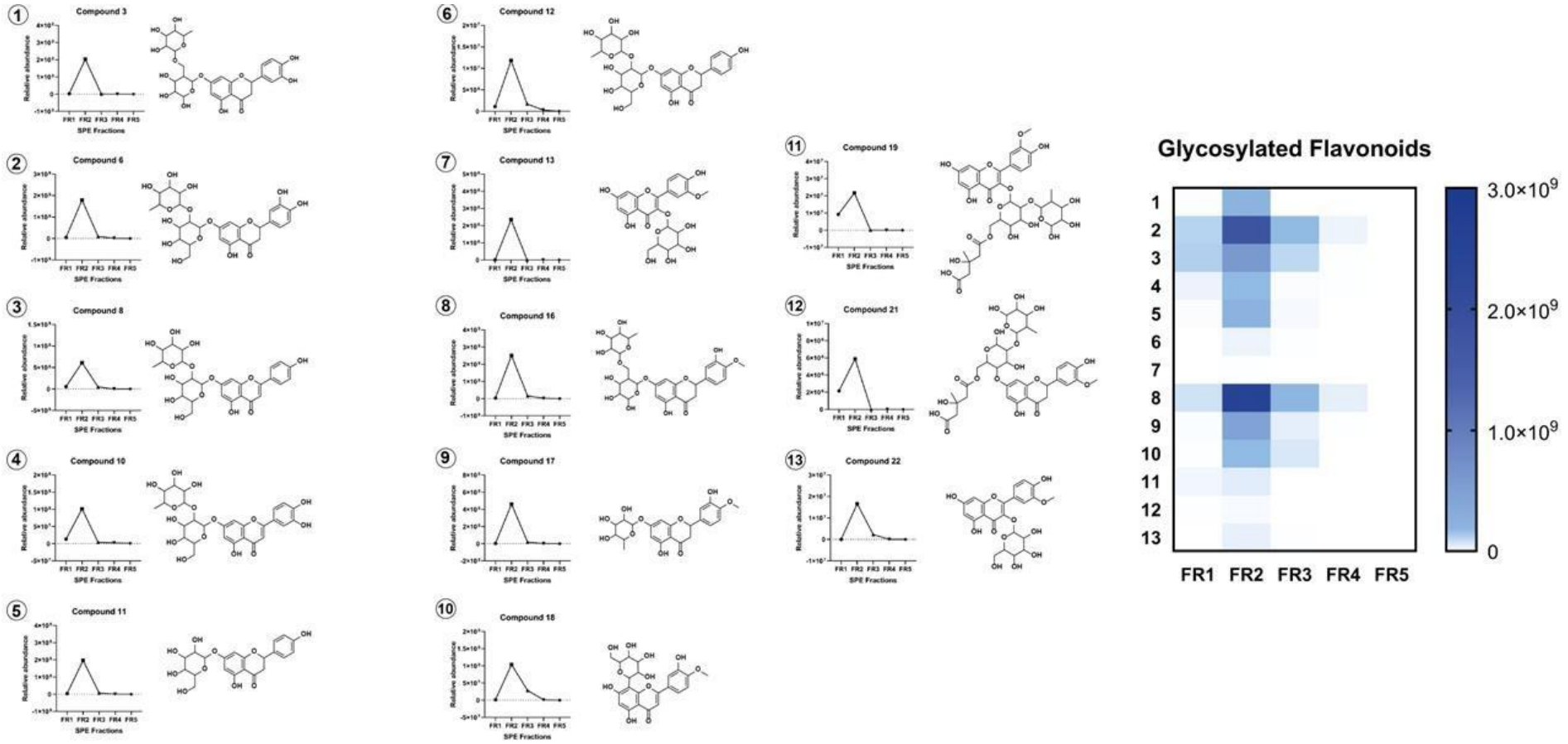


Source: Author's own.

## 5 CONCLUSÃO

Os dados de CL-EMAR do extrato EAE-CA, FR3 e FR4 de *Citrus aurantium*, agregado a ferramentas de desreplicação como o GNPS, e identificação por comparação com bases de dados, possibilitou a identificação de 65 compostos, sendo 57 no modo positivo e 8 substâncias no modo negativo de análise, pertencentes a classe de flavonoides, cumarinas, limonóide, compostos aromáticos e nitrogenados. Entre eles, 3 flavonoides (naringina, hesperidina e hesperitina) foram anotados a nível 1 de confiança, comparados com padrão.

As frações FR3 e FR4 mostraram-se promissoras no ensaio antifúngico sobre o fitopatógeno *Fusarium jinanense* com inibição micelial de 60,97 mg/mL e 57,33 mg/mL, respectivamente, enquanto o fungicida comercial Cercobin® apresentou uma inibição micelial de 47,92 mg/mL. Nessas duas frações os compostos principais identificados foram cumarinas, algumas delas preniladas e polimetoxiflavonas, essas substâncias menos polares são relatadas com potencial antimicrobiano devido ao caráter lipofílico que elas têm, facilitando a entrada na camada lipídica do microrganismo.

O ensaio antioxidante frente ao radical DPPH do extrato EAE-CA apresentou uma contração inibitória ($CI_{50}$) cerca de dez vezes maior do que o padrão positivo Trolox, sendo um resultado moderado para esse ensaio, observou-se também que o fracionamento em extração em fase sólida (SPE) não favoreceu a atividade antioxidante, pois todas as frações tiveram uma porcentagem de inibição menor do que o extrato EAE-CA. Dessa forma, pode ser atribuir o potencial antioxidante do extrato a interações sinérgicas entre as substâncias, que foi modificada no fracionamento.

Portanto, o trabalho evidenciou a importância do estudo da composição química das cascas de *C. aurantium*, pois esse refugo industrial pode ser usado no desenvolvimento de novos produtos ecológicos, a partir da compreensão dos mecanismos de ação do fungo (*Fusarium jinanense*) que é responsável por perdas significativas na produção de melão

## REFERÊNCIAS

ABOU, B. D.H.; IBRAHIM, B. M.; HASSAN, N. S.; YOUSUF, A. F.; EL GENGAIHI, S. Exploiting *Citrus aurantium* seeds and their secondary metabolites in the management of Alzheimer disease. **Toxicology reports**, v. 7, p.723-729, 2020.

AL ABOODY, M.S.; MICKYMARAY, S. Anti-fungal efficacy and mechanisms of flavonoids. **Antibiotics**, v. 9, n. 2, p.45, 2020.

ALVES, C. Q.; DAVIDL, J. M.; DAVID, J. P.; BAHIA, M. V.; AGUIAR, R, M. Métodos para determinação de atividade antioxidante in vitro em substratos orgânicos. **Química Nova**. v. 33, n. 10, p. 2202-2210, 2010.

ANNUNZIATA, F.; PINNA, C.; DALLAVALLE, S.; TAMBORINI, L.; PINTO, A. An Overview of Coumarin as a Versatile and Readily Accessible Scaffold with Broad-Ranging Biological Activities. **International Journal of Molecular Sciences**, v. 21, n.13, p. 4618, 2020.

APARECIDO, C.C. e ROSA, E.C. Avaliação morfologia e molecular para identificação de *Fusarium* sp. **Biológico***,* v. 81, p.1-7, 2019.

CROTTI, A. E. M., VESSECCHI, R., LOPES, J. L. C., & LOPES, N. P.. (2006). Espectrometria de massas com ionização por "electrospray": processos químicos envolvidos na formação de íons de substâncias orgânicas de baixo peso molecular. *Química Nova*, *29*(2), 287–292. https://doi.org/10.1590/S0100-40422006000200020

DEGIRMENCI, H.; ERKURT, H. Chemical profile and antioxidant potency of *Citrus aurantium* L. flower extracts with antibacterial effect against foodborne pathogens in rice pudding. **Lebensmittel-Wissenschaft & Technologie**, v. 126, p. 109273, 2020.

DEWICK, P. M. **Medicinal natural products: a biosynthetic approach**. 3. ed. Hoboken: Editora John Wiley & Sons; New Jersey-U.S. 2002, p. 137-186.

DIAS, R. C.S.; TERAO, D. Doença das cucurbitáceas. **Patologia pós-colheita: frutas, olerícolas e ornamentais tropicais**. Embrapa Agroindústria Tropical. Brasília, p. 595-628, 2006.

DING, L.; ZHANG, X.; ZHANG J. Antioxidant Activity In Vitro Guided Screening and Identification of Flavonoids Antioxidants in the Extract from *Tetrastigma hemsleyanum* Diels et Gilg. **International Journal of Analytical Chemistry**. 2021 Nov 23, p. 7195125, 2021.

GHINI, R.; HIROSHI K. **Resistência de fungos a fungicidas**. 2. ed. Jaguariúna, SP. Embrapa Meio Ambiente, 2002. 78p, II., 22 cm.

HAMEDI, A.; MOHAMMAD, M. Z.; AKRAM J.; SAEED, A.; REZA, H.; ARDALAN, P. *Citrus aurantium* (bitter orange) seeds oil: pharmacognostic, anti-inflammatory and anti-nociceptive properties. **Trends in Pharmaceutical Sciences**, v. 5, n. 3, p. 153-164, 2019.

HEGAZI, A. G.; EL HADY, F. K. A. Egyptian propolis: 3. Antioxidant, antimicrobial activities and chemical composition of propolis from reclaimed lands. **Zeitschrift für Naturforschung C**, v. 57, n. 3-4, p. 395-402, 2002.

JABEEN, H.; SALEEMI, S.; RAZZAQ, H.; YAQUB, A.; SHAKOOR, S.; & QURESHI, R. Investigating the scavenging of reactive oxygen species by antioxidants via theoretical and experimental methods. **Journal of Photochemistry and Photobiology B: Biology**, *180*, p. 268-275, 2018.

KIST, B.B; CARVALHO, C.D; BELING, R.R. **Anuário Brasileiro de Horti&Fruti 2022** – Santa Cruz do Sul: Editora Gazeta Santa Cruz, p.96, 2022. Disponível em: https://www.editoragazeta.com.br/sitewp/wp content/uploads/2022/04/HORTIFRUTI_2022.pdf> Acesso em 14 de abril de 2023.

KULKARNI, A. S.; VIKRAM V. N.; MOHAMMAD, Z.; HAJERA, N. K.; SANDHYA, S. B.; SANDIP, T. T. Investigation of Orange Peel Ethanolic Extract as an Anticataract Agent. **World Journal of Pharmacy and Pharmaceutical Sciences**, v.7, n.2, p. 1025-1033, 2017.

LIMA, E. N.; OSTER, A. H.; BORDALLO, P. N.; ARAÚJO, A. A.; SILVA, D. E.; LIMA, C. S. A novel lineage in the *Fusarium incarnatum-equiseti* species complex is one of the causal agents of fusarium rot on melon fruits in Northeast Brazil. **Plant Pathology**, v. 70, n. 1, p.133-143, 2021.

LI, Y., WANG, X., CHEN, Q., HOU, Y., XIA, Q., & ZHAO, P. (2016). Metabolomics analysis of the larval head of the silkworm, Bombyx mori. *International Journal of Molecular Sciences*, *17*(9), 1460.

MONTAGNER, C.; DE SOUZA, S.M.; GROPOSO, C.; DELLE MONACHE, F.; SMÂNIA, E.F.; SMÂNIA Jr, A. Antifungal activity of coumarins. **Zeitschrift für Naturforschung C**, v. 63, n. 1-2, p.21-28, 2008.

MORADI, K.; ASHTARIAN, H.; DANZIMA, N.Y.; SAEEDI, H.; BIJAN, B.; AKBARI, F.; MOHAMMADI, M. M. Essential oil from *Citrus aurantium* alleviates anxiety of patients undergoing coronary angiography: a single-blind, randomized controlled trial. **Chinese journal of integrative medicine**, v. 27, p.177-182, 2021.

MOURA, R. B.; AREAS, T. F. Laranja da terra: evidências científicas para diferentes aplicações terapêuticas. **Revista Fitos**. v. 7, n. 2, p. 110-118, 2013.

NAZARI, V.; AZARPIRA, R., N.; HELI, H. Development of self-nanoemulsifying drug delivery systems for oil extracts of *Citrus aurantium* L. blossoms and Rose damascena and evaluation of anticancer properties. **Journal of Drug Delivery Science and Technology**, v. 47, p. 330-336, 2018.

NICOLESCU, T. O. (2017). Interpretation of mass spectra. *Mass Spectrometry*, 23-78.

NOTHIAS, L. F., PETRAS, D., SCHMID, R., DÜHRKOP, K., RAINER, J., SARVEPALLI, A., ... & DORRESTEIN, P. C. (2020). Feature-based molecular networking in the GNPS analysis environment. *Nature methods*, *17*(9), 905-908.

OLIVEIRA, G. L. S. Determinação da capacidade antioxidante de produtos naturais in vitro pelo método do DPPH•: estudo de revisão. **Revista Brasileira de Plantas Medicinais**. v. 17, n. 1, p. 36-44, 2015.

OMOTAYO, O.P.; OMOTAYO, A.O.; MWANZA, M.; BABALOLA, O.O. Prevalence of mycotoxins and their consequences on human health. **Toxicological research**, v. 35, p.1-7, 2017.

OSTER, A.H.; SILVA, E.O.; BORBALLO, P.N.; ZOCOLO, G.H.; SILVEIRA, M.R.S.; OIRAM FILHO, F.; DE ARAÚJO, A.A.C. Luz ultravioleta pulsada no controle de podridão pós-colheita e na qualidade de melão para exportação. Embrapa Agroindústria Tropical–Boletim de Pesquisa e Desenvolvimento (INFOTECA-E). **Boletim de pesquisa**, 173, ISSN 1679-6543, 2018.

OULEBSIR, C.; MEFTI-KORTEBY, H.; DJAZOULI, Z. E.; ZEBIB, B.; MERAH, O. Essential Oil of *Citrus aurantium* L. Leaves: Composition, antioxidant activity, elastase and collagenase inhibition. **Agronomy**, v. 12, n. 6, p.1466, 2022.

PAVIA, D. L.; LAMPMAN, G. M.; KRIZ, G. S.; VYVYAN, J. R. **Introdução à espectroscopia**. 4. ed. Cengage Learning, 2010. 692 p.

PILON, A. C., VIEIRA, N. C., AMARAL, J. G., MONTEIRO, A. F., SILVA, R. R. da ., SPÍNDOLA, L. S., CASTRO-GAMBOA, I., & LOPES, N. P.. (2021). Redes Moleculares: Uma análise sobre anotações e descoberta de novos ativos. *Química Nova*, *44*(9), 1168–1179. https://doi.org/10.21577/0100-4042.20170777

PREVEDELLO, M.T. and COMACHIO, G. Antioxidantes e sua relação com os radicais livres, e Doenças Crônicas Não Transmissíveis: uma revisão de literatura Antioxidants and their relationship with free radicals, and Chronic Non communicable Diseases: a literature review. **Brazilian Journal of Development**, *7*(6), pp.55244-55285, 2021.

PUTON, B. M. S.; BERNARDI, J. L; ORO, C. E. D.; BOMBANA, V. B.; DARIFF, A. P.; BECKER, J.; PAROUL, N.; CANSIAN, R. L. Concentração Inibitória Mínima E Atividade Antioxidante Do Extrato De Plectranthus Ornatus Codd. (Lamiaceae) Extraído Por Diferentes Solventes. **Revista Perspectiva, Erechim**. *42*(159), p. 109-118, 2018.

SILVERSTEIN, R. M.; WEBSTER, F. X.; KIEMLE, D. J. **Identificação espectrométrica de compostos orgânicos.** 7. ed. Rio de Janeiro, Editora LTC, 2007. 490 p.

SIMÕES, C. M. O.; SCHENKEL, E. P.; GOSMAN, G.; MELLO, J. C. P.; MENTEZ, L. A.; PETROVICK, P. R. **Farmacognosia: da planta ao medicamento**. 6. ed. Porto Alegre: Editora da UFRGS; Florianópolis: Editora da UFSC, 2007. 1102 p.

SUNTAR, I.; KHAN, H.; PATEL, S.; CELANO, R.; RASTRELLI, L. An overview on *Citrus aurantium* L.: Its functions as food ingredient and therapeutic agent. **Oxidative Medicine and Cellular Longevity**. v. 2018, p. 7864269-7864269, 2018.